Design, synthesis, and evaluation of novel 3-carboranyl-1,8-naphthalimide derivatives as potential anticancer agents.

Sebastian Rykowski[a], Dorota Gurda-Woźna[b,1], Marta Orlicka-Płocka[b,1], Agnieszka Fedoruk-Wyszomirska[b], Małgorzata Giel-Pietraszuk[b], Eliza Wyszko[b], Aleksandra Kowalczyk[c], Paweł Stączek[c], Andrzej Bak[d], Agnieszka Kiliszek[b], Wojciech Rypniewski[b], Agnieszka B. Olejniczak[a,*]

[a]Institute of Medical Biology, Polish Academy of Sciences, 106 Lodowa St., Łódź 93-232, Poland

[b]Institute of Bioorganic Chemistry, Polish Academy of Sciences, 12/14 Z. Noskowskiego St., 61-704 Poznan, Poland

[c]Department of Molecular Microbiology, Faculty of Biology and Environmental Protection, University of Lodz, 12/16 Banacha St., Łódź 90-237, Poland

[d]Department of Chemistry, University of Silesia, Szkolna 9 St., 40-007 Katowice, Poland

Table of contents

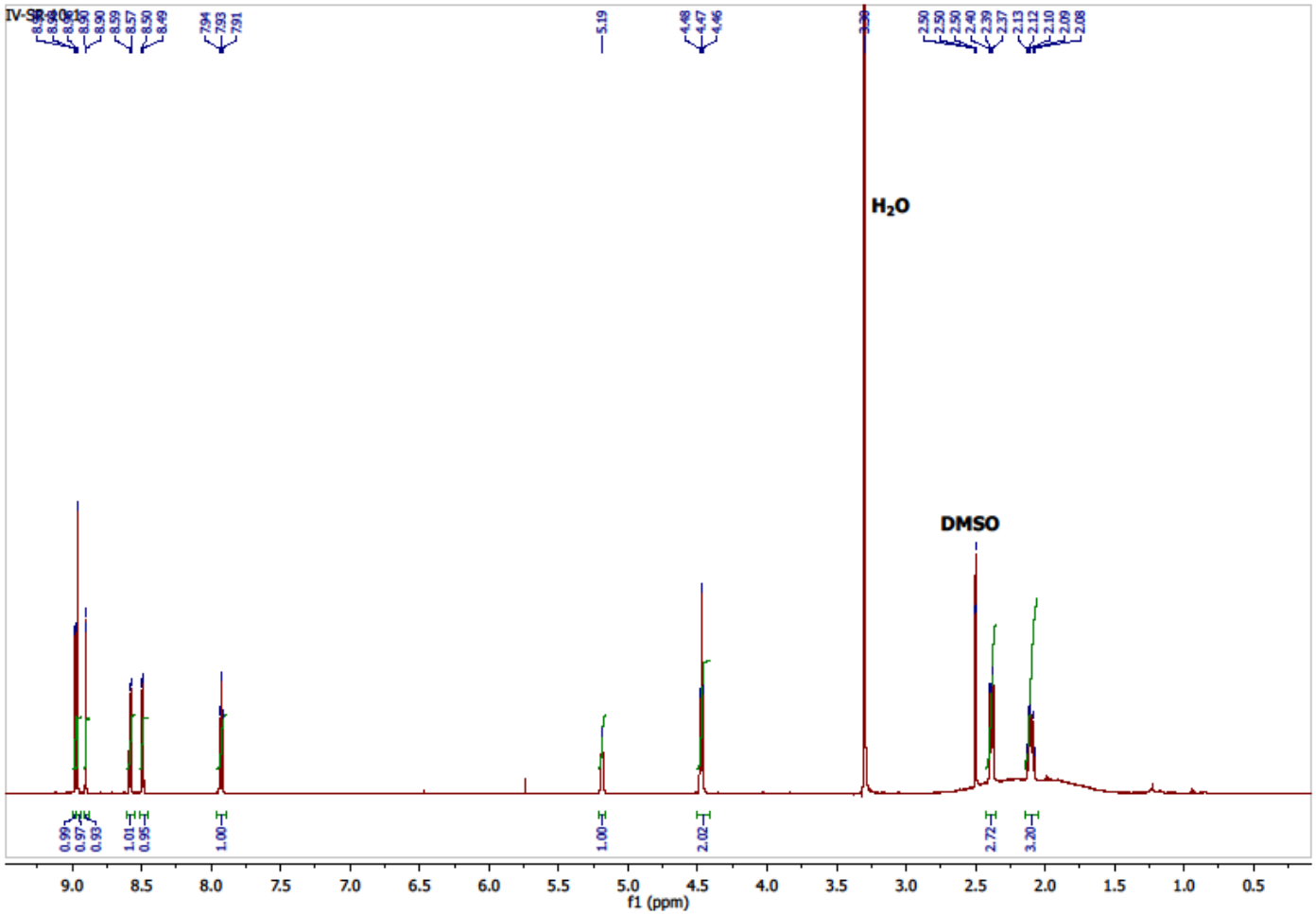

Figure S1. ^{1}H NMR spectrum of **6**.

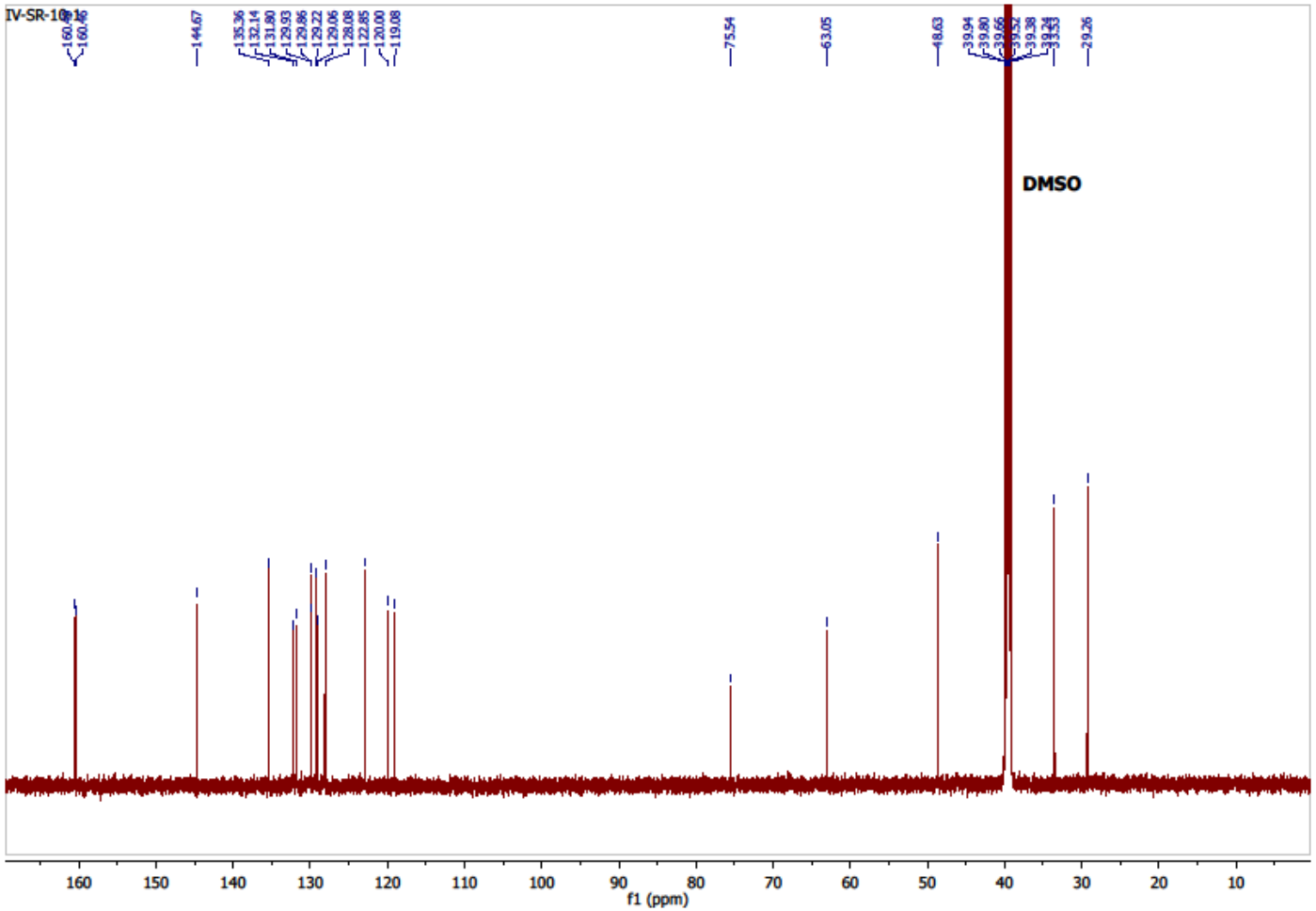

Figure S2. ^{13}C NMR spectrum of **6**.

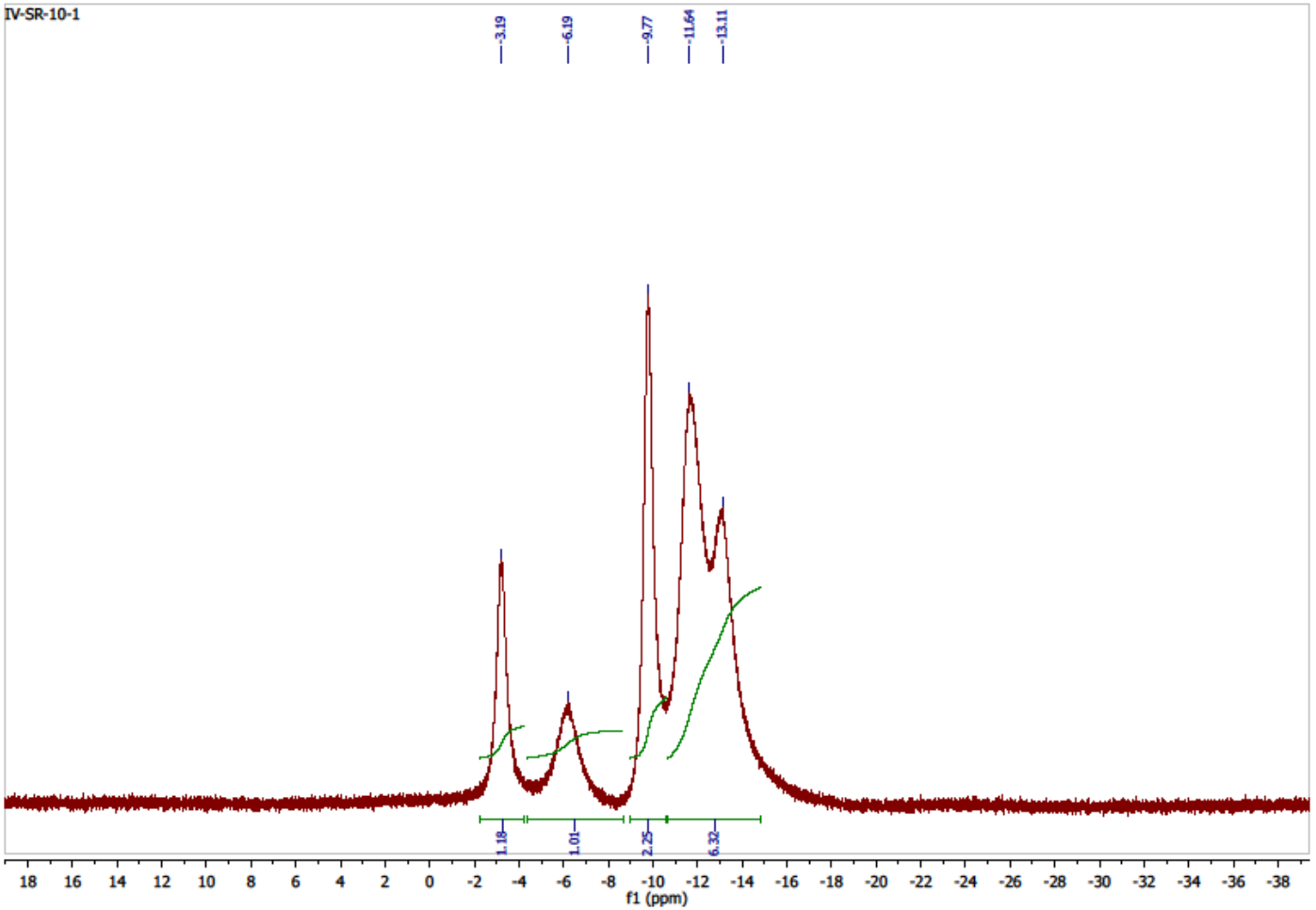

Figure S3. ^{11}B NMR {^{1}H BB} spectrum of **6**.

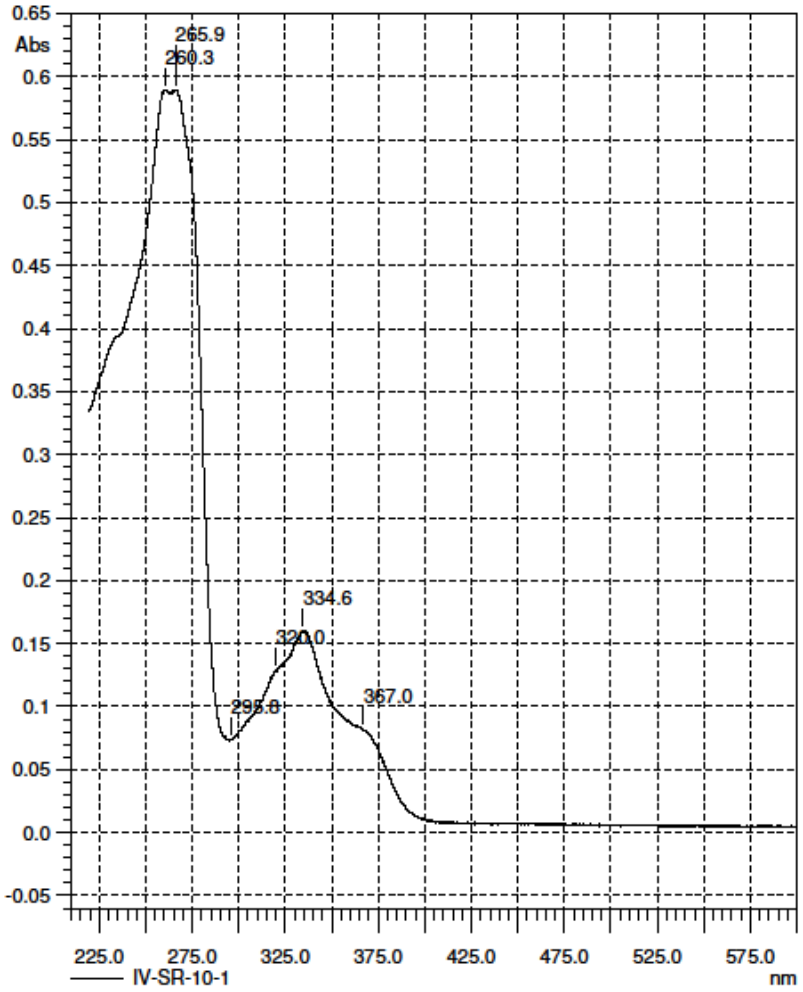

Figure S4. UV spectrum of **6**.

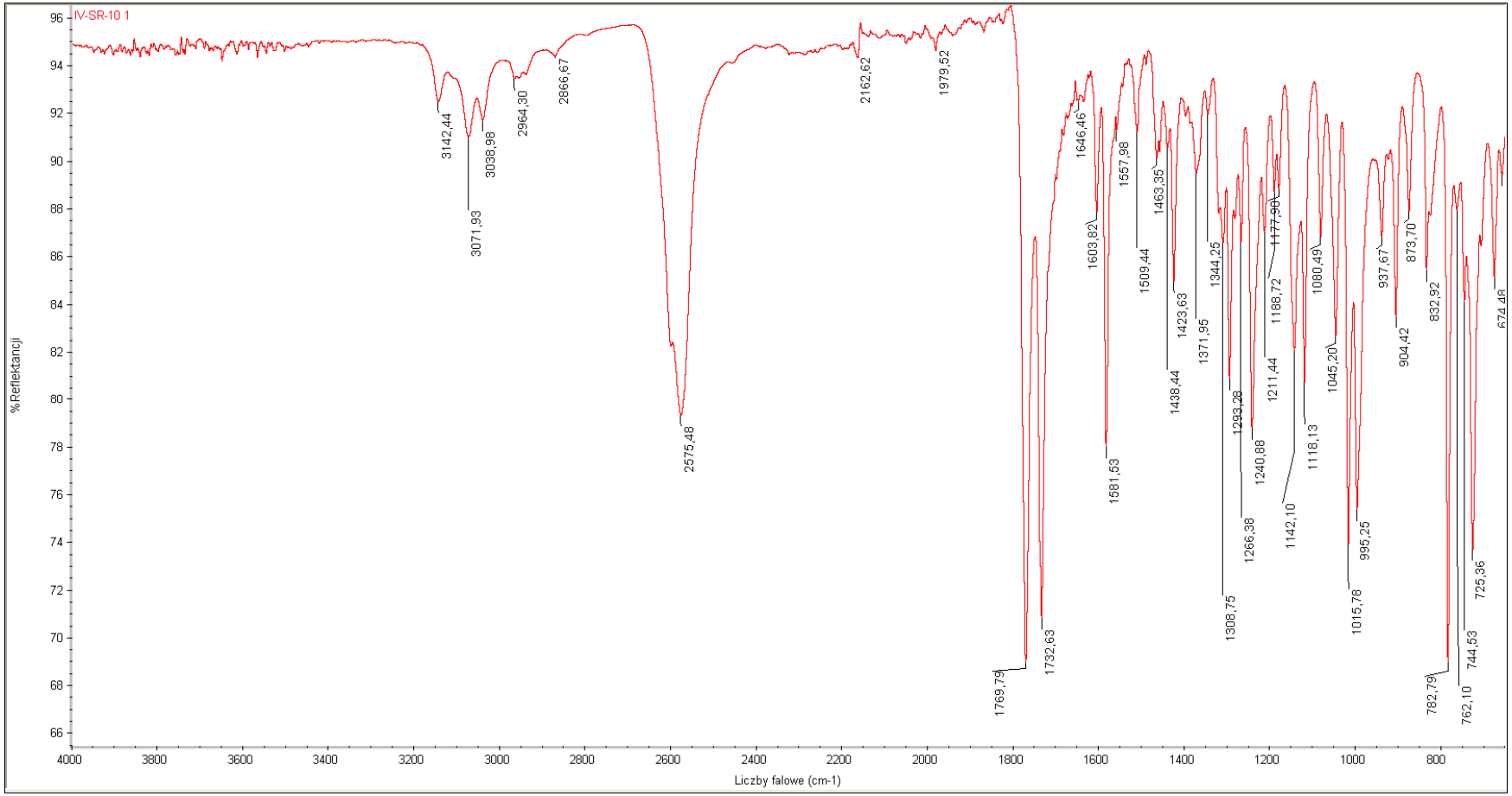

Figure S5. IR spectrum of **6**.

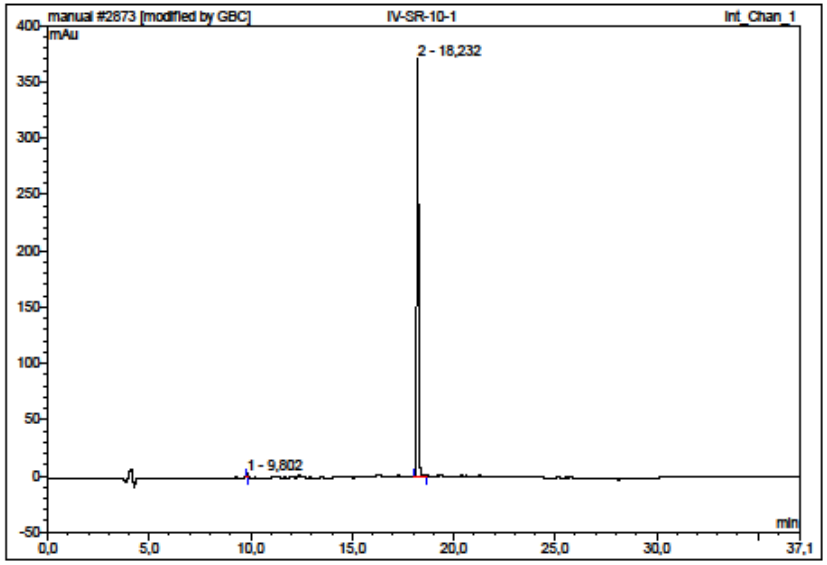

No.	Ret.Time min	Peak Name	Height mAu	Area mAu*min	Rel.Area %	Amount	Type
1	9,80	n.a.	2,965	0,240	0,63	n.a.	BMB*
2	18,23	n.a.	371,895	37,820	99,37	n.a.	BMB
Total:			374,860	38,060	100,00	0,000	

Figure S6. HPLC analysis of **6**.

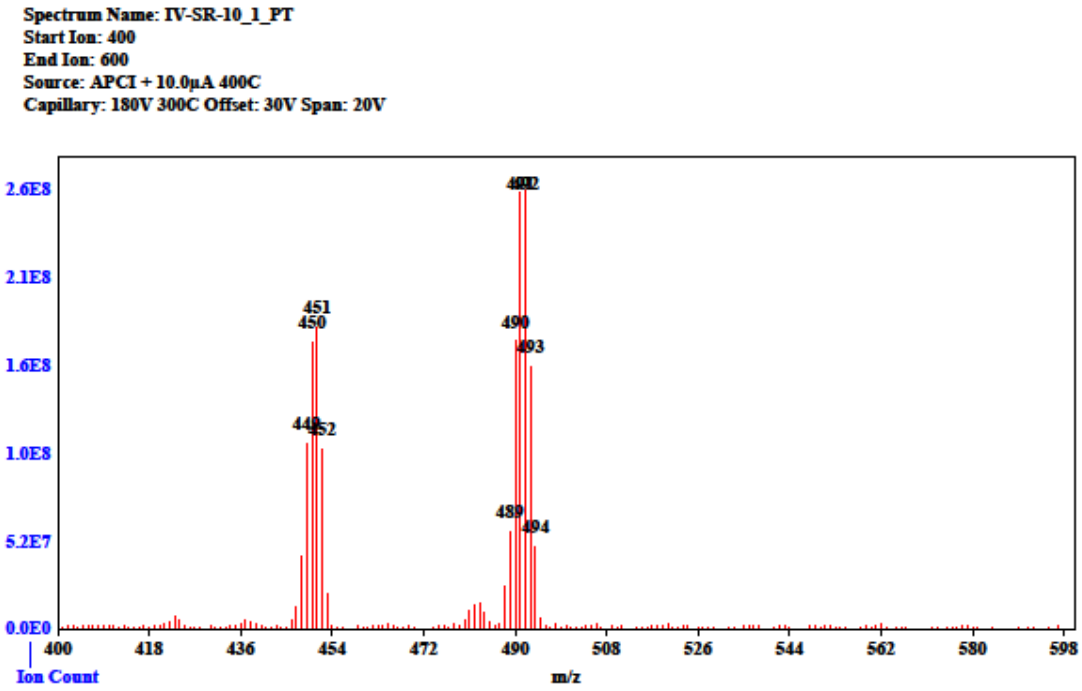

Figure S7. MS spectrum of **6**.

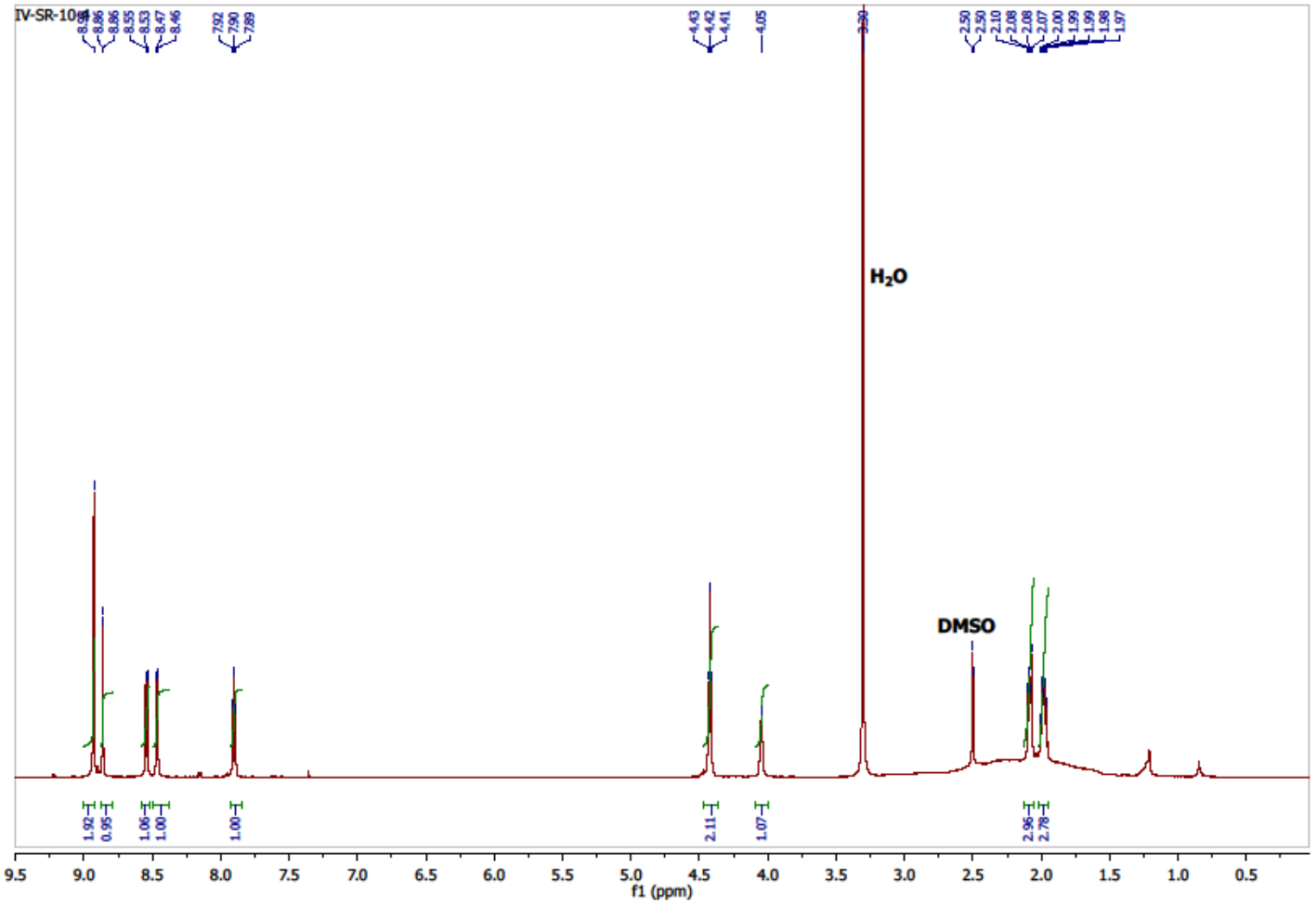

Figure S8. ^{1}H NMR spectrum of **7**.

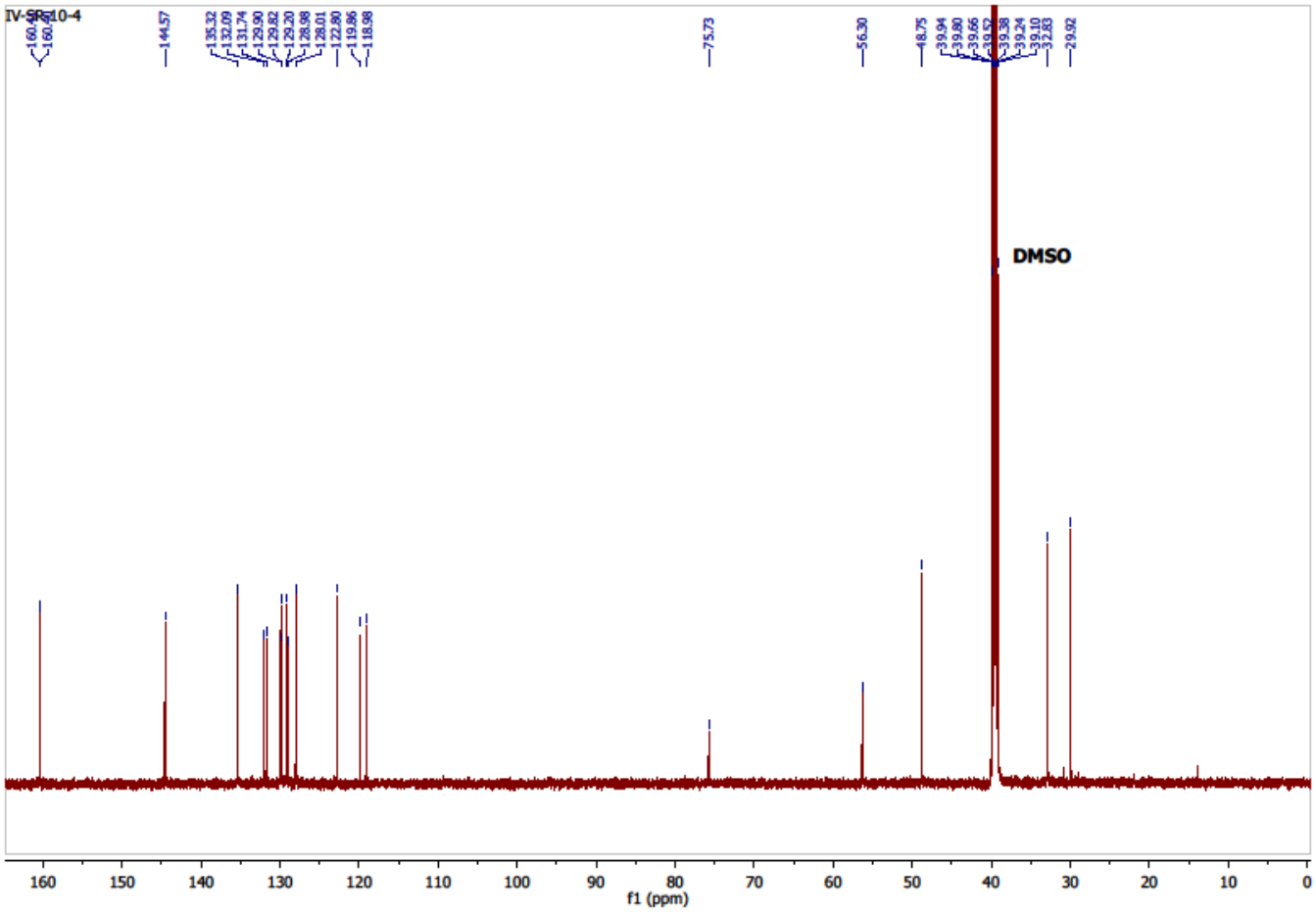

Figure S9. ^{13}C NMR spectrum of **7**.

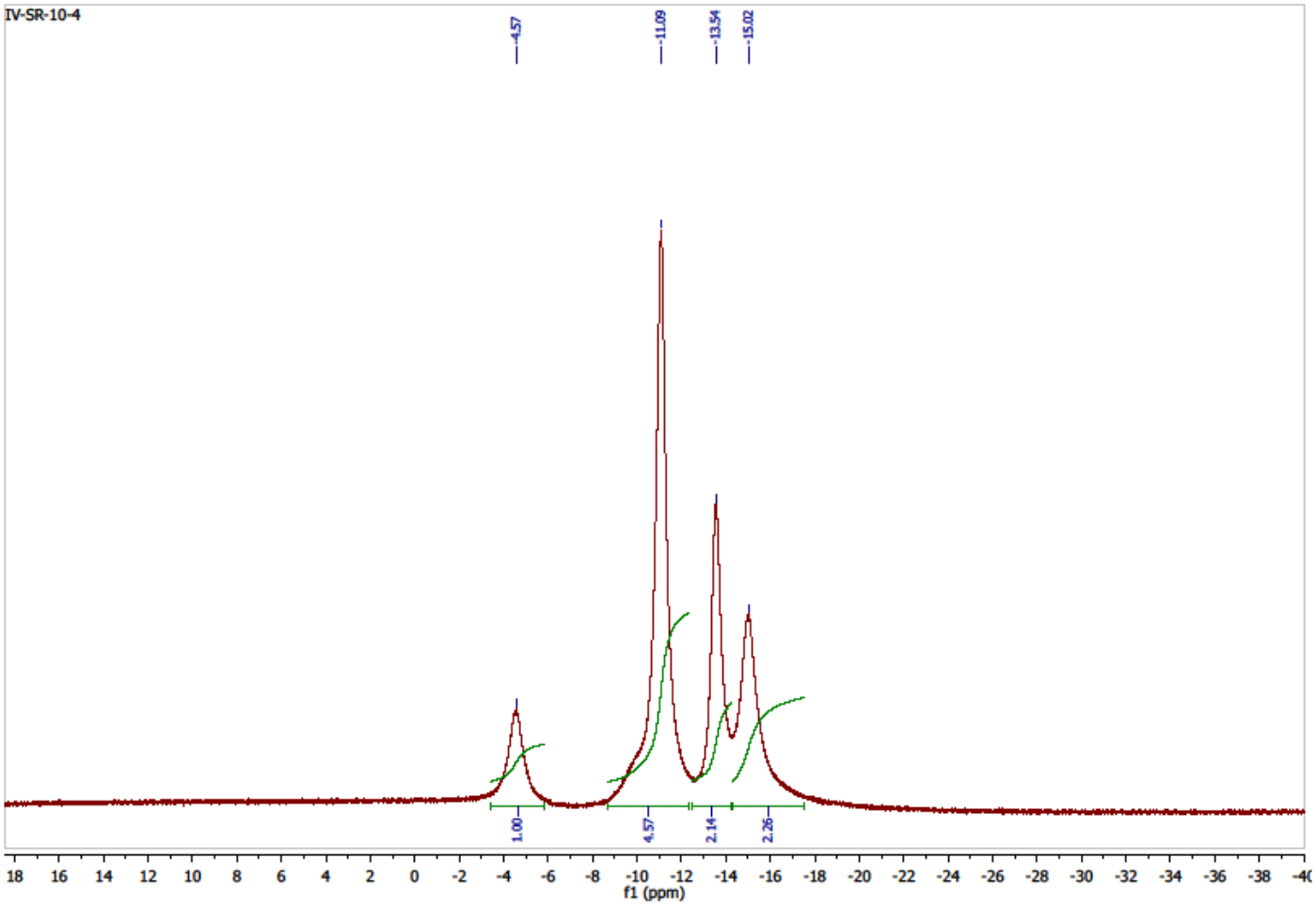

Figure S10. ^{11}B NMR {^{1}H BB} spectrum of **7**.

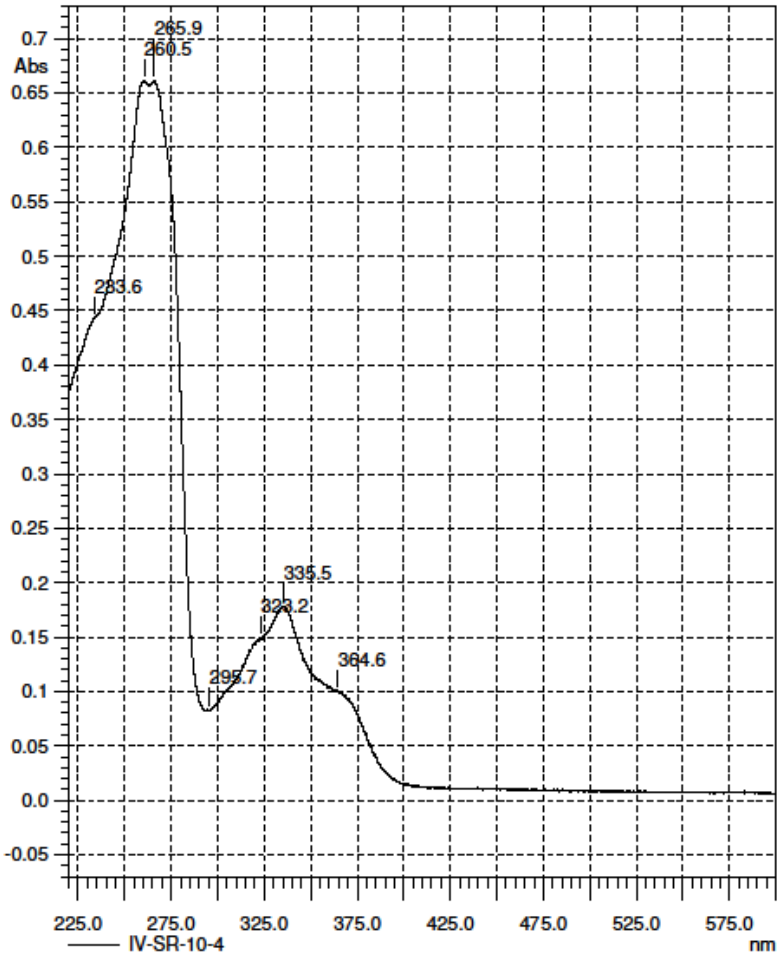

Figure S11. UV spectrum of **7**.

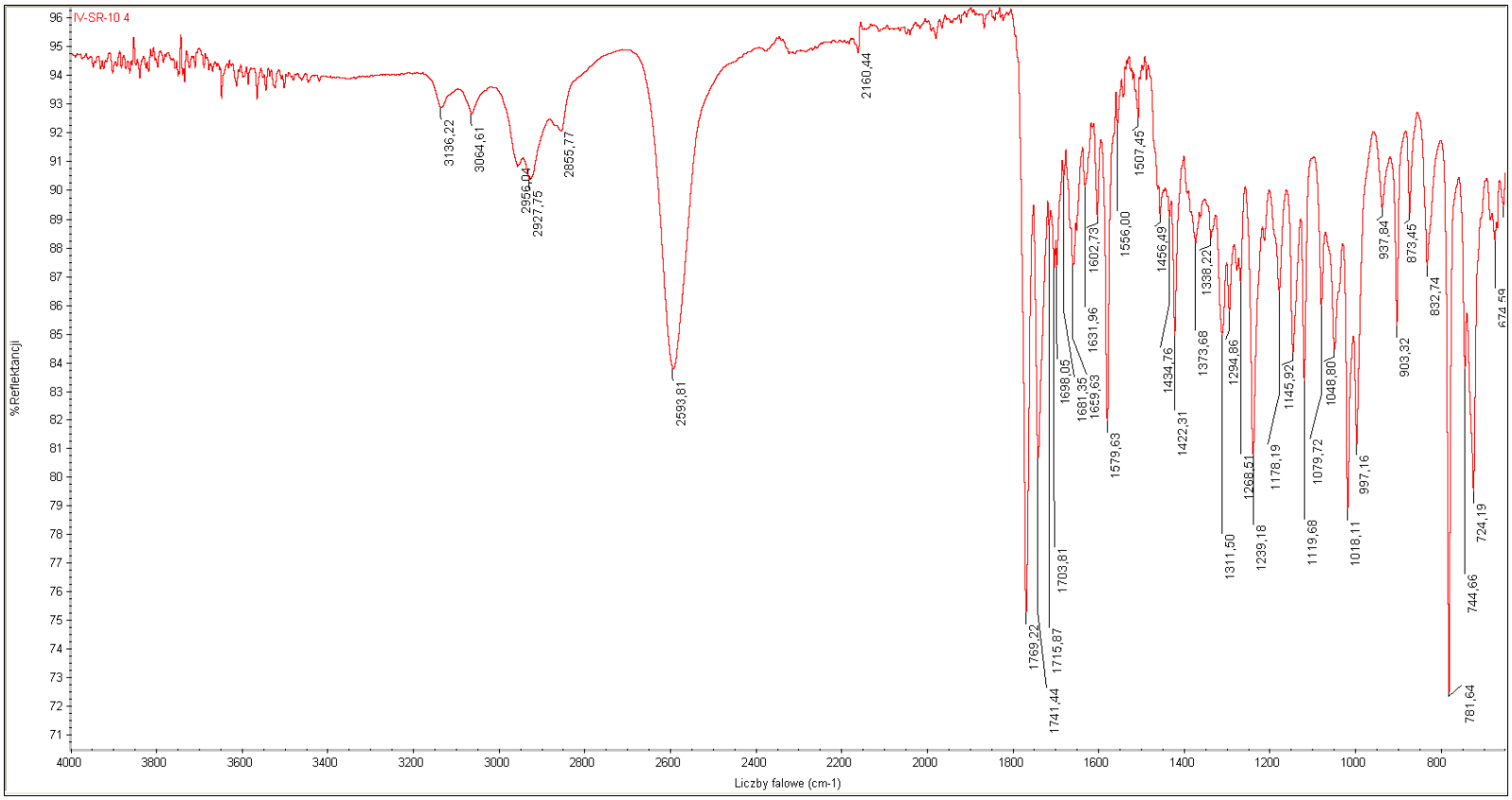

Figure S12. IR spectrum of **7**.

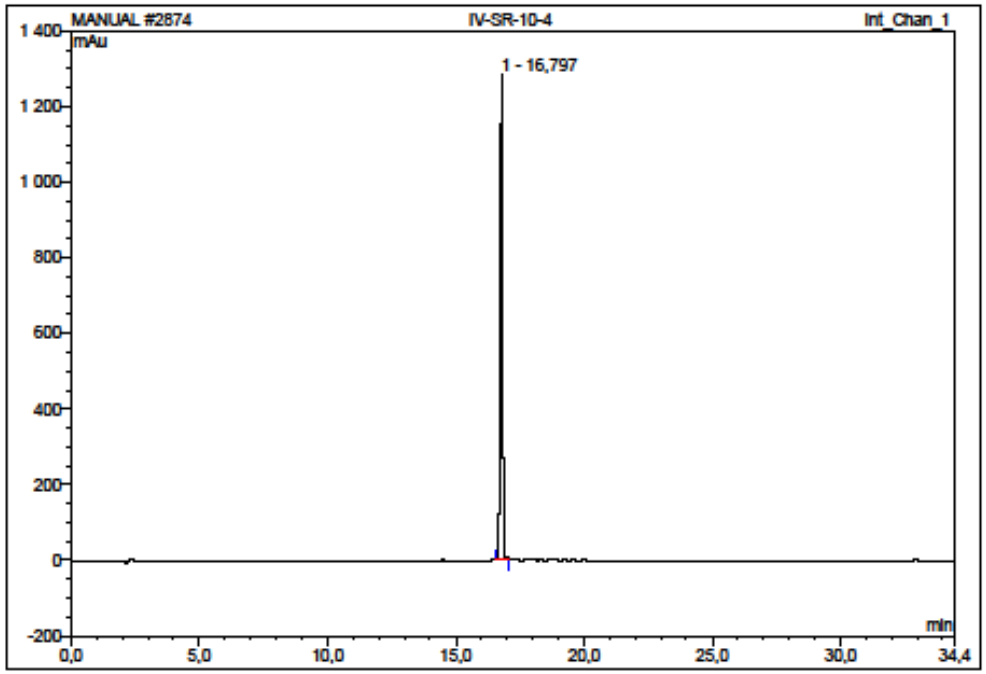

No.	Ret.Time min	Peak Name	Height mAu	Area mAu*min	Rel.Area %	Amount	Type
1	16,80	n.a.	1281,764	135,115	100,00	n.a.	BMB
Total:			1281,764	135,115	100,00	0,000	

Figure S13. HPLC analysis of **7**.

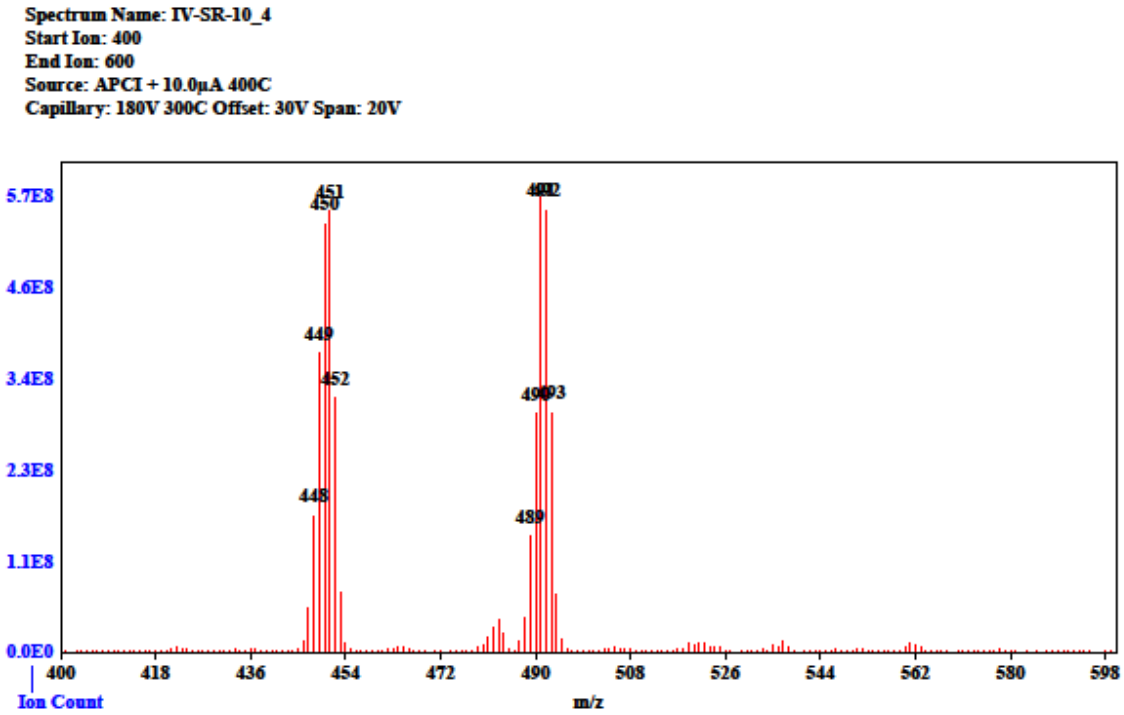

Figure S14. MS spectrum of **7**.

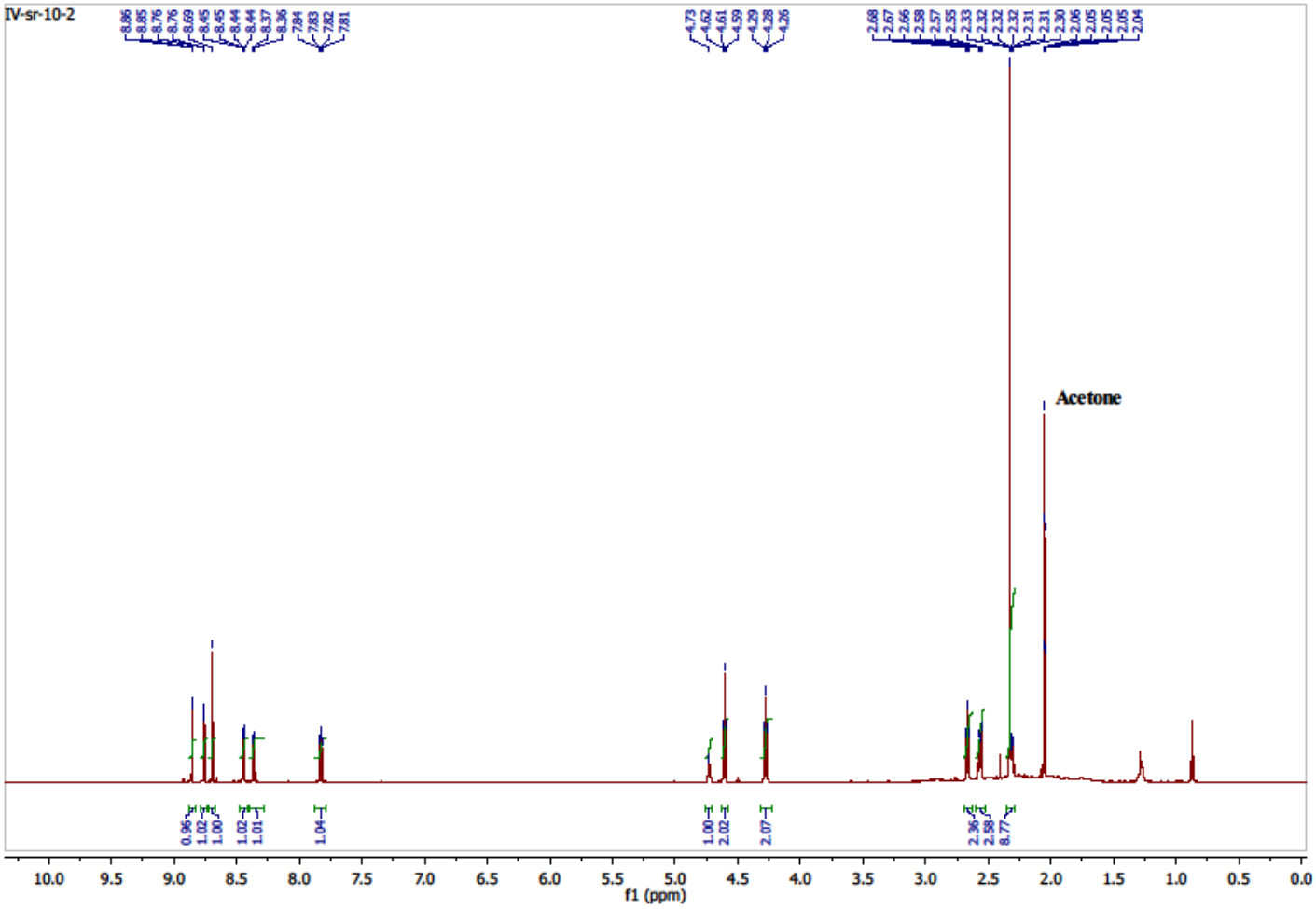

Figure S15. ^{1}H NMR spectrum of **8**.

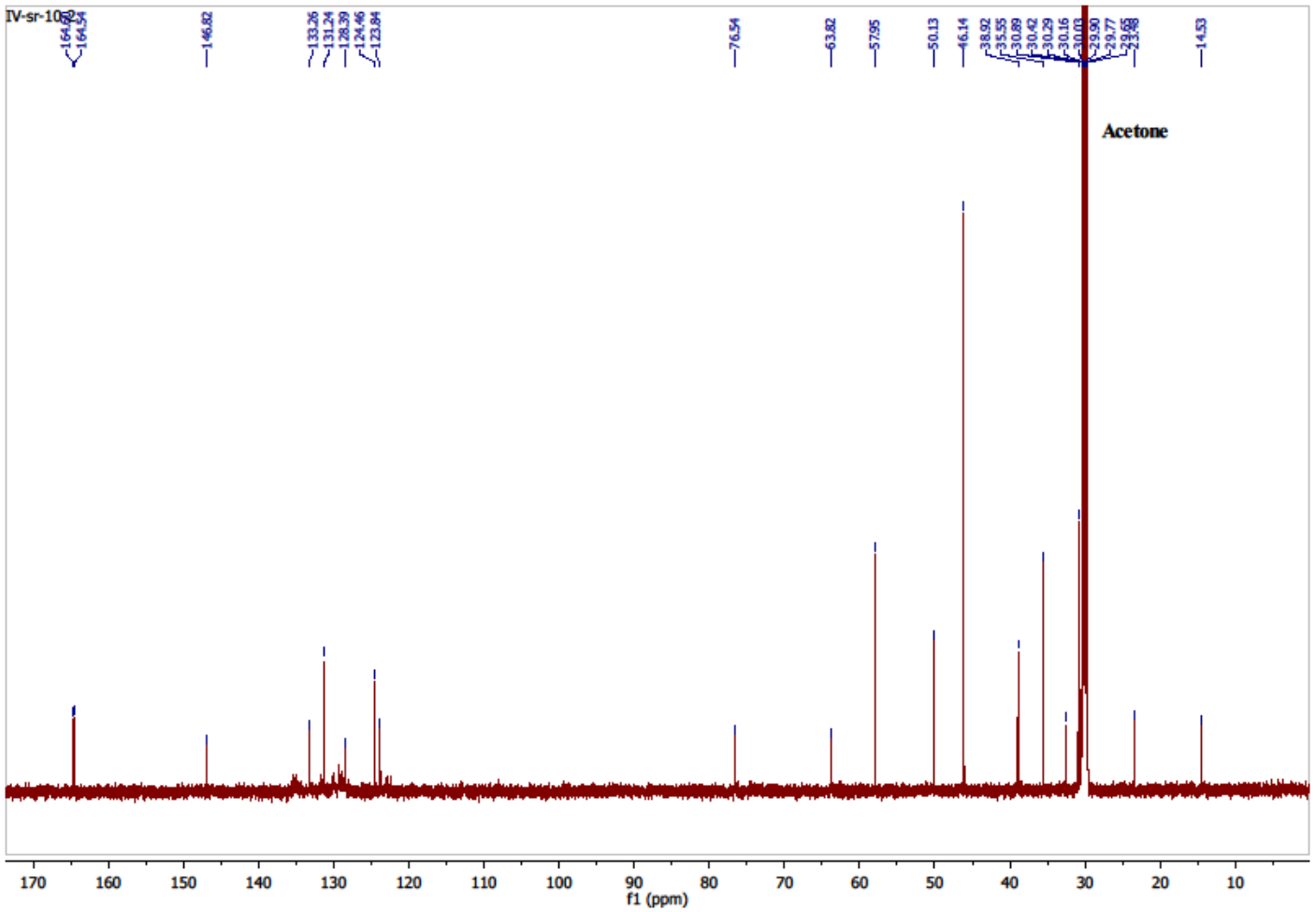

Figure S16. ^{13}C NMR spectrum of **8**.

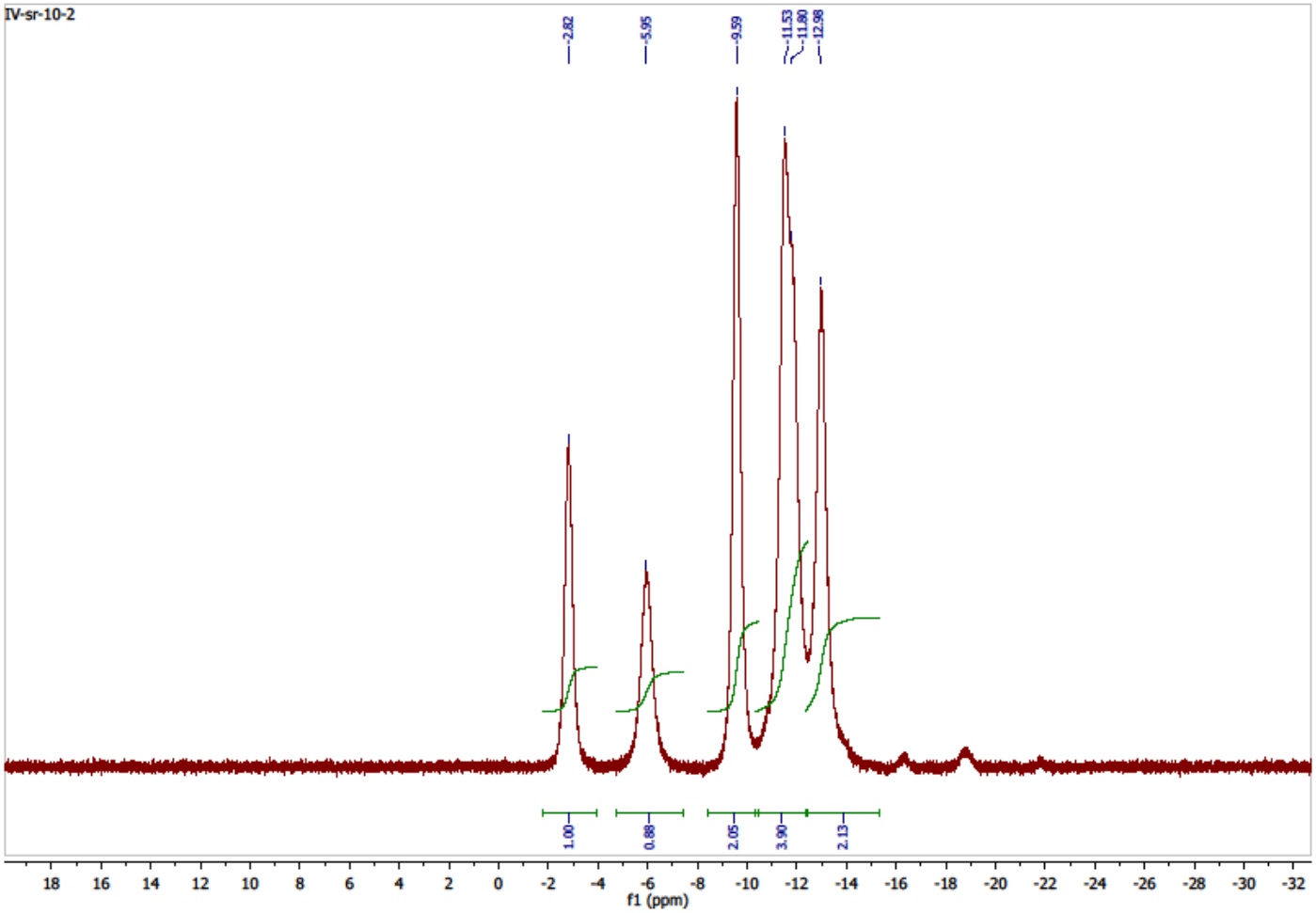

Figure S17. ^{11}B NMR {^{1}H BB} spectrum of **8**.

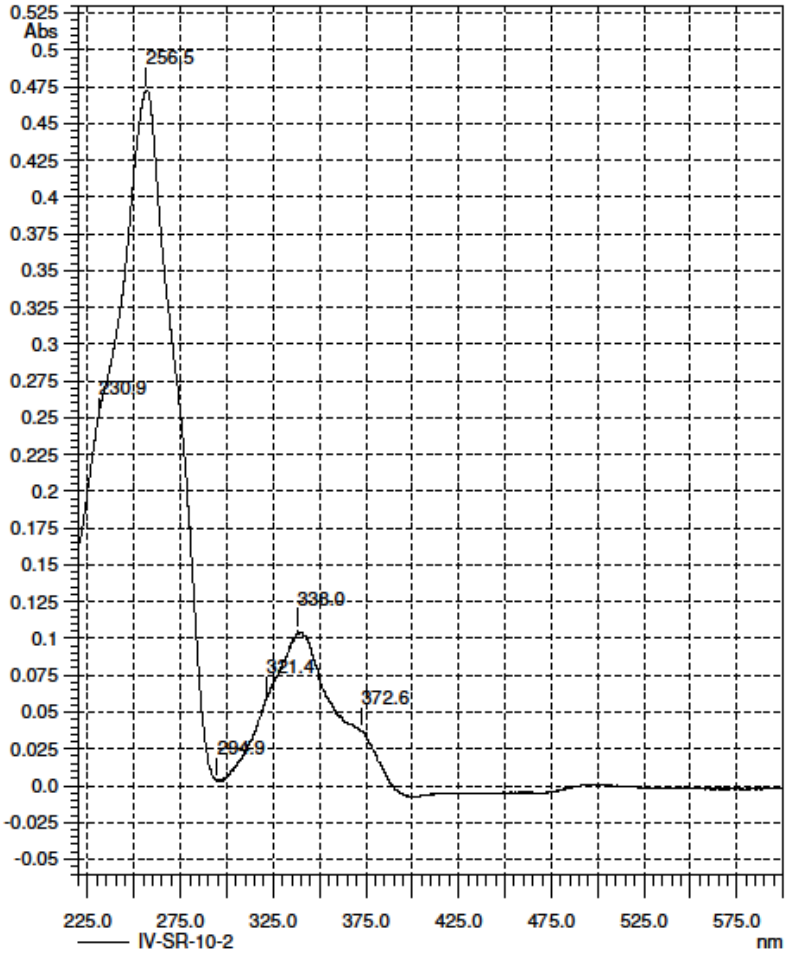

Figure S18. UV spectrum of **8**.

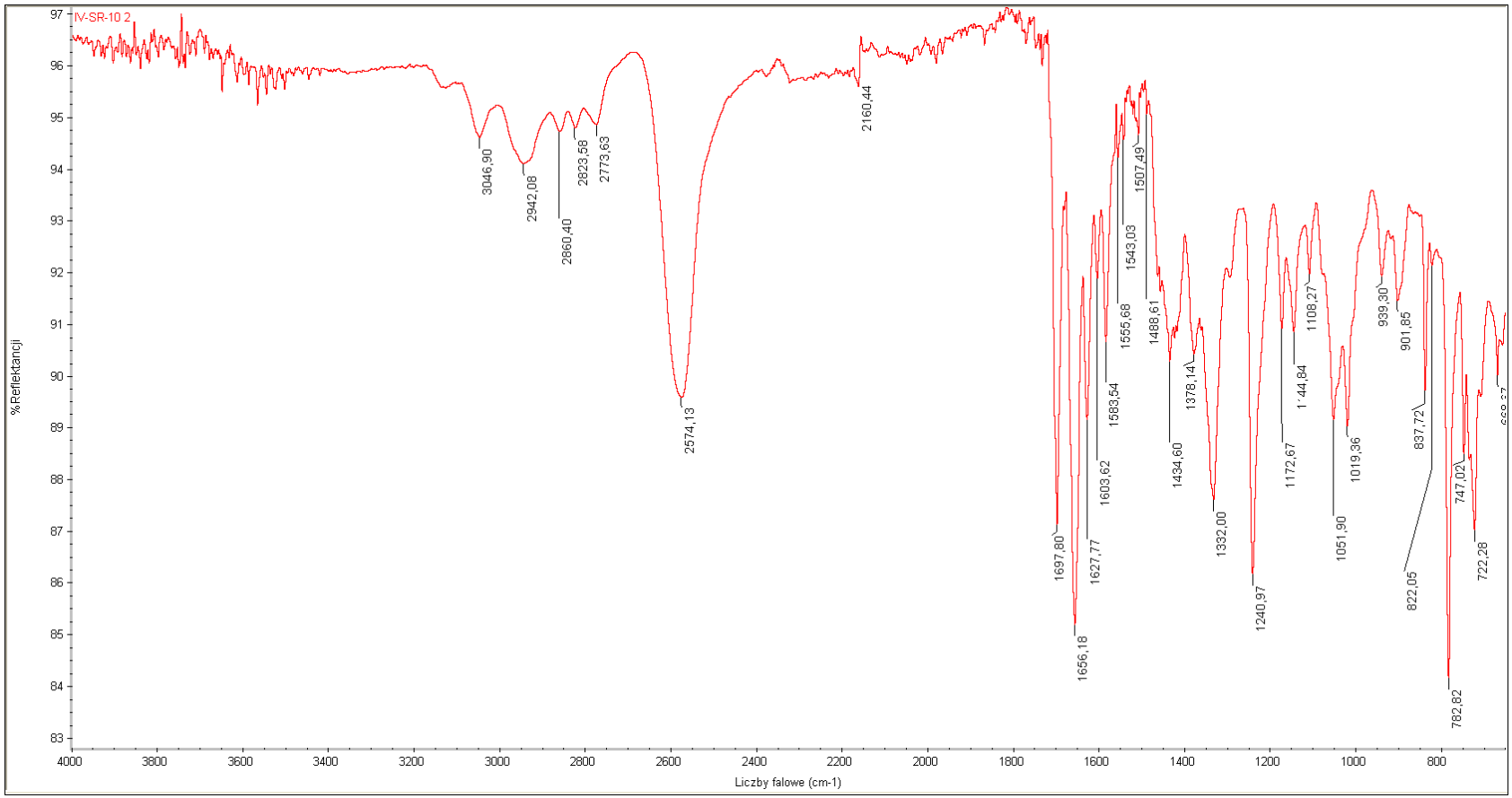

Figure S19. IR spectrum of **8**.

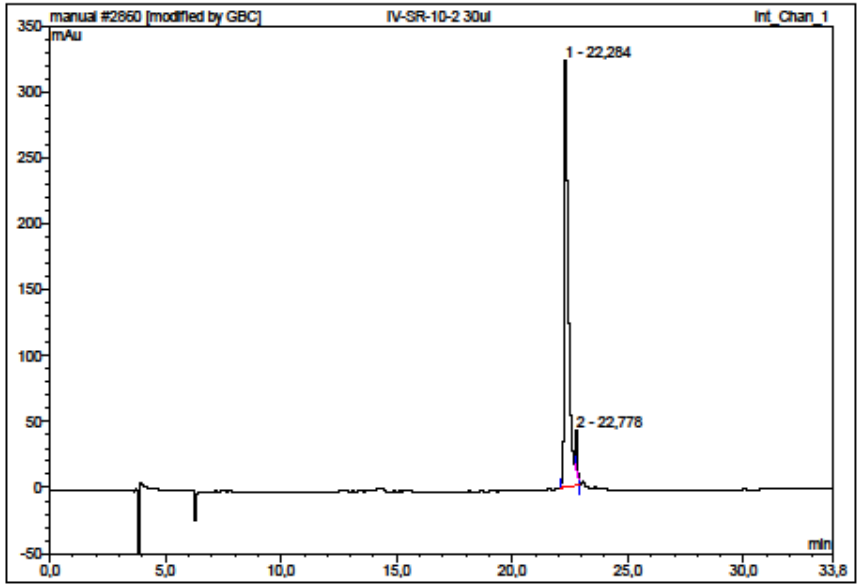

No.	Ret.Time min	Peak Name	Height mAu	Area mAu*min	Rel.Area %	Amount	Type
1	22,28	n.a.	324,260	69,327	96,50	n.a.	BMB*
2	22,78	n.a.	30,615	2,511	3,50	n.a.	Rd*
Total:			354,875	71,838	100,00	0,000	

Figure S20. HPLC analysis of **8**.

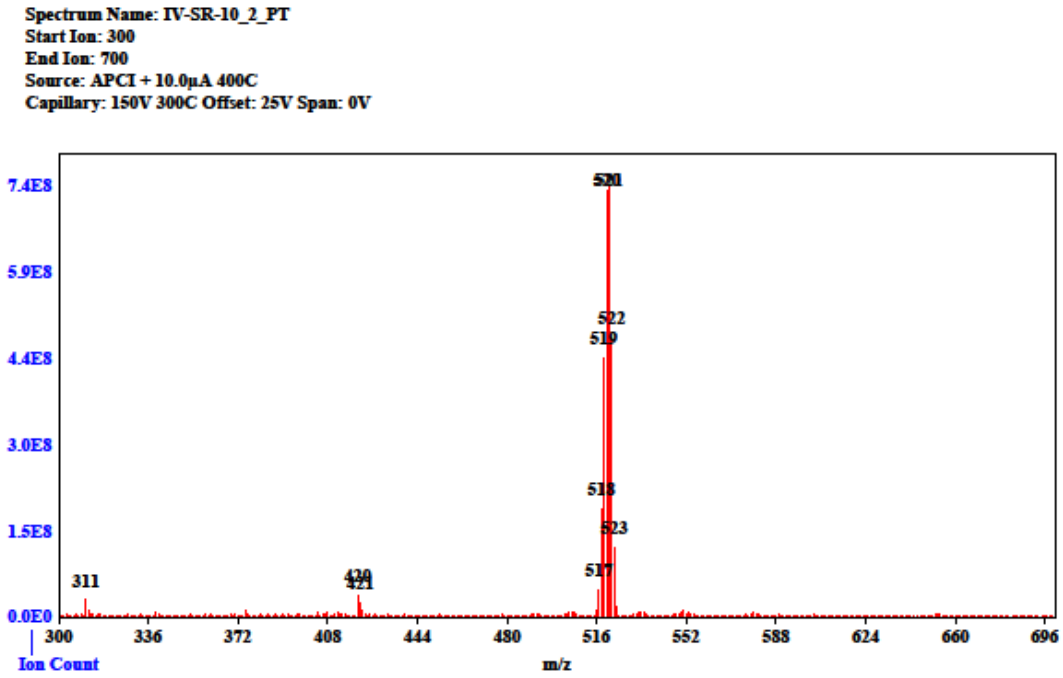

Figure S21. MS spectrum of **8**.

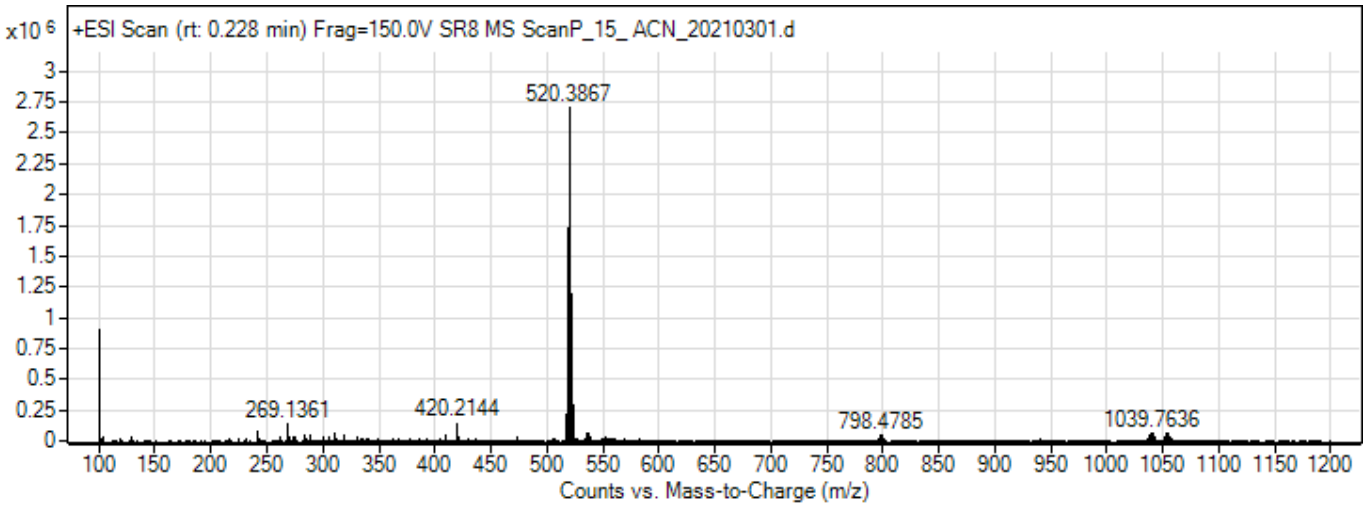

Figure S22. HRMS spectrum of **8**.

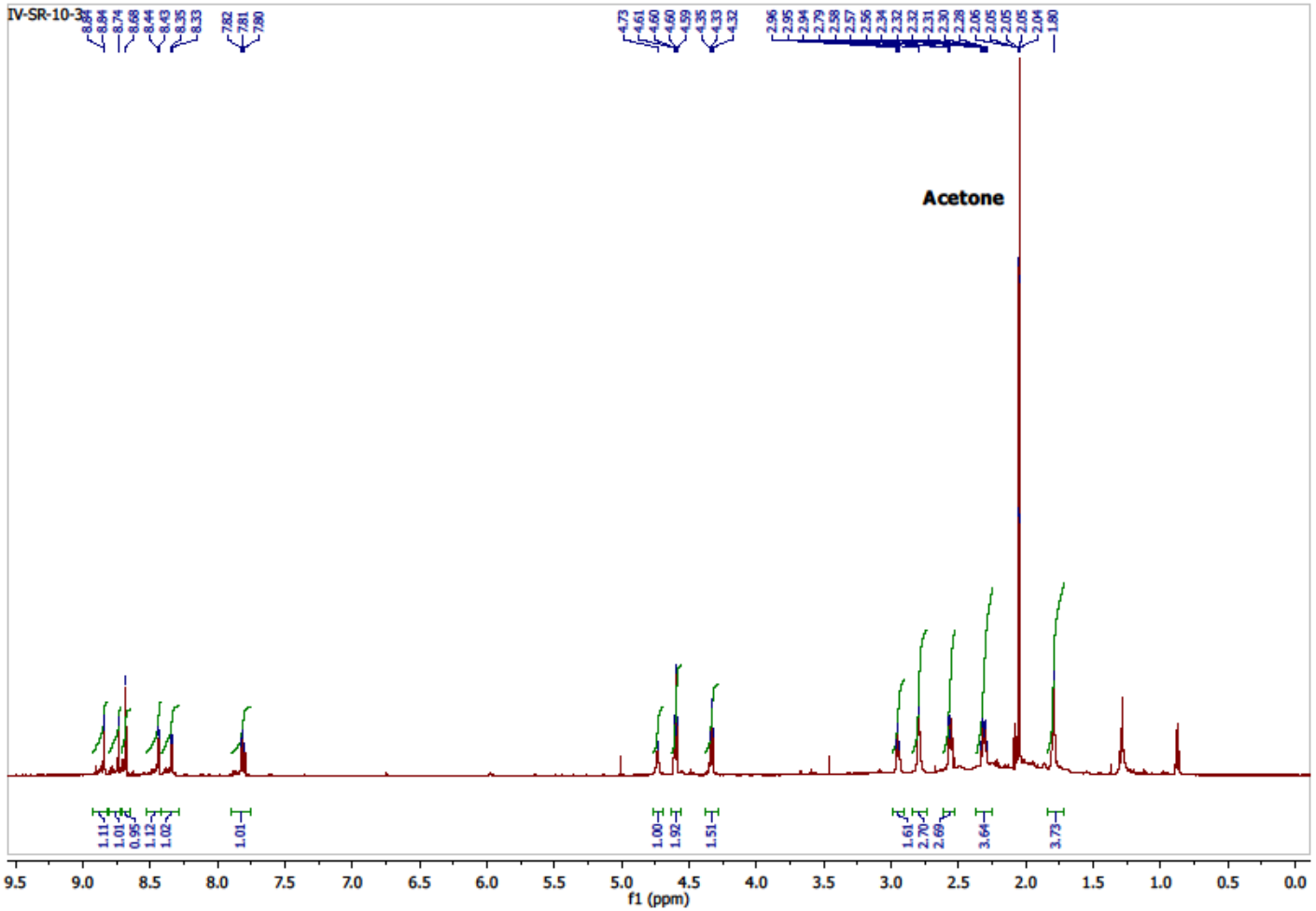

Figure S23. ^{1}H NMR spectrum of **9**.

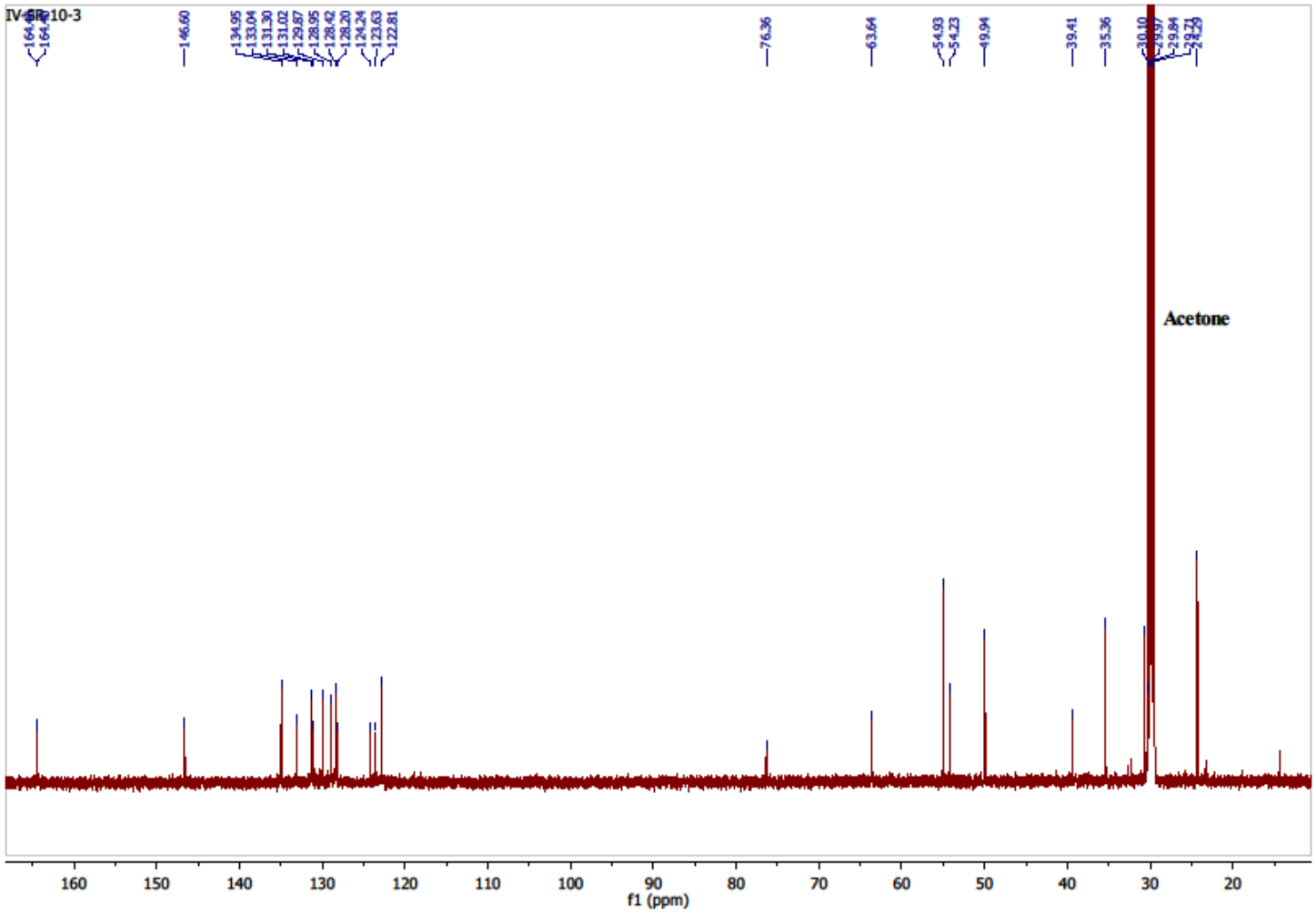

Figure S24. ^{13}C NMR spectrum of **9**.

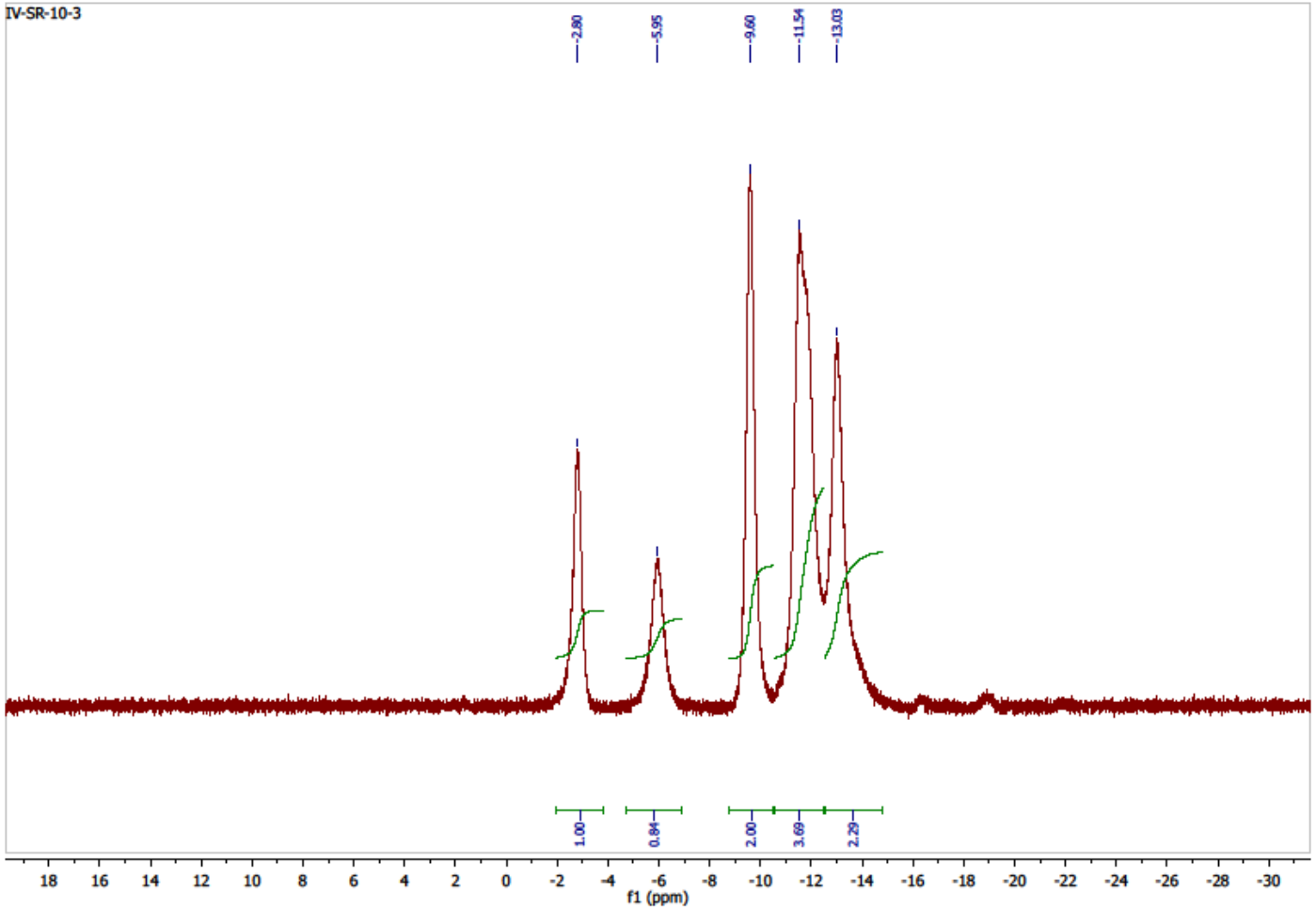

Figure S25. ^{11}B NMR {^{1}H BB} spectrum of **9**.

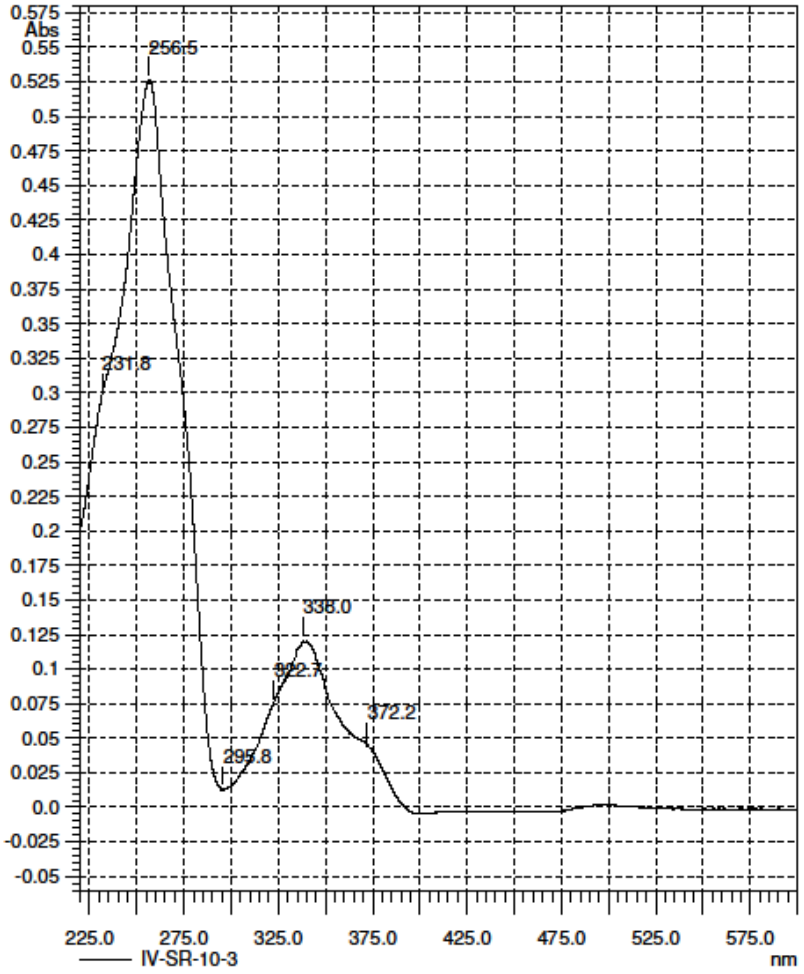

Figure S26. UV spectrum of **9**.

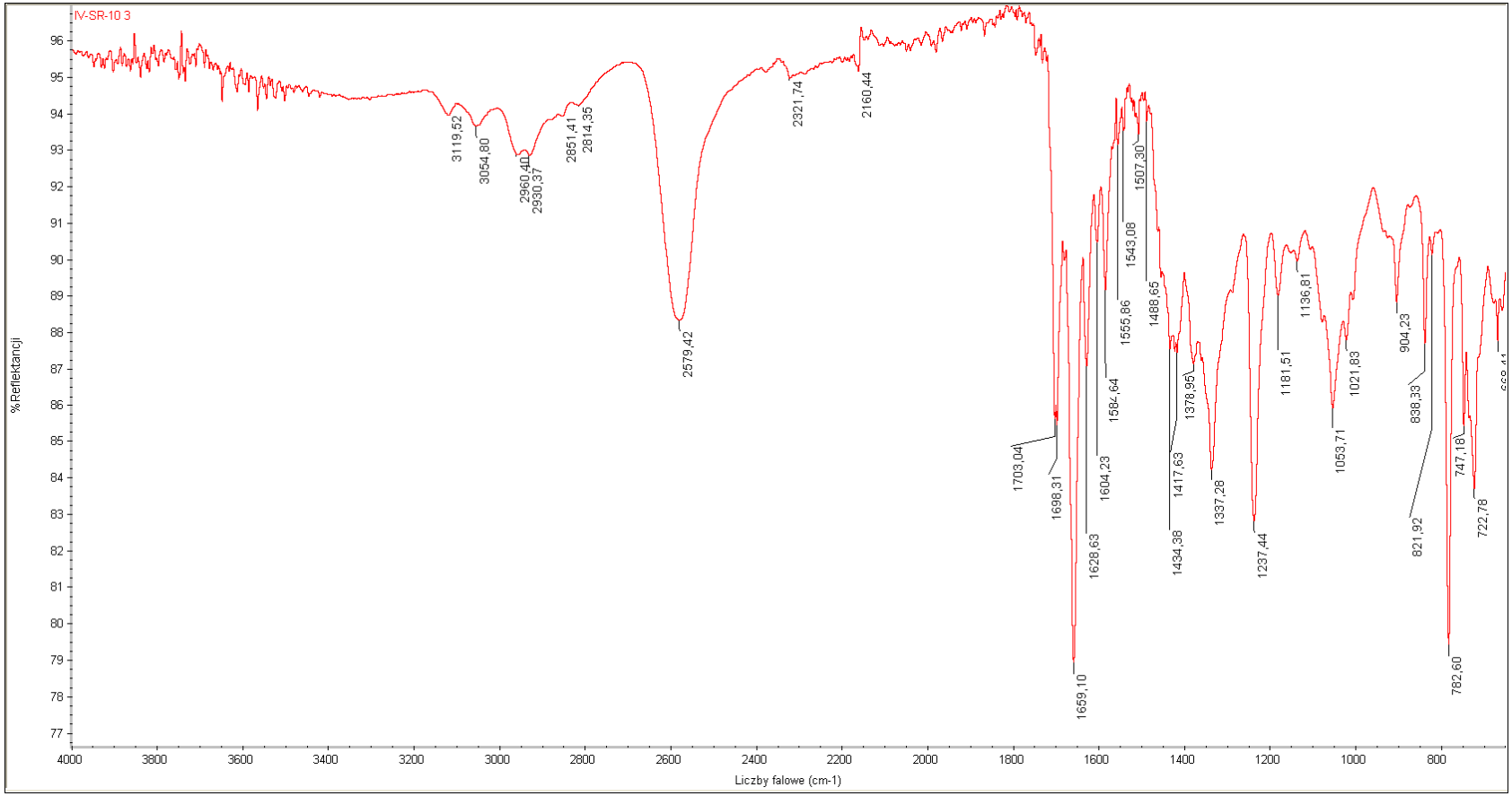

Figure S27. IR spectrum of **9**.

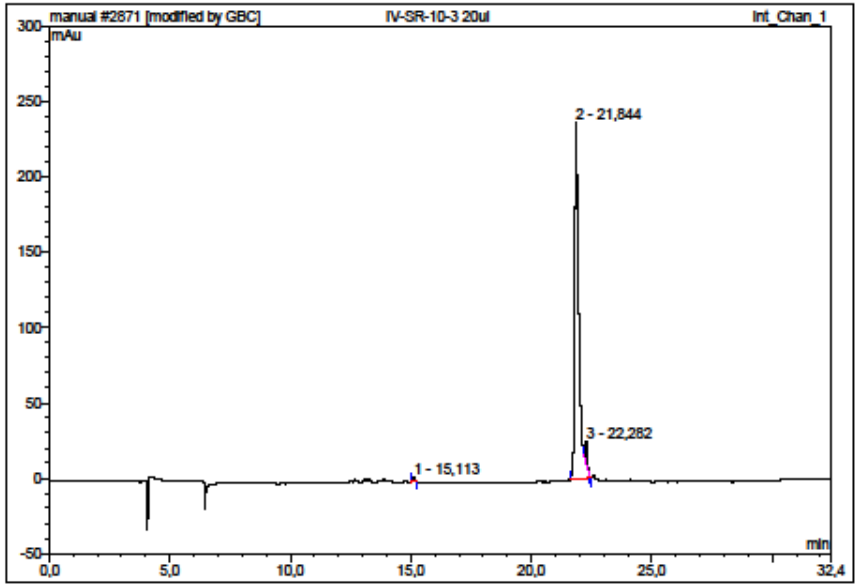

No.	Ret.Time min	Peak Name	Height mAu	Area mAu*min	Rel.Area %	Amount	Type
1	15,11	n.a.	3,035	0,348	0,72	n.a.	BMB*
2	21,84	n.a.	236,872	46,733	96,65	n.a.	BMB*
3	22,28	n.a.	15,135	1,272	2,63	n.a.	Rd*
Total:			255,042	48,353	100,00	0,000	

Figure S28. HPLC analysis of **9**.

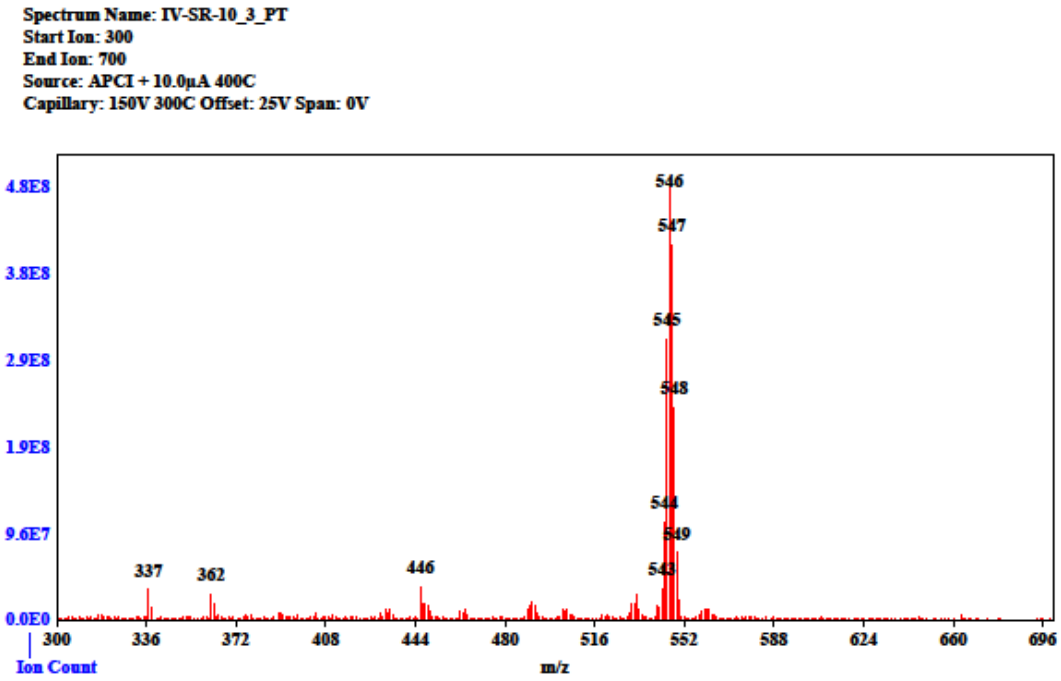

Figure S29. MS spectrum of **9**.

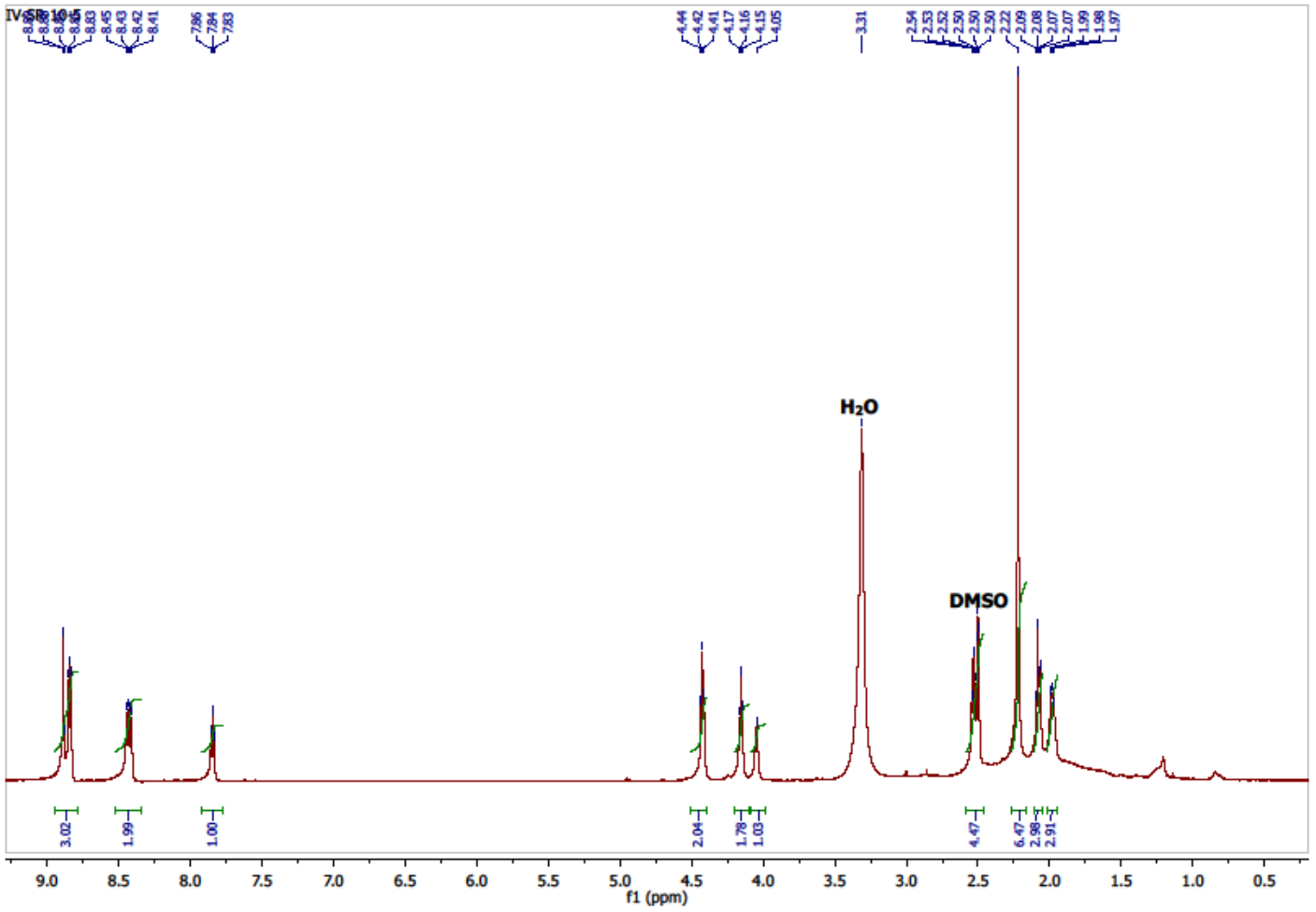

Figure S30. ^{1}H NMR spectrum of **10**.

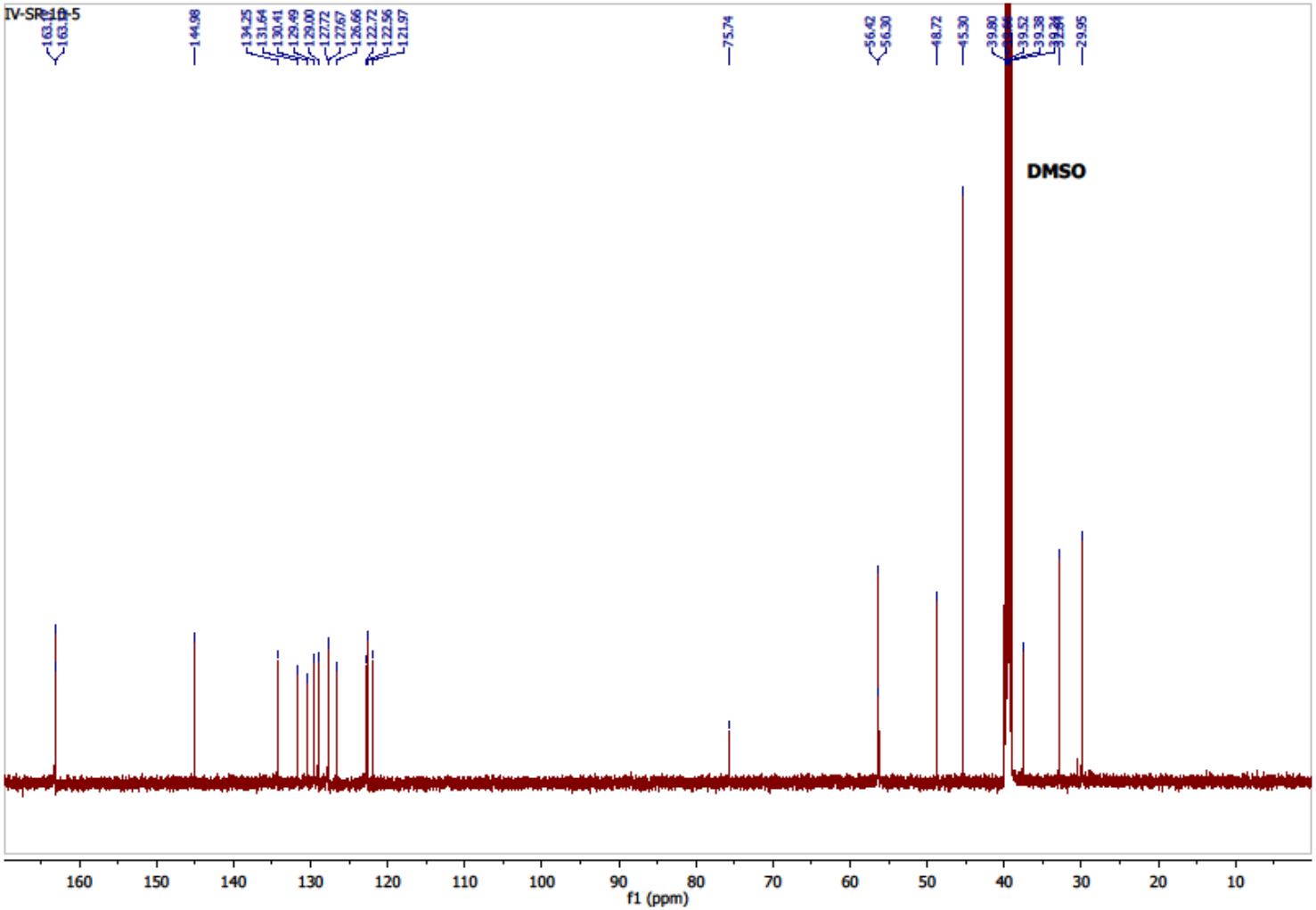

Figure S31. ^{13}C NMR spectrum of **10**.

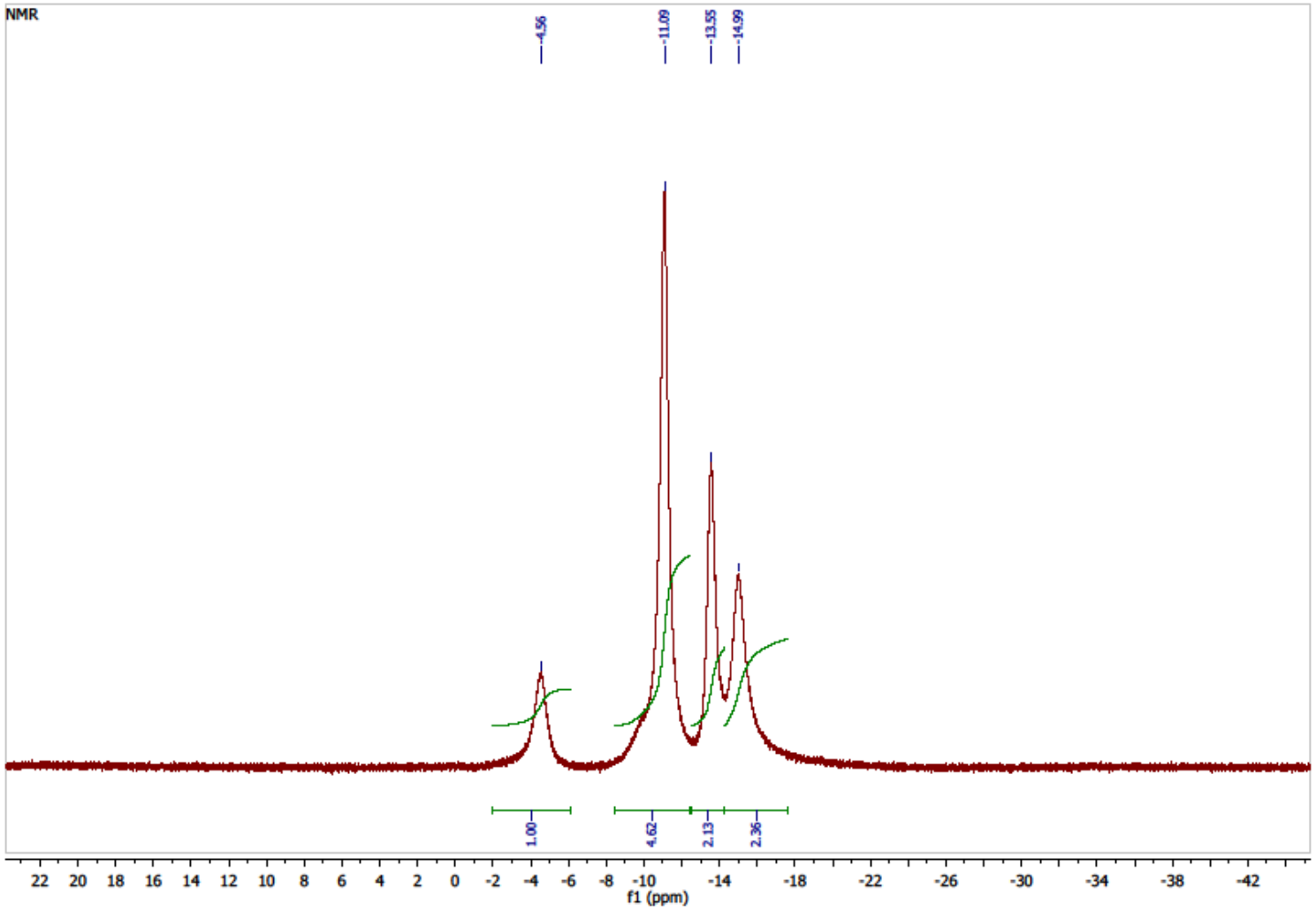

Figure S32. ^{11}B NMR $\{^{1}H$ BB$\}$ spectrum of **10**.

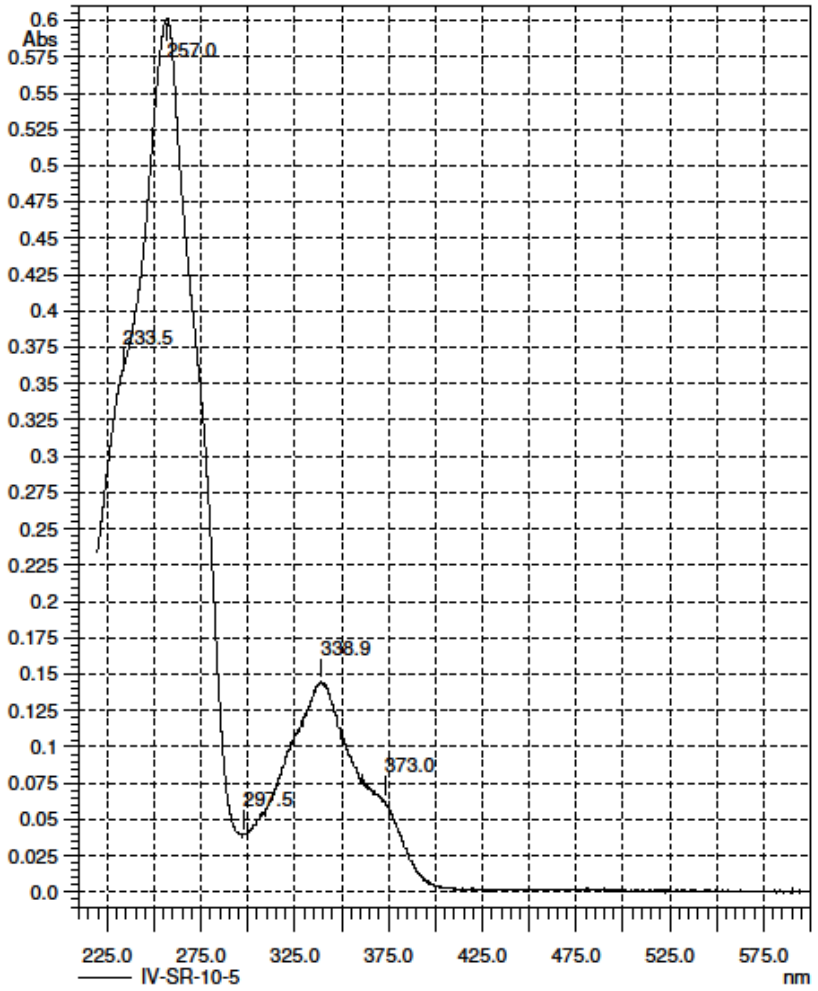

Figure S33. UV spectrum of **10**.

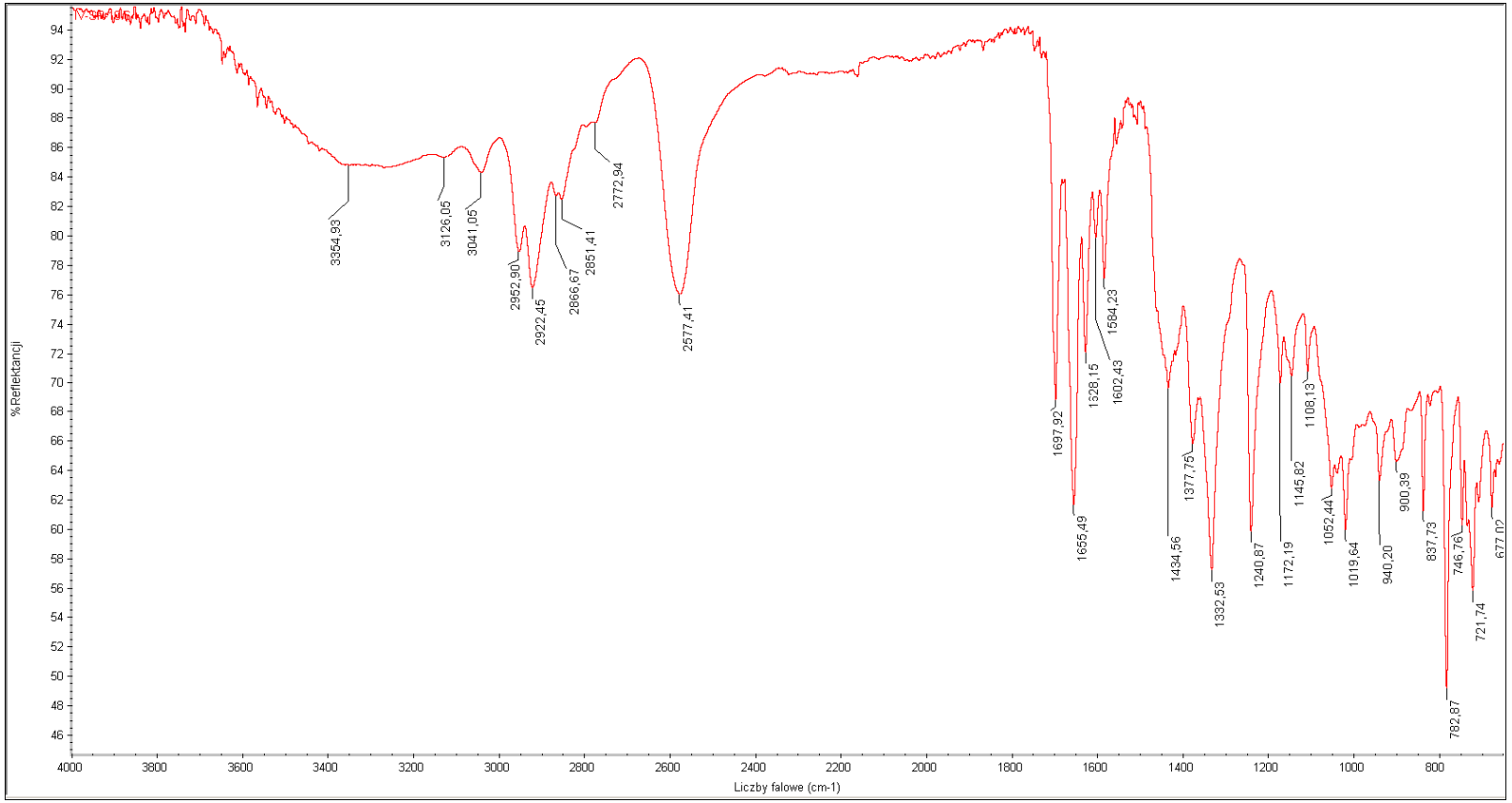

Figure S34. IR spectrum of **10**.

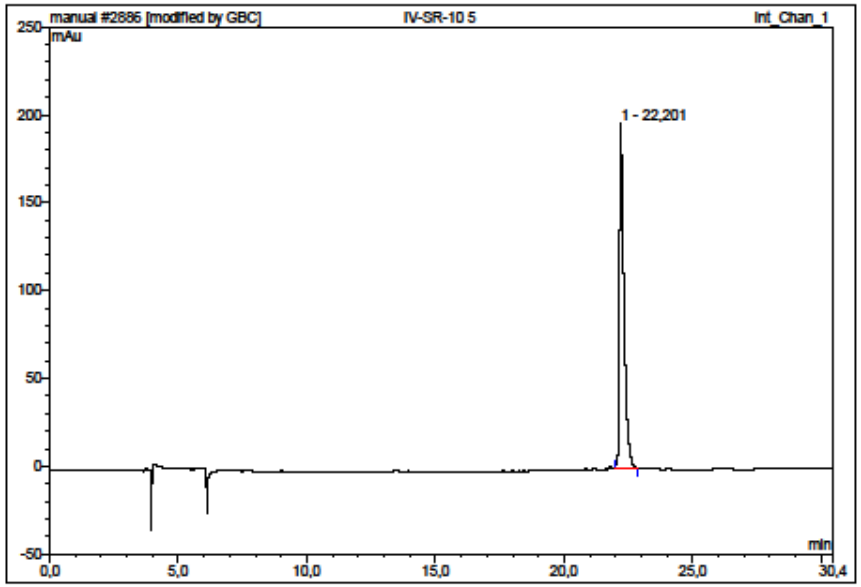

No.	Ret.Time min	Peak Name	Height mAu	Area mAu*min	Rel.Area %	Amount	Type
1	22,20	n.a.	196,209	39,594	100,00	n.a.	BMB
Total:			196,209	39,594	100,00	0,000	

Figure S35. HPLC analysis of **10**.

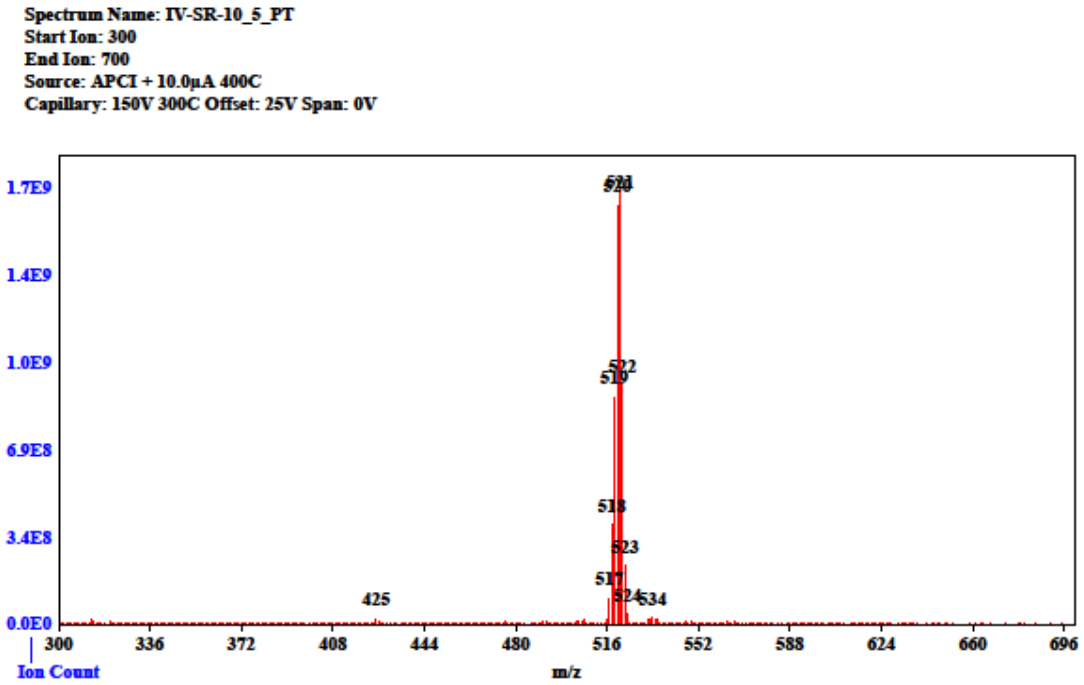

Figure S36. MS spectrum of **10**.

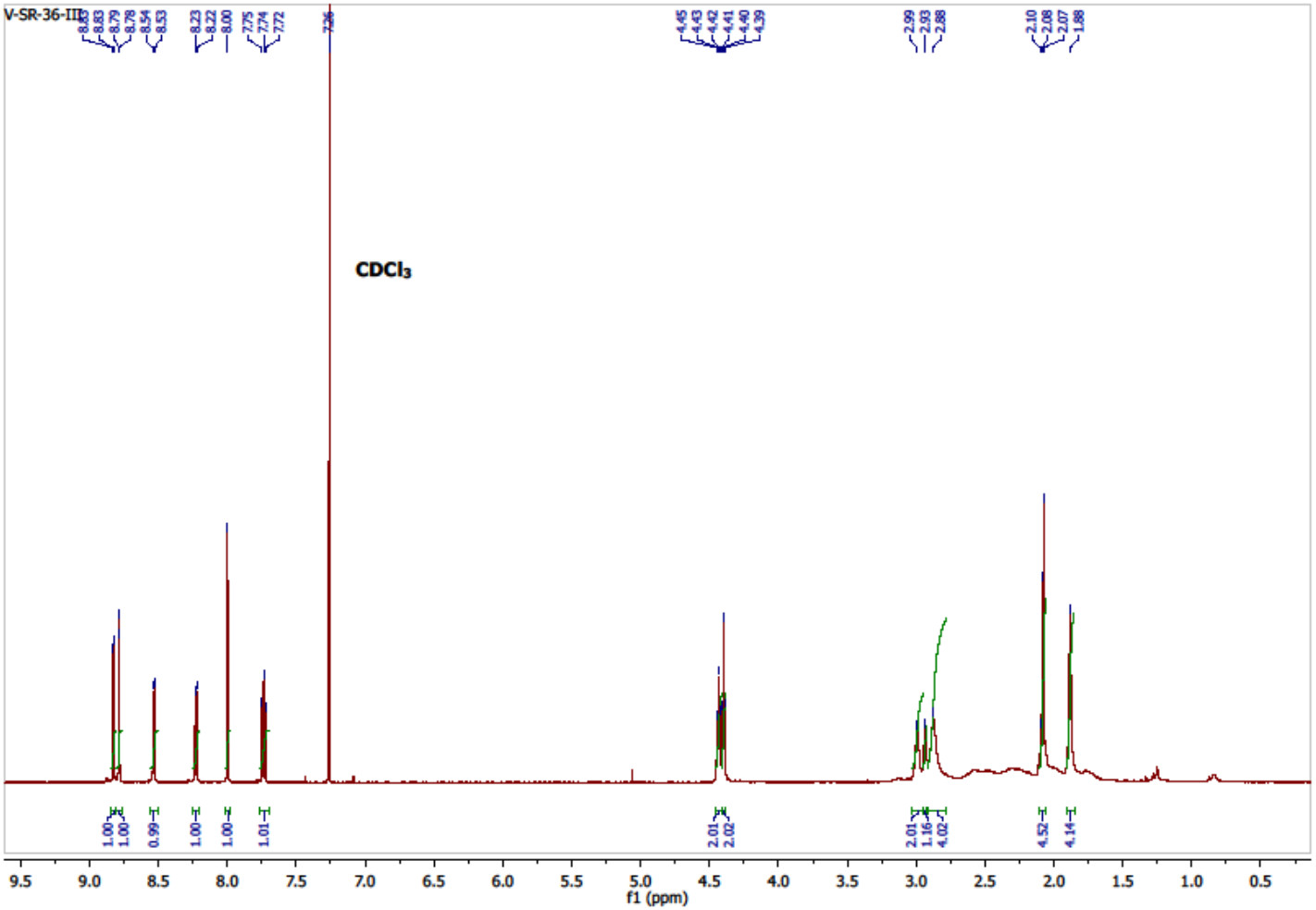

Figure S37. ^{1}H NMR spectrum of **11**.

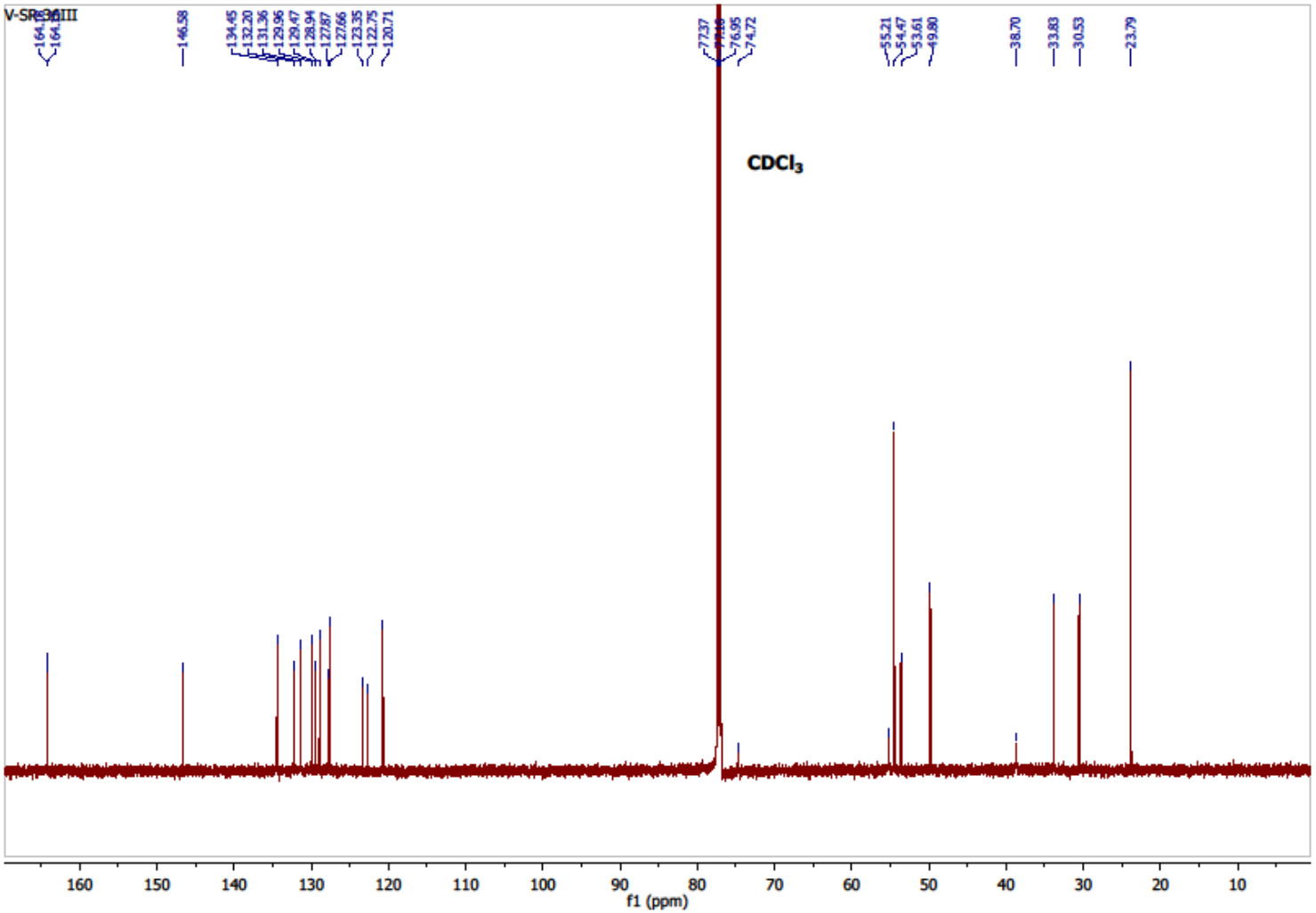

Figure S38. ^{13}C NMR spectrum of **11**.

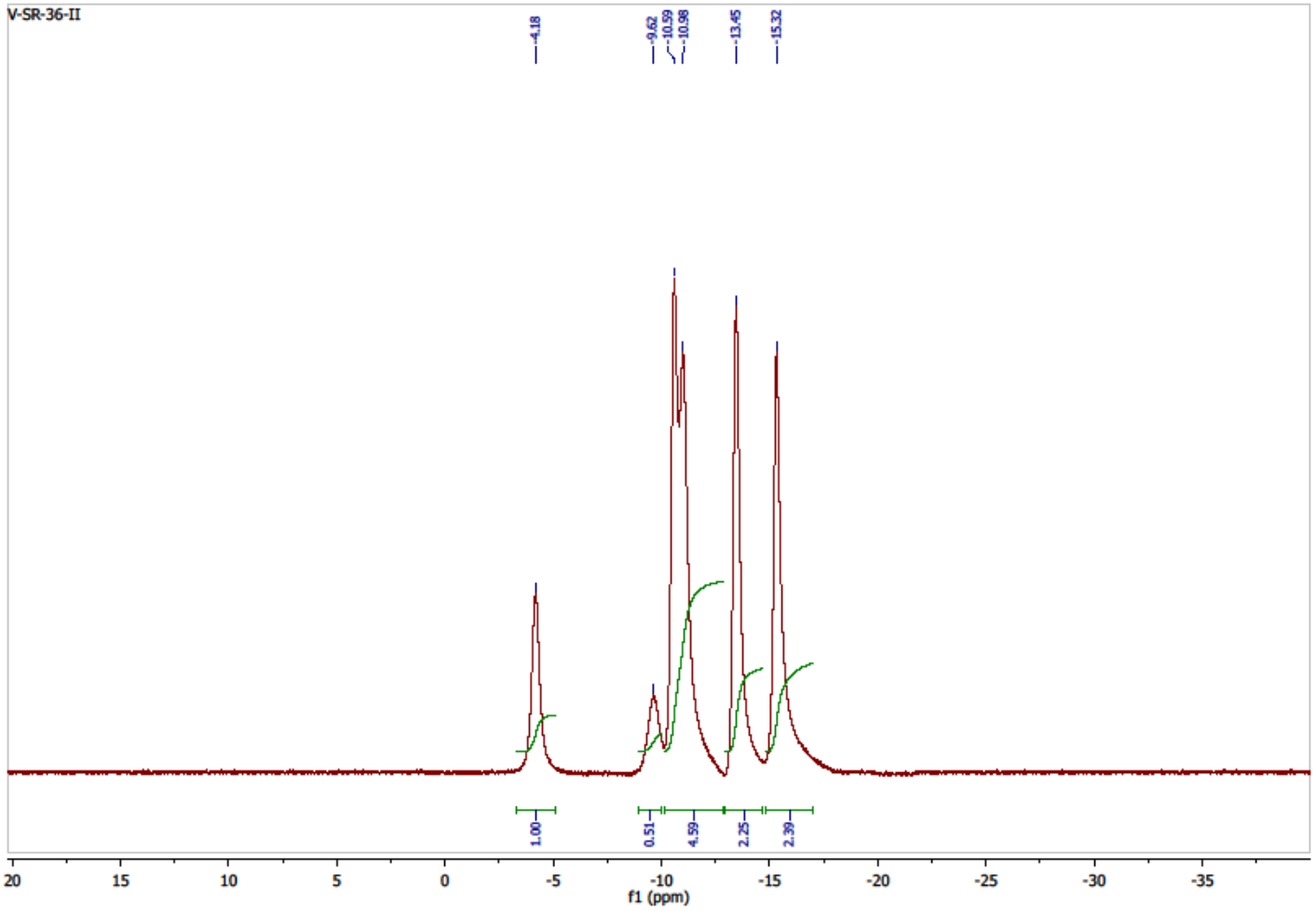

Figure S39. ^{11}B NMR {^{1}H BB} spectrum of **11**.

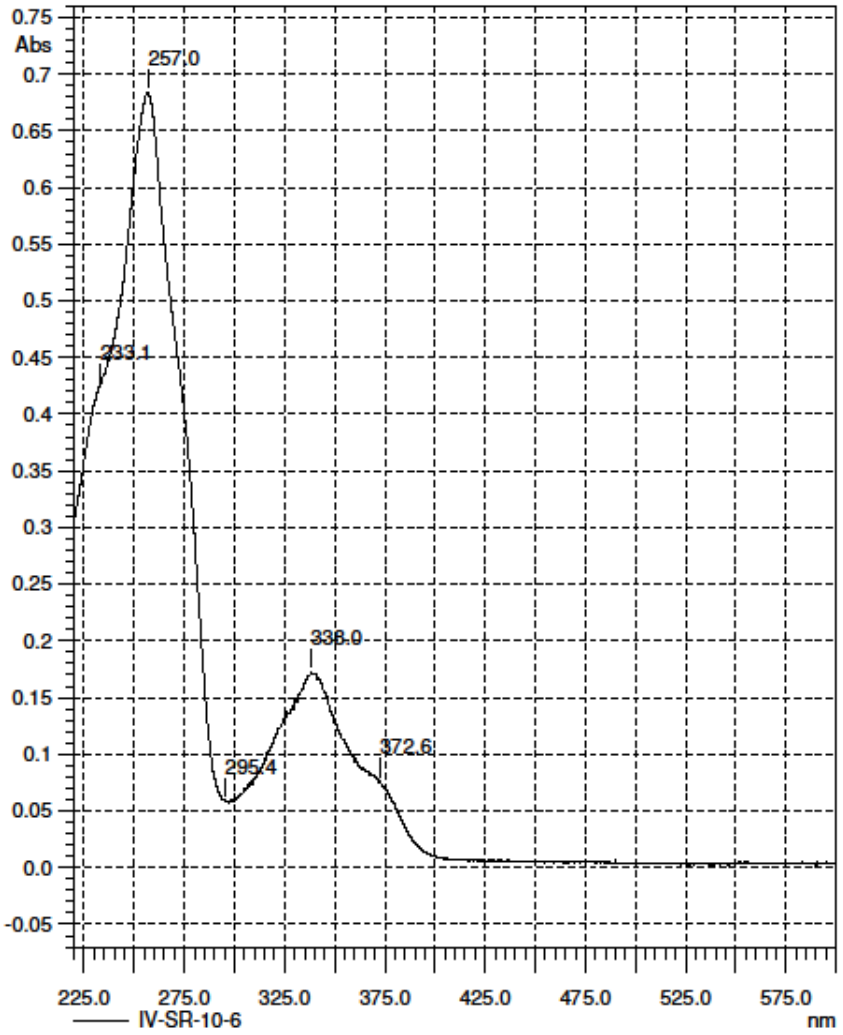

Figure S40. UV spectrum of **11**.

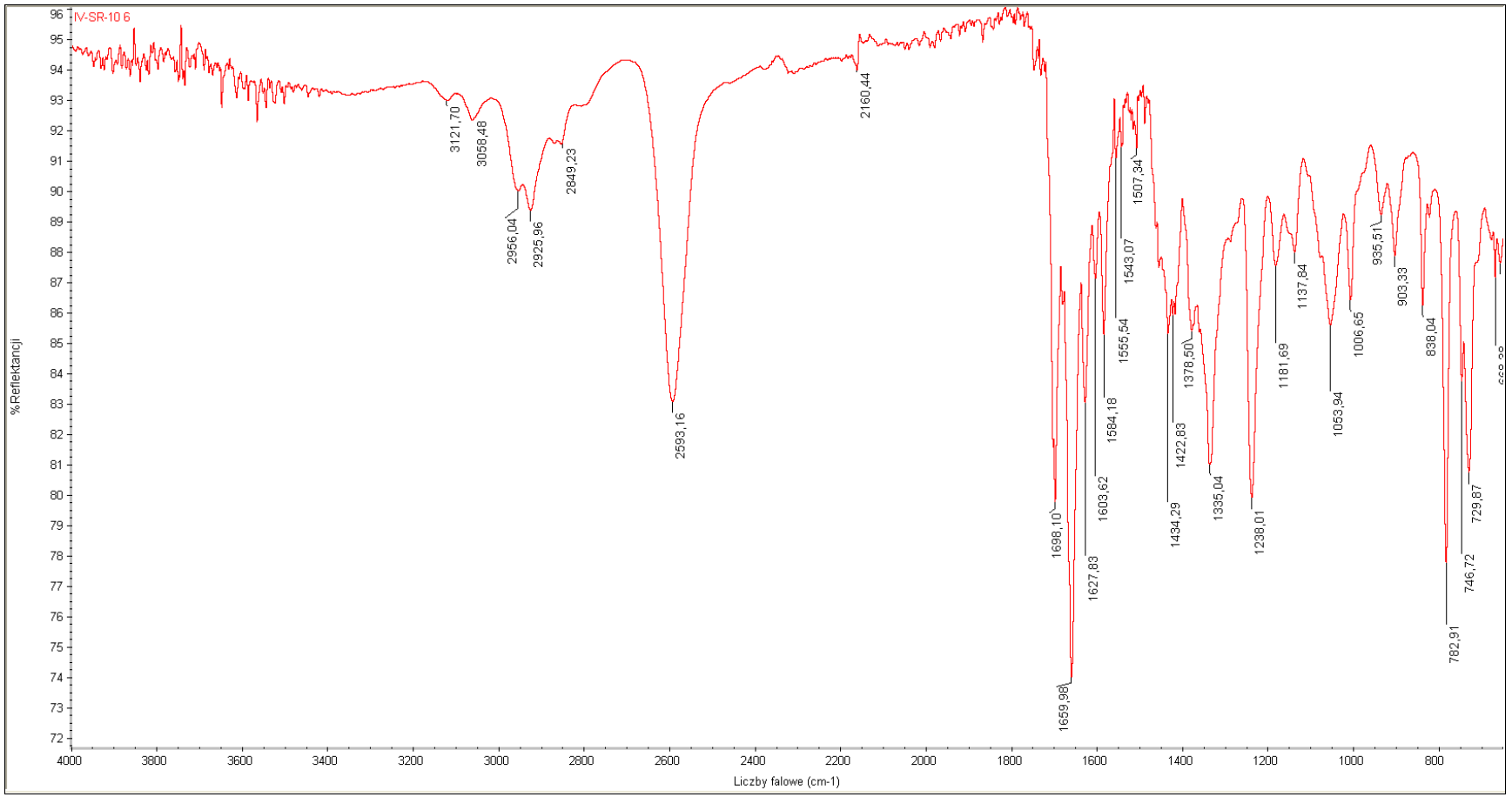

Figure S41. IR spectrum of **11**.

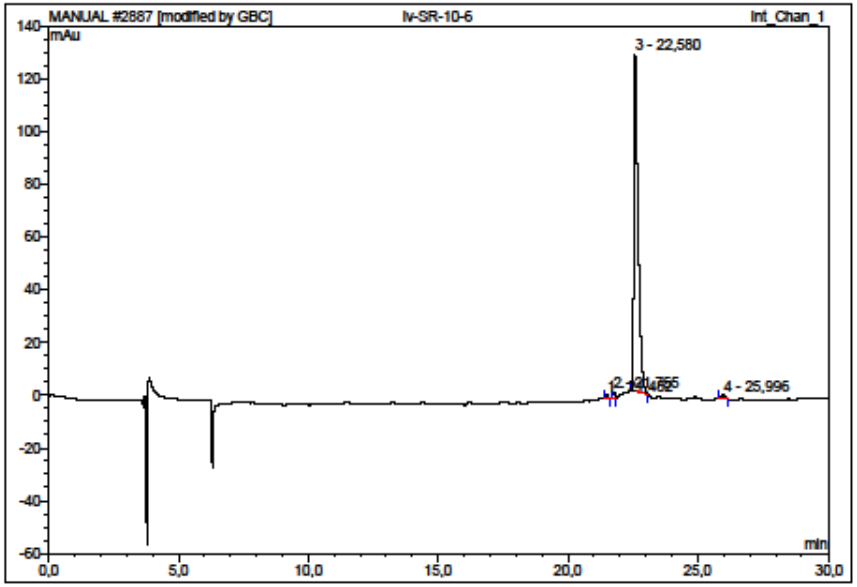

No.	Ret.Time min	Peak Name	Height mAu	Area mAu*min	Rel.Area %	Amount	Type
1	21,48	n.a.	0,983	0,114	0,46	n.a.	BMB*
2	21,76	n.a.	2,363	0,226	0,91	n.a.	BMB*
3	22,58	n.a.	127,847	24,210	97,63	n.a.	BMB*
4	26,00	n.a.	1,303	0,248	1,00	n.a.	BMB*
Total:			132,495	24,798	100,00	0,000	

Figure S42. HPLC analysis of **11**.

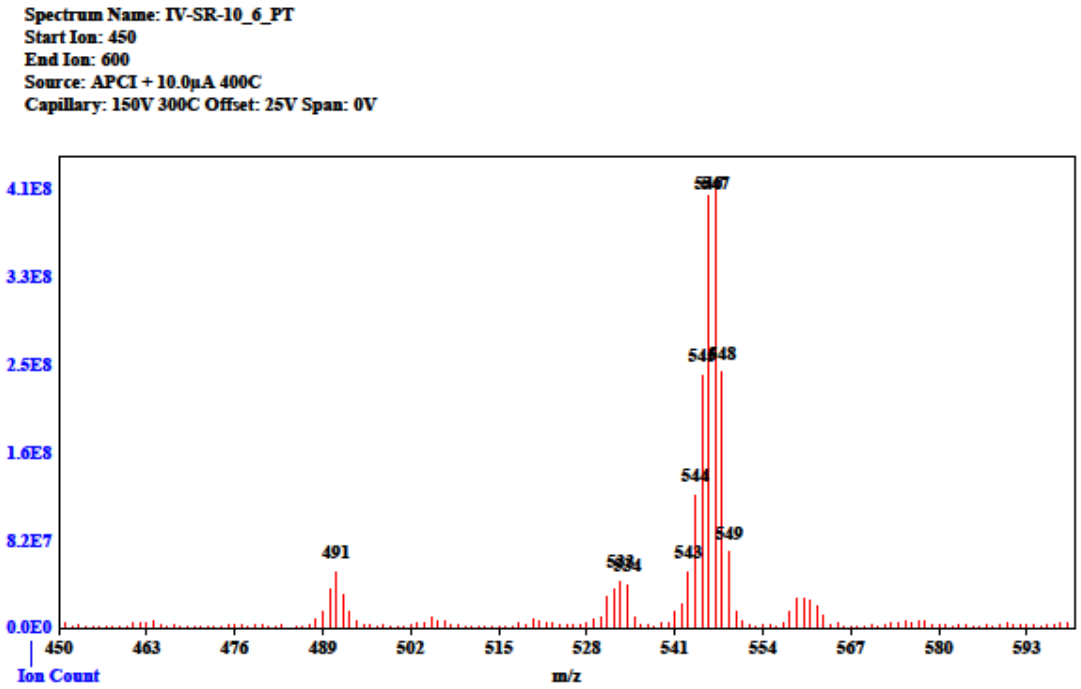

Figure S43. MS spectrum of **11**.

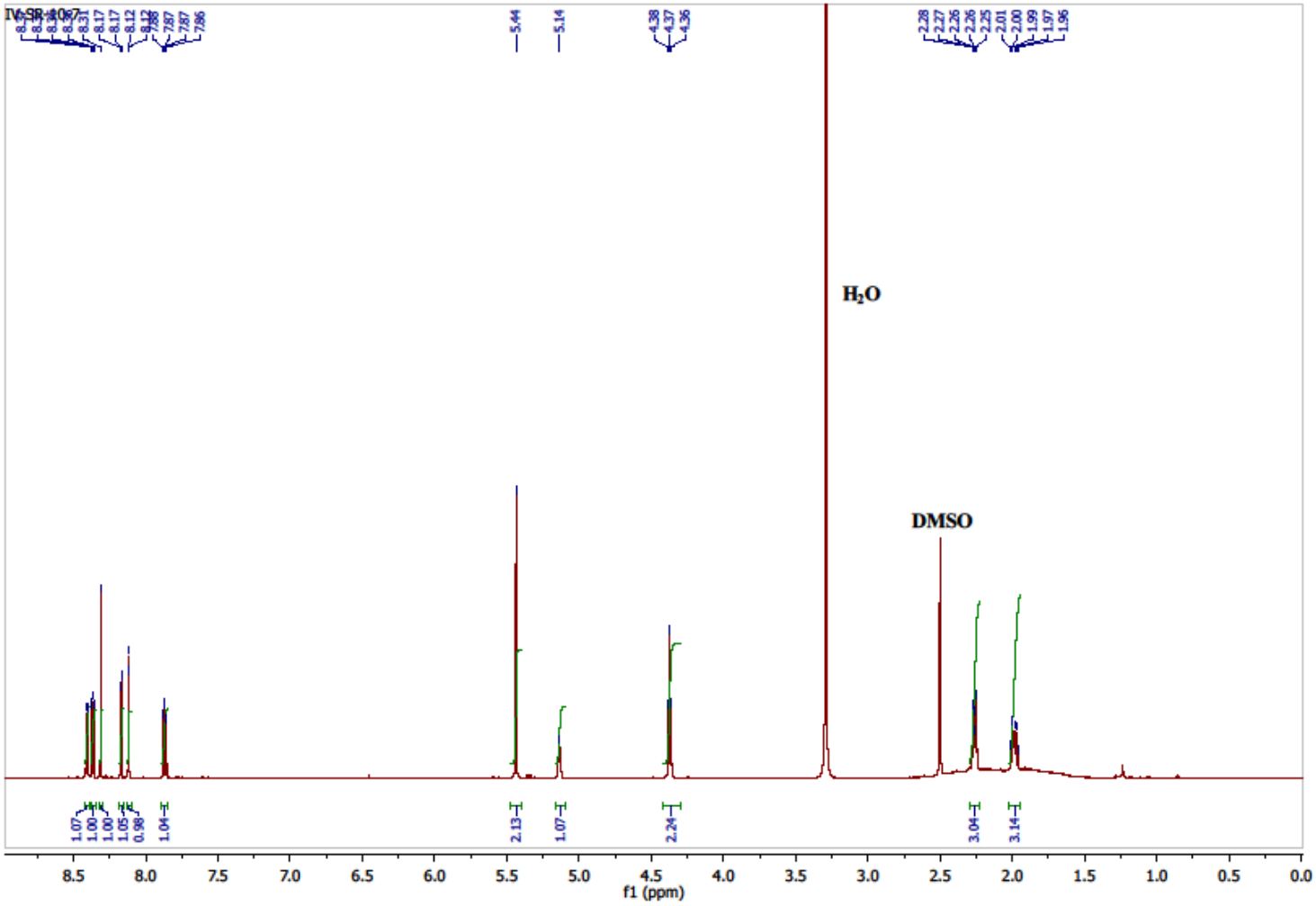

Figure S44. ^{1}H NMR spectrum of **15**.

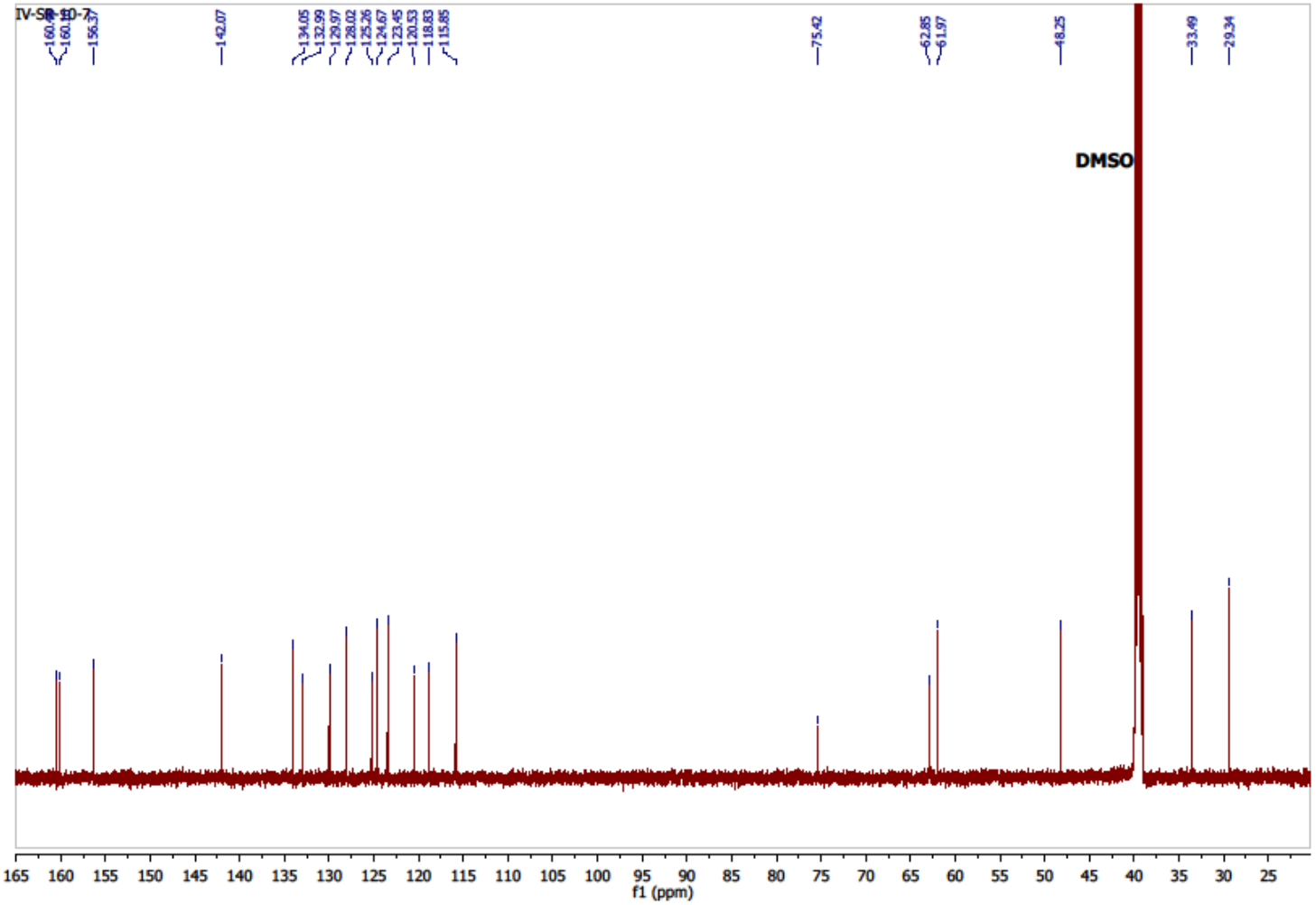

Figure S45. ^{13}C NMR spectrum of **15**.

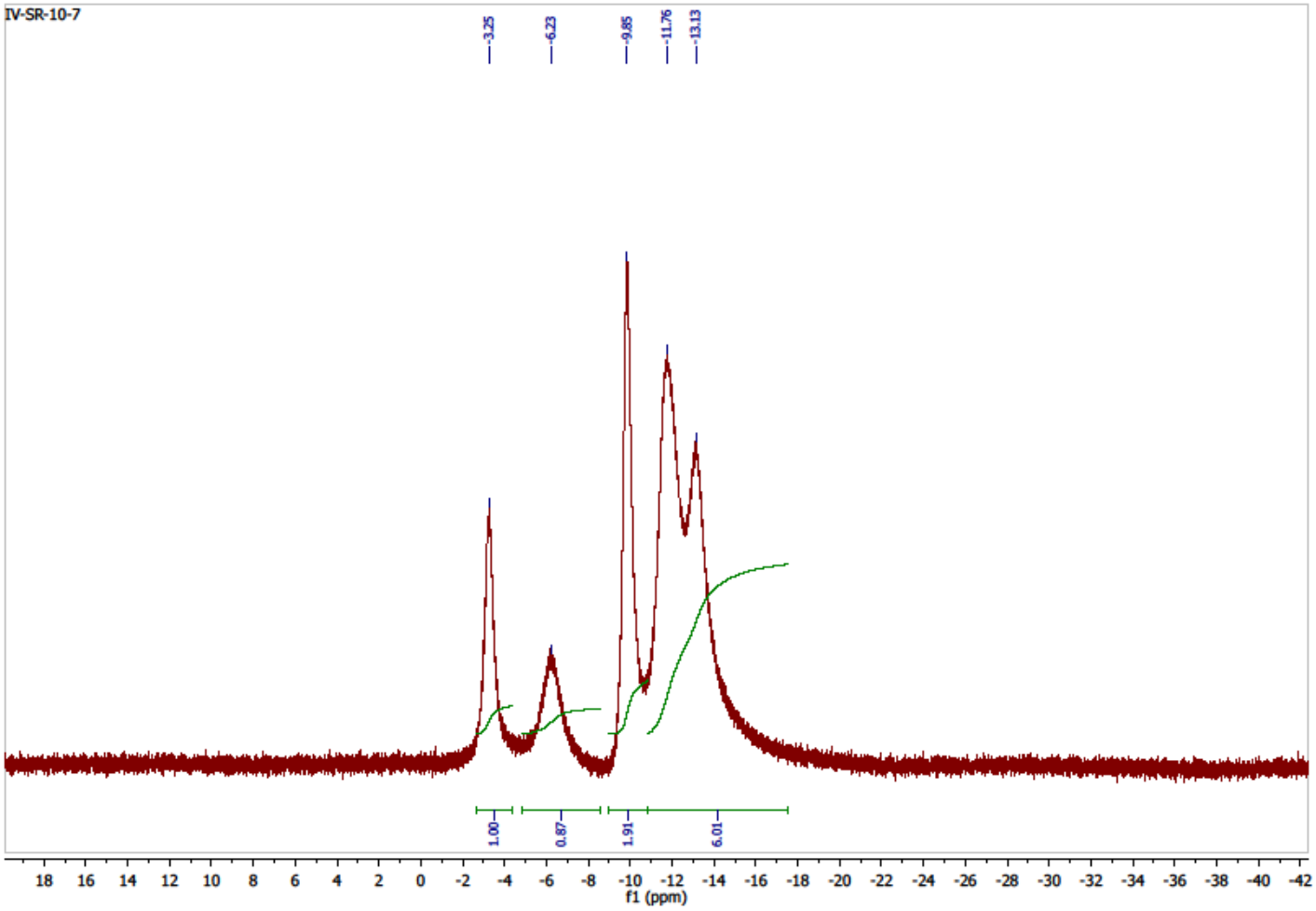

Figure S46. ^{11}B NMR $\{^{1}H$ BB$\}$ spectrum of **15**.

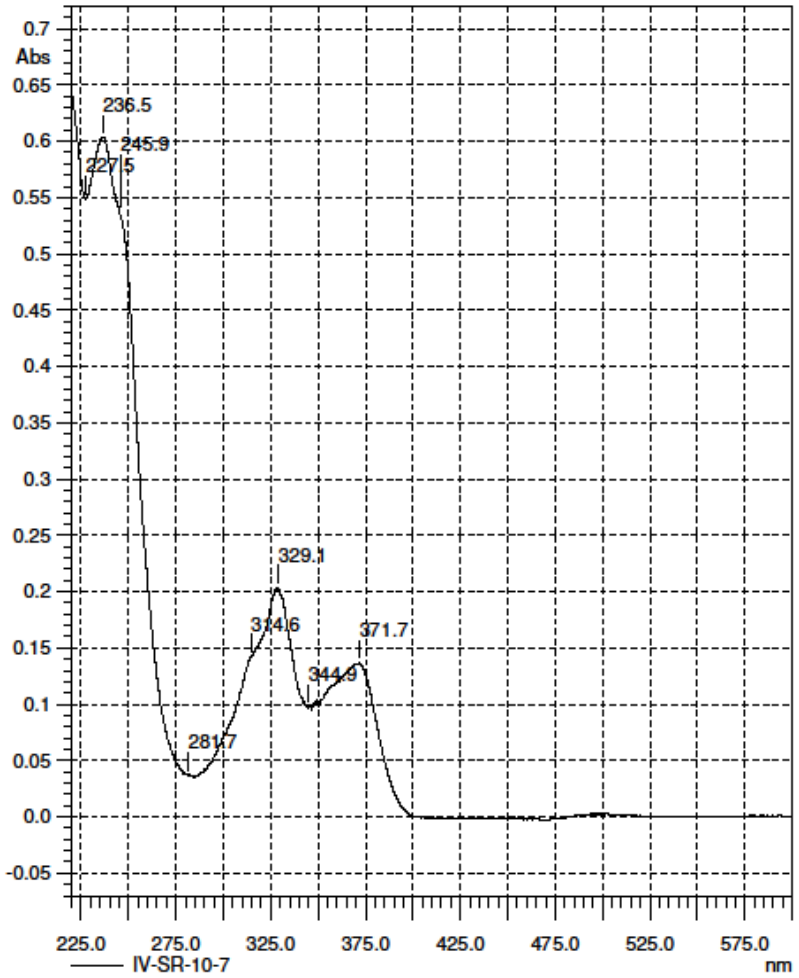

Figure S47. UV spectrum of **15**.

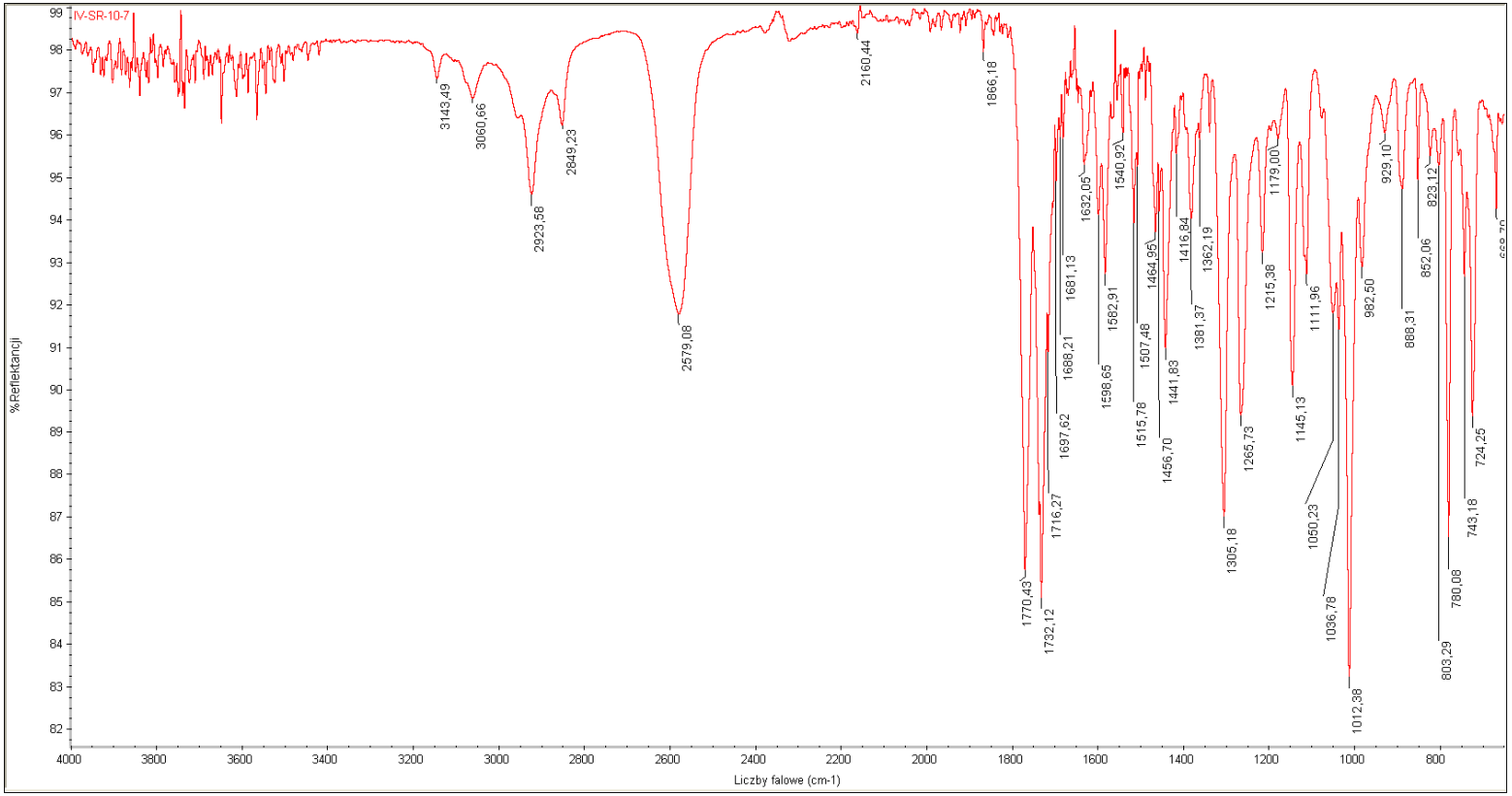

Figure S48. IR spectrum of **15**.

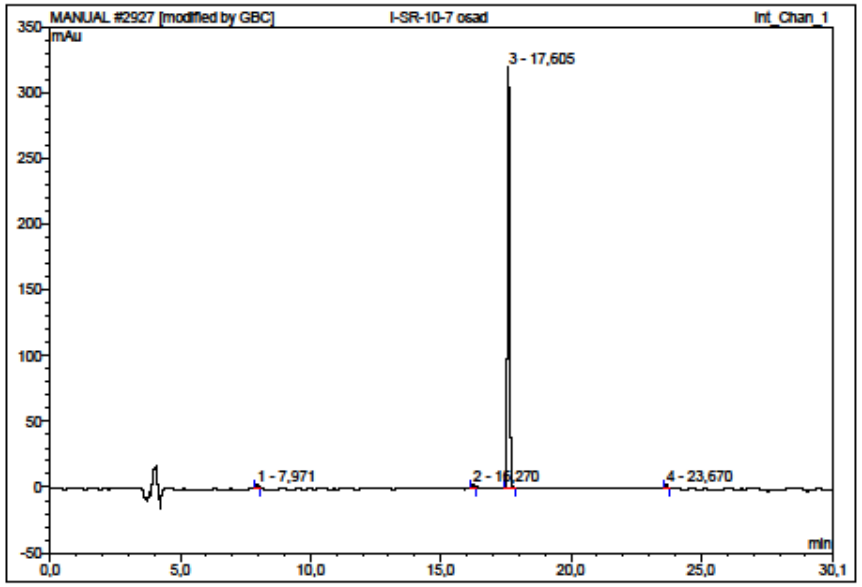

No.	Ret.Time min	Peak Name	Height mAu	Area mAu*min	Rel.Area %	Amount	Type
1	7,97	n.a.	2,487	0,249	0,75	n.a.	BMB*
2	16,27	n.a.	2,121	0,185	0,56	n.a.	BMB*
3	17,61	n.a.	320,685	32,546	98,09	n.a.	BMB
4	23,67	n.a.	2,109	0,199	0,60	n.a.	BMB*
Total:			327,402	33,179	100,00	0,000	

Figure S49. HPLC analysis of **15**.

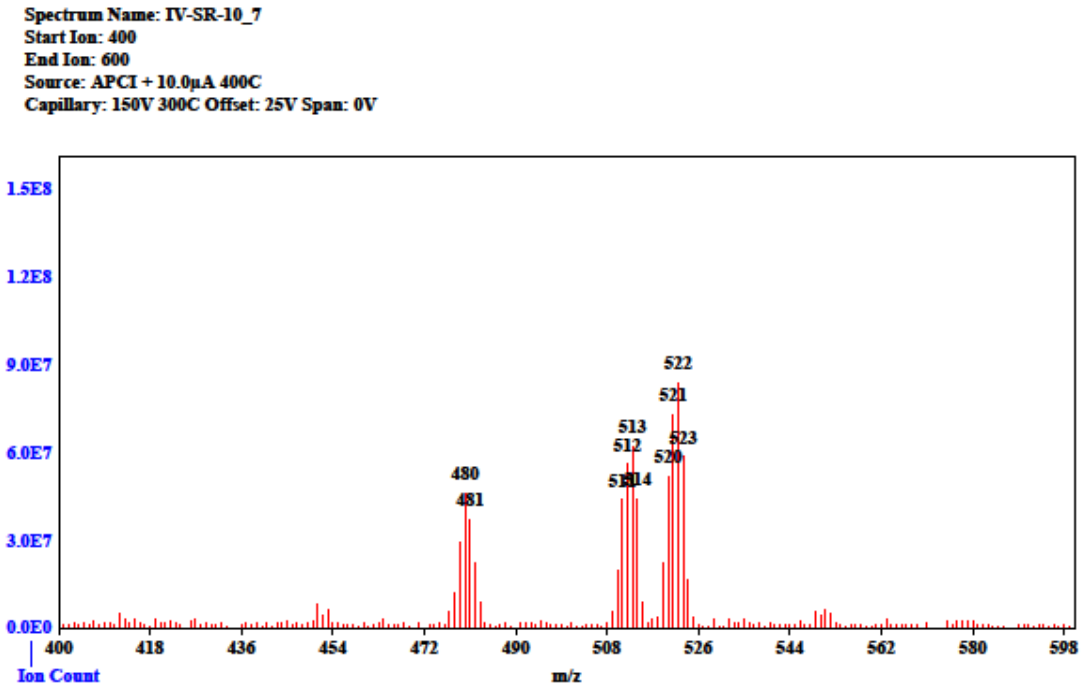

Figure S50. MS spectrum of **15**.

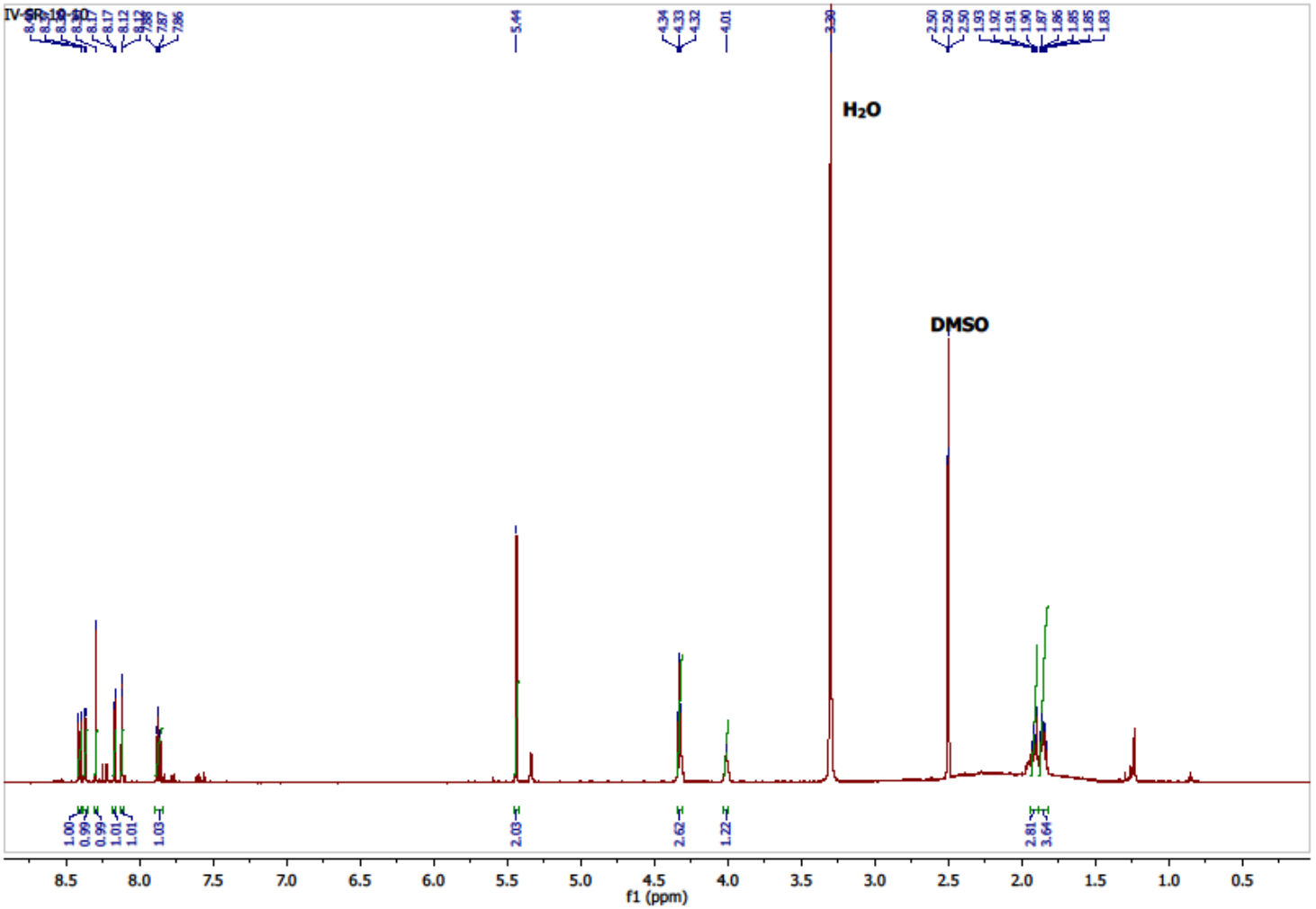

Figure S51. ^{1}H NMR spectrum of **16**.

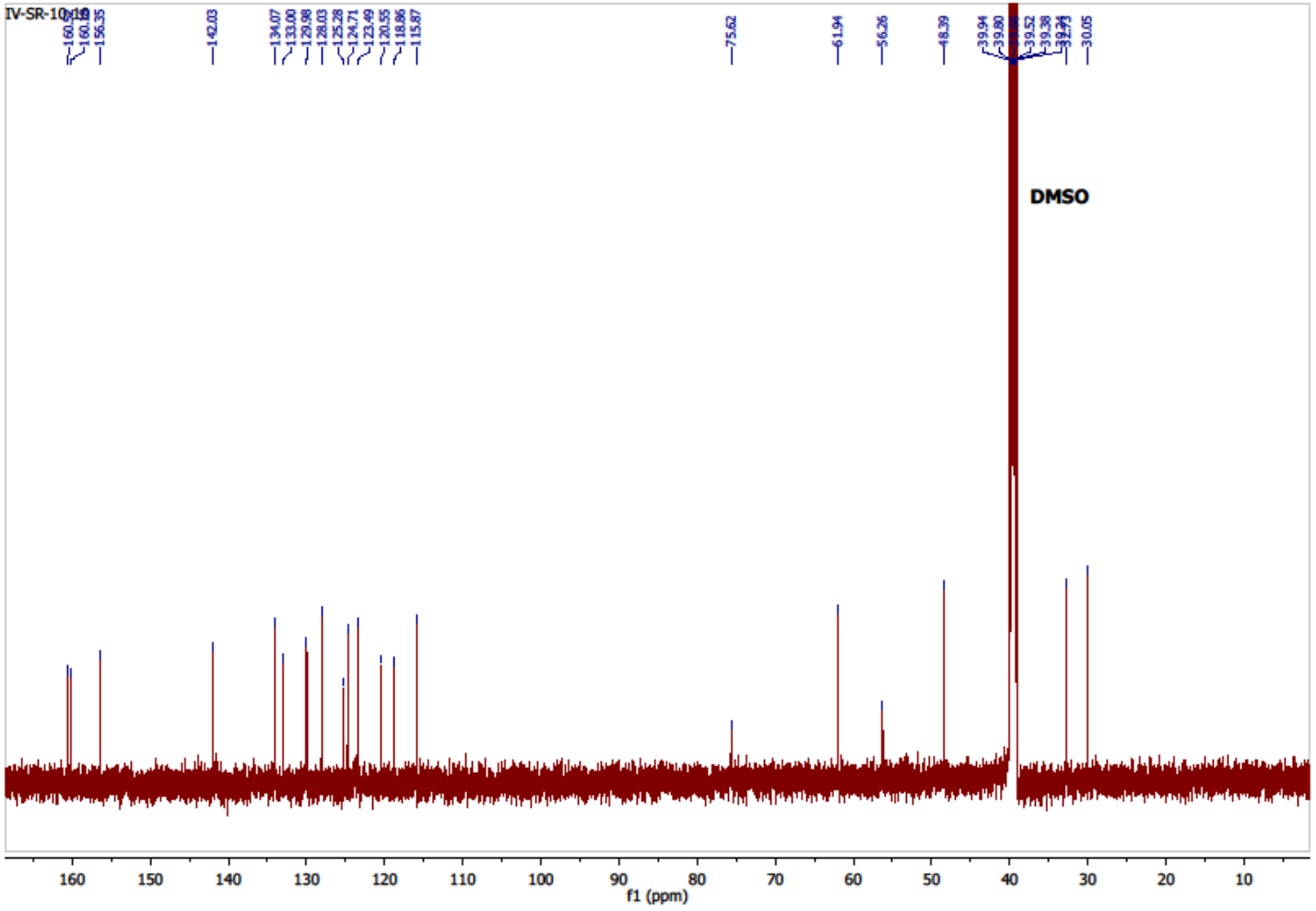

Figure S52. ^{13}C NMR spectrum of **16**.

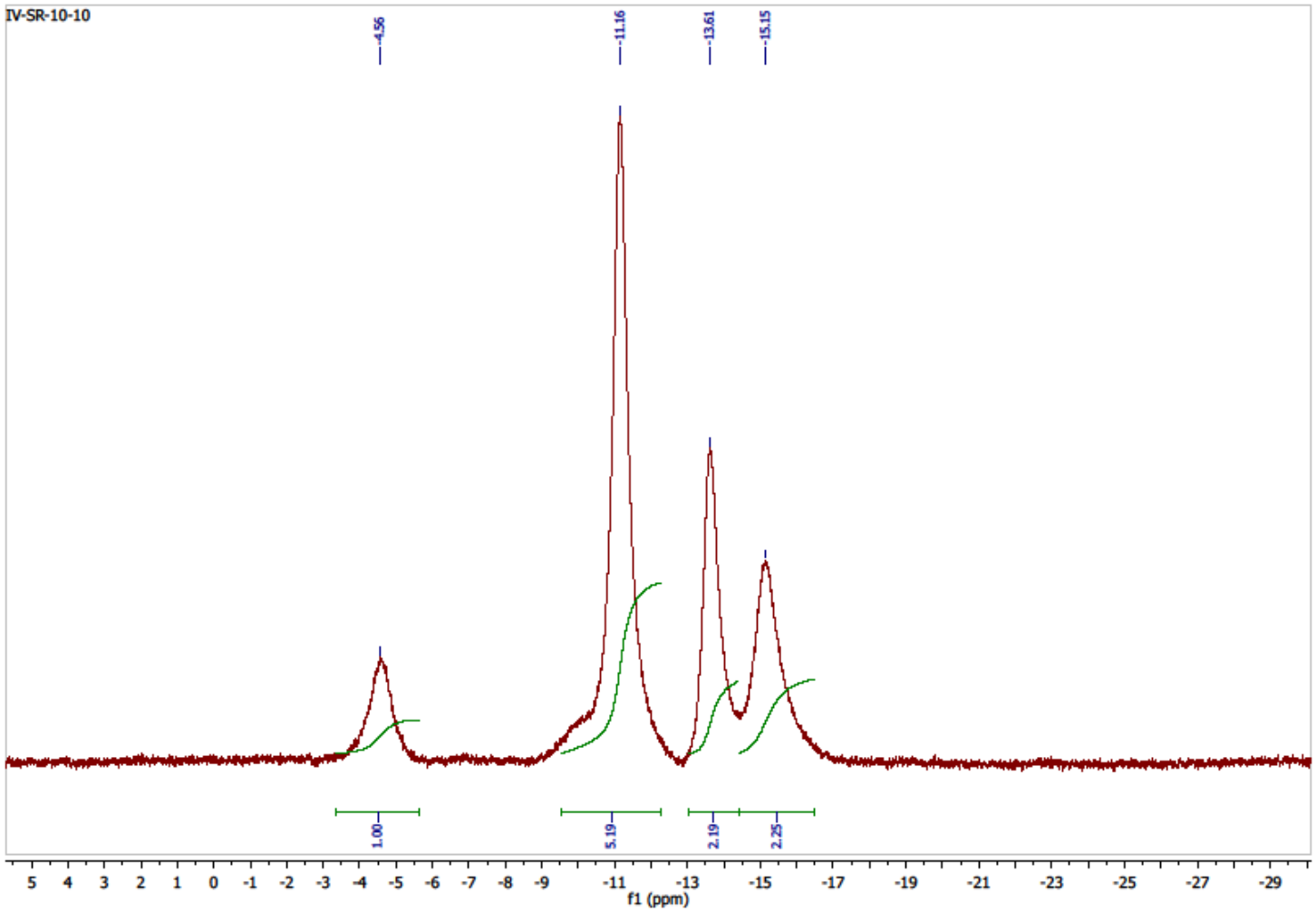

Figure S53. ^{11}B NMR $\{^{1}H$ BB$\}$ spectrum of **16**.

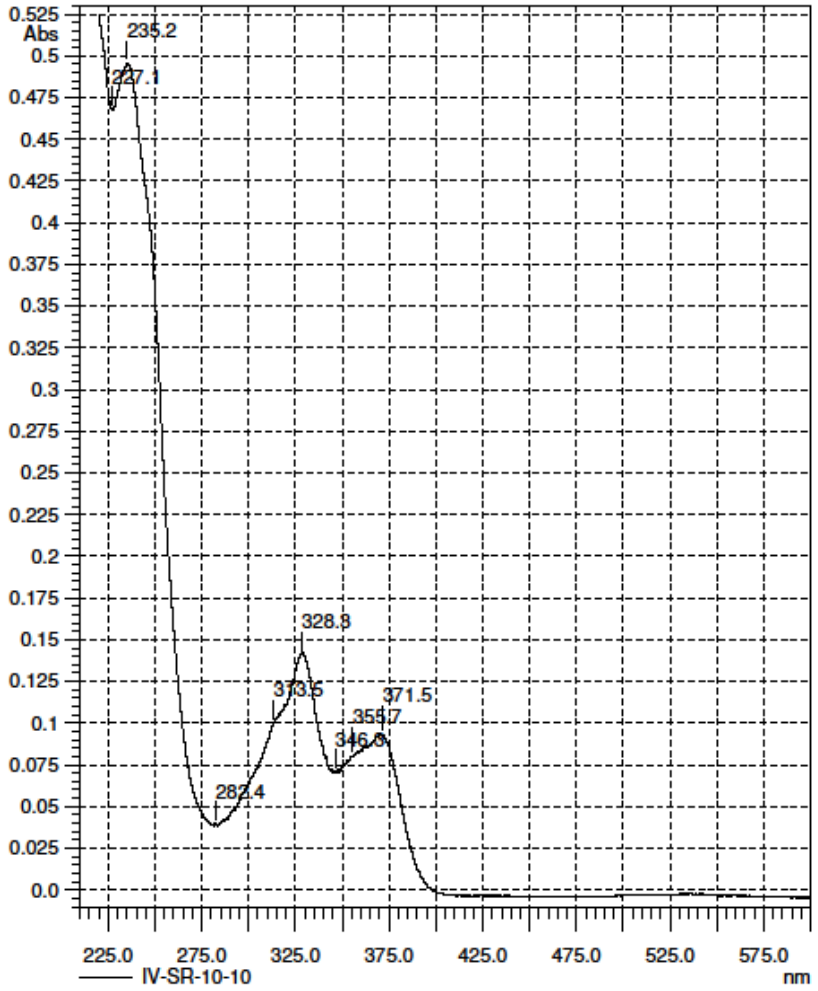

Figure S54. UV spectrum of **16**.

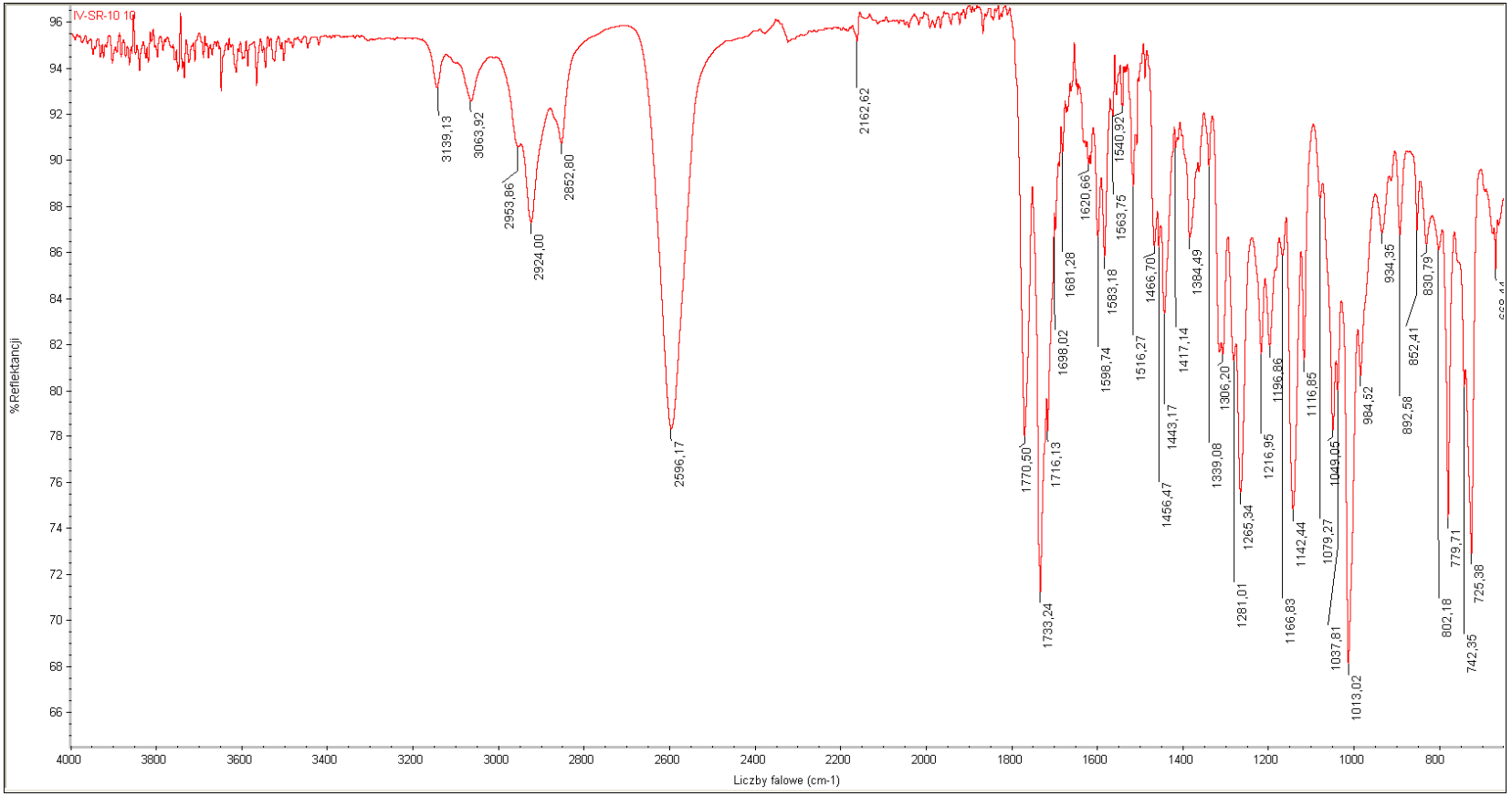

Figure S55. IR spectrum of **16**.

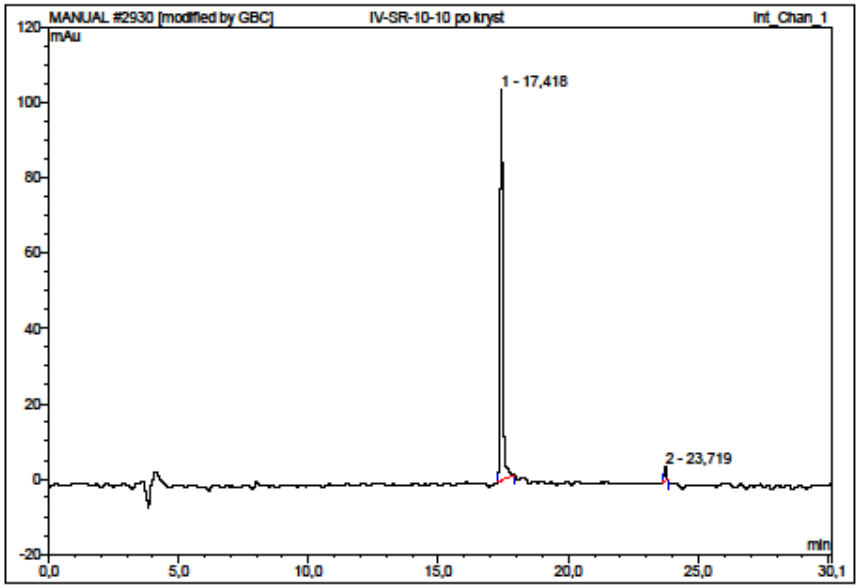

No.	Ret.Time min	Peak Name	Height mAu	Area mAu*min	Rel.Area %	Amount	Type
1	17,42	n.a.	103,998	11,152	96,15	n.a.	BMB
2	23,72	n.a.	4,200	0,446	3,85	n.a.	BMB*
Total:			108,198	11,598	100,00	0,000	

Figure S56. HPLC analysis of **16**.

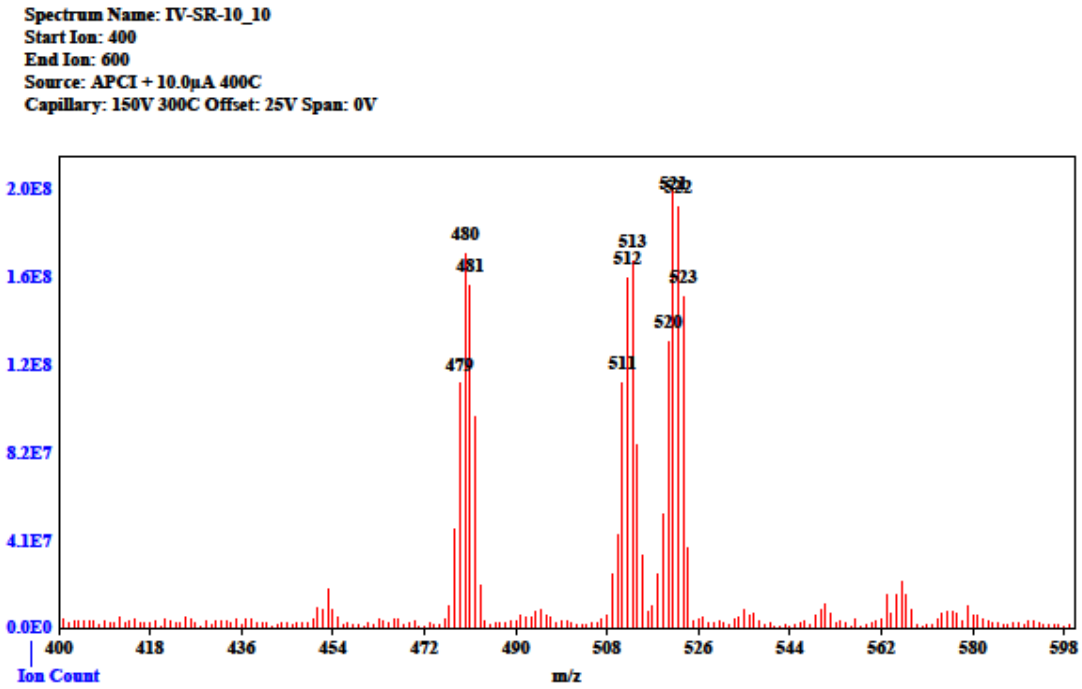

Figure S57. MS spectrum of **16**.

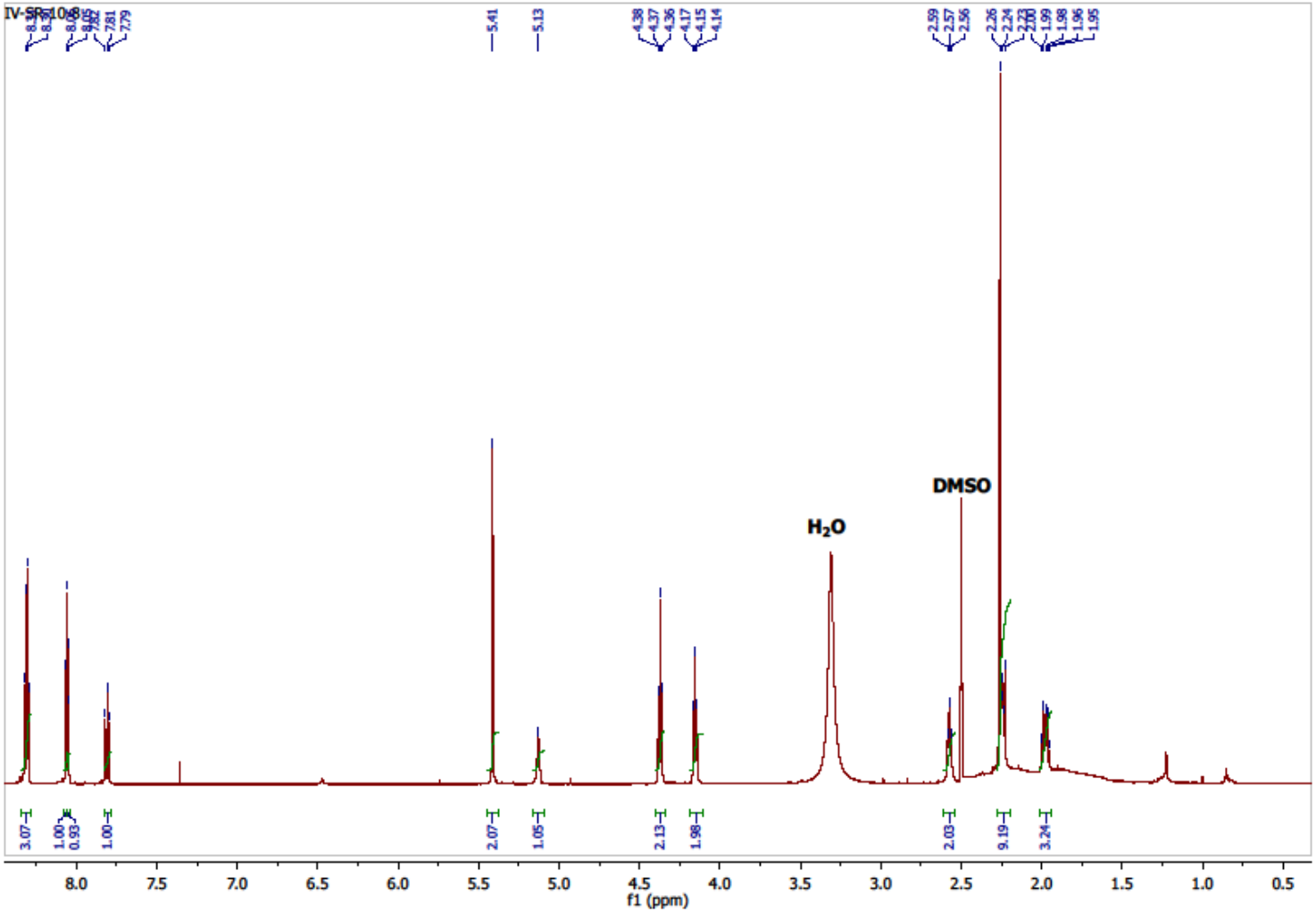

Figure S58. ^{1}H NMR spectrum of **17**.

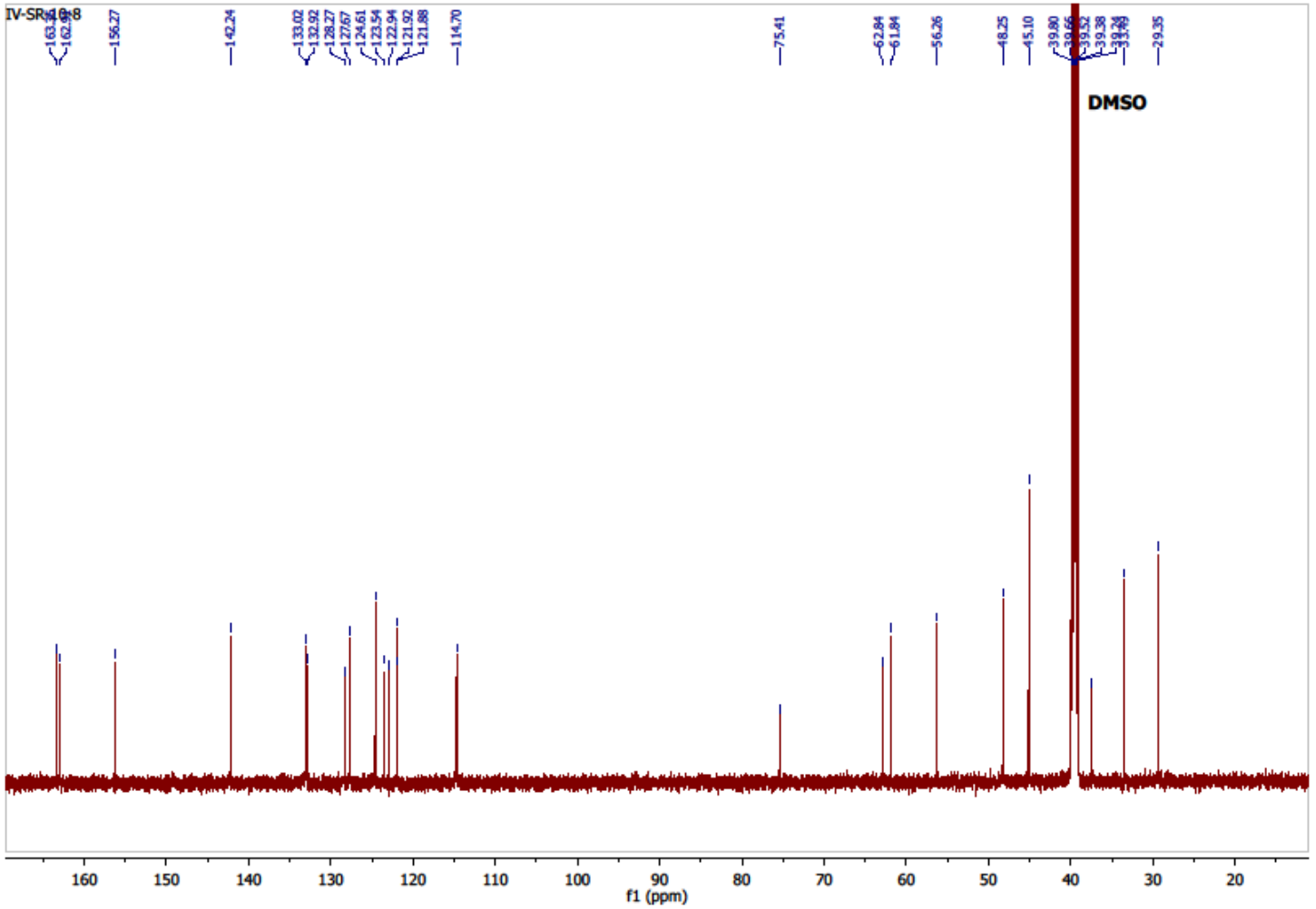

Figure S59. ^{13}C NMR spectrum of **17**.

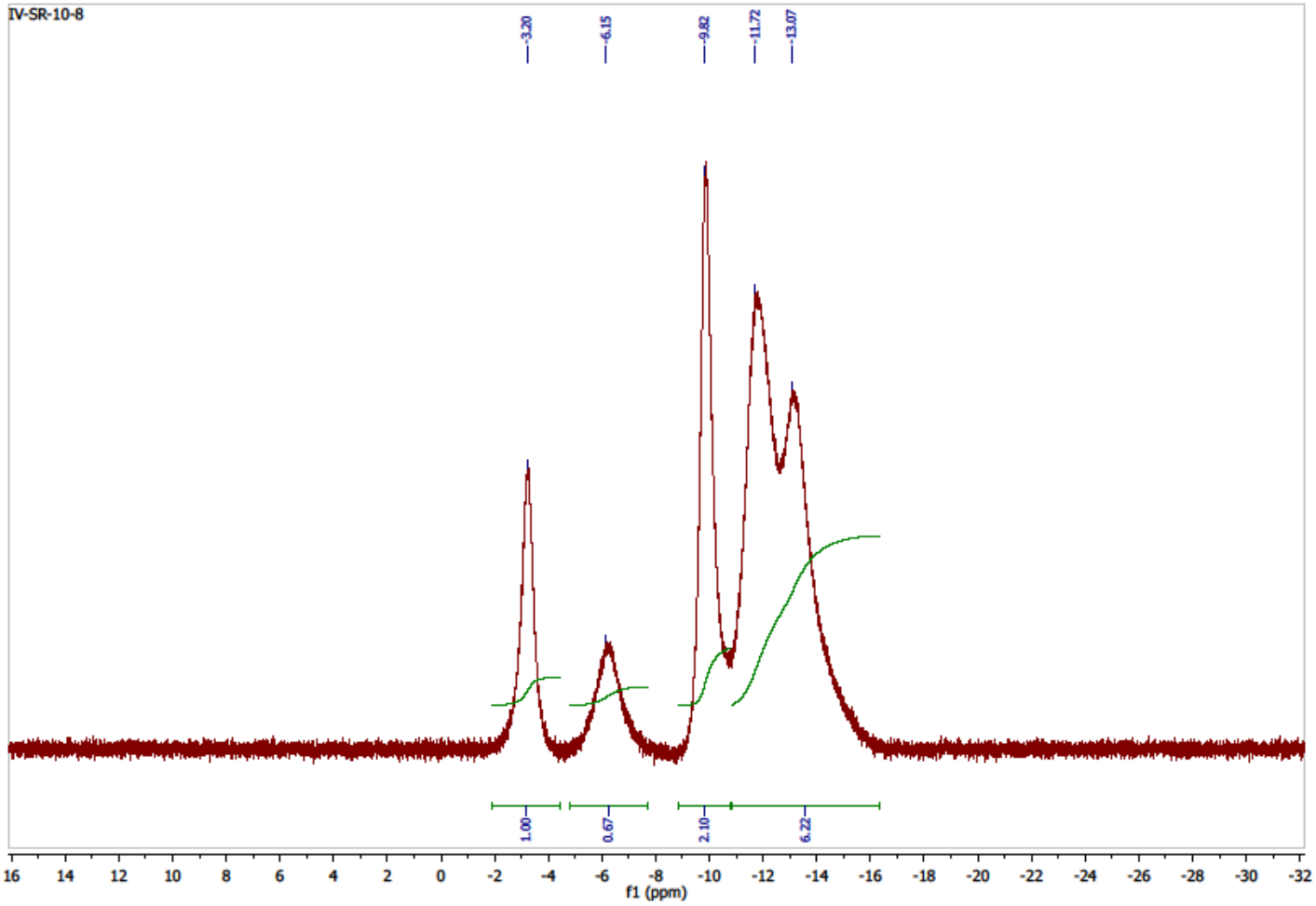

Figure S60. ^{11}B NMR {^{1}H BB} spectrum of **17**.

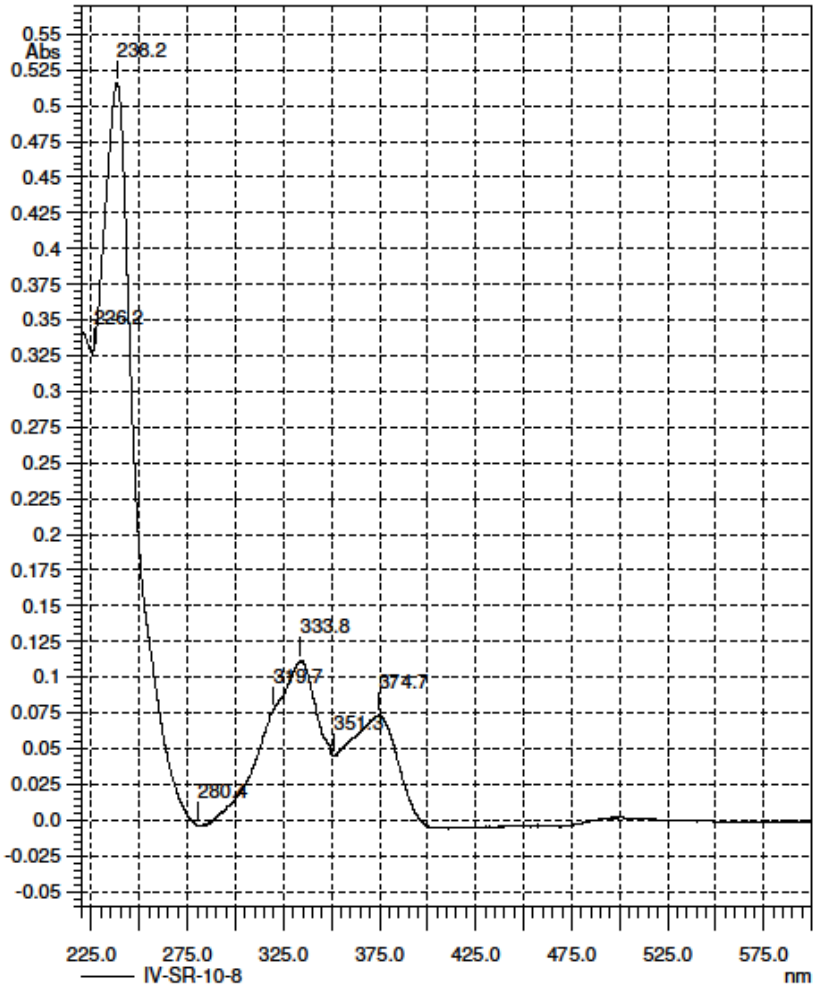

Figure S61. UV spectrum of **17**.

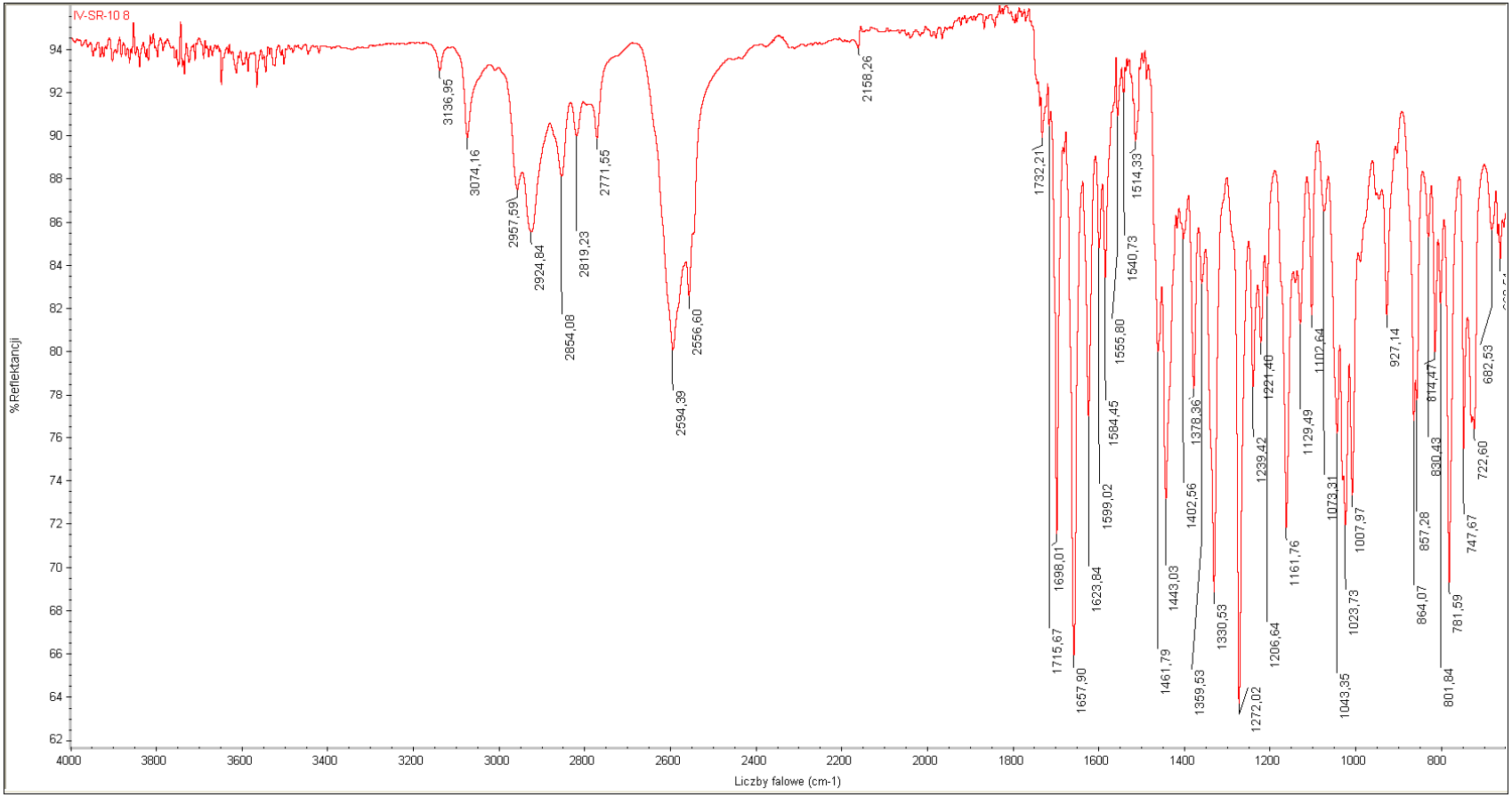

Figure S62. IR spectrum of **17**.

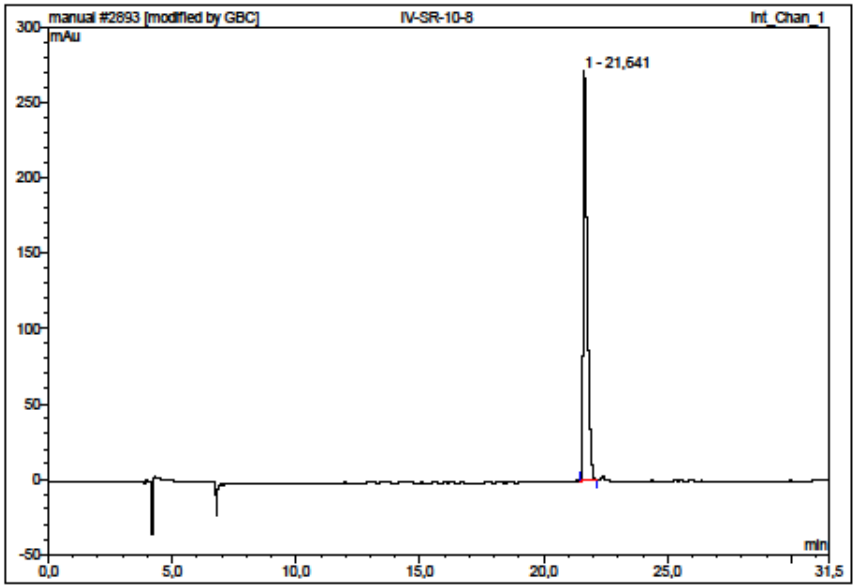

No.	Ret.Time min	Peak Name	Height mAu	Area mAu*min	Rel.Area %	Amount	Type
1	21,64	n.a.	272,839	51,467	100,00	n.a.	BMB
Total:			272,839	51,467	100,00	0,000	

Figure S63. HPLC analysis of **17**.

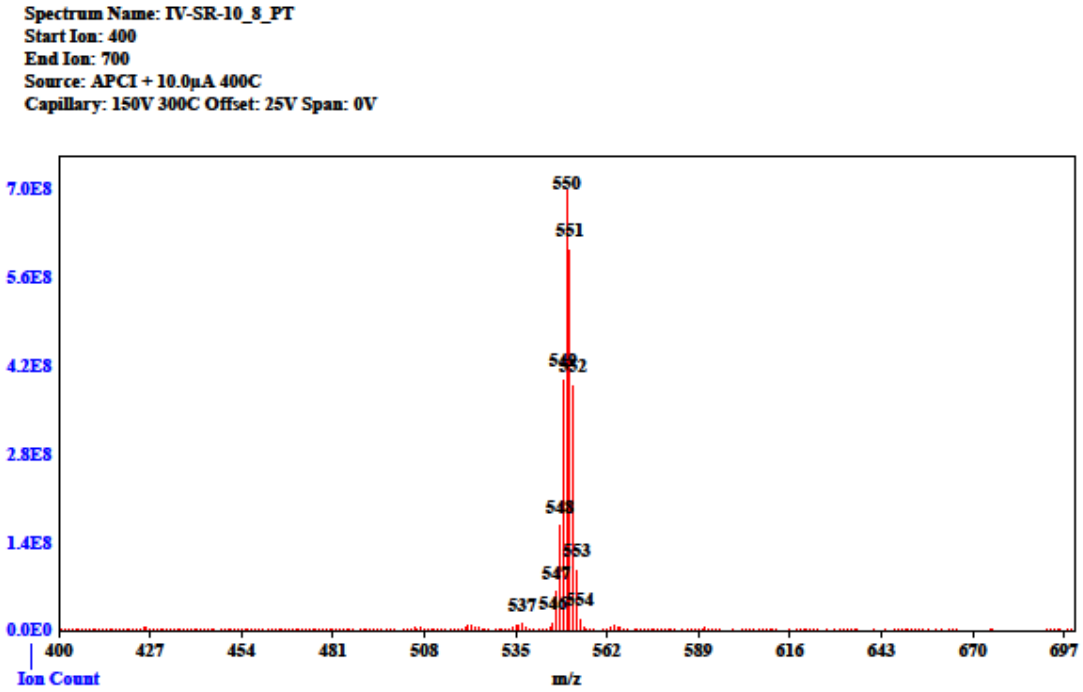

Figure S64. MS spectrum of **17**.

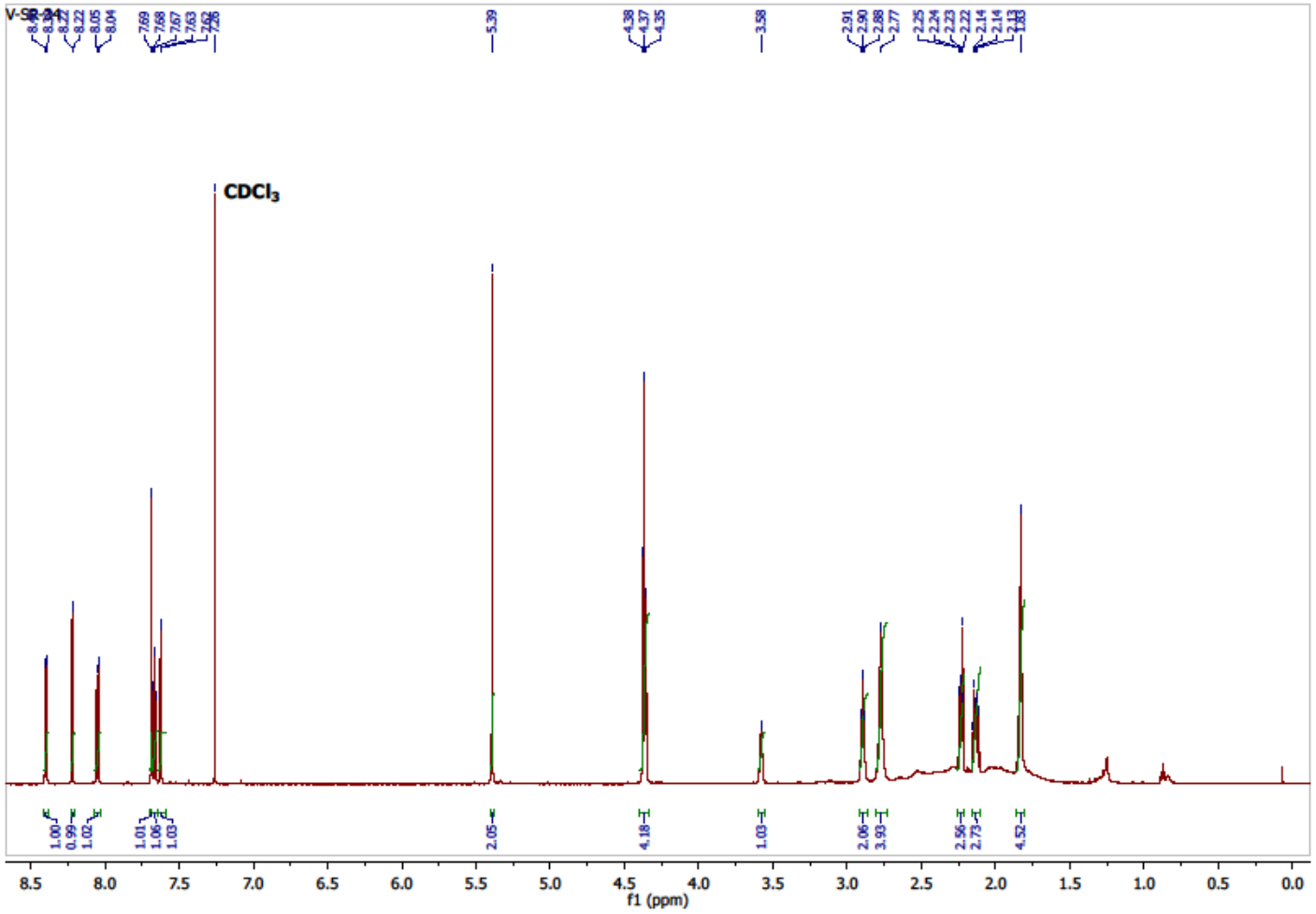

Figure S65. ^{1}H NMR spectrum of **18**.

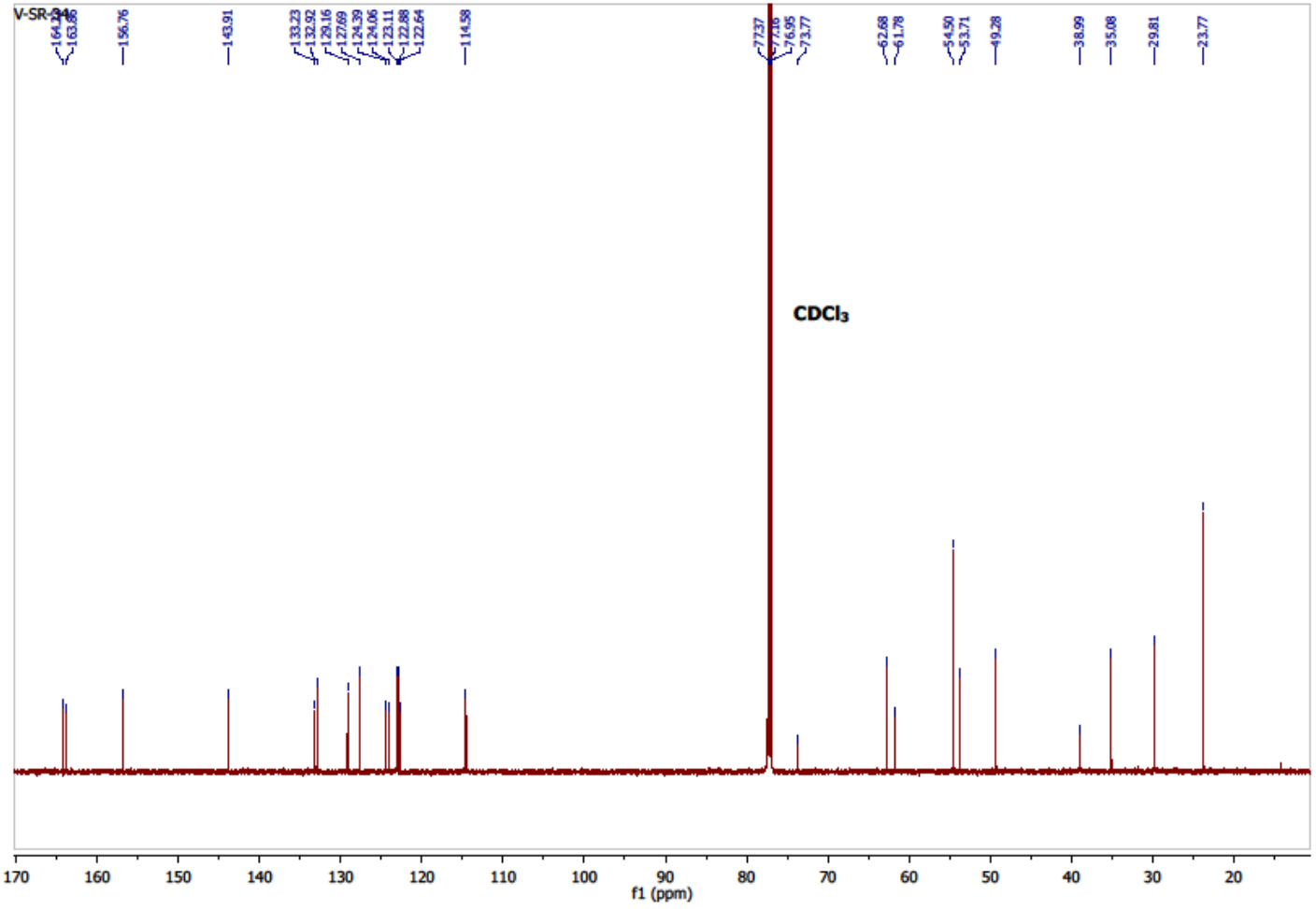

Figure S66. ^{13}C NMR spectrum of **18**.

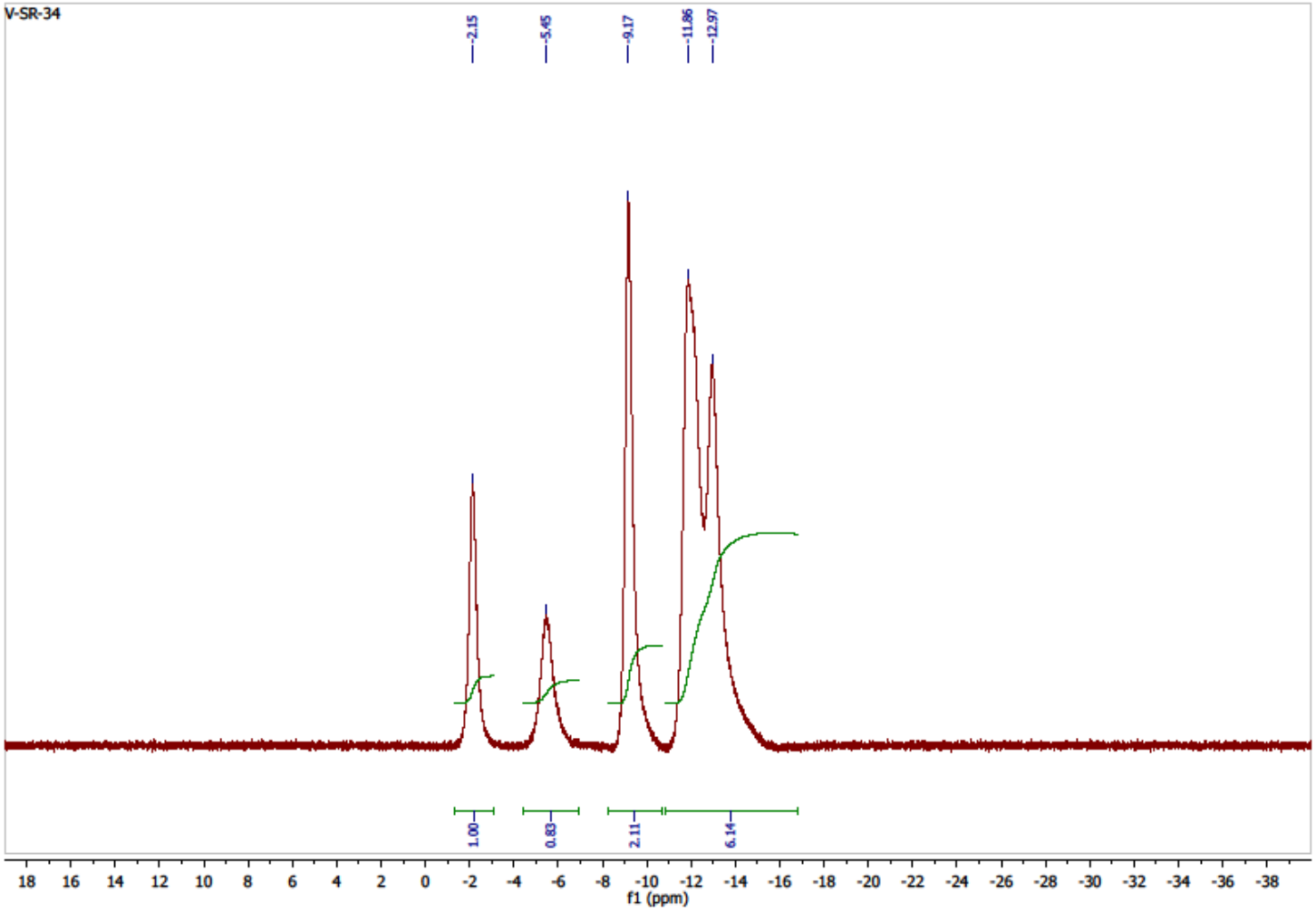

Figure S67. ^{11}B NMR {^{1}H BB} spectrum of **18**.

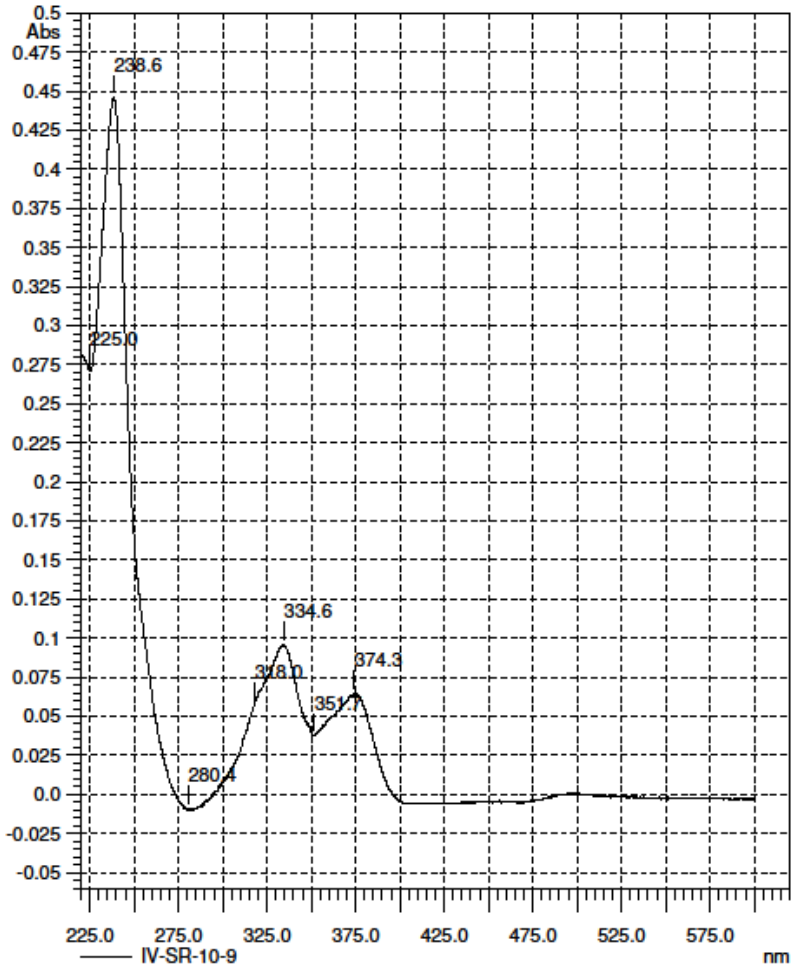

Figure S68. UV spectrum of **18**.

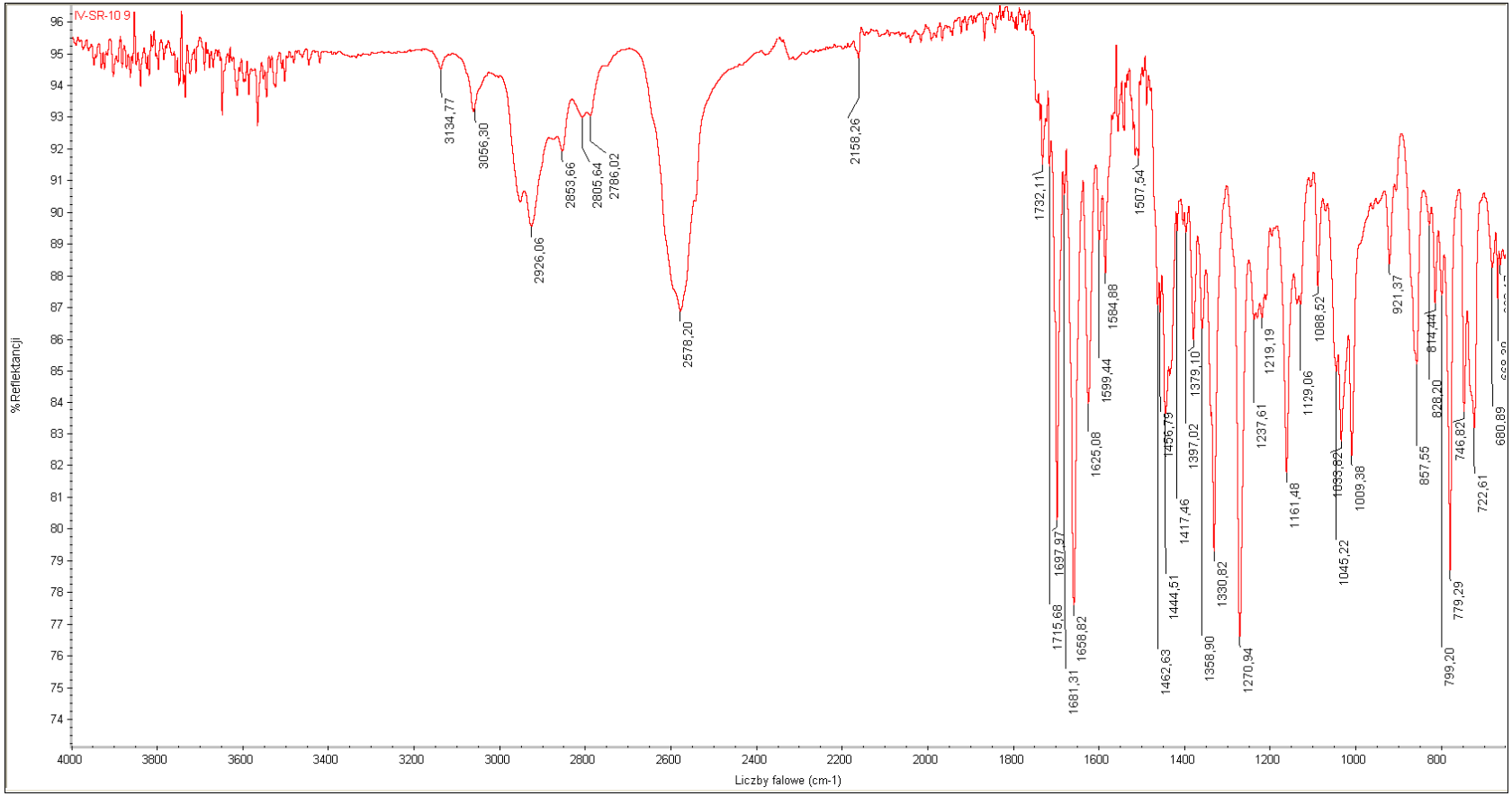

Figure S69. IR spectrum of **18**.

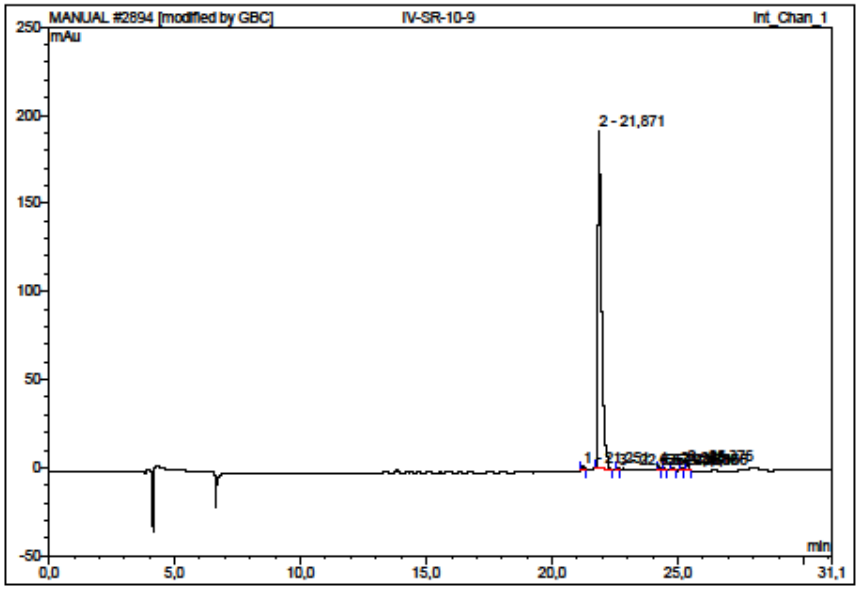

No.	Ret.Time min	Peak Name	Height mAu	Area mAu*min	Rel.Area %	Amount	Type
1	21,25	n.a.	1,985	0,193	0,56	n.a.	BMB*
2	21,87	n.a.	191,502	33,011	96,79	n.a.	BMB
3	22,64	n.a.	0,708	0,071	0,21	n.a.	BMB*
4	24,27	n.a.	1,989	0,186	0,54	n.a.	BMB*
5	24,48	n.a.	0,728	0,065	0,19	n.a.	BMB*
6	24,80	n.a.	1,215	0,127	0,37	n.a.	BMB*
7	25,17	n.a.	0,822	0,078	0,23	n.a.	BMB*
8	25,38	n.a.	2,904	0,375	1,10	n.a.	BMB*
Total:			201,851	34,106	100,00	0,000	

Figure S70. HPLC analysis of **18**.

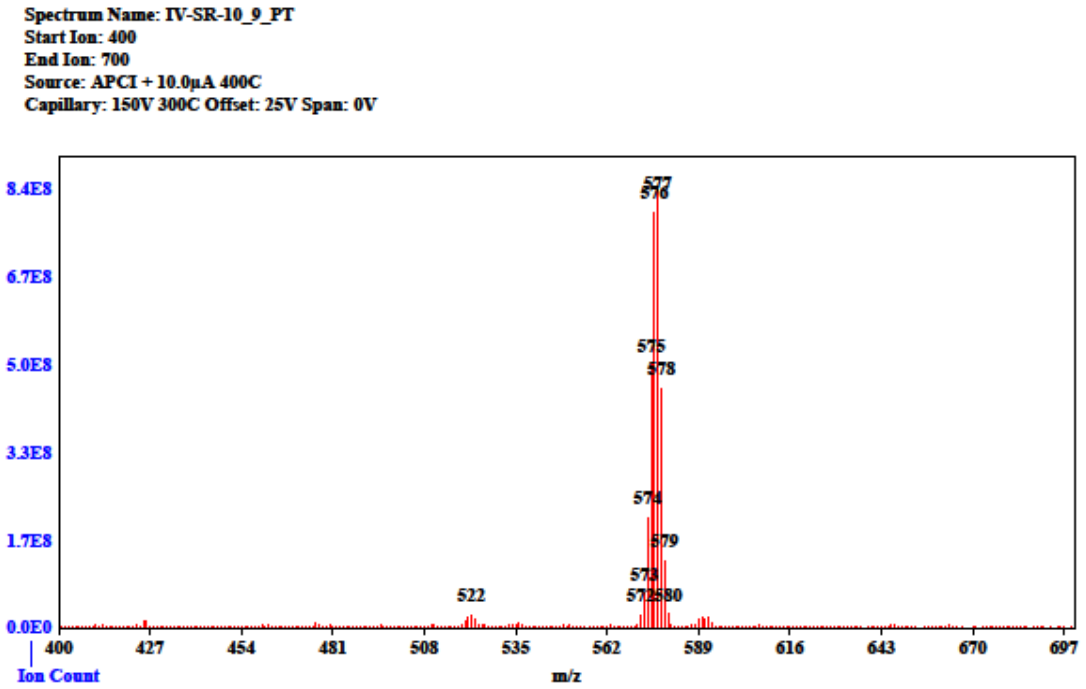

Figure S71. MS spectrum of **18**.

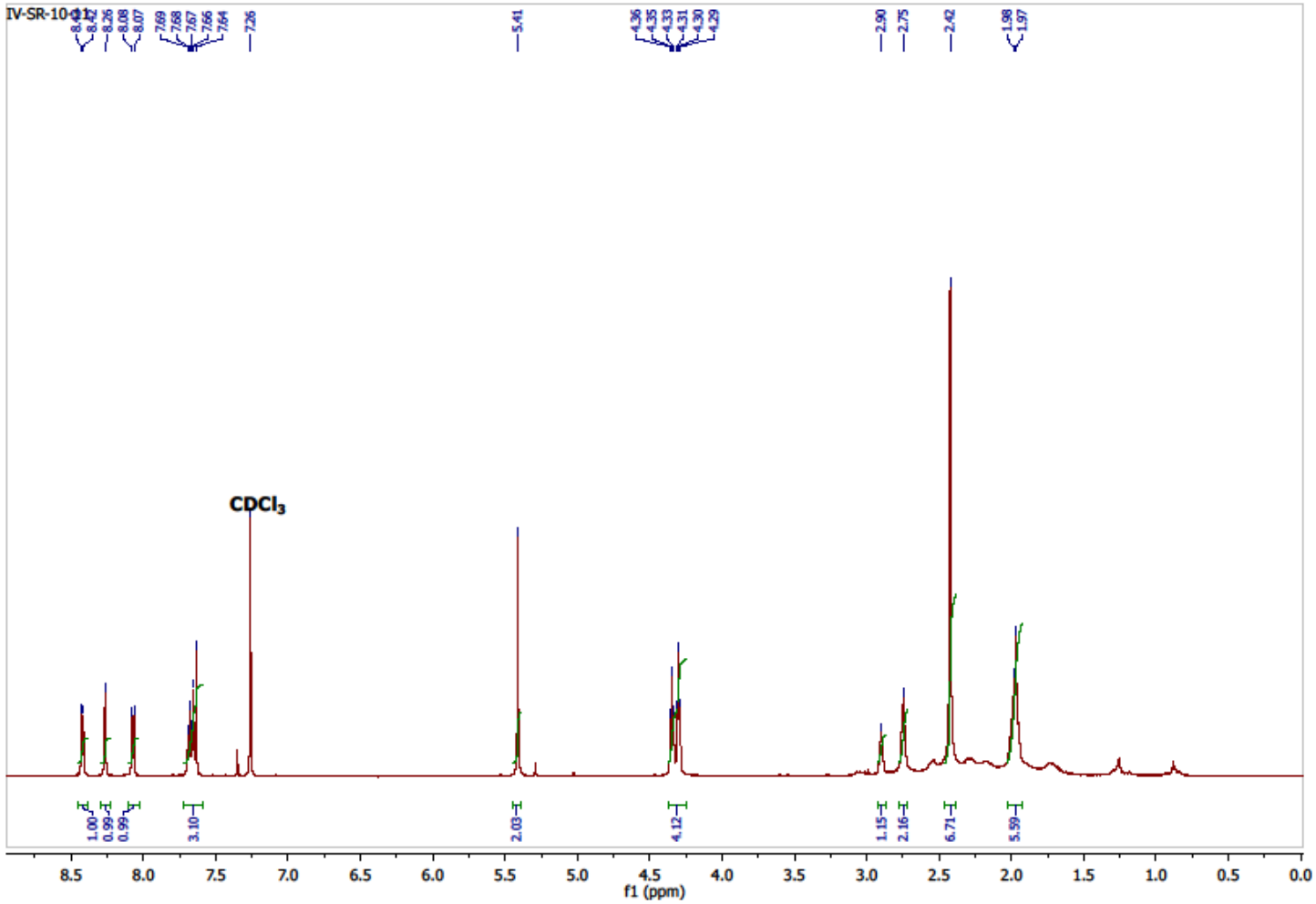

Figure S72. ^{1}H NMR spectrum of **19**.

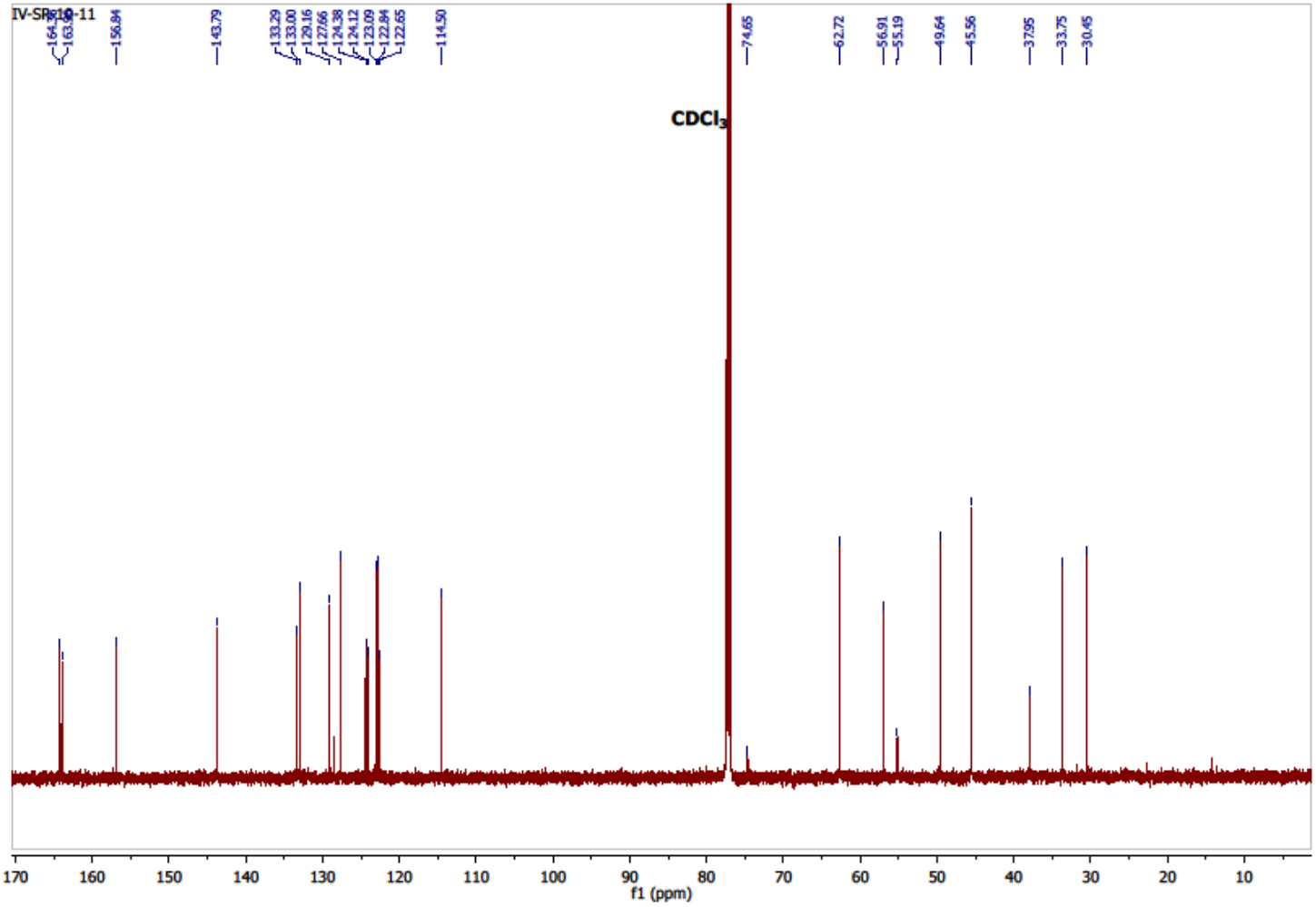

Figure S73. ^{13}C NMR spectrum of **19**.

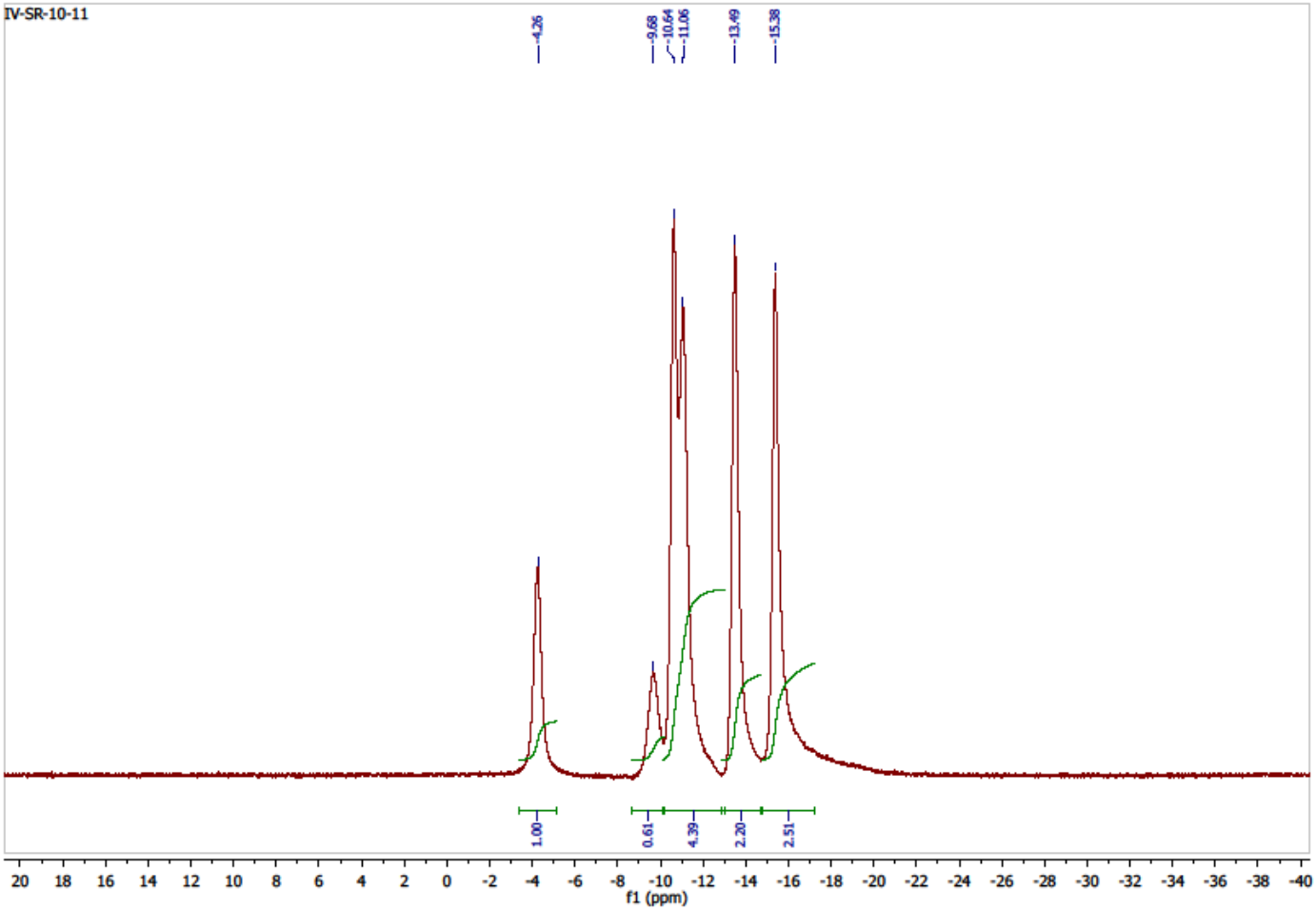

Figure S74. ^{11}B NMR {^{1}H BB} spectrum of **19**.

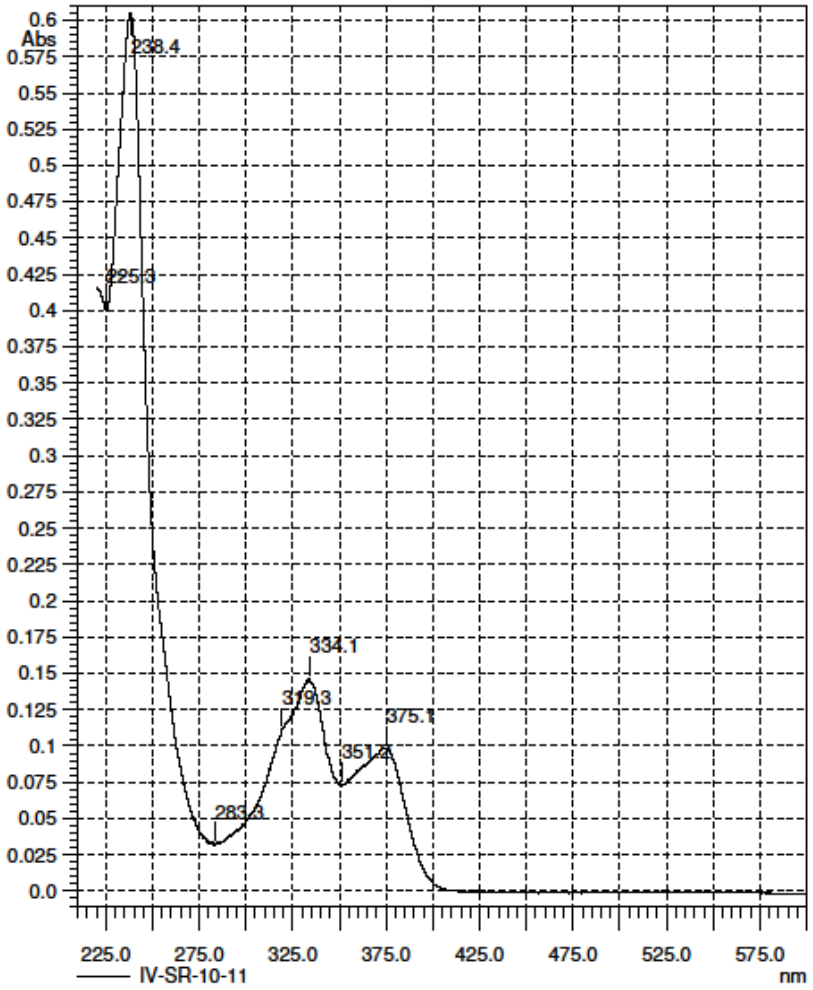

Figure S75. UV spectrum of **19**.

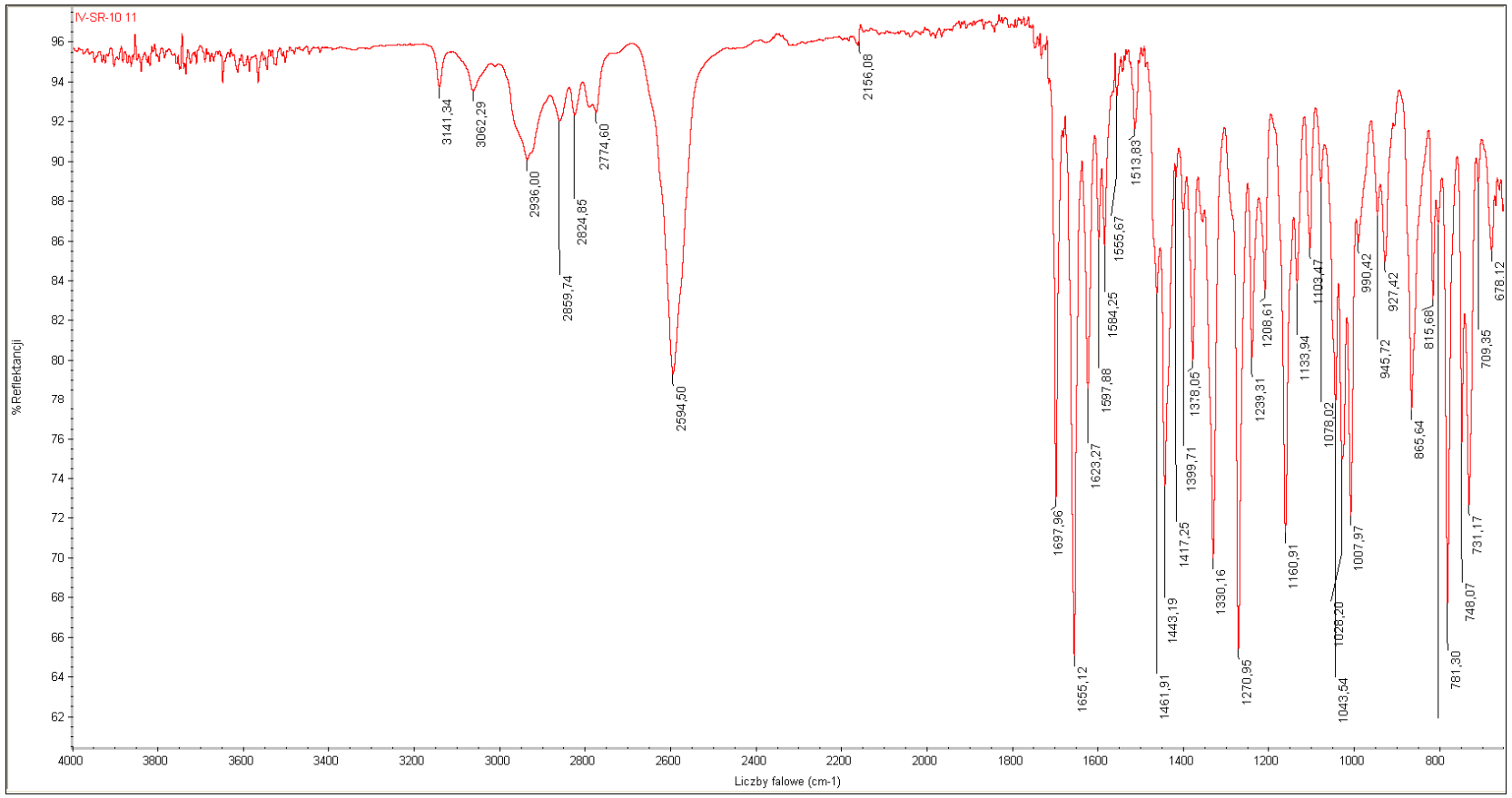

Figure S76. IR spectrum of **19**.

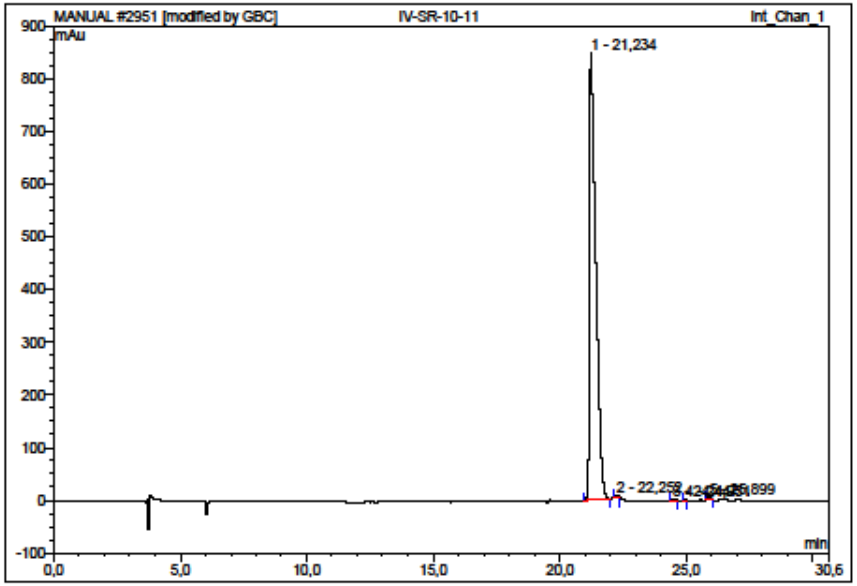

No.	Ret.Time min	Peak Name	Height mAu	Area mAu*min	Rel.Area %	Amount	Type
1	21,23	n.a.	849,952	248,891	99,30	n.a.	BMB
2	22,25	n.a.	4,583	0,672	0,27	n.a.	BM *
3	24,45	n.a.	1,821	0,243	0,10	n.a.	BMB*
4	24,95	n.a.	2,623	0,272	0,11	n.a.	BMB*
5	25,90	n.a.	4,032	0,565	0,23	n.a.	BMB*
Total:			863,010	250,642	100,00	0,000	

Figure S77. HPLC analysis of **19**.

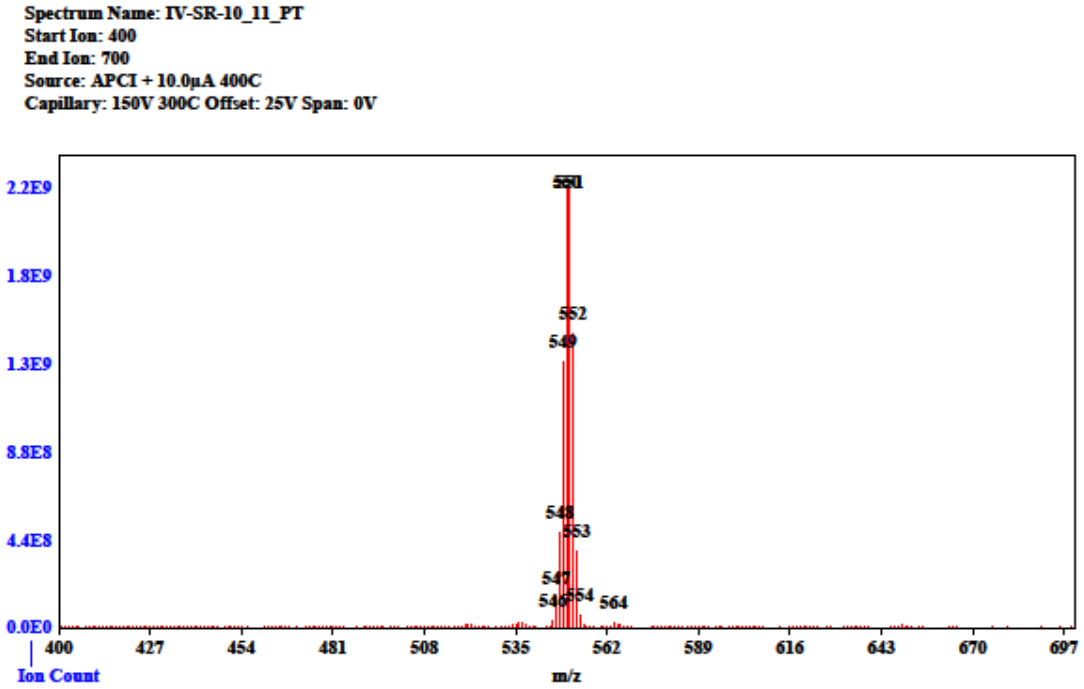

Figure S78. MS spectrum of **19**.

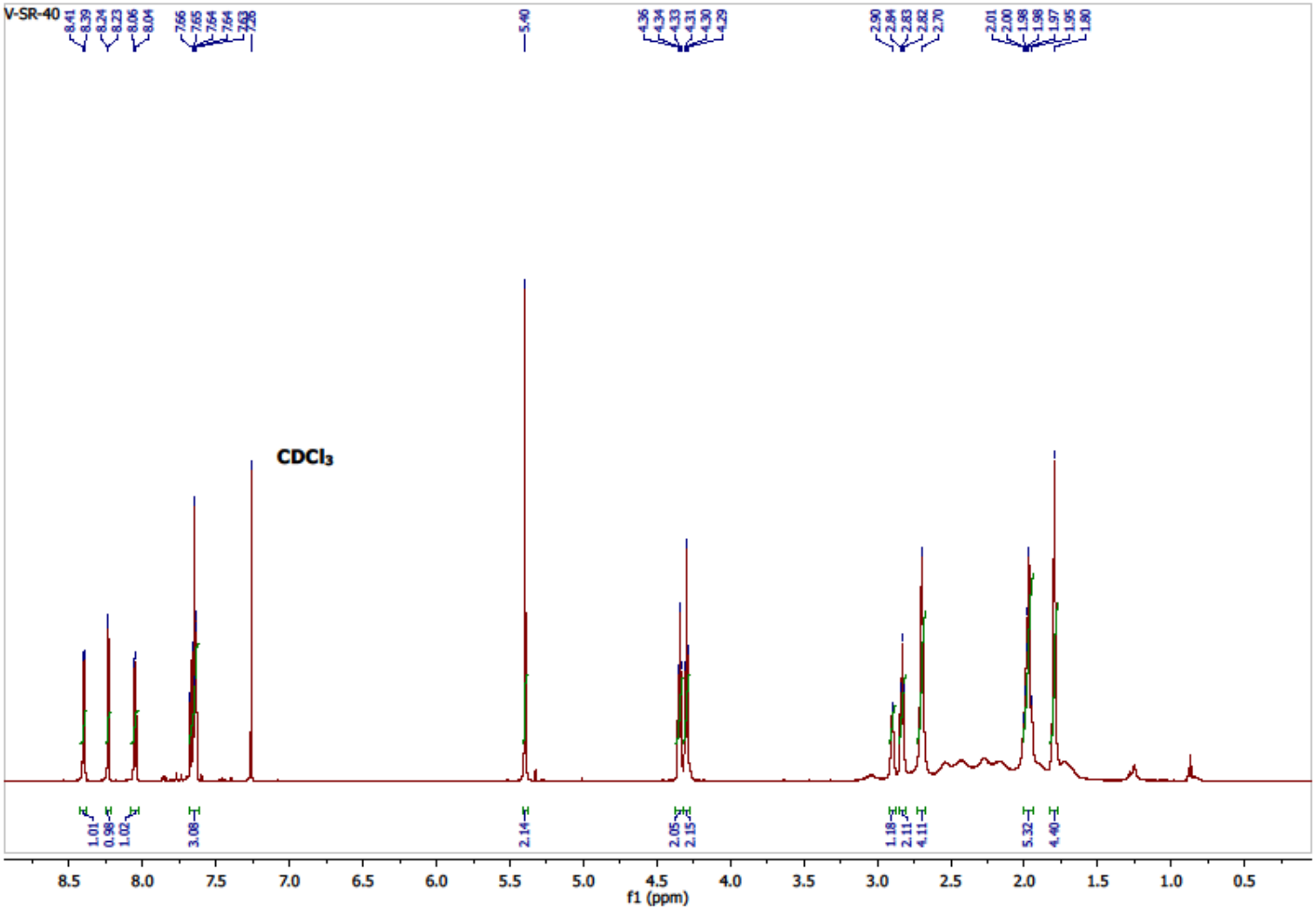

Figure S79. ^{1}H NMR spectrum of **20**.

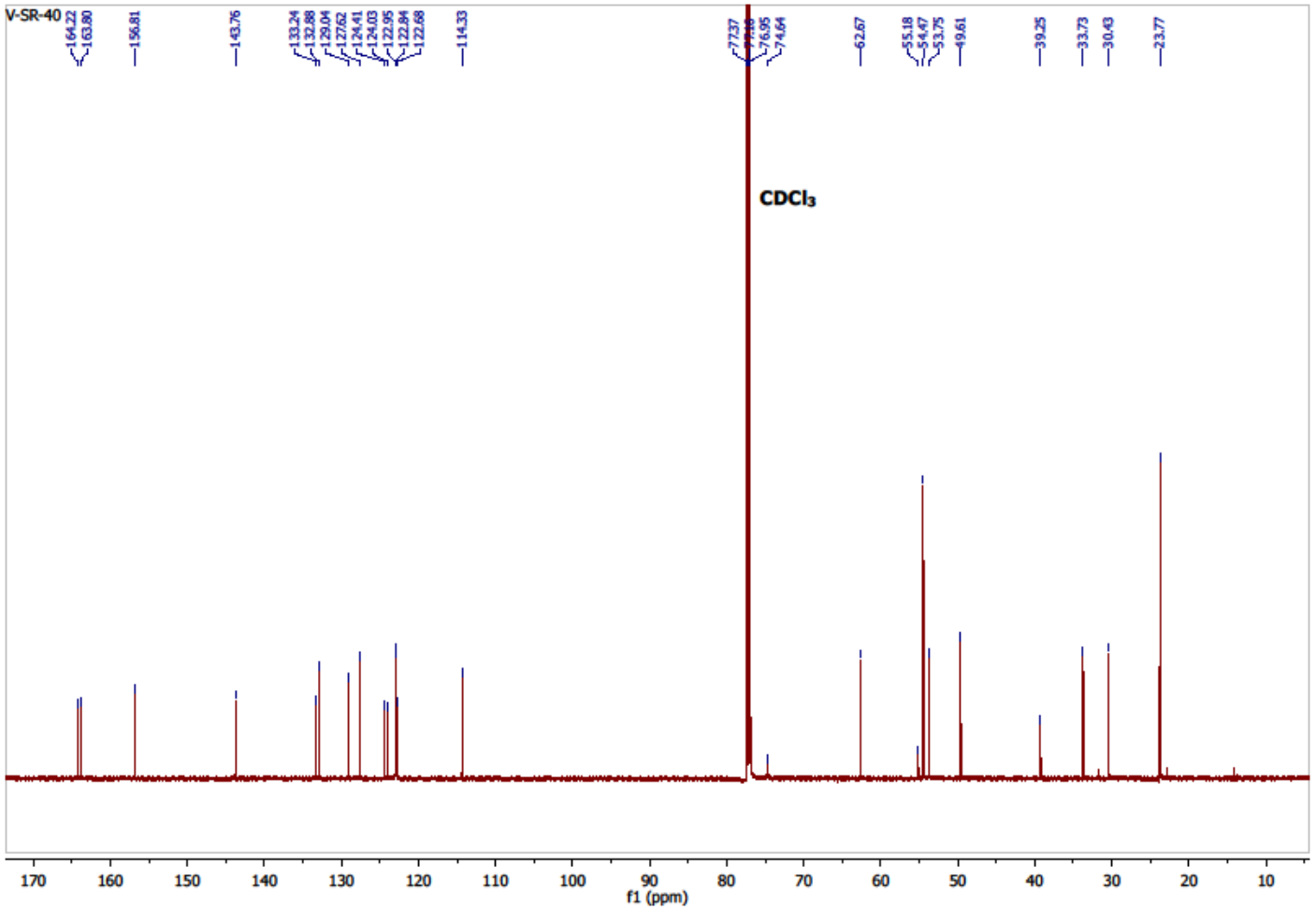

Figure S80. ^{13}C NMR spectrum of **20**.

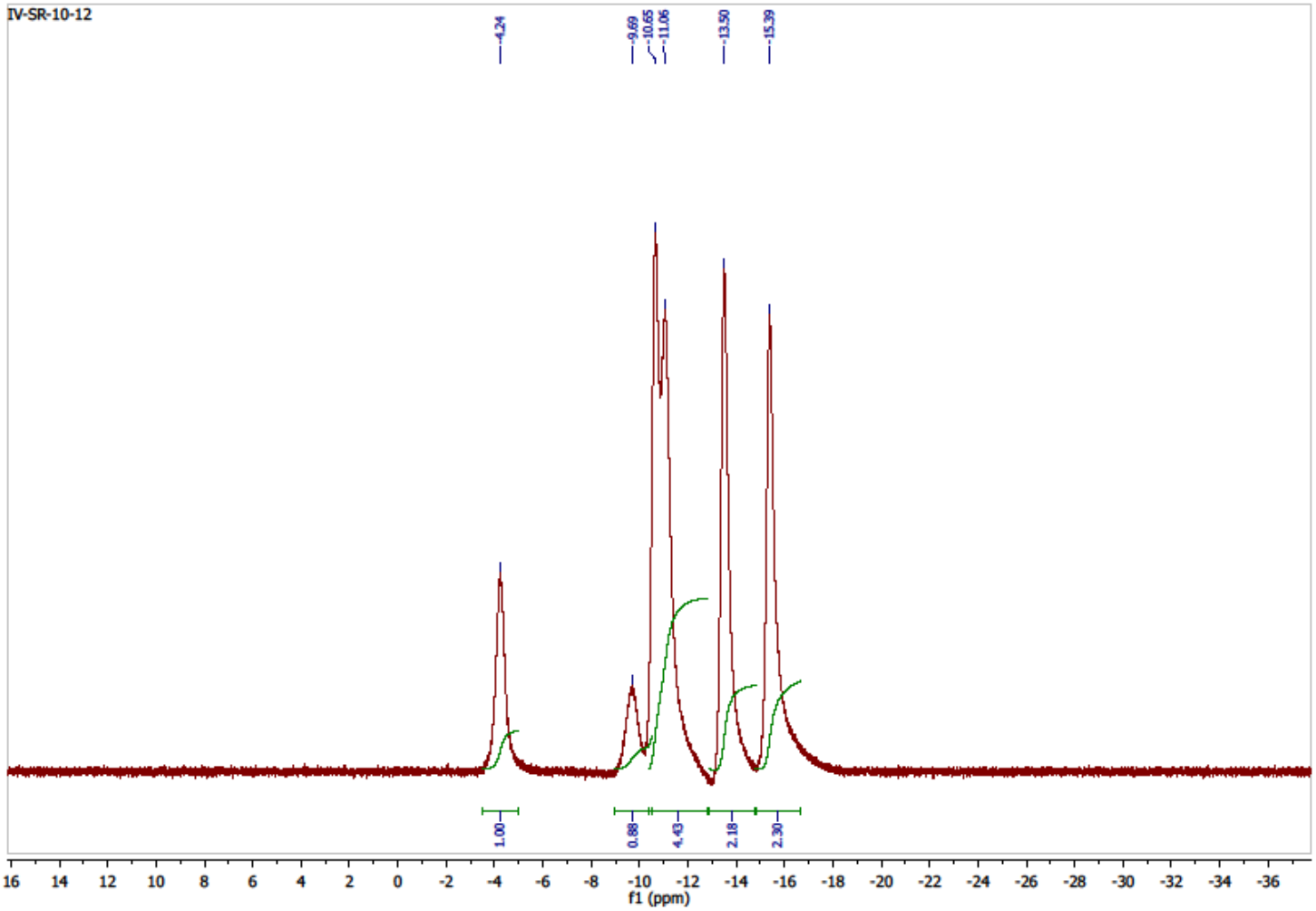

Figure S81. ^{11}B NMR {^{1}H BB} spectrum of **20**.

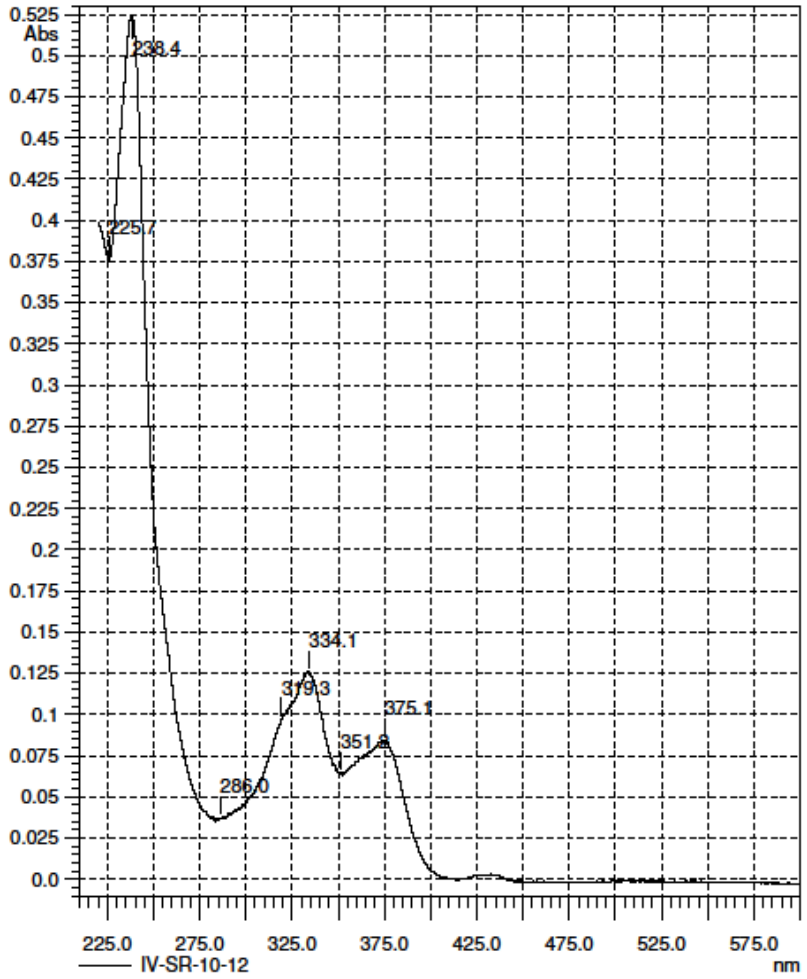

Figure S82. UV spectrum of **20**.

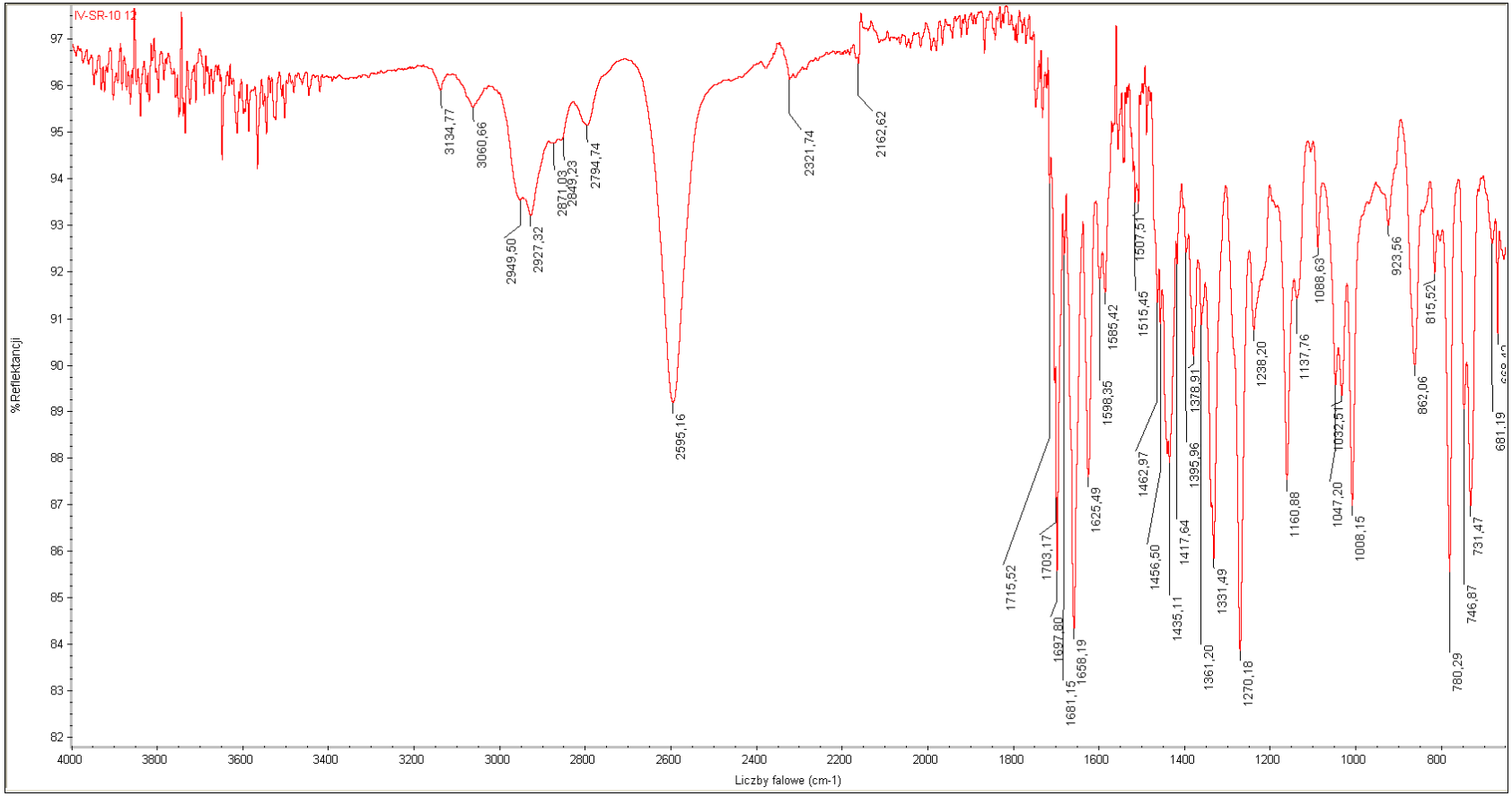

Figure S83. IR spectrum of **20**.

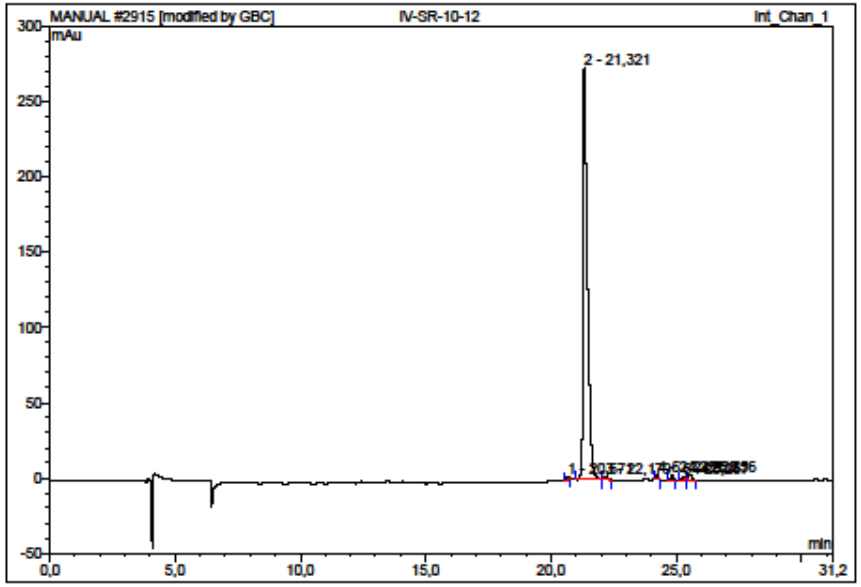

No.	Ret.Time min	Peak Name	Height mAu	Area mAu*min	Rel.Area %	Amount	Type
1	20,67	n.a.	2,376	0,234	0,40	n.a.	BMB*
2	21,32	n.a.	272,962	56,512	96,19	n.a.	BMB*
3	22,18	n.a.	1,980	0,366	0,62	n.a.	BMB*
4	24,25	n.a.	2,976	0,286	0,49	n.a.	BMB*
5	24,82	n.a.	2,954	0,408	0,69	n.a.	BMB*
6	25,27	n.a.	2,065	0,283	0,48	n.a.	BMb*
7	25,56	n.a.	3,923	0,659	1,12	n.a.	bMB*
Total:			289,235	58,748	100,00	0,000	

Figure S84. HPLC analysis of **20**.

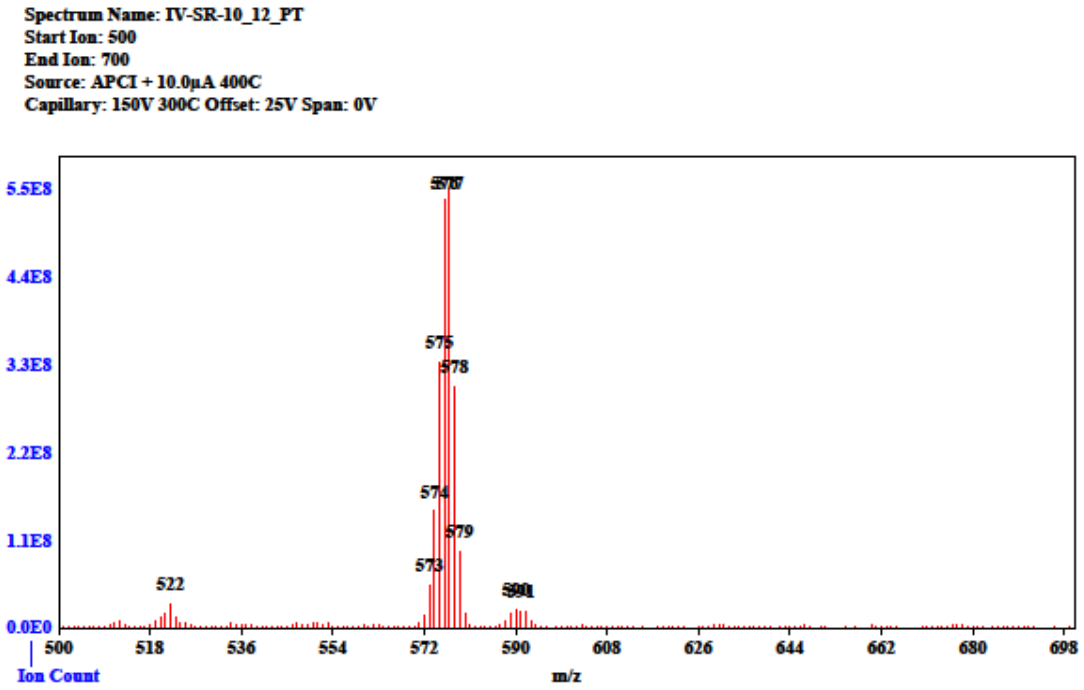

Figure S85. MS spectrum of **20**.

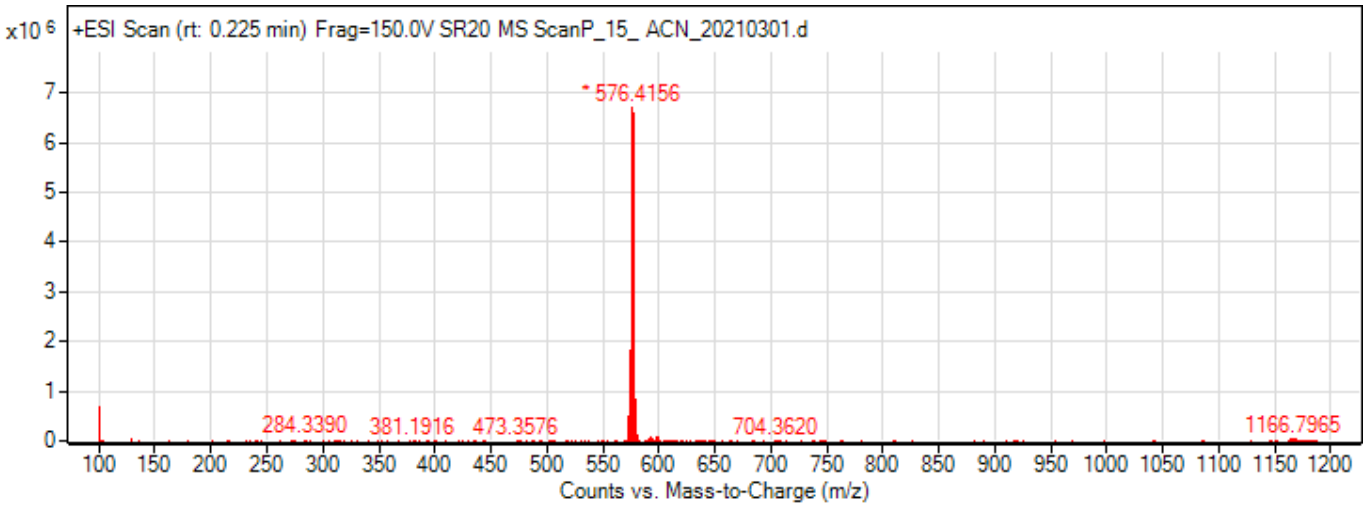

Figure S86. HRMS spectrum of **20**.

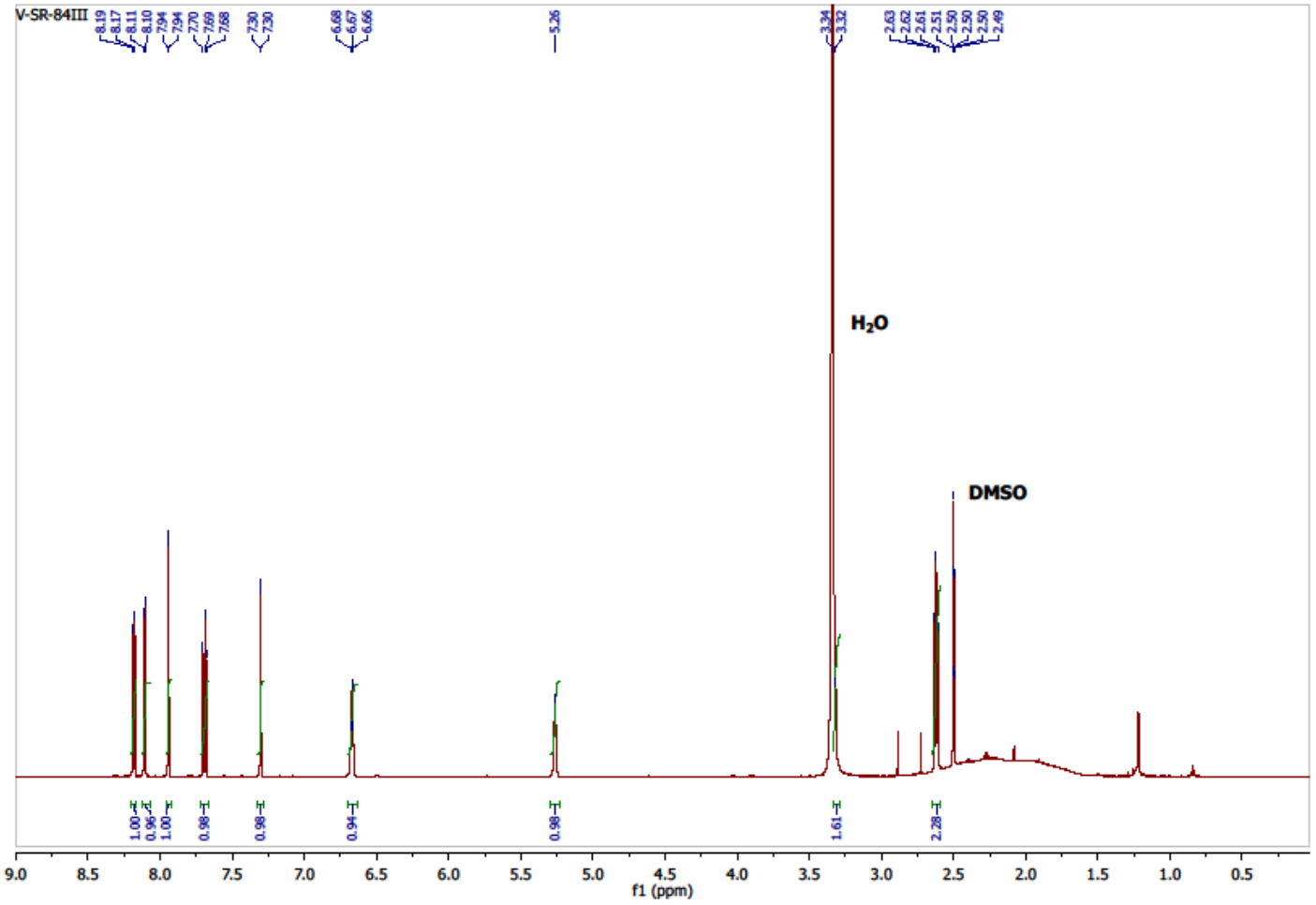

Figure S87. ^{1}H NMR spectrum of **31**.

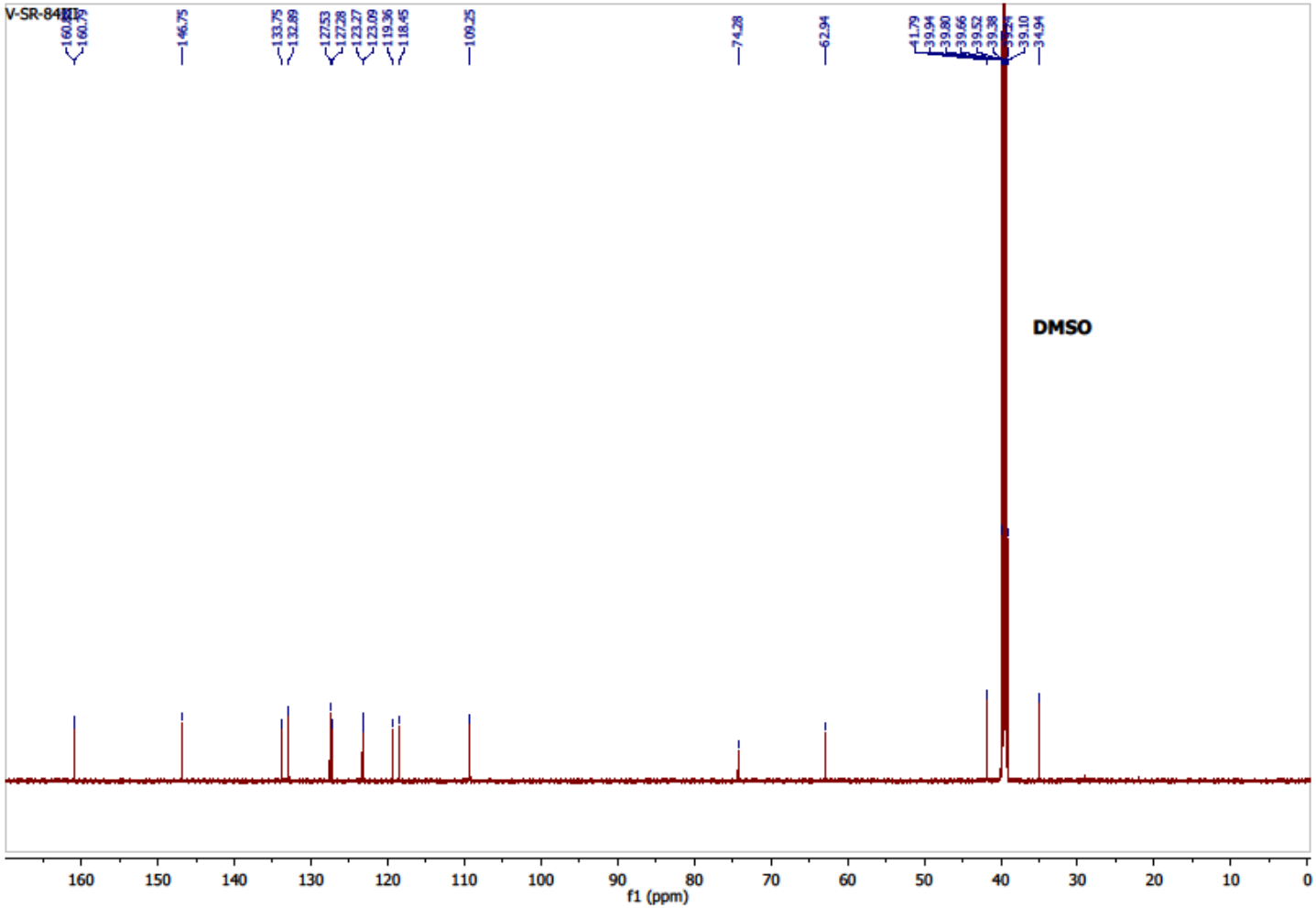

Figure S88. ^{13}C NMR spectrum of **31**.

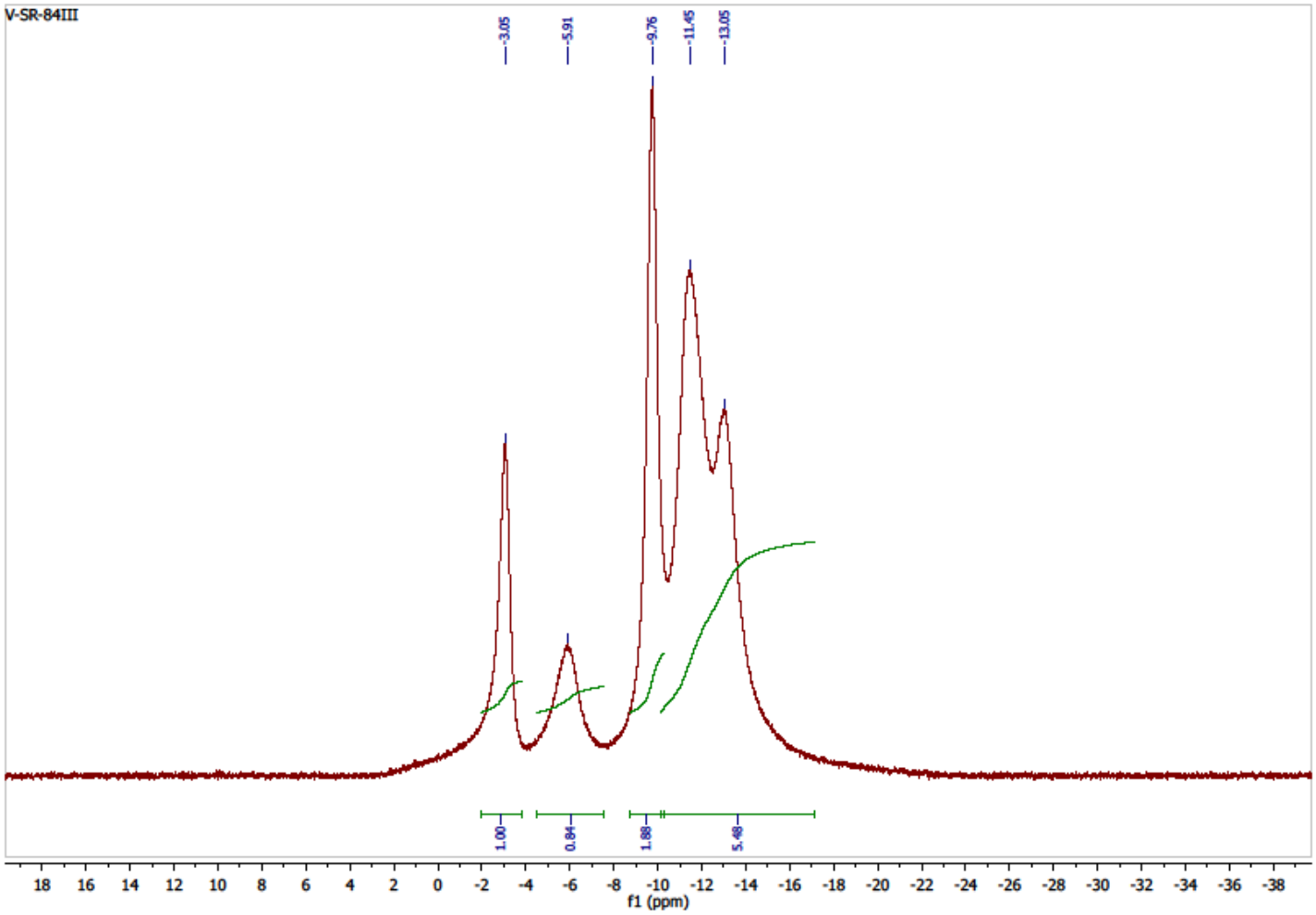

Figure S89. ^{11}B NMR $\{^{1}H$ BB$\}$ spectrum of **31**.

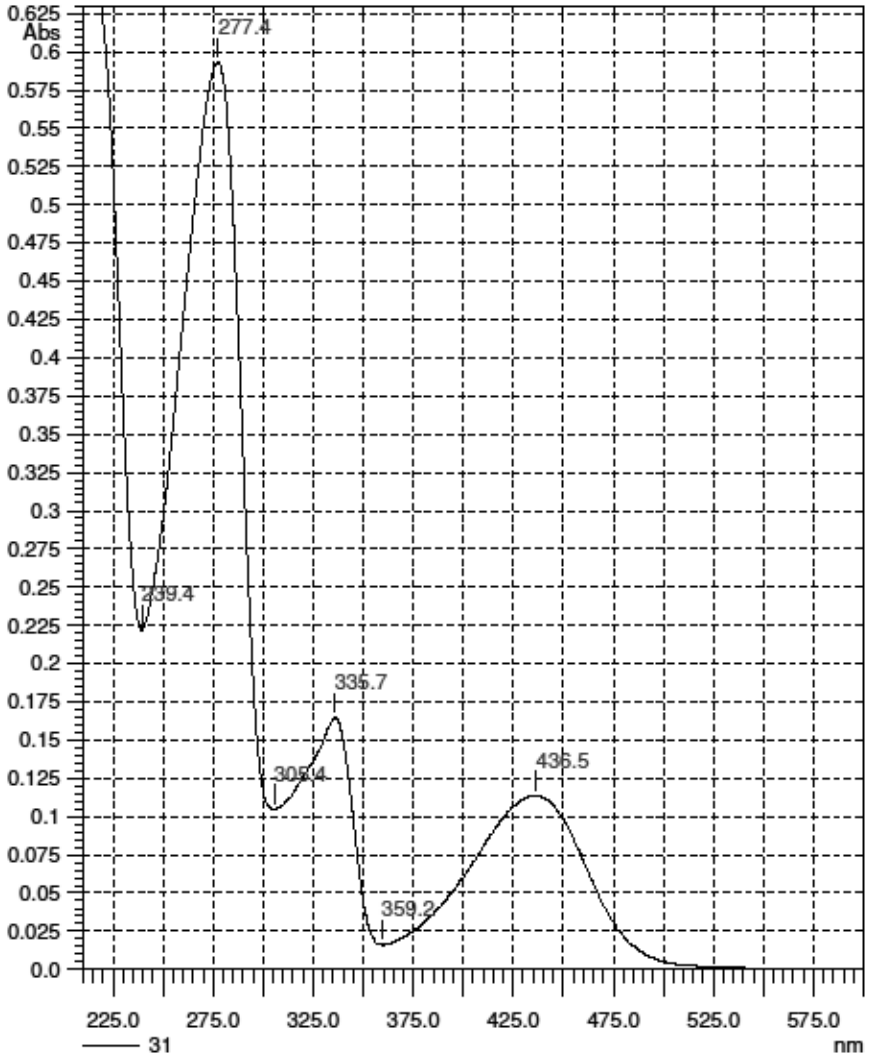

Figure S90. UV spectrum of **31**.

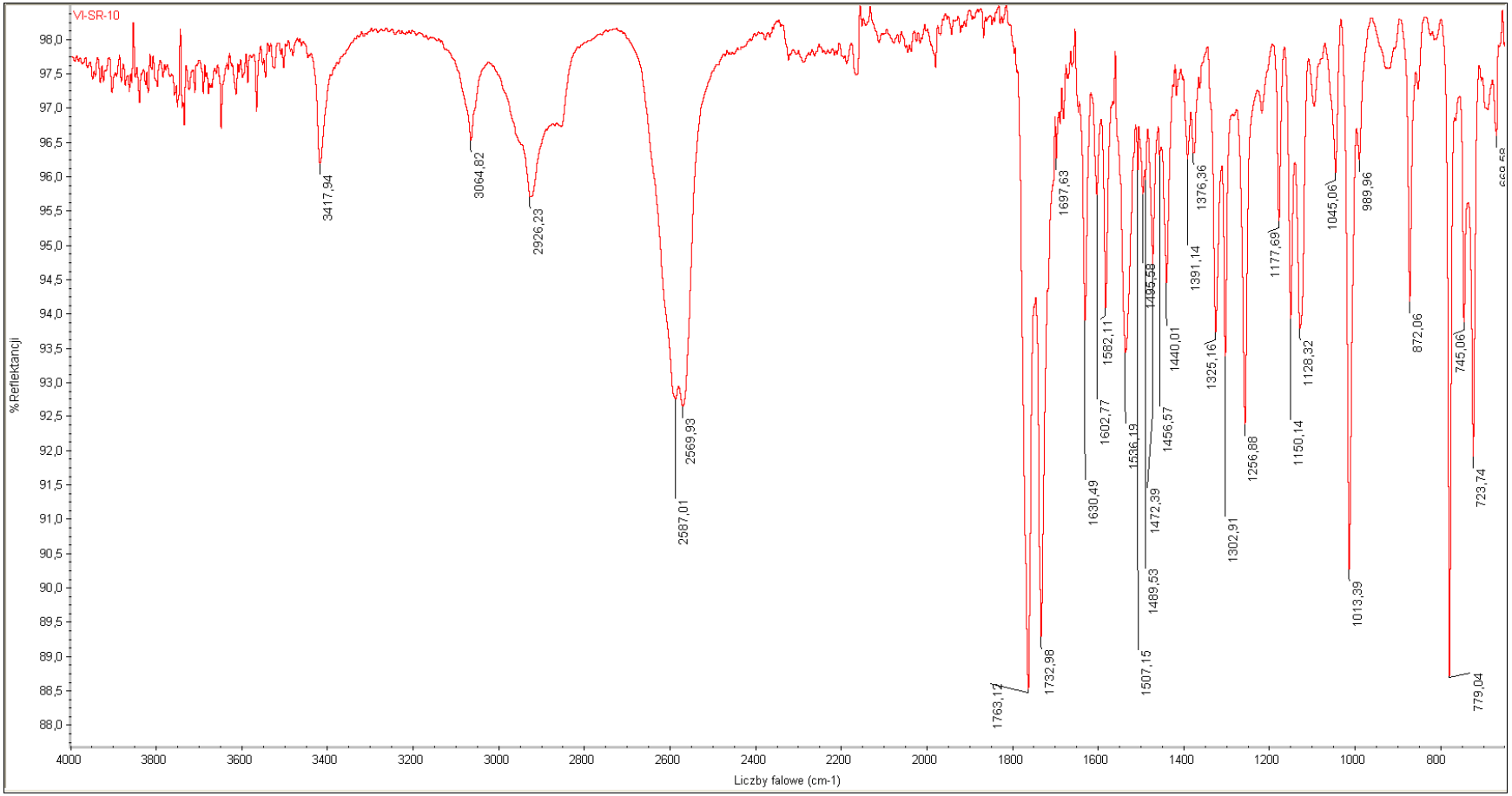

Figure S91. IR spectrum of **31**.

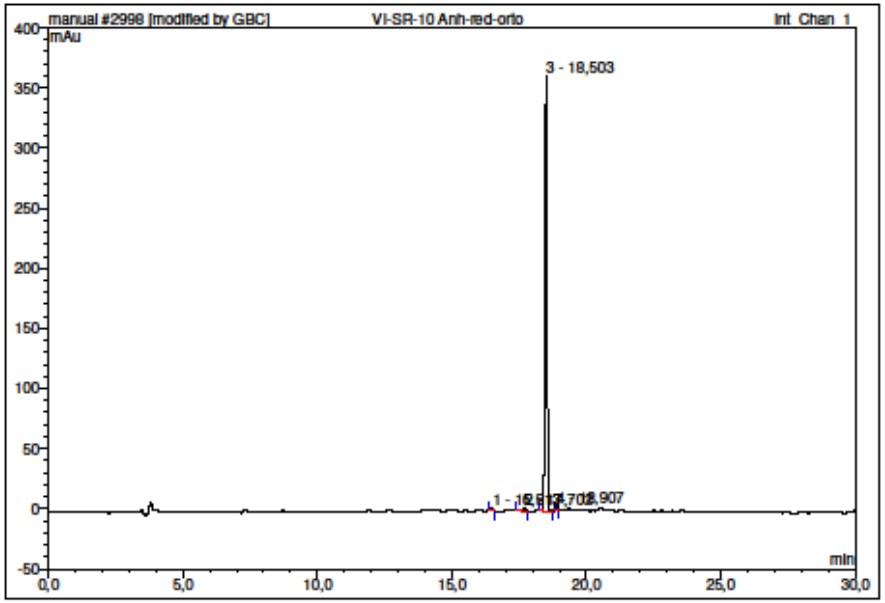

No.	Ret.Time min	Peak Name	Height mAu	Area mAu*min	Rel.Area %	Amount	Type
1	16,51	n.a.	1,476	0,158	0,49	n.a.	BMB*
2	17,70	n.a.	1,962	0,465	1,44	n.a.	BMB*
3	18,50	n.a.	361,479	31,441	97,33	n.a.	BMB
4	18,91	n.a.	3,089	0,240	0,74	n.a.	BMB*
Total:			368,005	32,304	100,00	0,000	

Figure S92. HPLC analysis of **31**.

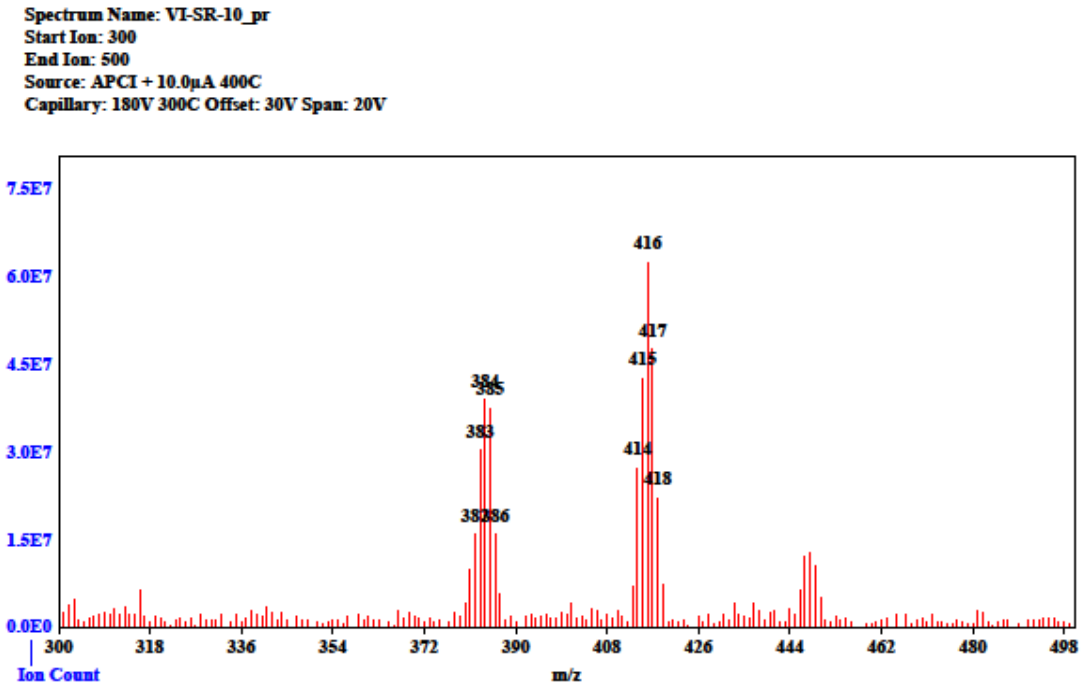

Figure S93. MS spectrum of **31**.

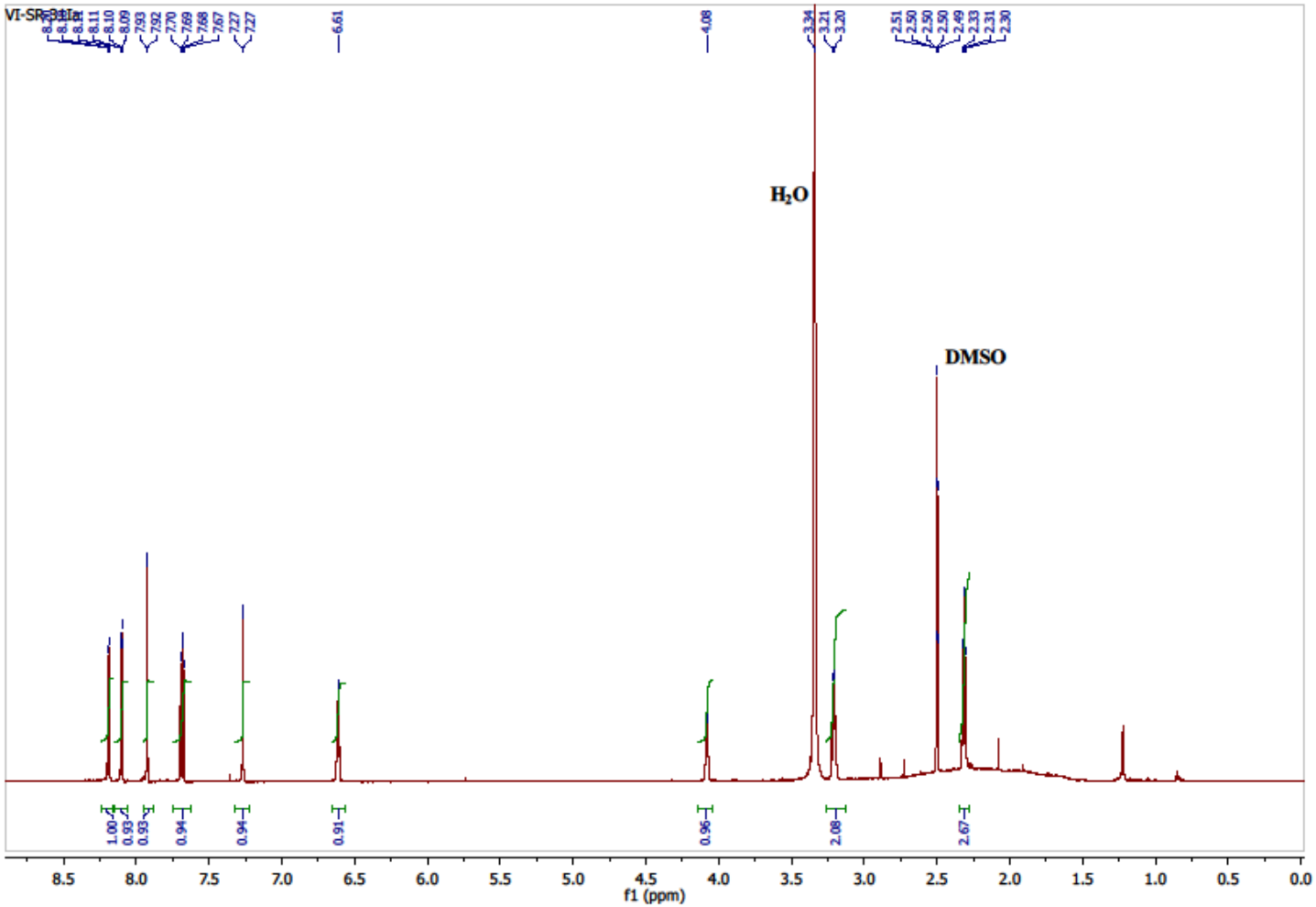

Figure S94. ^{1}H NMR spectrum of **32**.

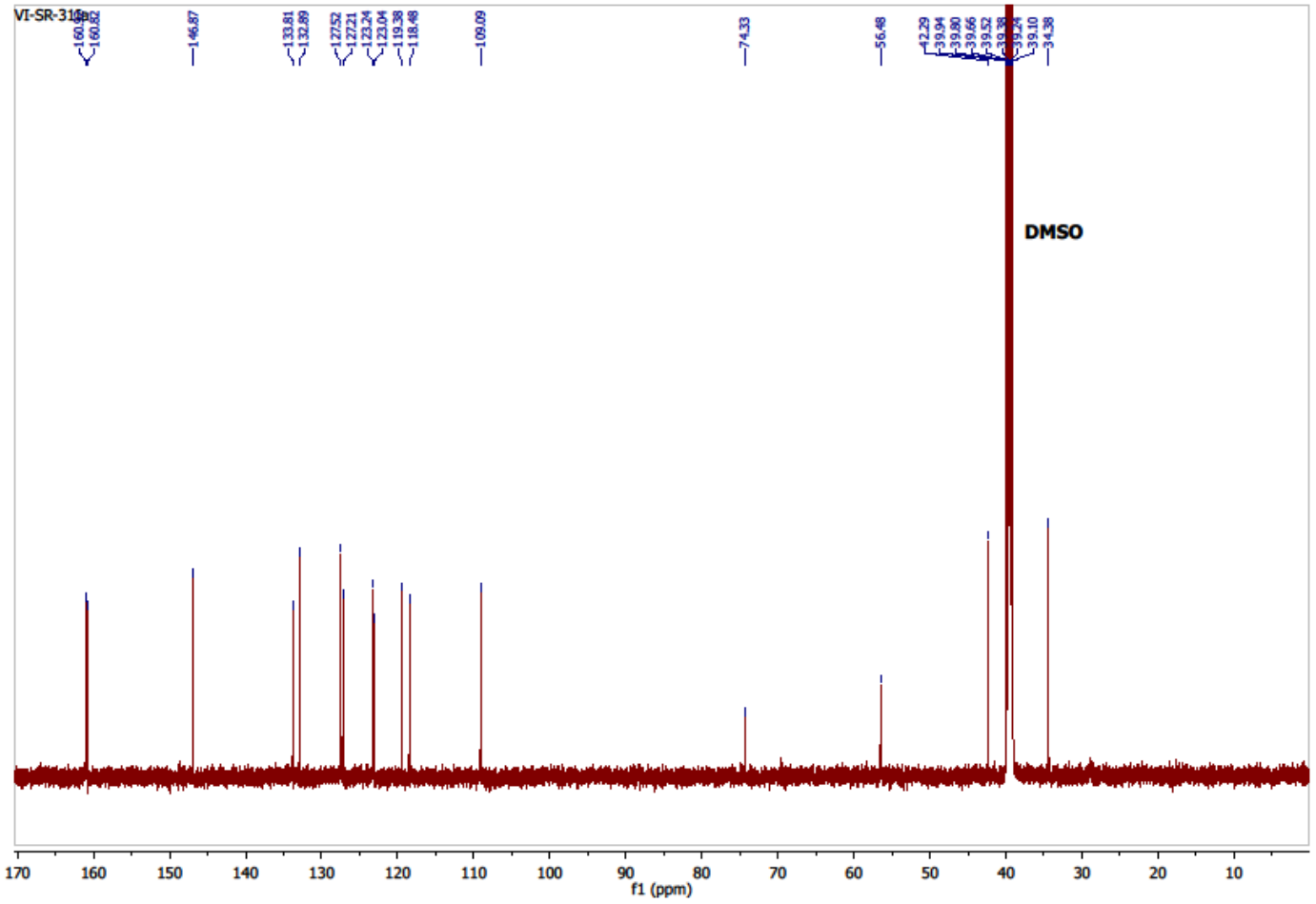

Figure S95. ^{13}C NMR spectrum of **32**.

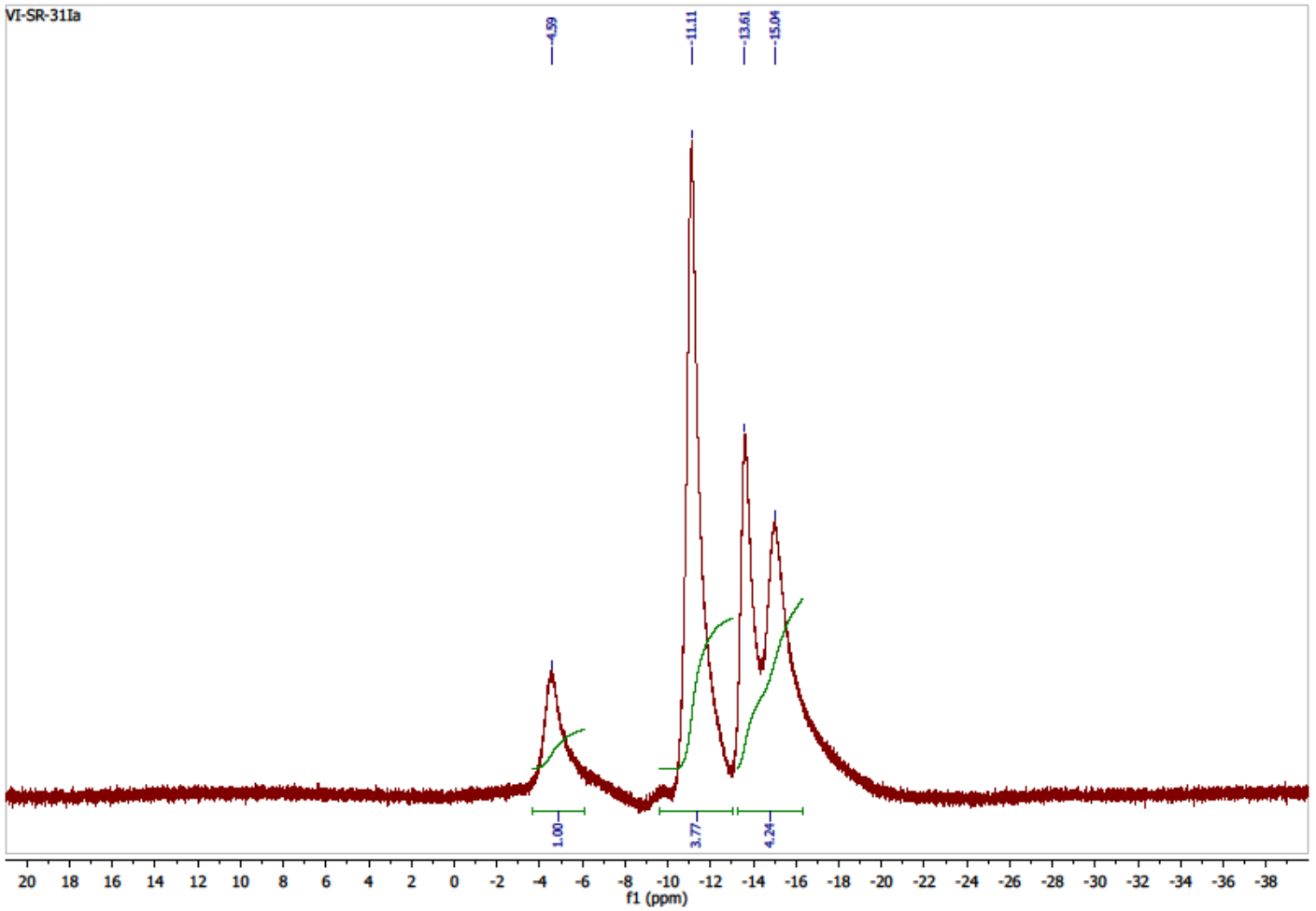

Figure S96. ^{11}B NMR {^{1}H BB} spectrum of **32**.

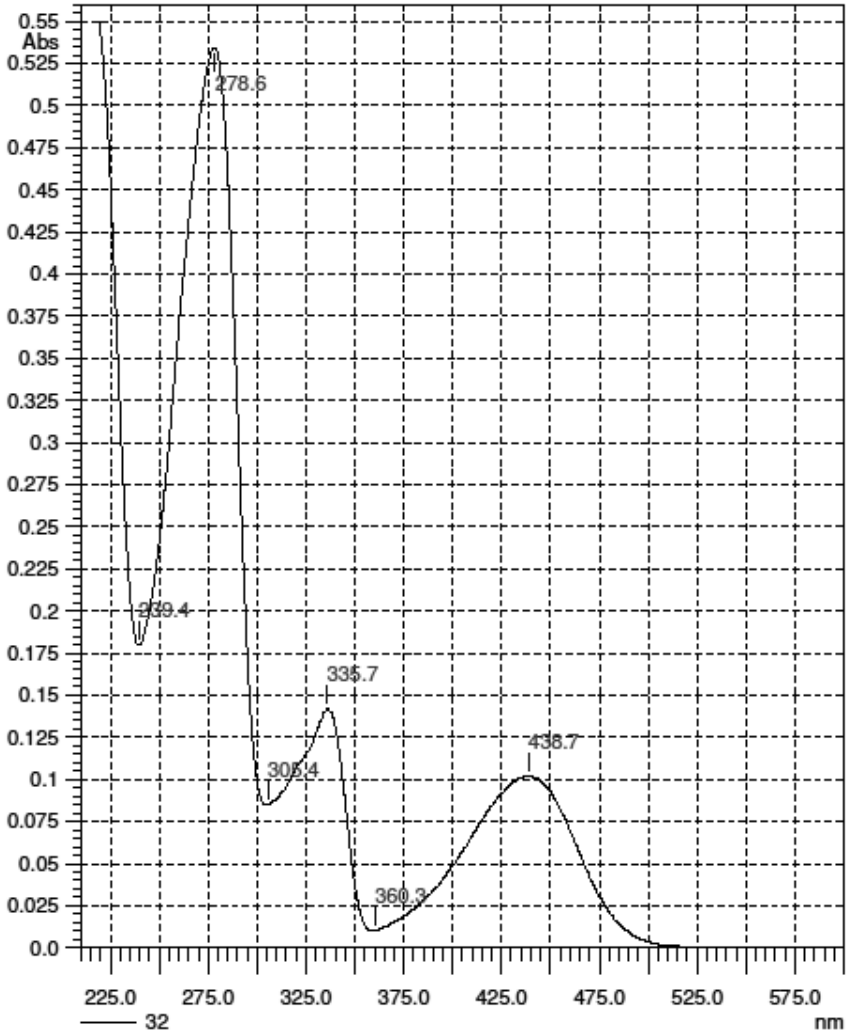

Figure S97. UV spectrum of **32**.

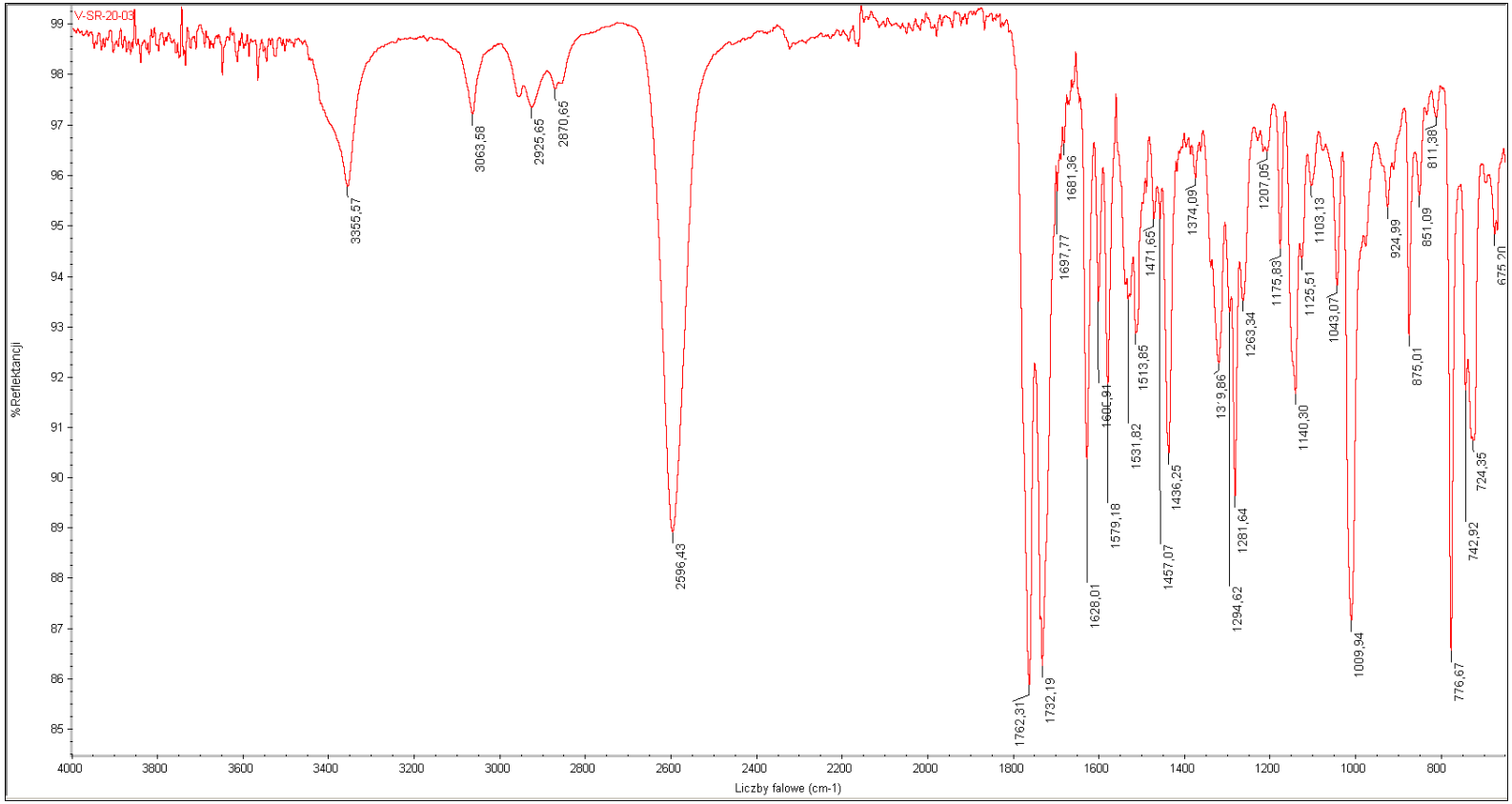

Figure S98. IR spectrum of **32**.

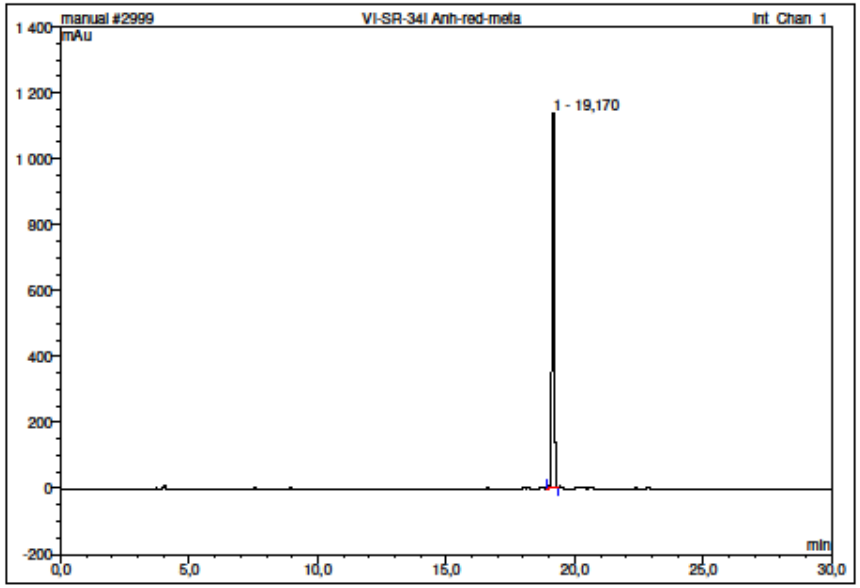

No.	Ret.Time min	Peak Name	Height mAu	Area mAu*min	Rel.Area %	Amount	Type
1	19,17	n.a.	1137,513	110,542	100,00	n.a.	BMB
Total:			1137,513	110,542	100,00	0,000	

Figure S99. HPLC analysis of **32**.

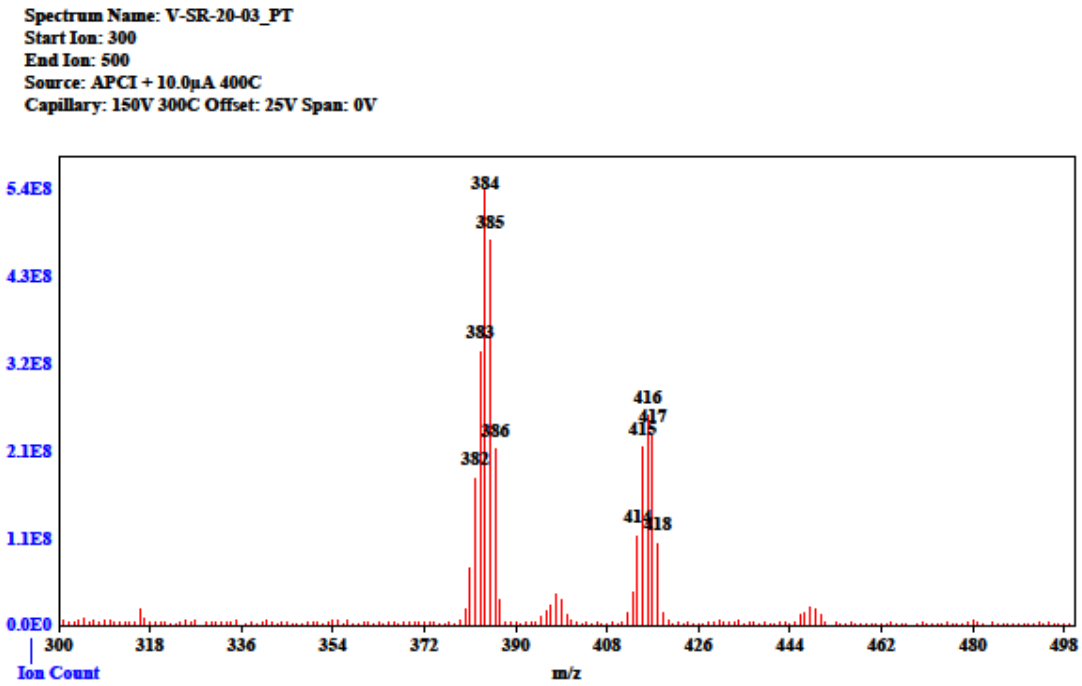

Figure S100. MS spectrum of **32**.

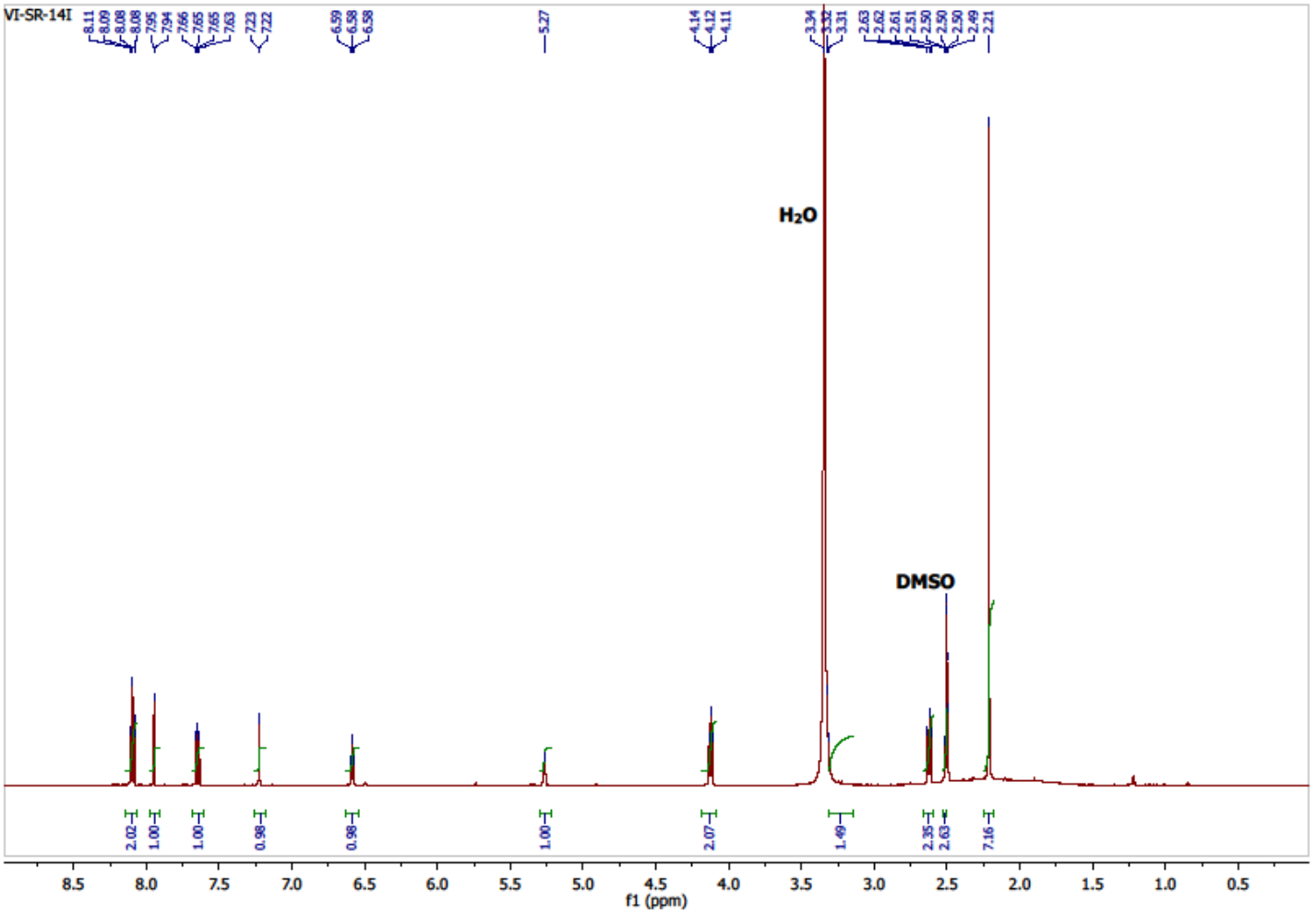

Figure S101. ^{1}H NMR spectrum of **33**.

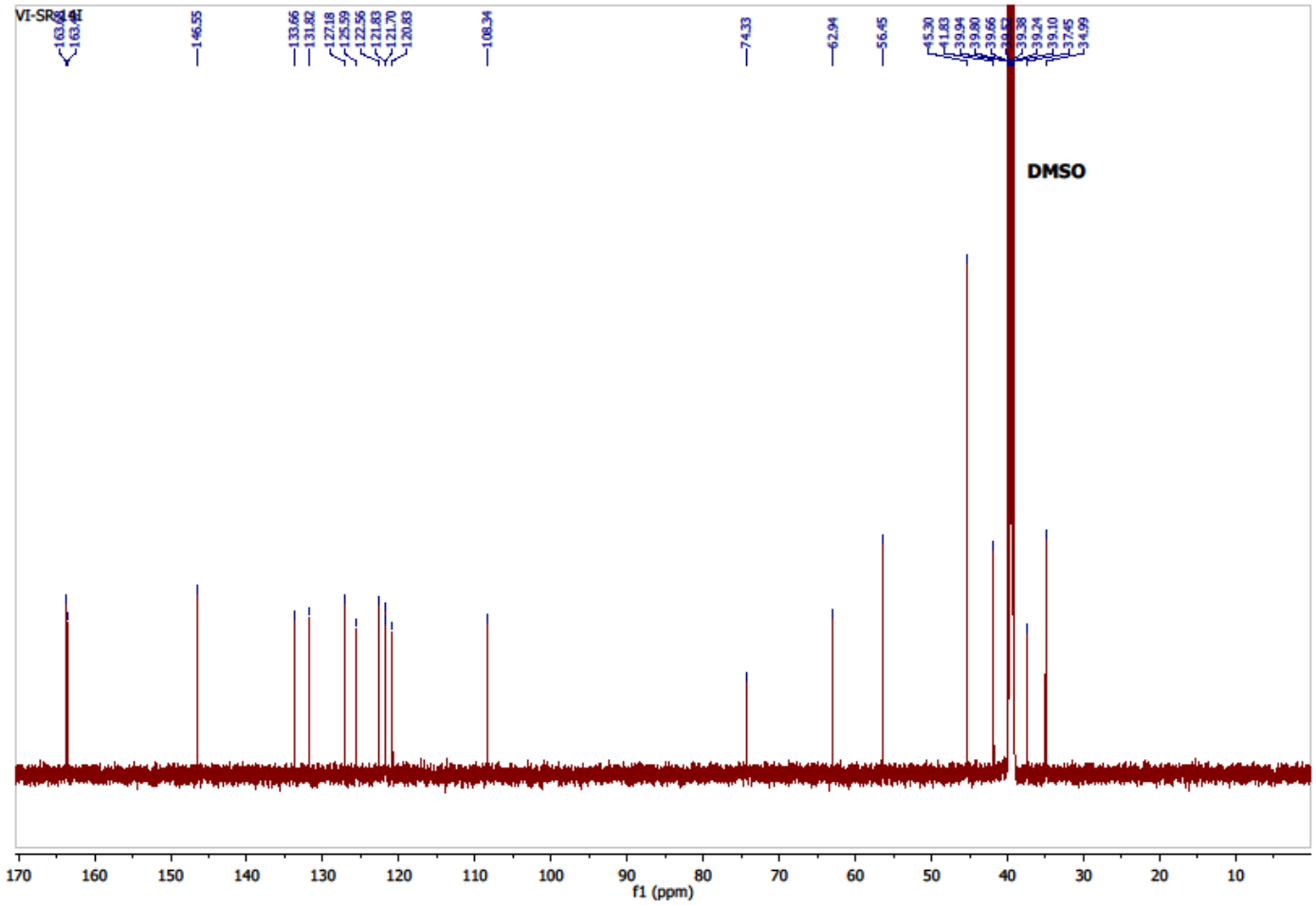

Figure S102. ^{13}C NMR spectrum of **33**.

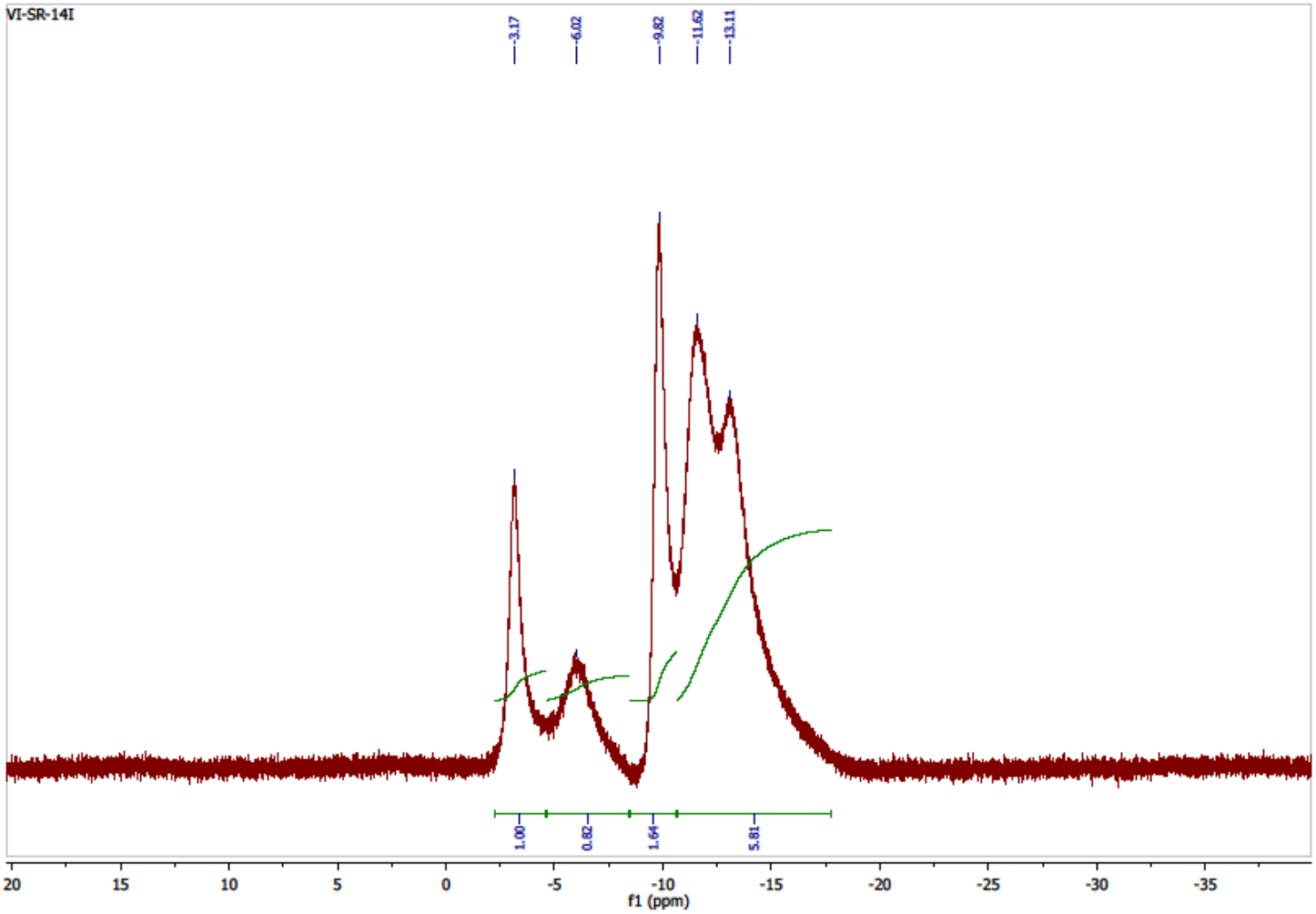

Figure S103. ^{11}B NMR {^{1}H BB} spectrum of **33**.

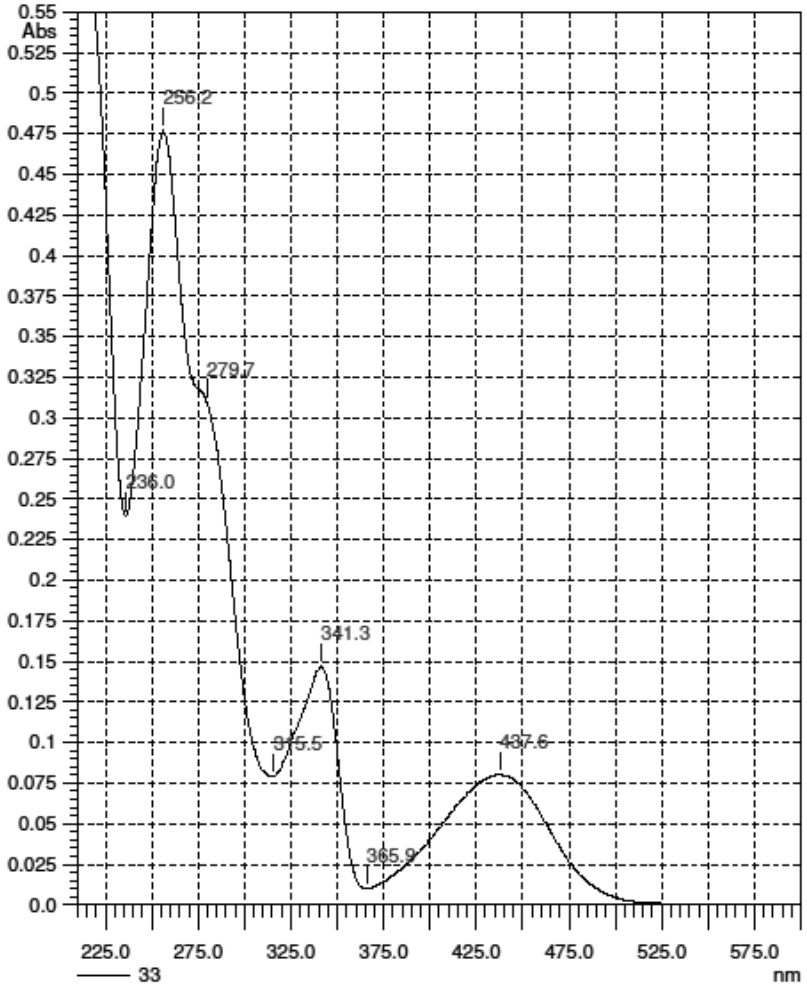

Figure S104. UV spectrum of **33**.

Figure S105. IR spectrum of **33**.

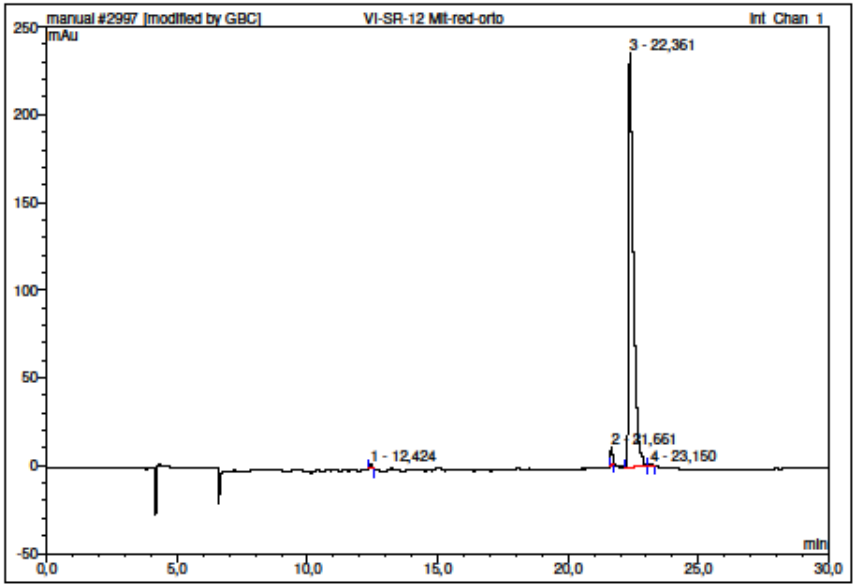

No.	Ret.Time min	Peak Name	Height mAu	Area mAu*min	Rel.Area %	Amount	Type
1	12,42	n.a.	2,295	0,298	0,58	n.a.	BMB*
2	21,66	n.a.	10,037	0,950	1,85	n.a.	BMB*
3	22,36	n.a.	235,948	49,811	97,15	n.a.	BMB*
4	23,15	n.a.	1,591	0,215	0,42	n.a.	BMB*
Total:			249,872	51,275	100,00	0,000	

Figure S106. HPLC analysis of **33**.

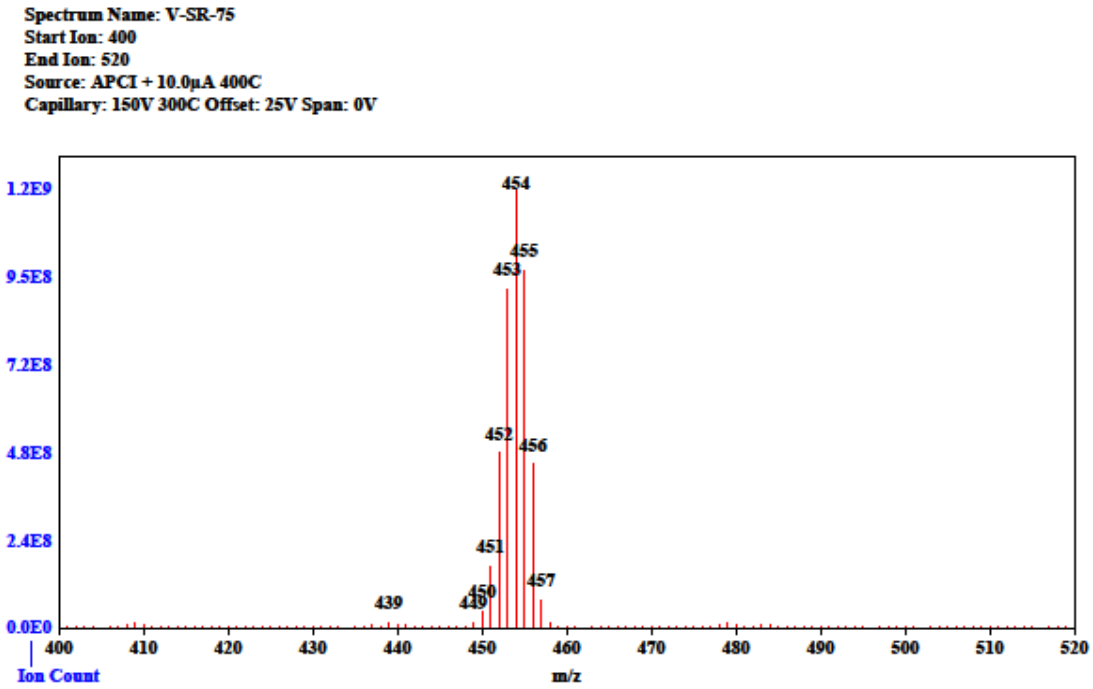

Figure S107. MS spectrum of **33**.

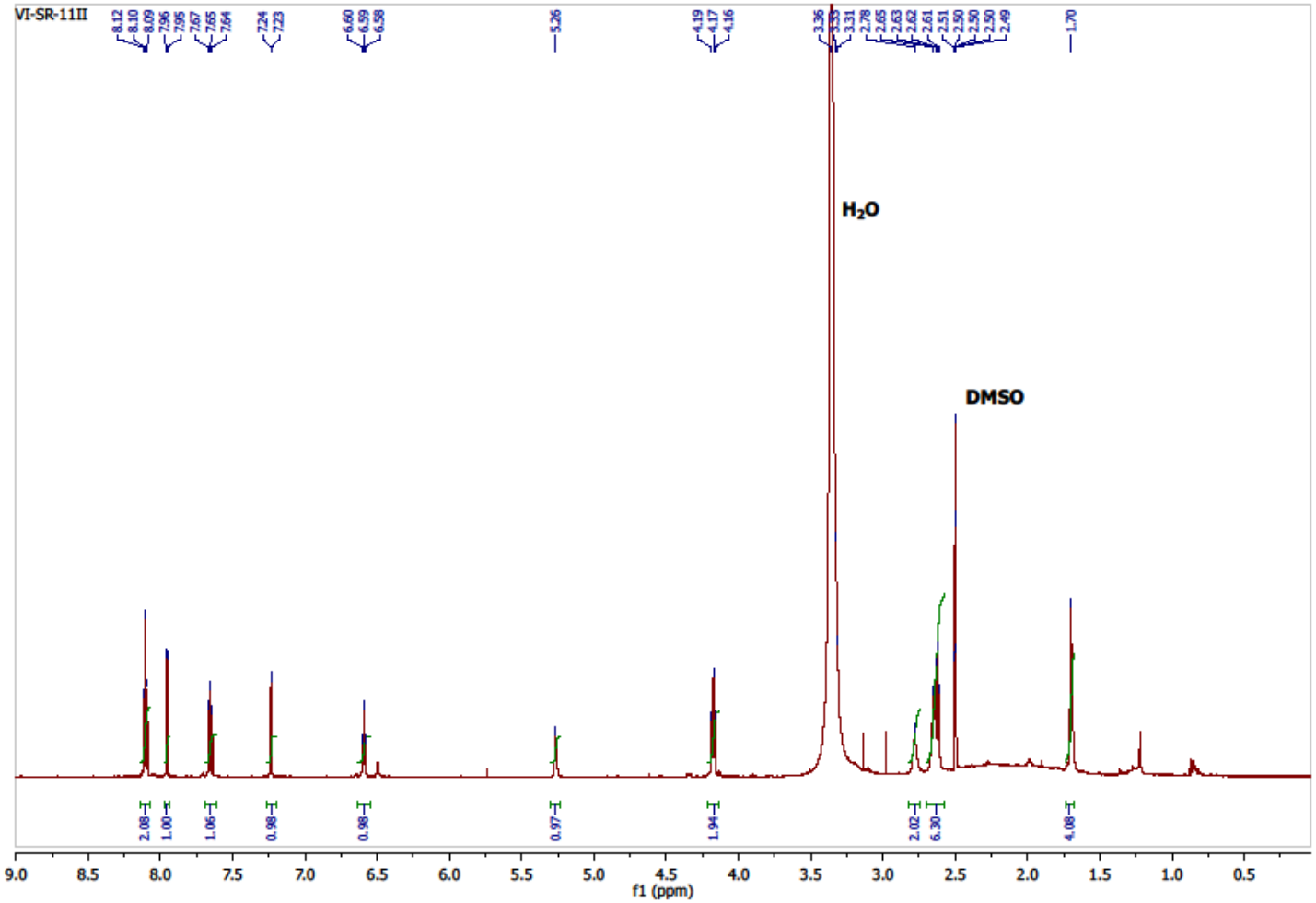

Figure S108. ^{1}H NMR spectrum of **34**.

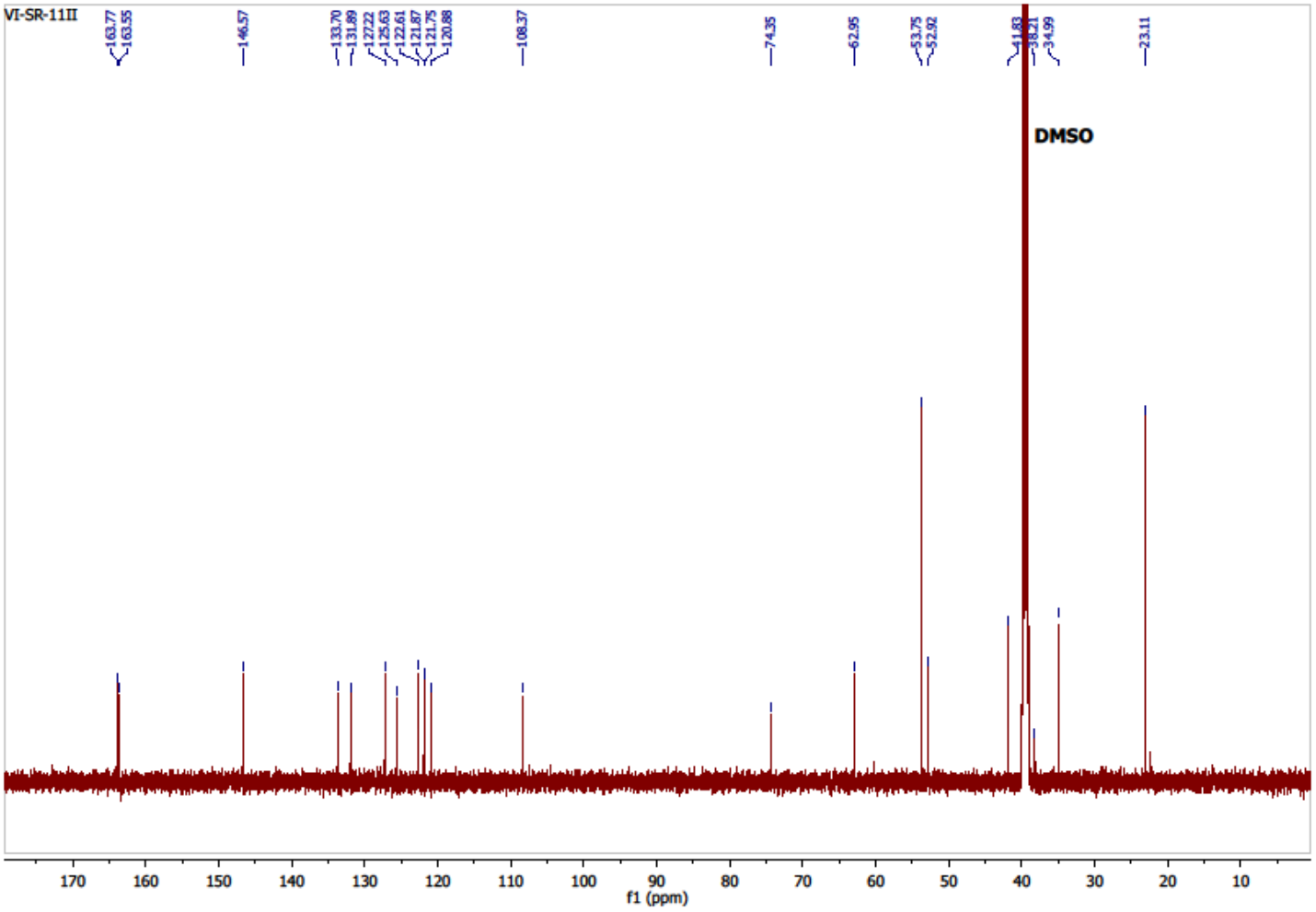

Figure S109. ^{13}C NMR spectrum of **34**.

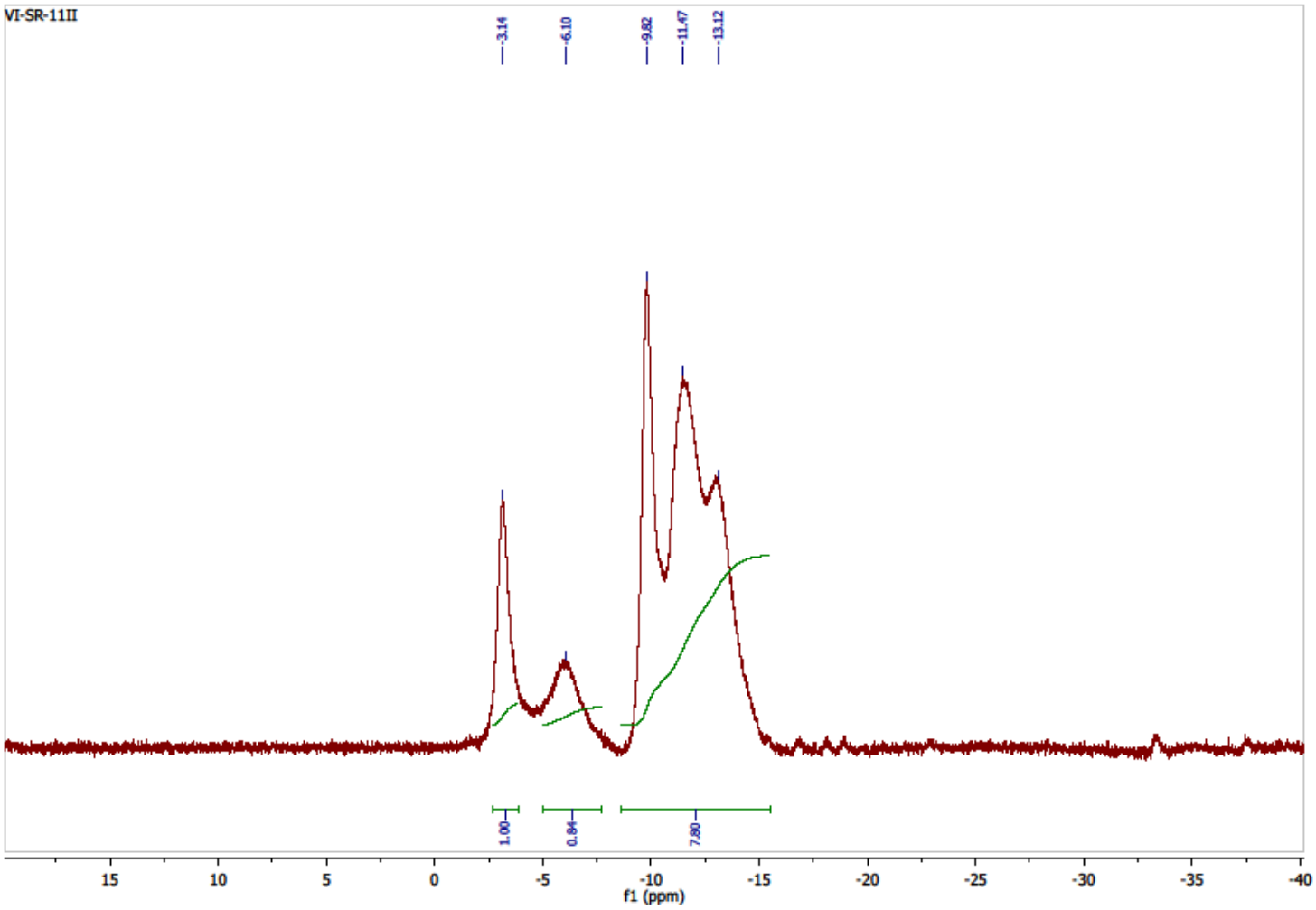

Figure S110. ^{11}B NMR {^{1}H BB} spectrum of **34**.

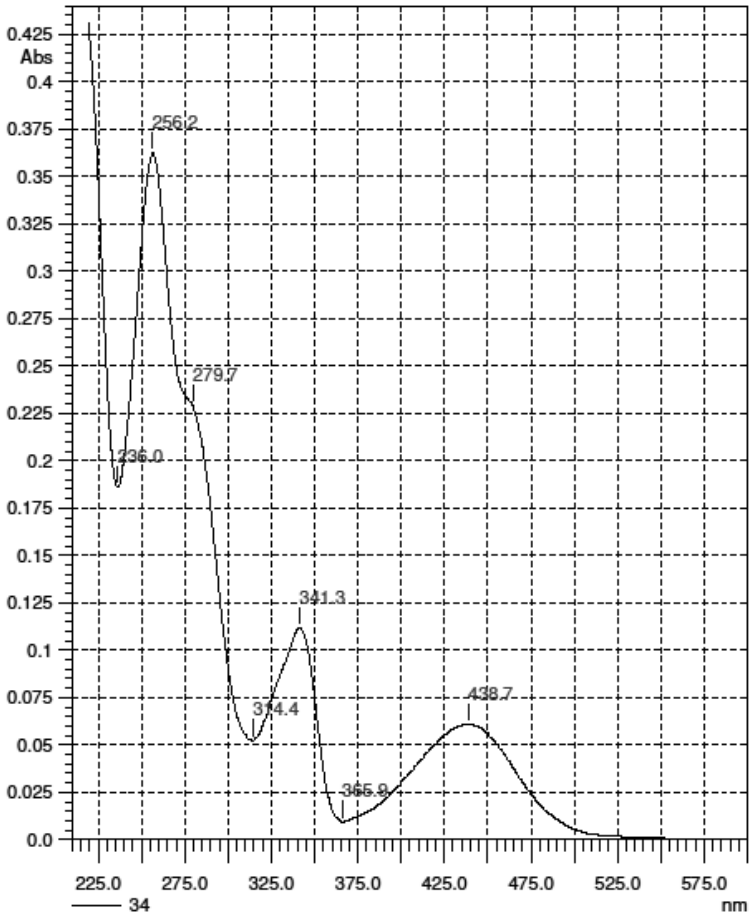

Figure S111. UV spectrum of **34**.

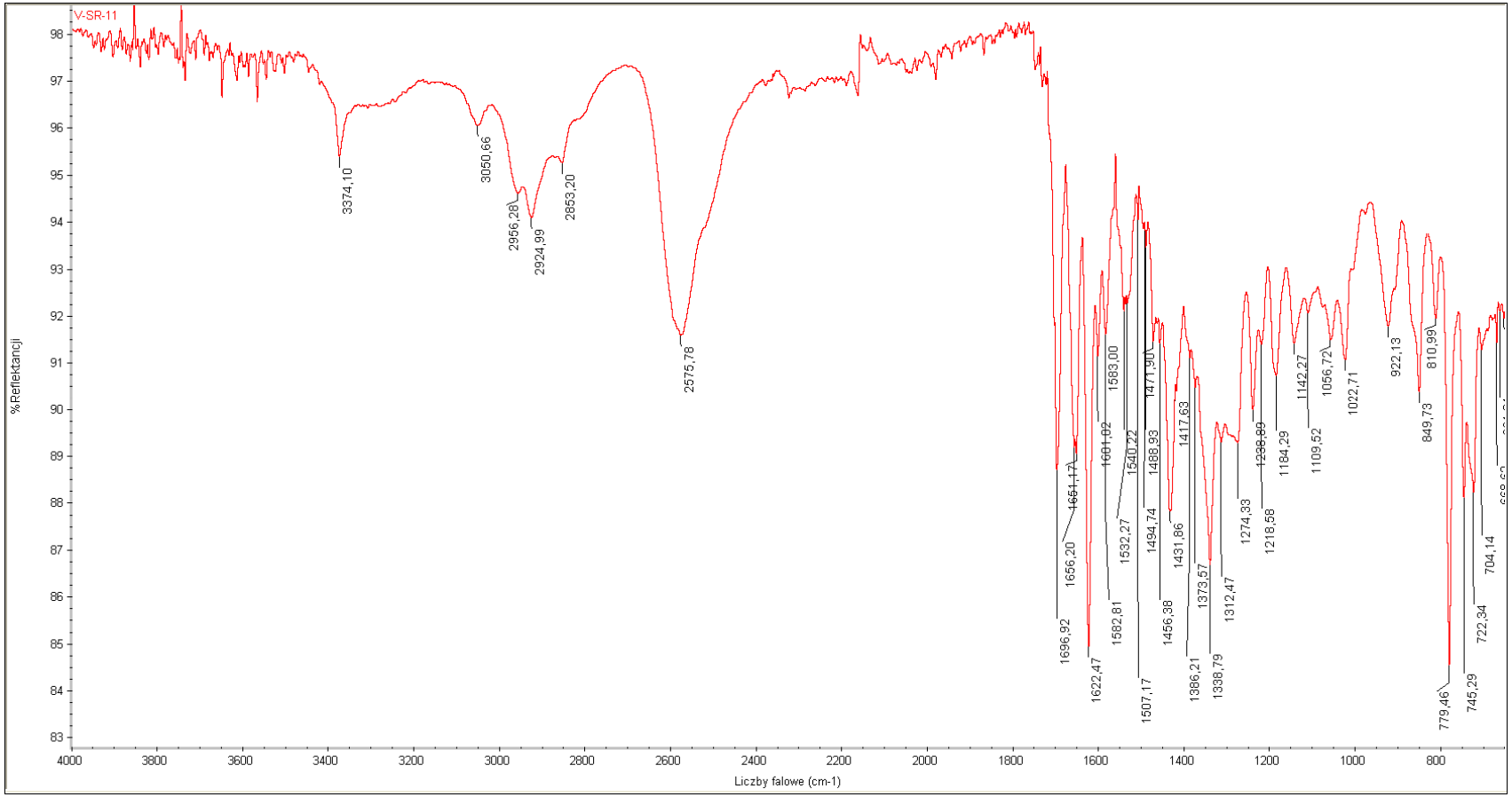

Figure S112. IR spectrum of **34**.

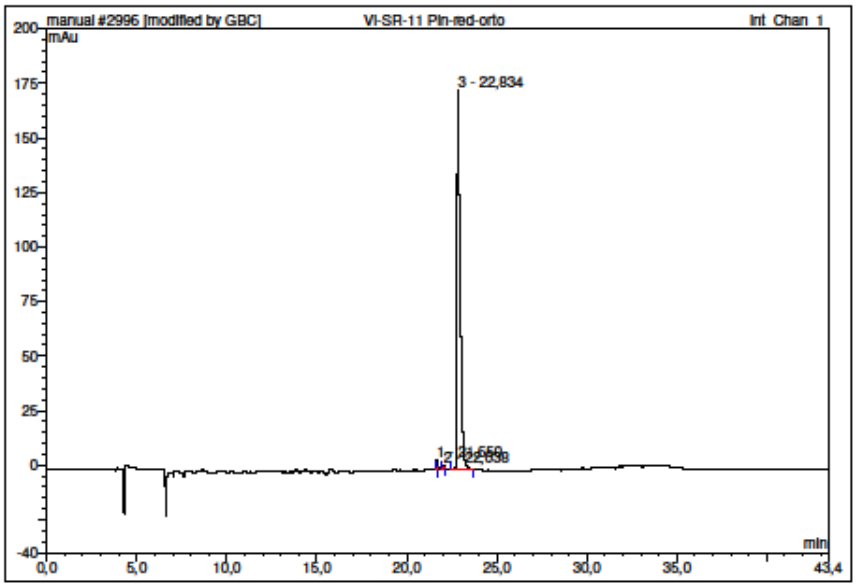

No.	Ret.Time min	Peak Name	Height mAu	Area mAu*min	Rel.Area %	Amount	Type
1	21,65	n.a.	3,876	0,366	1,01	n.a.	BMB*
2	22,04	n.a.	1,402	0,149	0,41	n.a.	BMB*
3	22,83	n.a.	173,815	35,568	98,57	n.a.	BMB
Total:			179,093	36,083	100,00	0,000	

Figure S113. HPLC analysis of **34**.

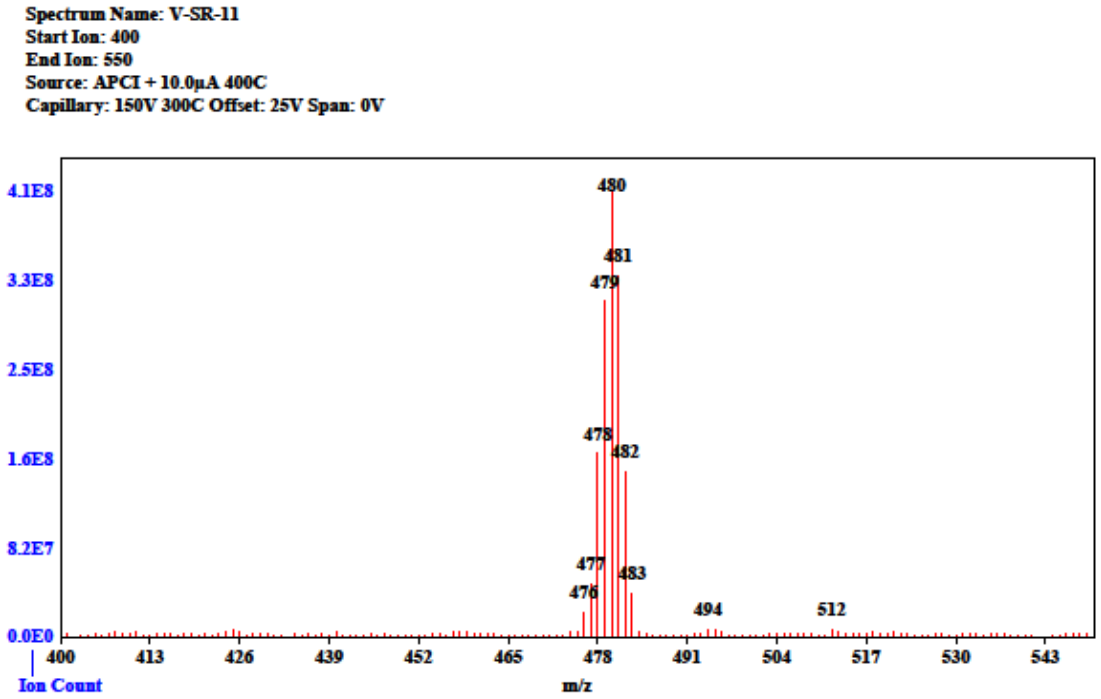

Figure S114. MS spectrum of **34**.

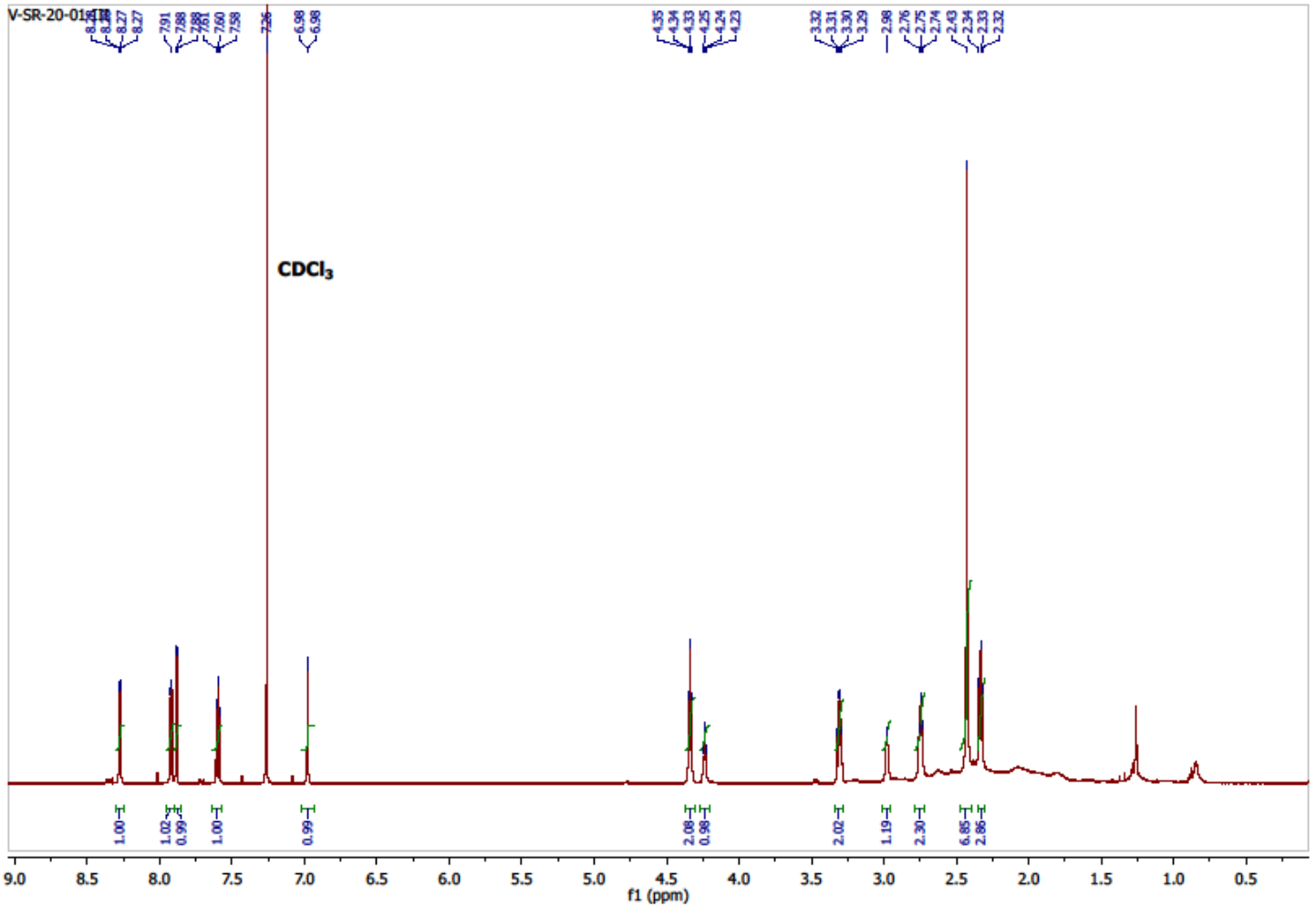

Figure S115. ^{1}H NMR spectrum of **35**.

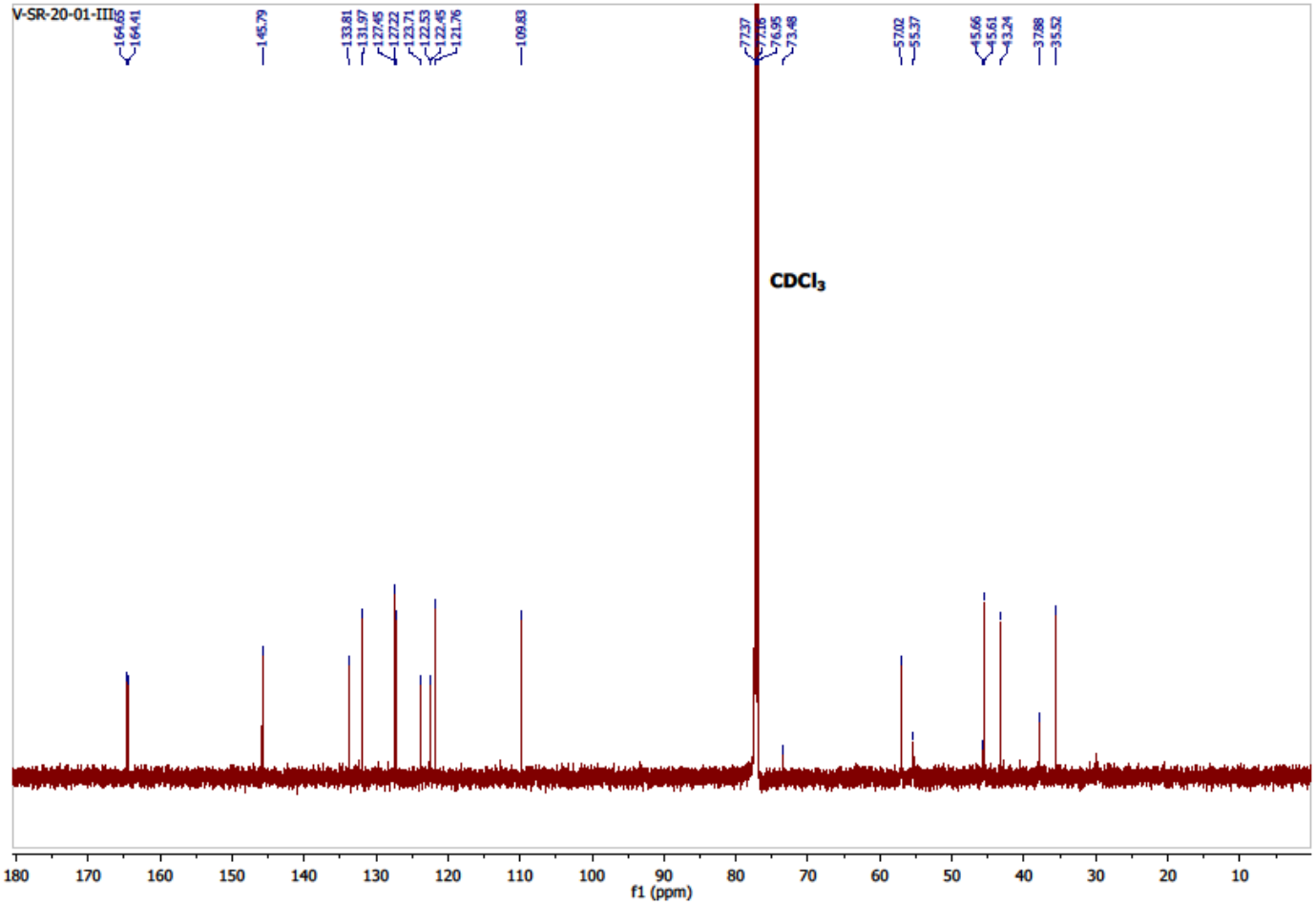

Figure S116. ^{13}C NMR spectrum of **35**.

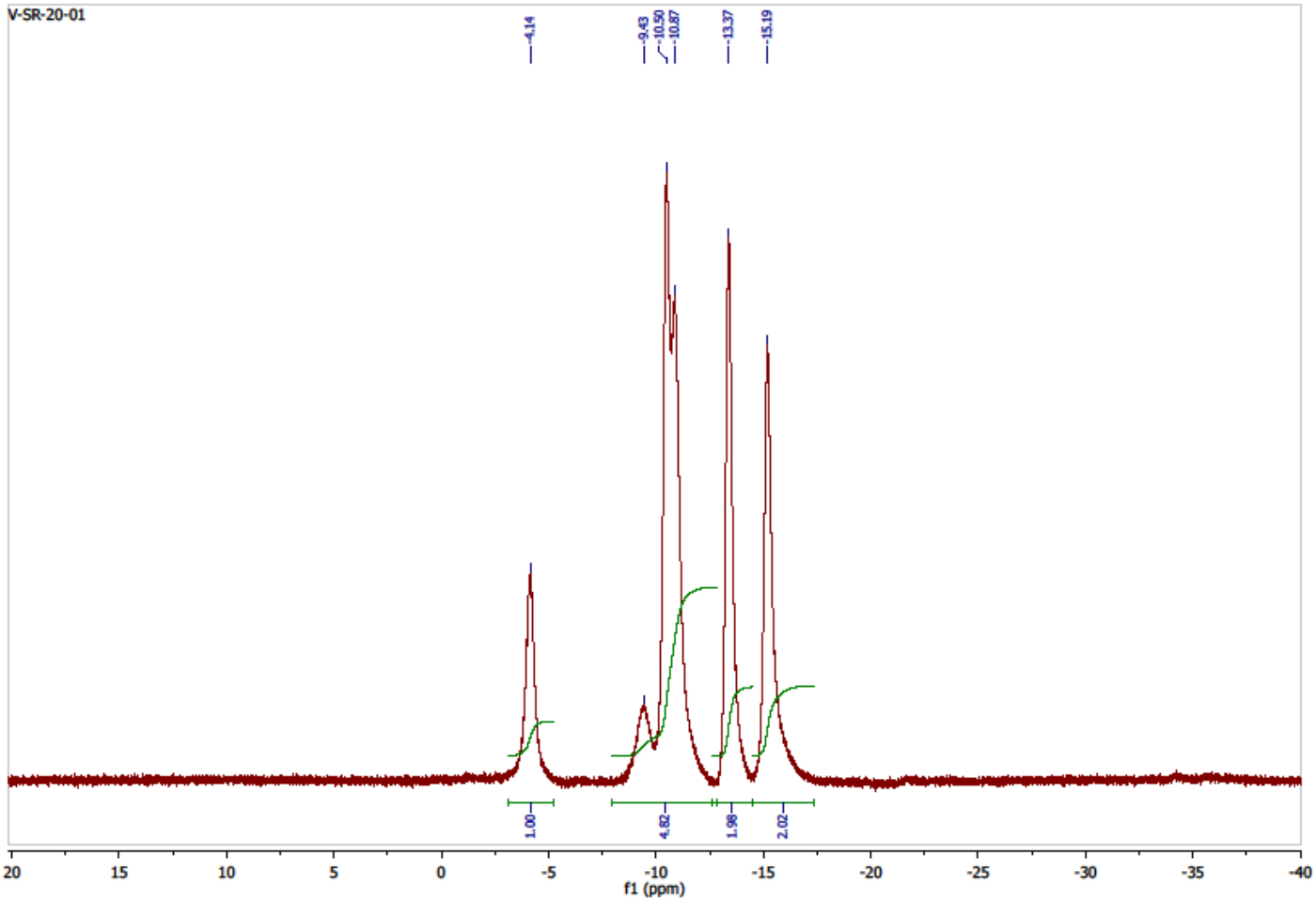

Figure S117. ^{11}B NMR {^{1}H BB} spectrum of **35**.

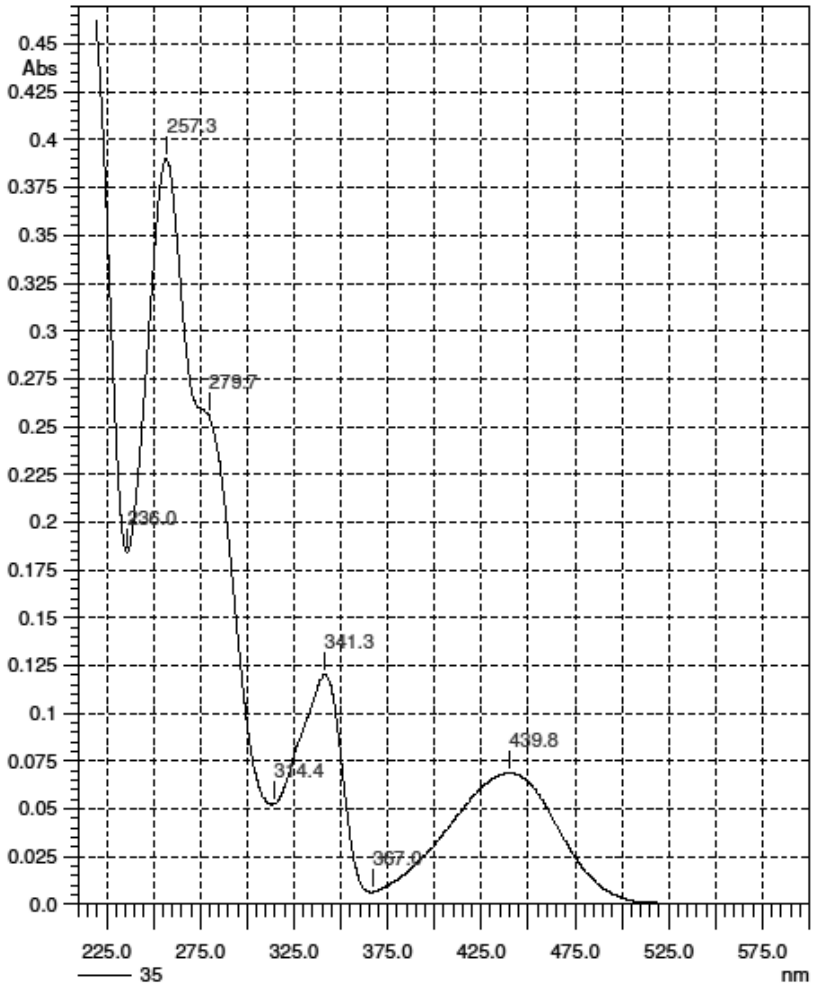

Figure S118. UV spectrum of **35**.

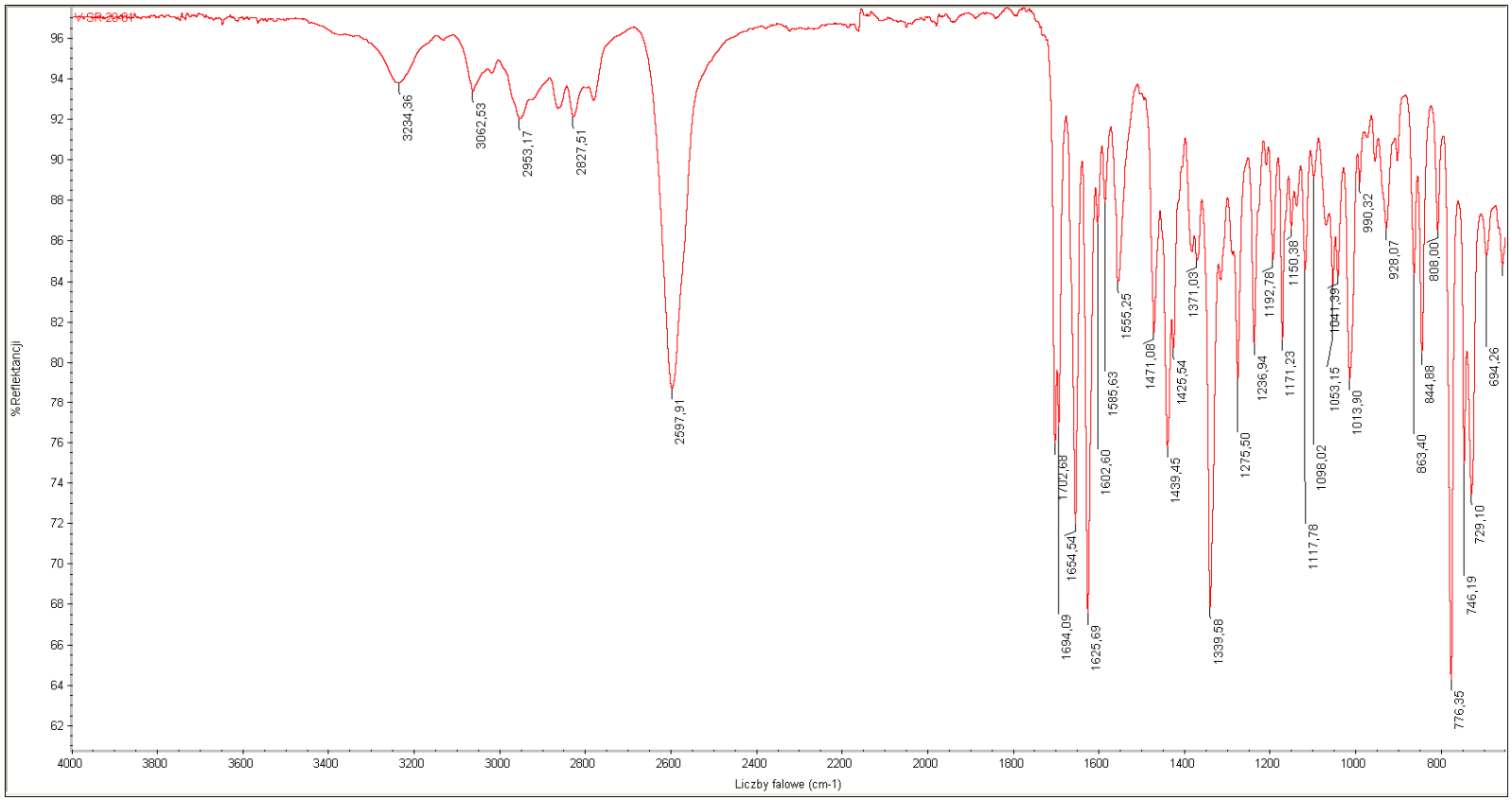

Figure S119. IR spectrum of **35**.

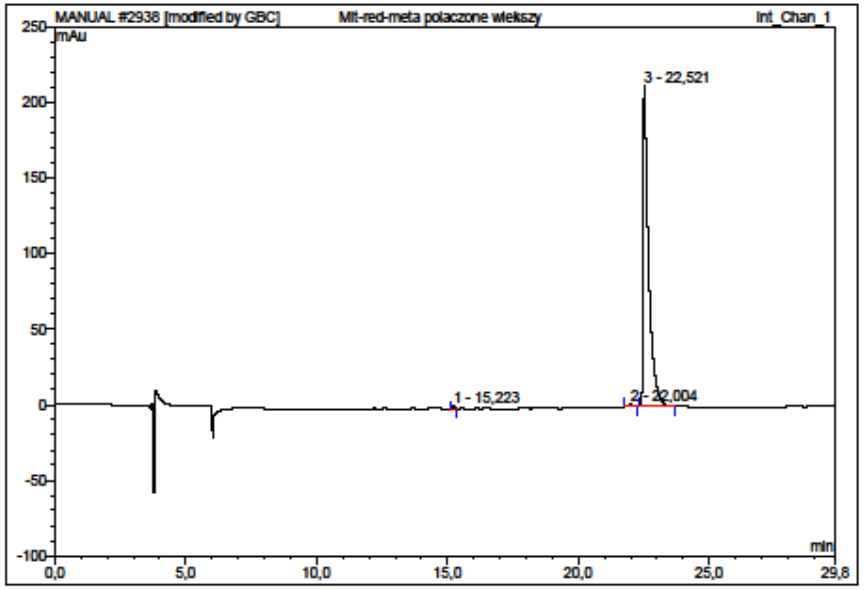

No.	Ret.Time min	Peak Name	Height mAu	Area mAu*min	Rel.Area %	Amount	Type
1	15,22	n.a.	1,554	0,181	0,34	n.a.	BMB*
2	22,00	n.a.	1,349	0,437	0,82	n.a.	BMB*
3	22,52	n.a.	211,994	52,373	98,83	n.a.	BMB
Total:			214,897	52,991	100,00	0,000	

Figure S120. HPLC analysis of **35**.

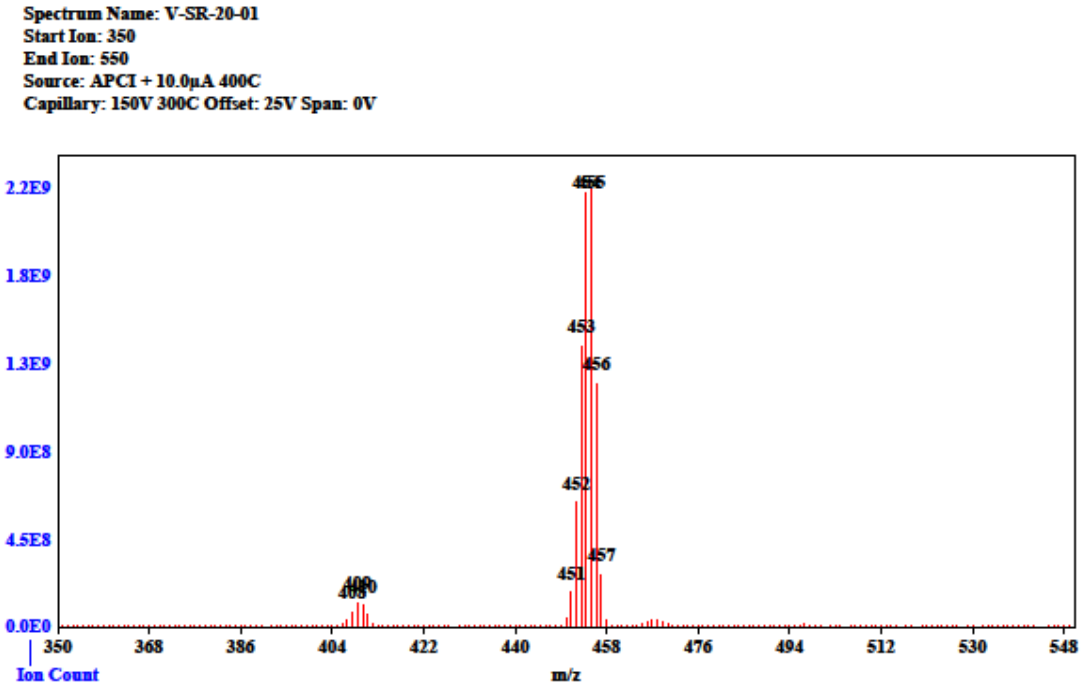

Figure S121. MS spectrum of **35**.

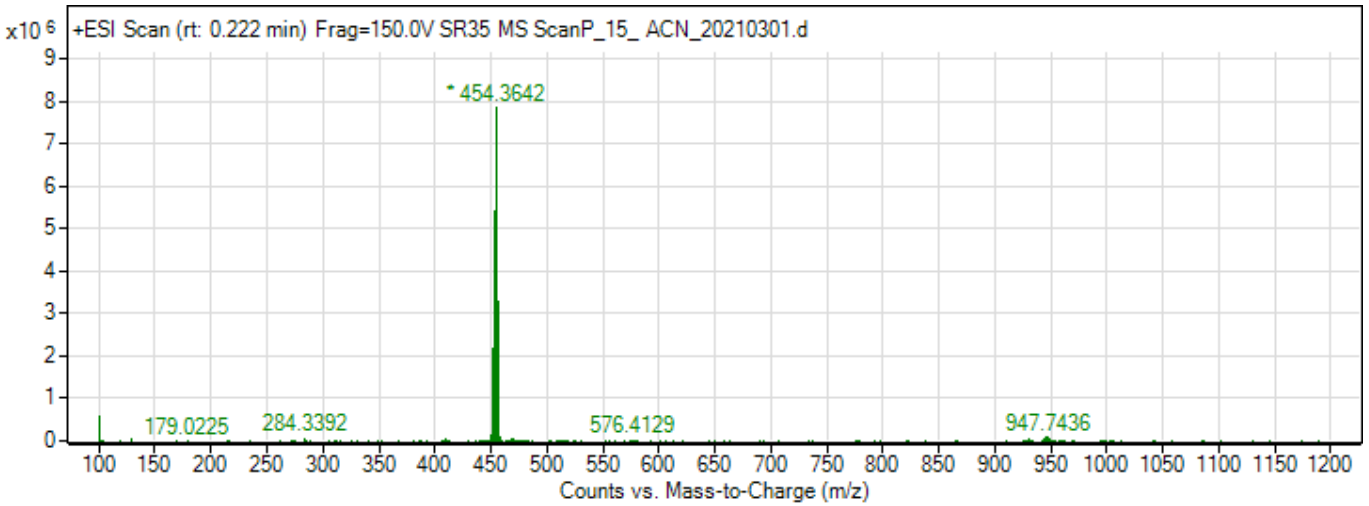

Figure S122. HRMS spectrum of **35**.

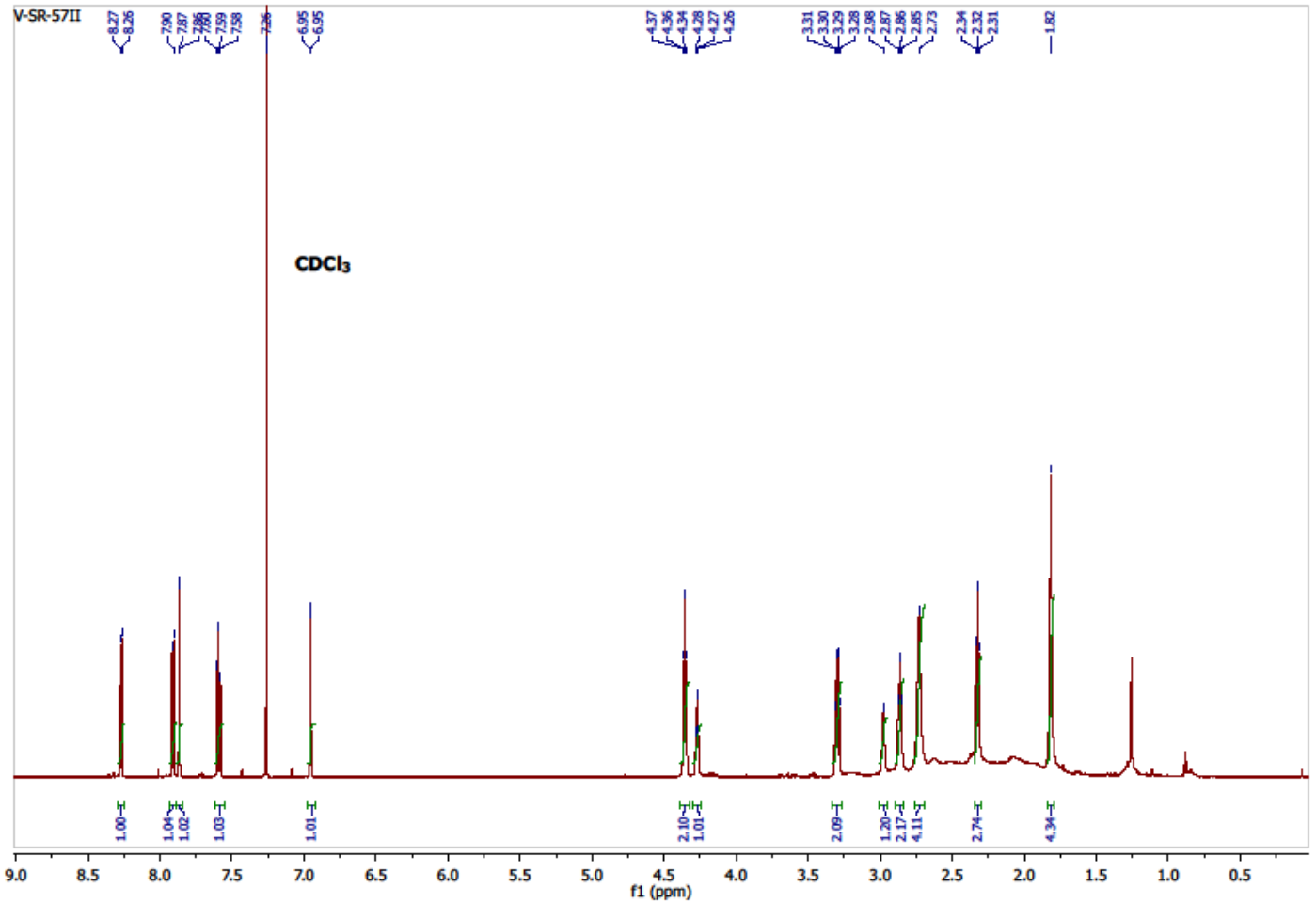

Figure S123. ^{1}H NMR spectrum of **36**.

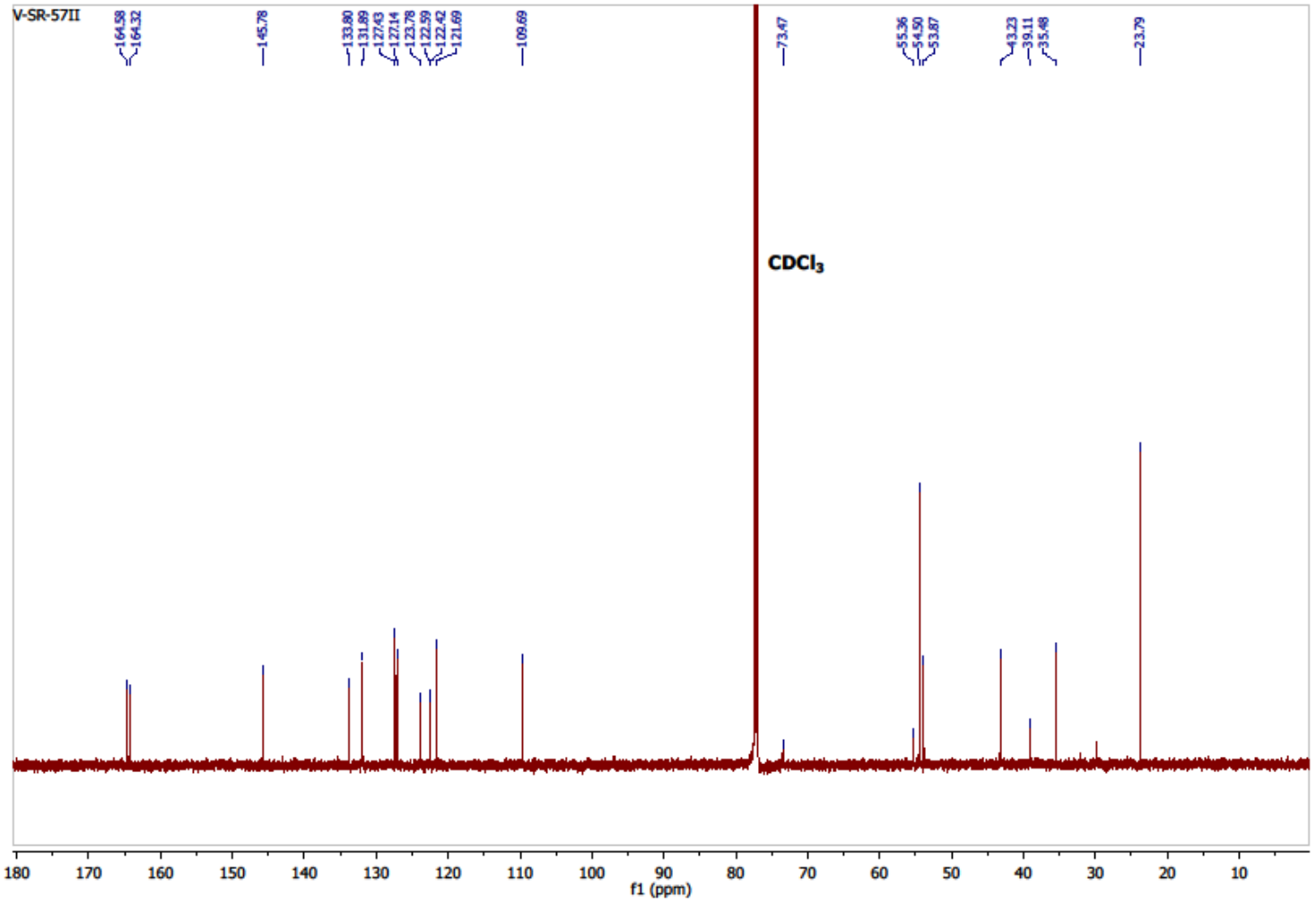

Figure S124. ^{13}C NMR spectrum of **36**.

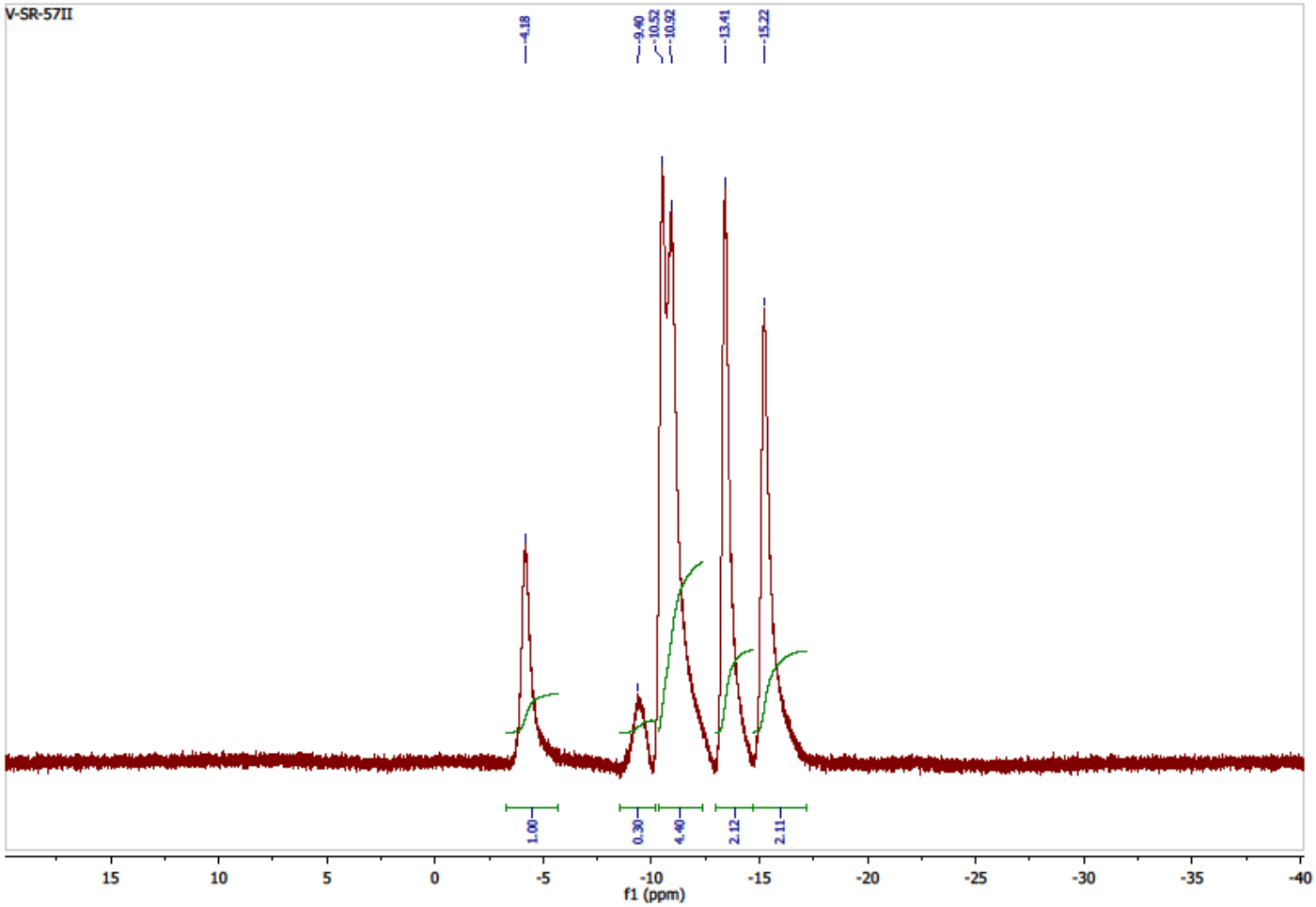

Figure S125. ^{11}B NMR {^{1}H BB} spectrum of **36**.

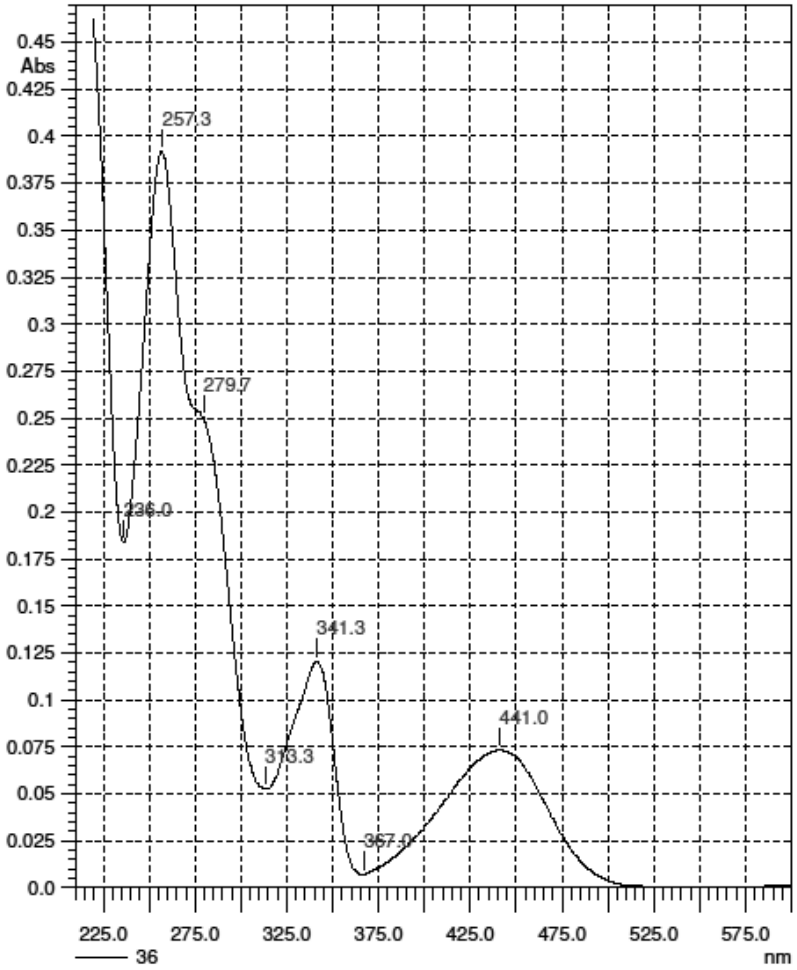

Figure S126. UV spectrum of **36**.

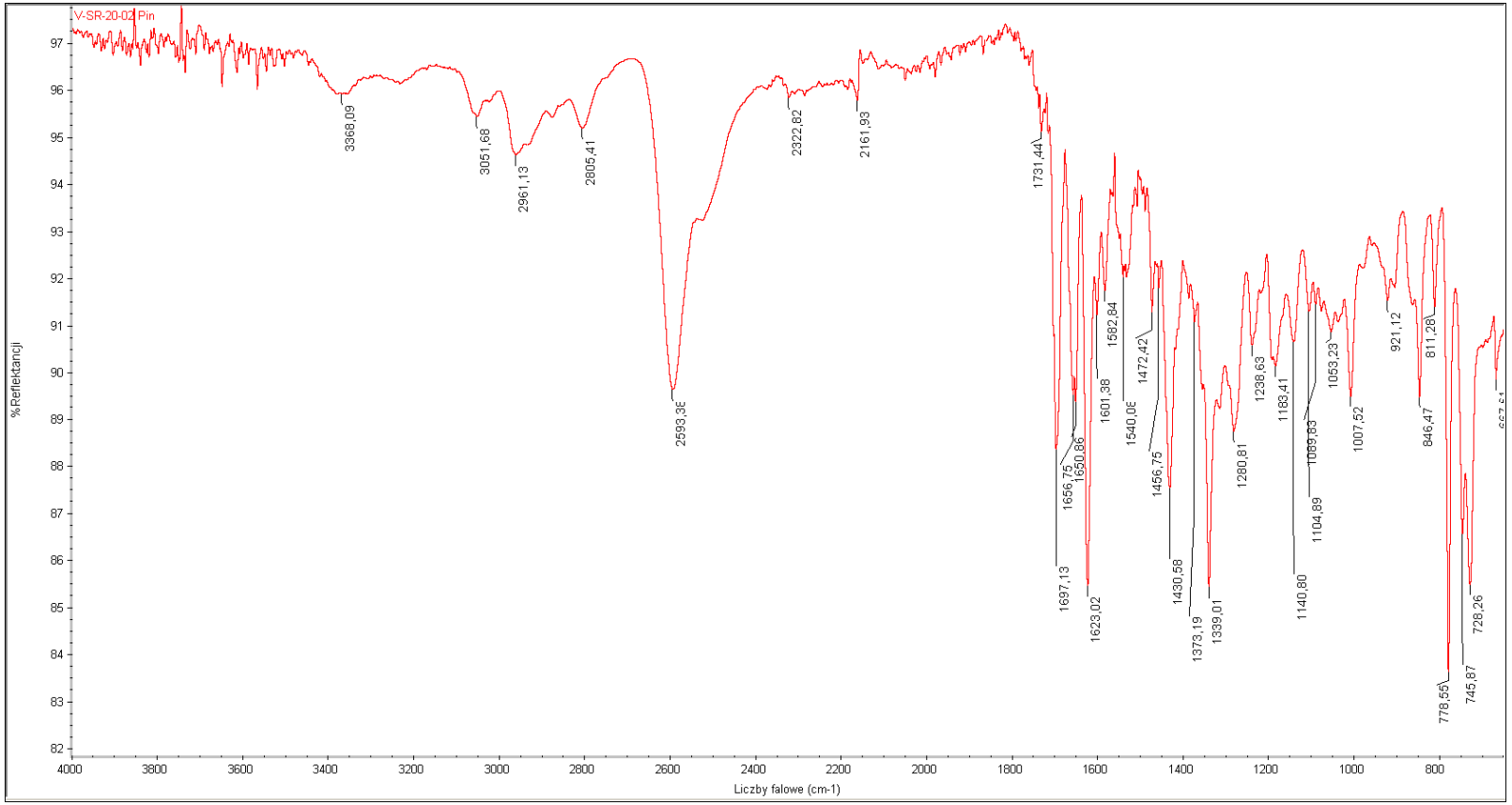

Figure S127. IR spectrum of **36**.

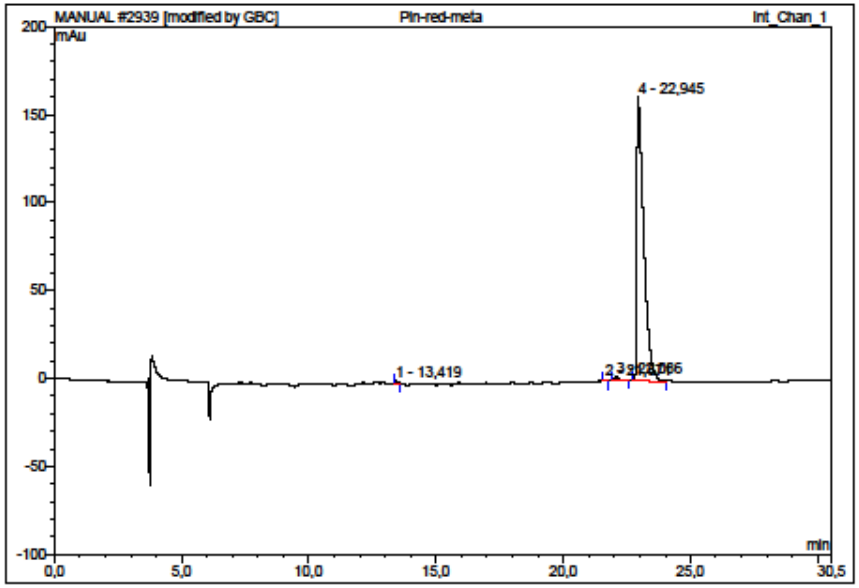

No.	Ret.Time min	Peak Name	Height mAu	Area mAu*min	Rel.Area %	Amount	Type
1	13,42	n.a.	1,566	0,193	0,36	n.a.	BMB*
2	21,67	n.a.	0,901	0,100	0,19	n.a.	BMB*
3	22,09	n.a.	2,307	0,591	1,12	n.a.	BMB*
4	22,95	n.a.	161,591	52,121	98,33	n.a.	BMB
Total:			166,365	53,005	100,00	0,000	

Figure S128. HPLC analysis of **36**.

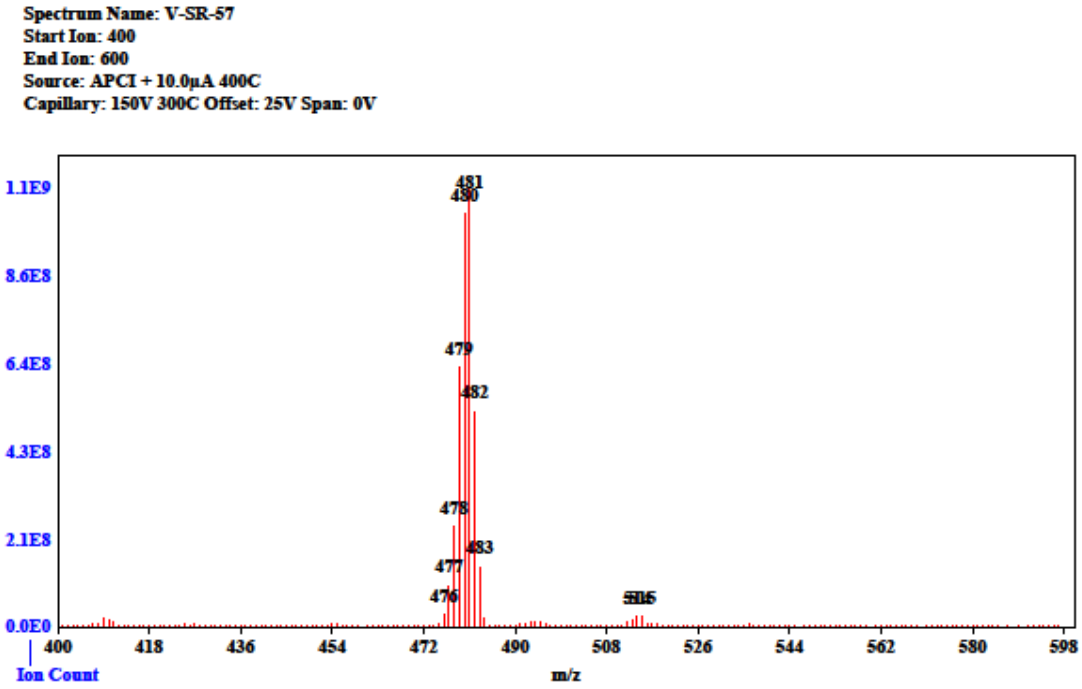

Figure S129. MS spectrum of **36**.

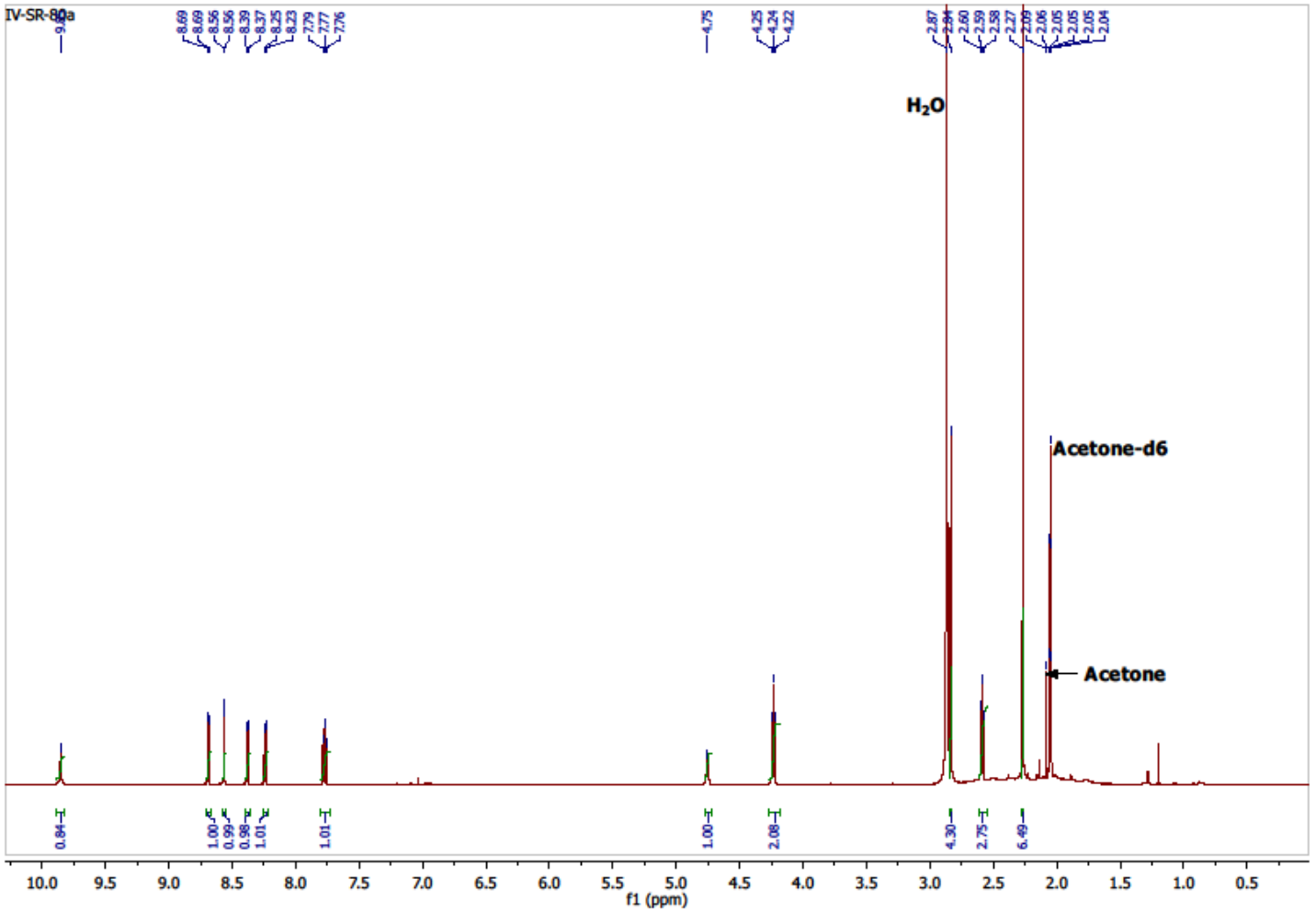

Figure S130. ^{1}H NMR spectrum of **39**.

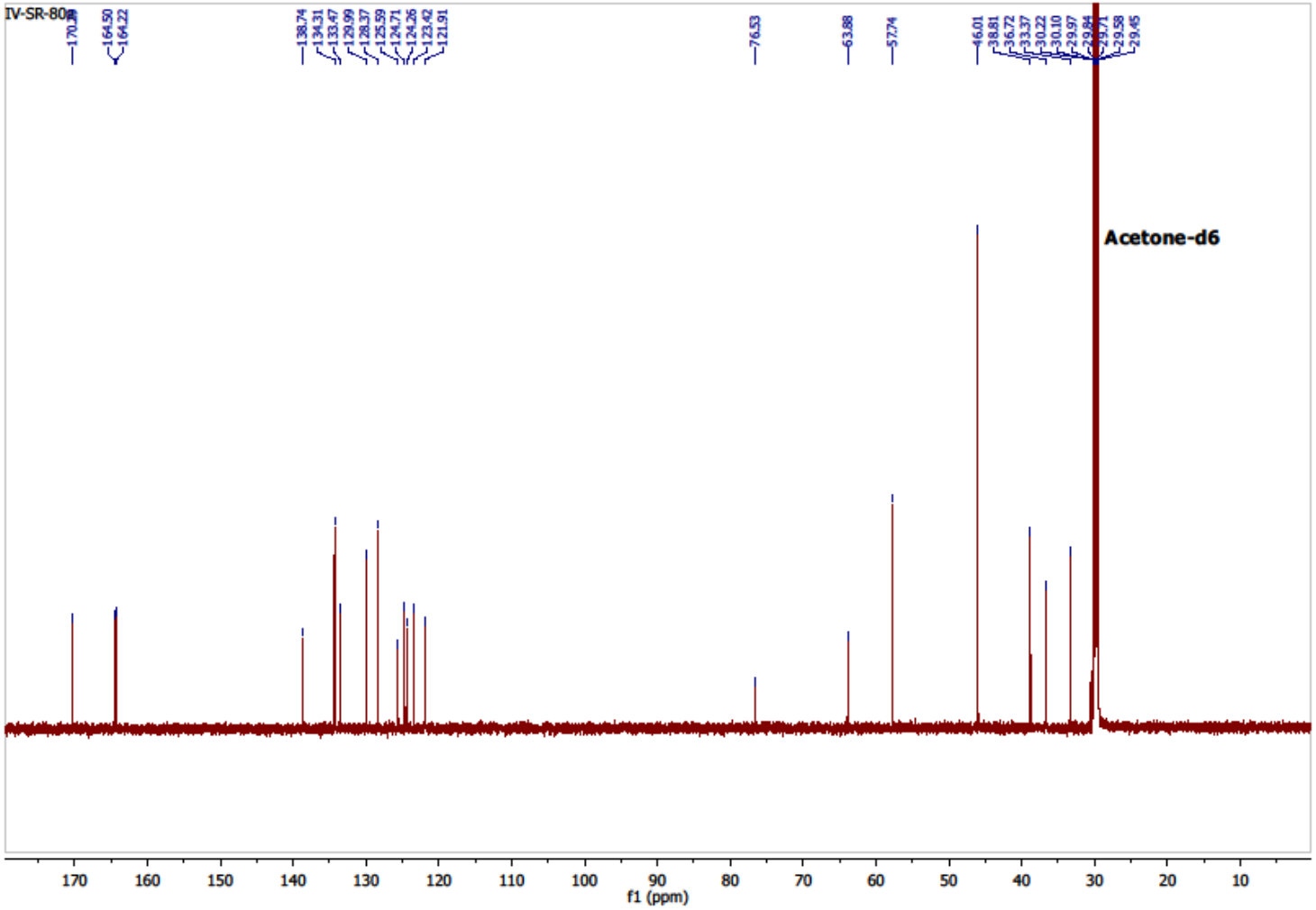

Figure S131. ^{13}C NMR spectrum of **39**.

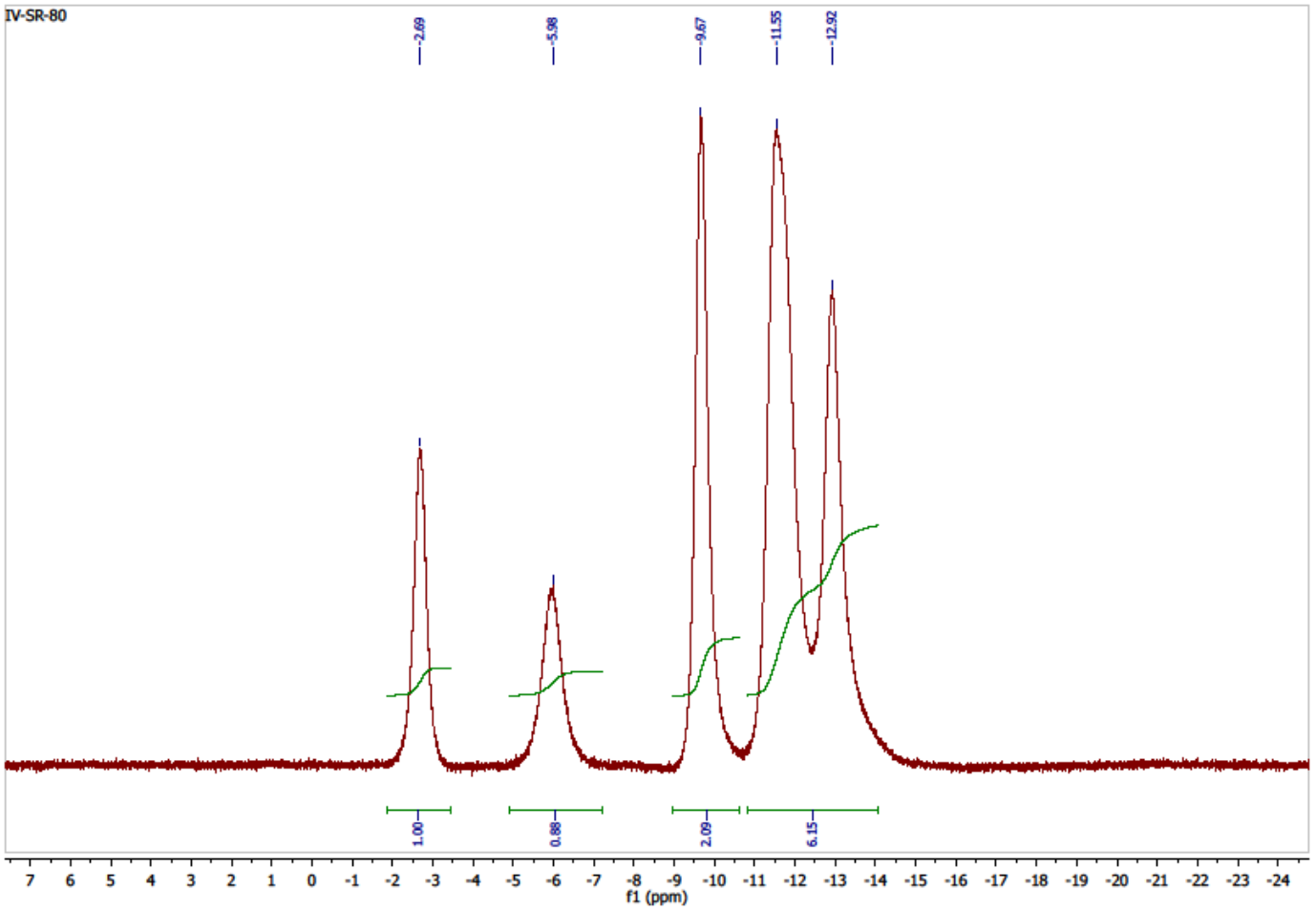

Figure S132. ^{11}B NMR {^{1}H BB} spectrum of **39**.

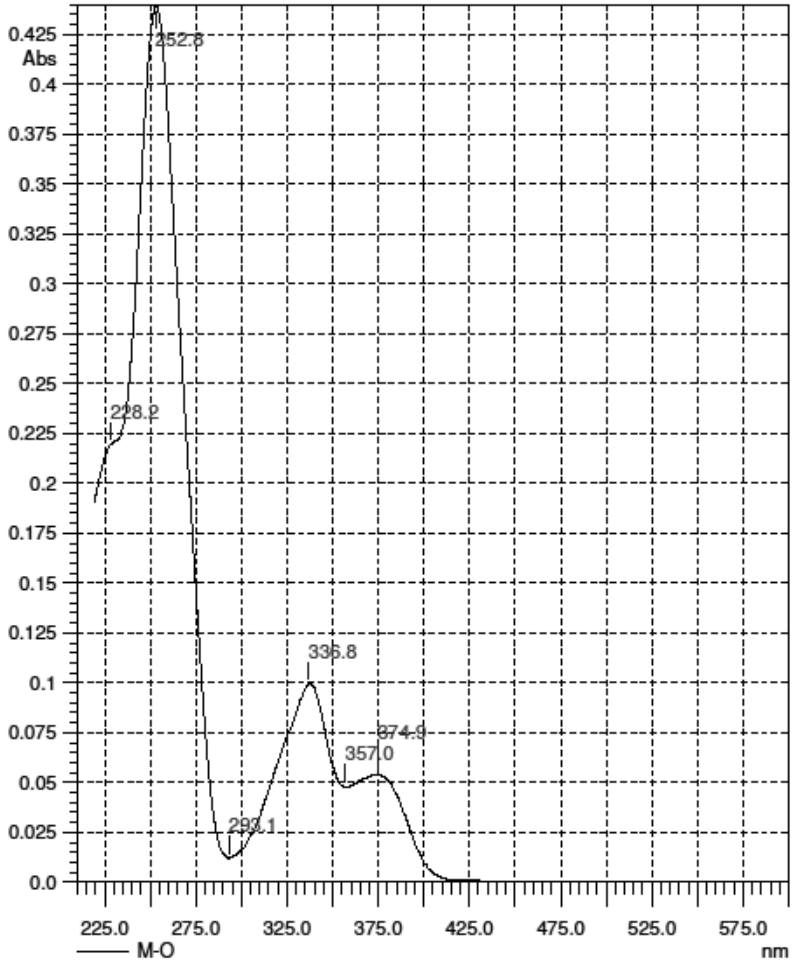

Figure S133. UV spectrum of **39**.

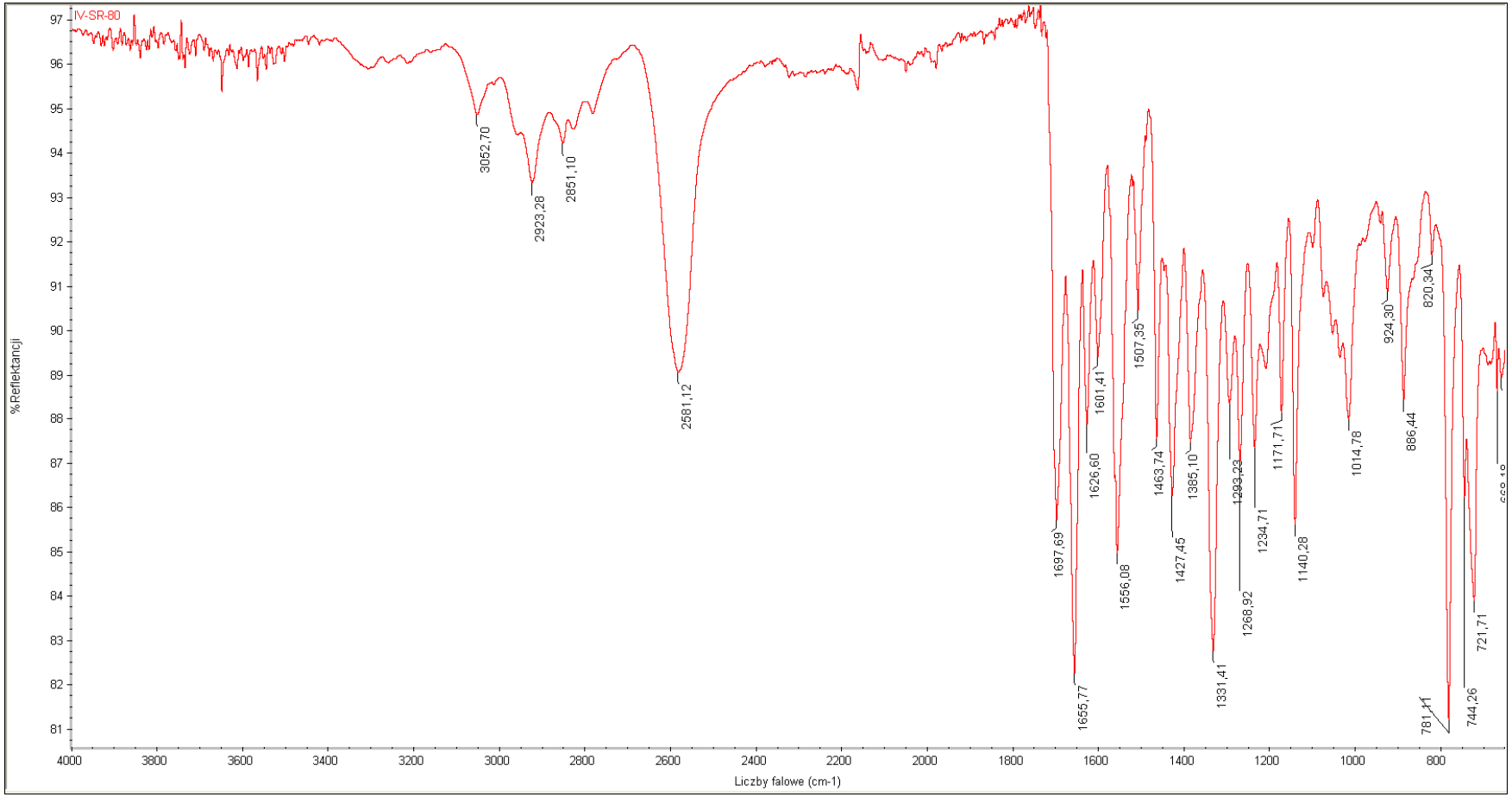

Figure S134. IR spectrum of **39**.

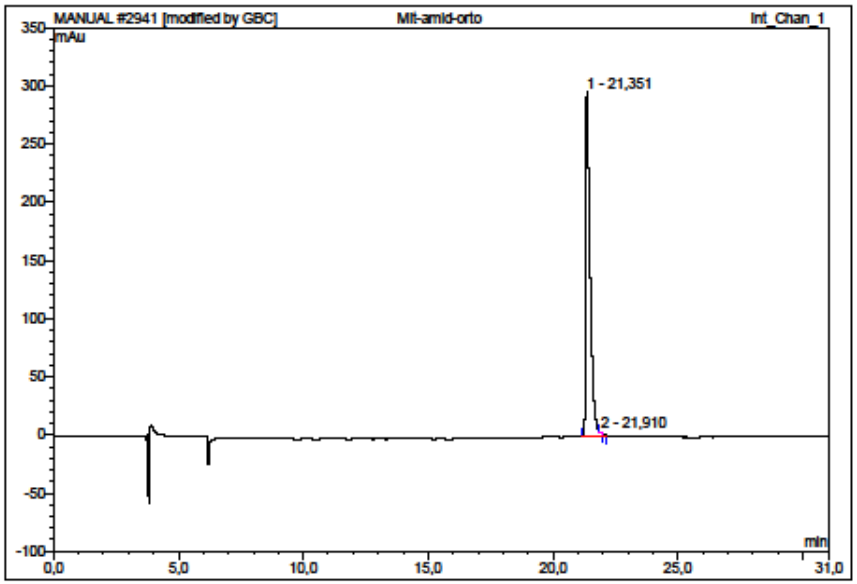

No.	Ret.Time min	Peak Name	Height mAu	Area mAu*min	Rel.Area %	Amount	Type
1	21,35	n.a.	296,387	60,775	99,89	n.a.	BMB*
2	21,91	n.a.	0,740	0,068	0,11	n.a.	Rd*
Total:			297,127	60,843	100,00	0,000	

Figure S135. HPLC analysis of **39**.

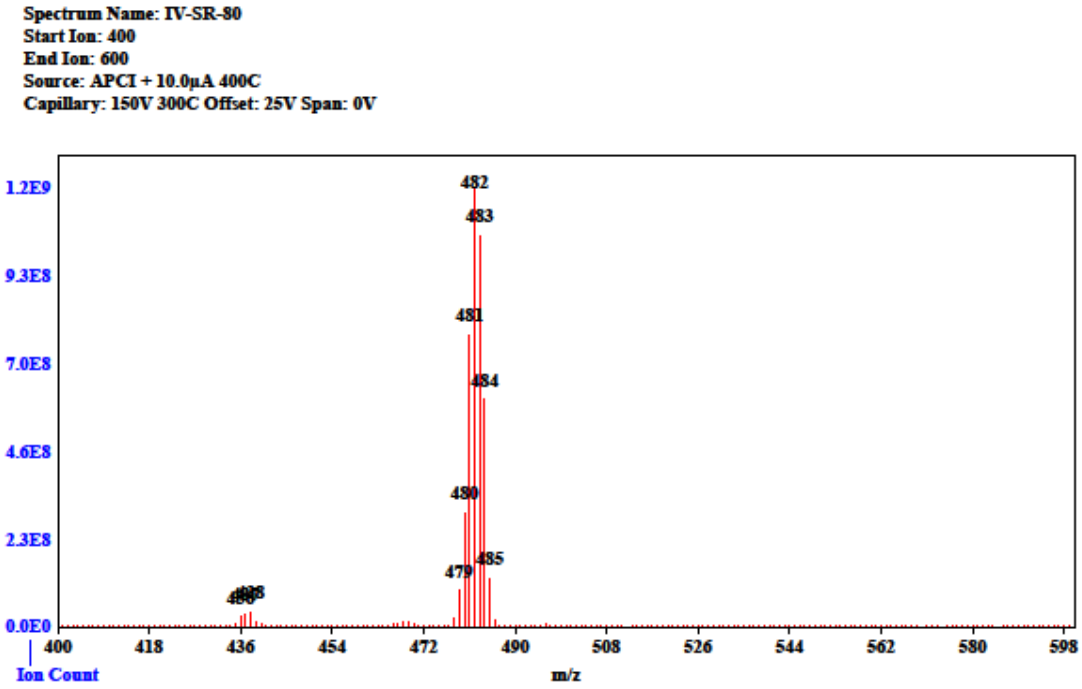

Figure S136. MS spectrum of **39**.

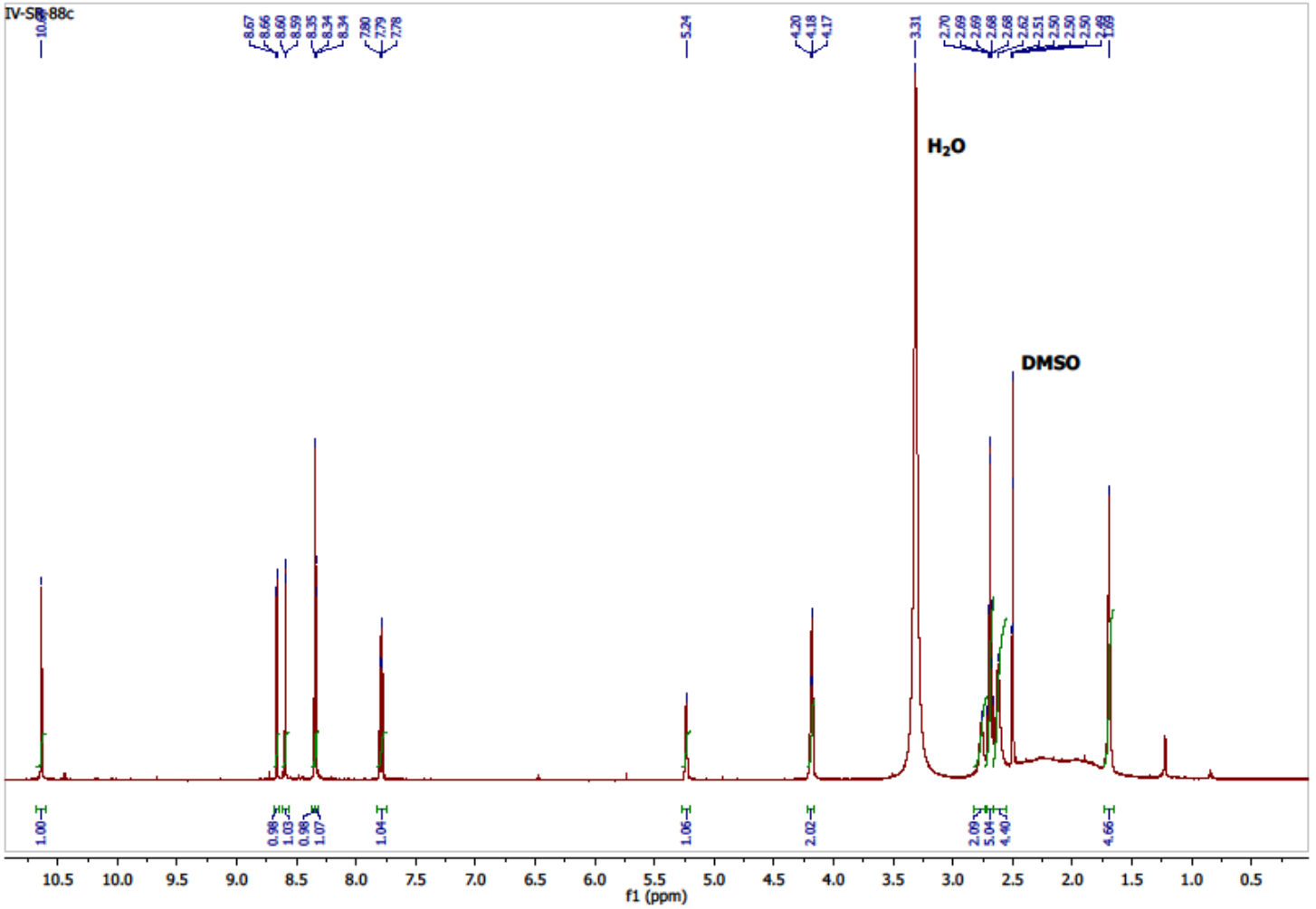

Figure S137. ^{1}H NMR spectrum of **40**.

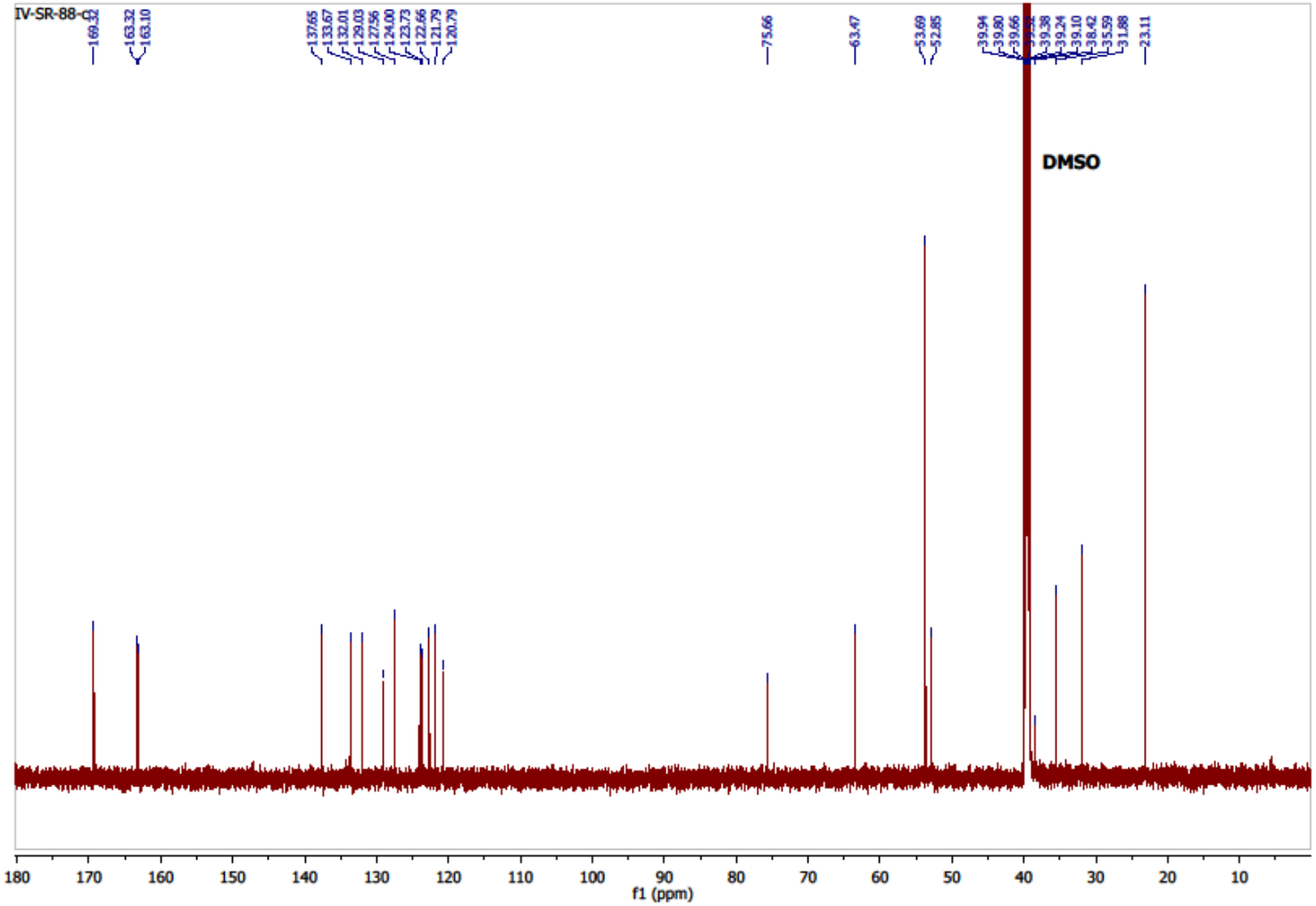

Figure S138. ^{13}C NMR spectrum of **40**.

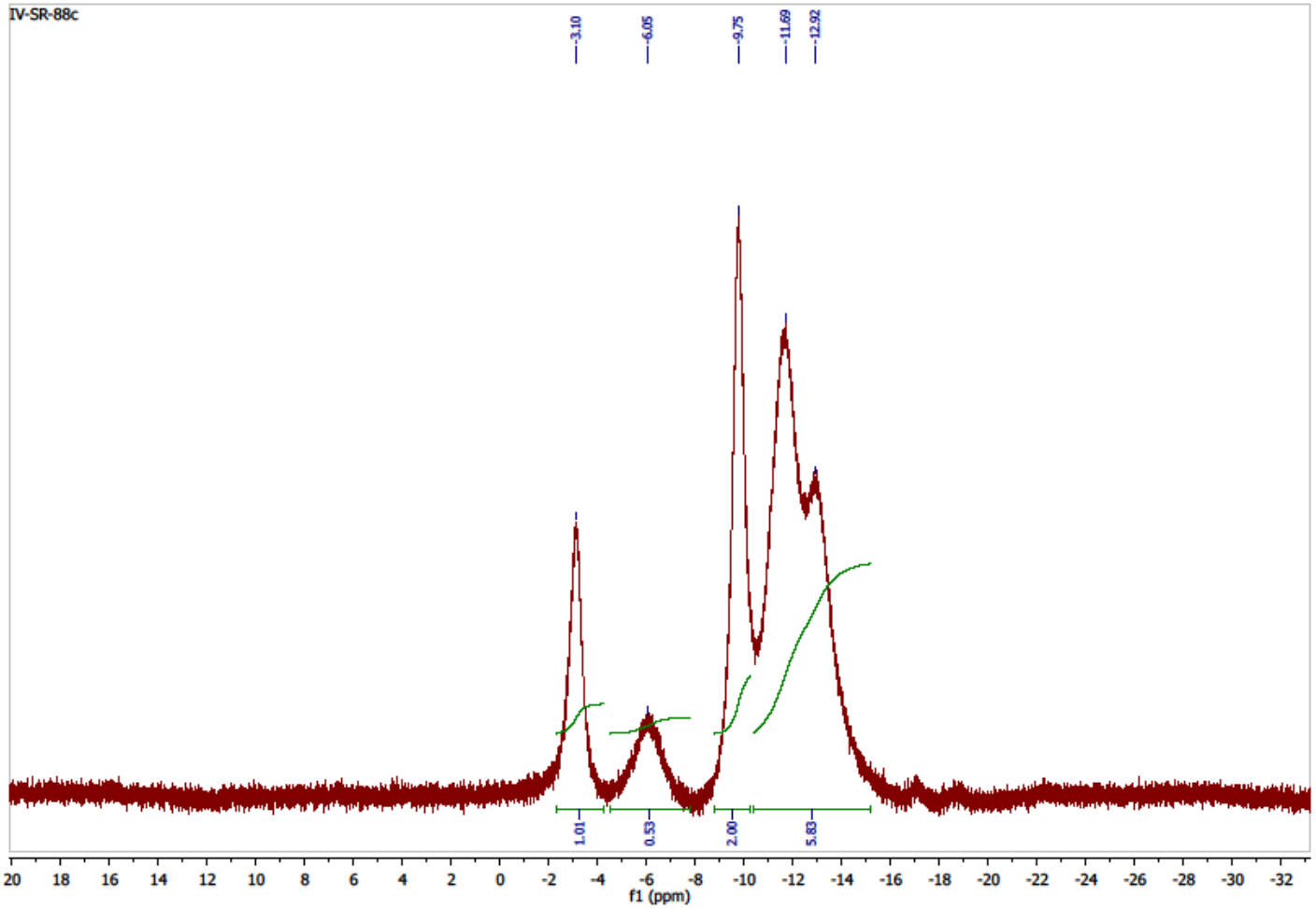

Figure S139. ^{11}B NMR {^{1}H BB} spectrum of **40**.

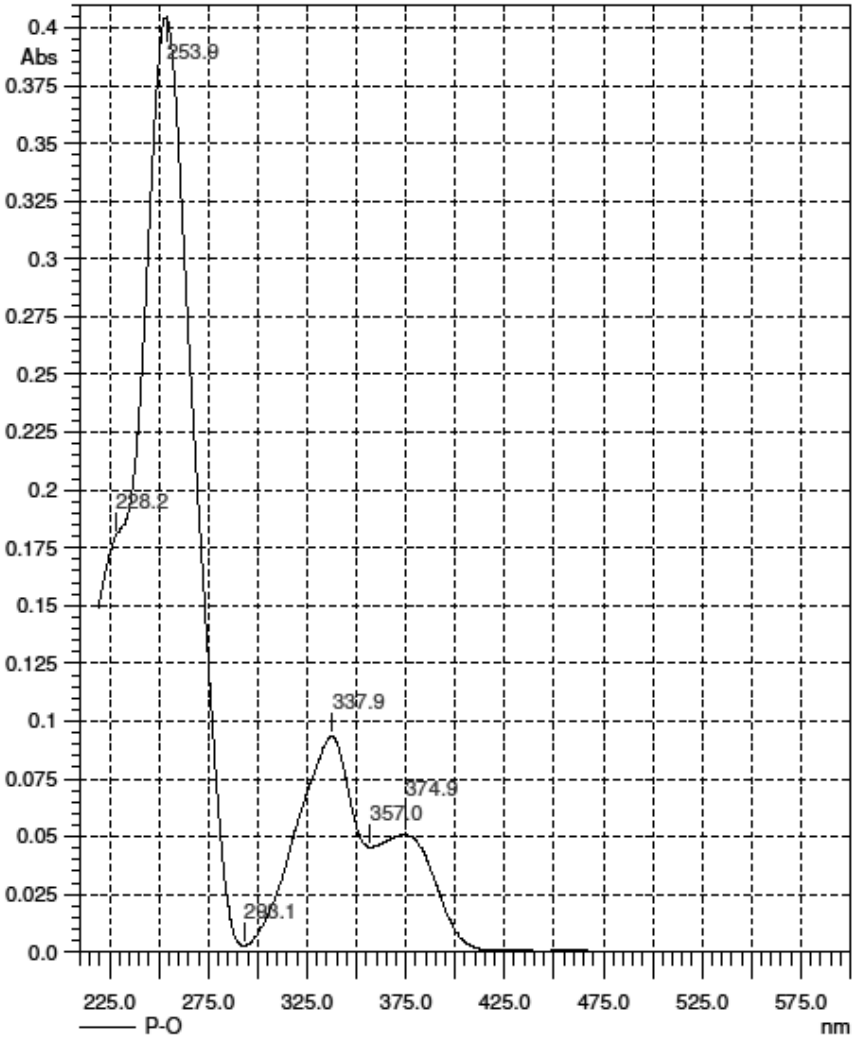

Figure S140. UV spectrum of **40**.

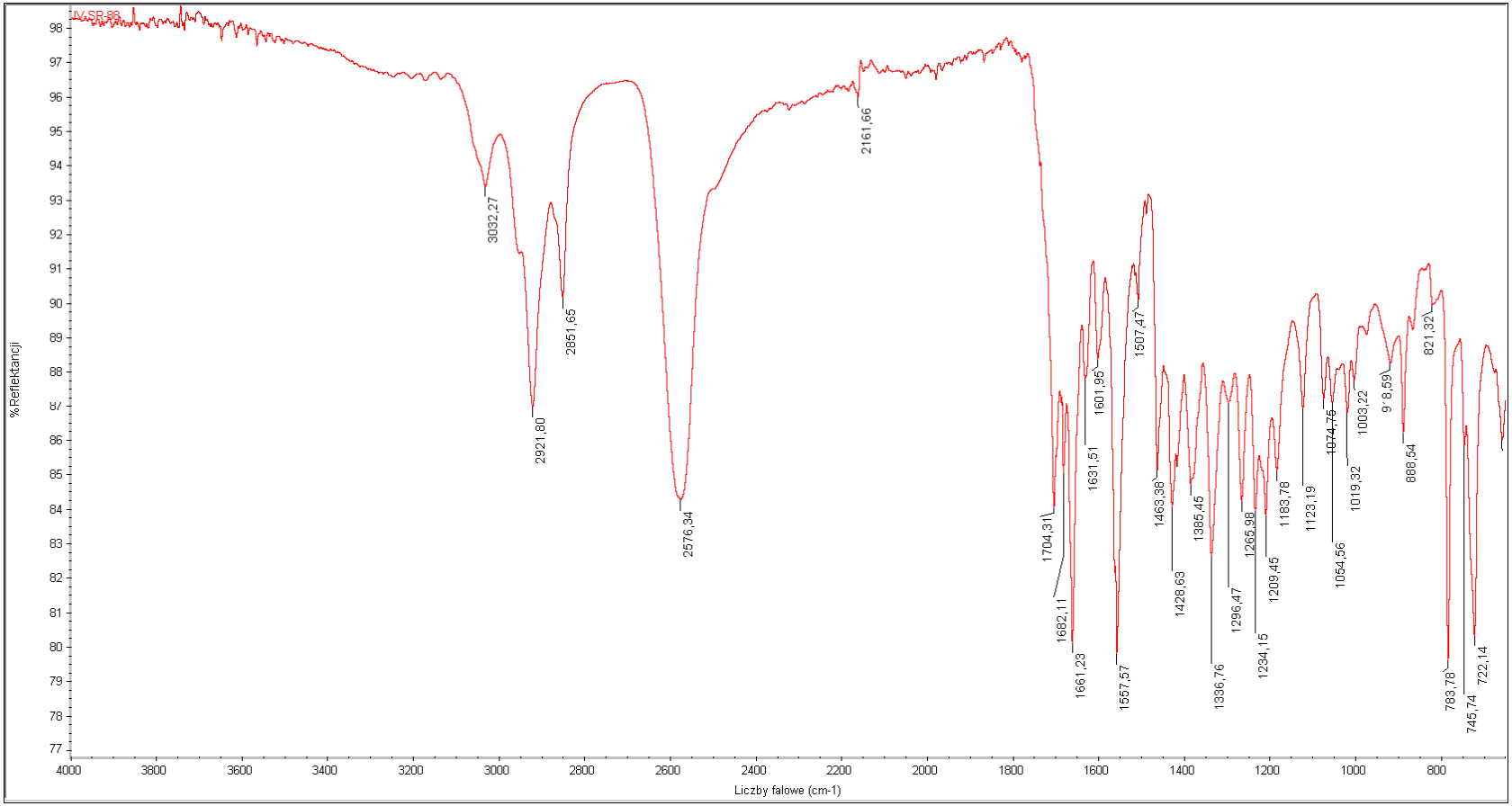

Figure S141. IR spectrum of **40**.

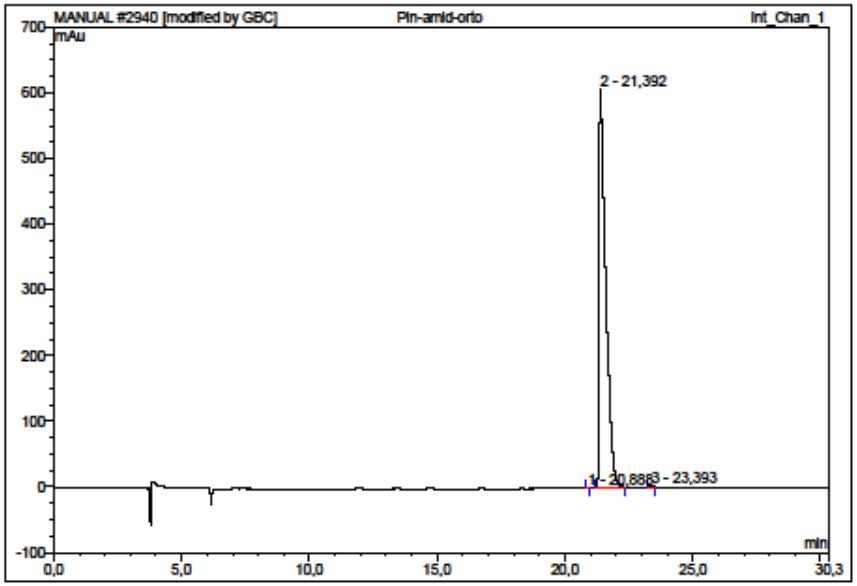

No.	Ret.Time min	Peak Name	Height mAu	Area mAu*min	Rel.Area %	Amount	Type
1	20,89	n.a.	0,743	0,064	0,03	n.a.	BMB*
2	21,39	n.a.	606,469	181,277	99,65	n.a.	BMB
3	23,39	n.a.	3,461	0,571	0,31	n.a.	BMB*
Total:			610,674	181,911	100,00	0,000	

Figure S142. HPLC analysis of **40**.

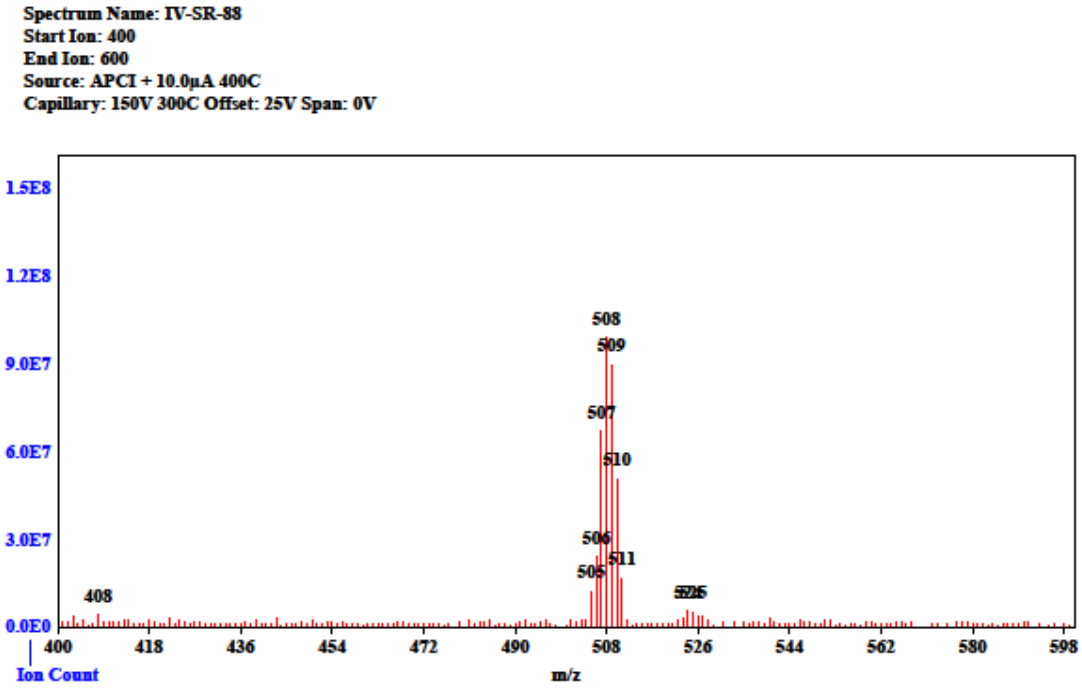

Figure S143. MS spectrum of **40**.

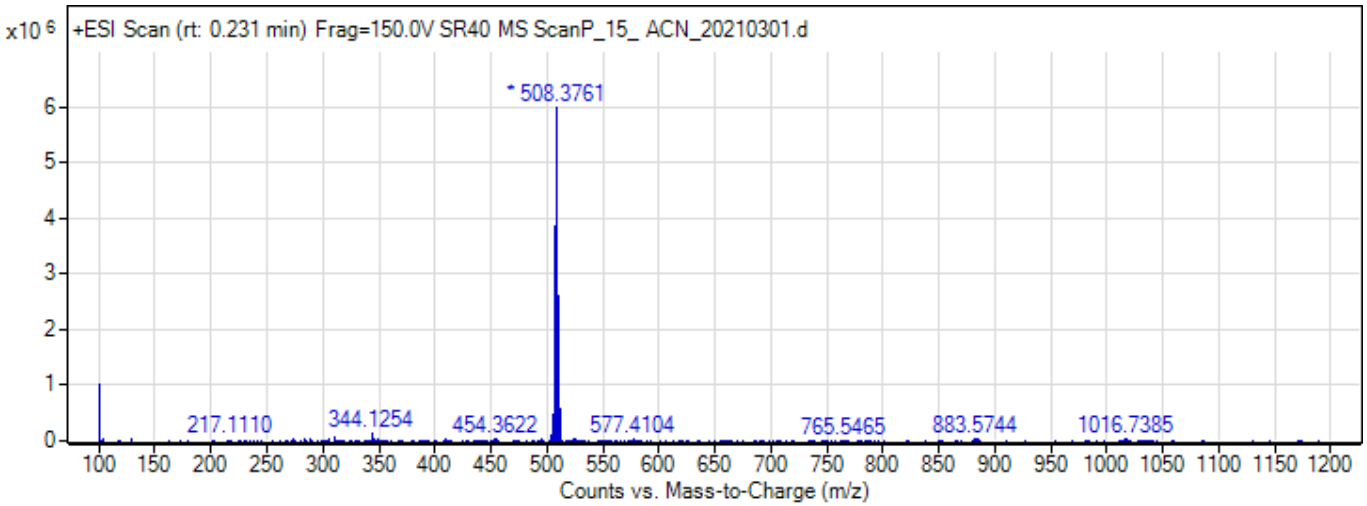

Figure S144. HRMS spectrum of **40**.

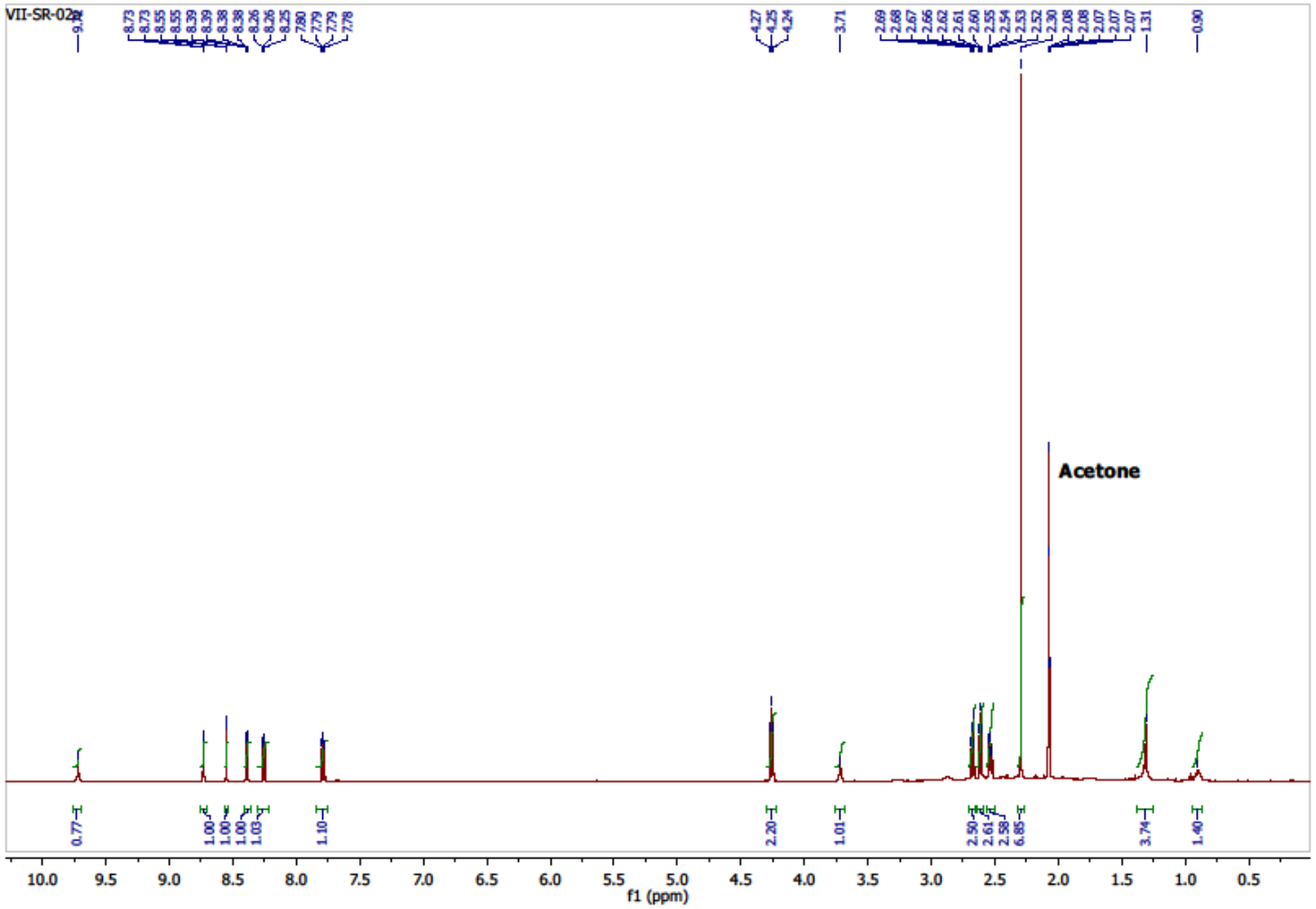

Figure S145. ^{1}H NMR spectrum of **41**.

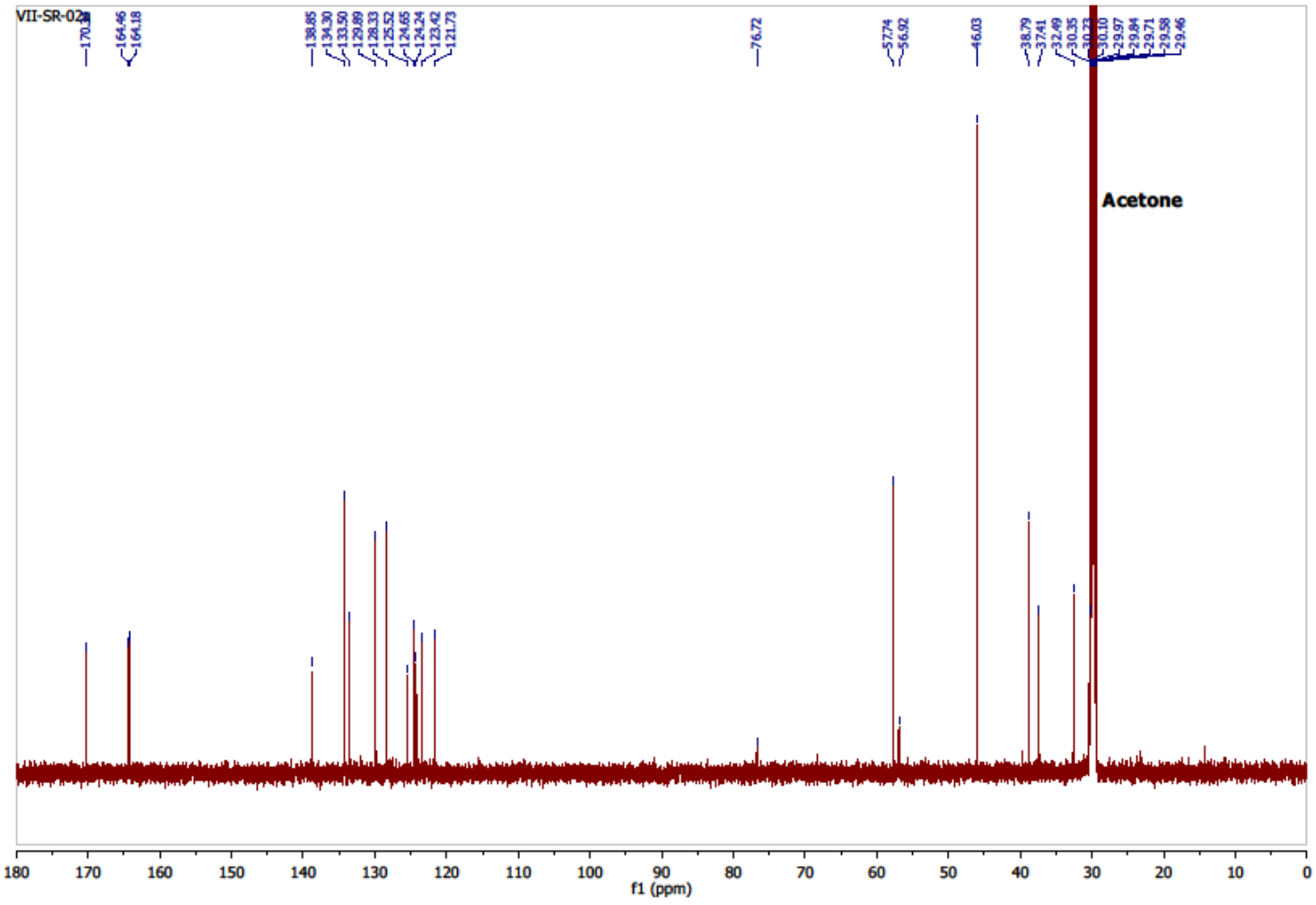

Figure S146. ^{13}C NMR spectrum of **41**.

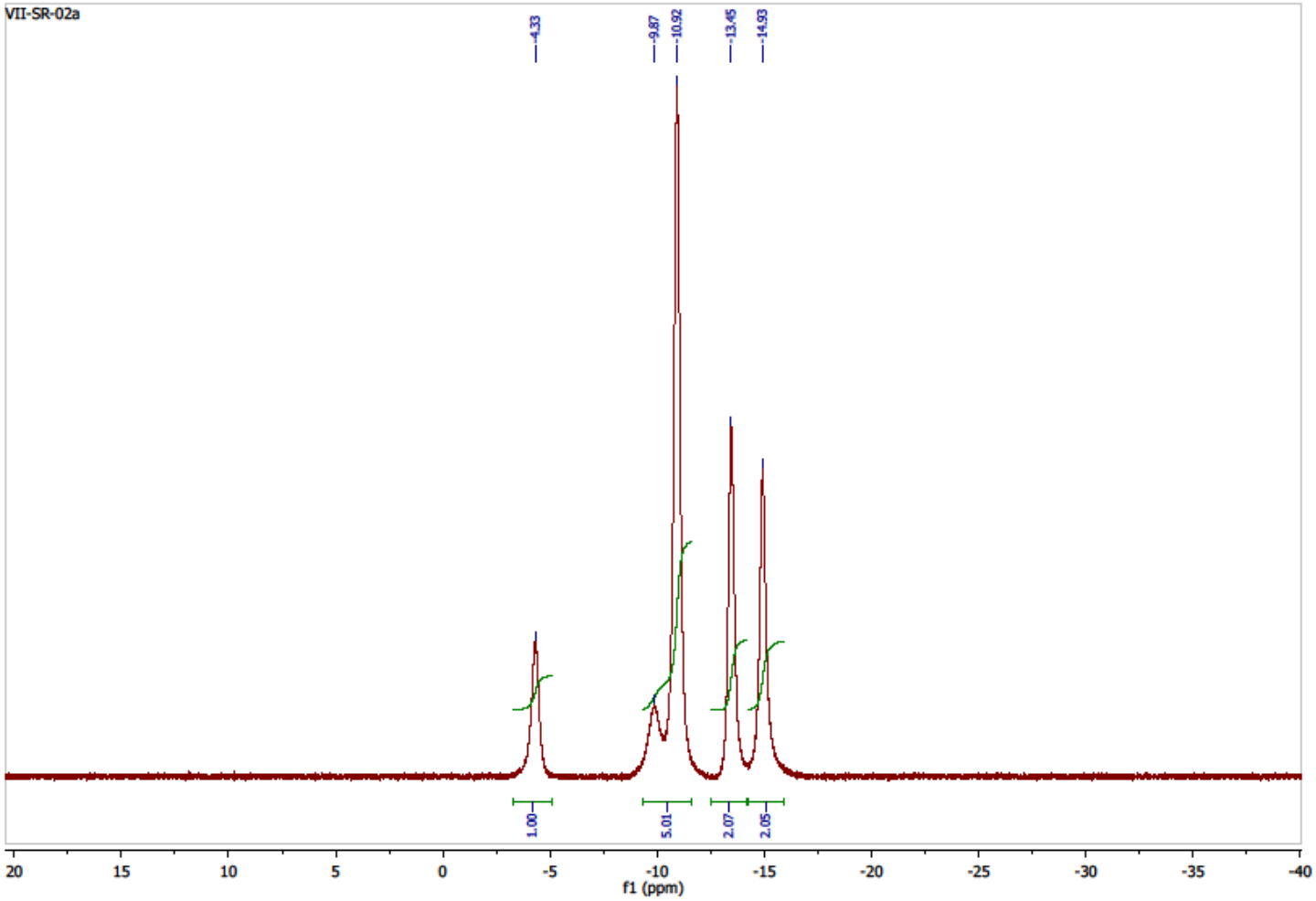

Figure S147. IR spectrum of **41**.

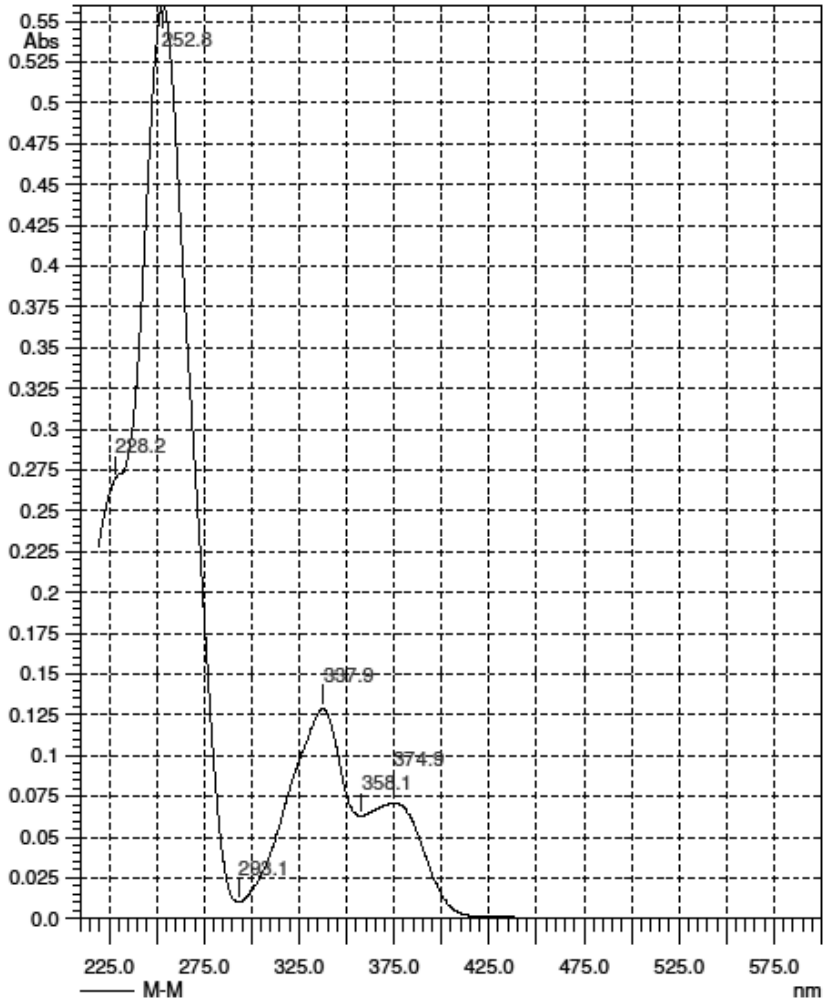

Figure S148. UV spectrum of **41**.

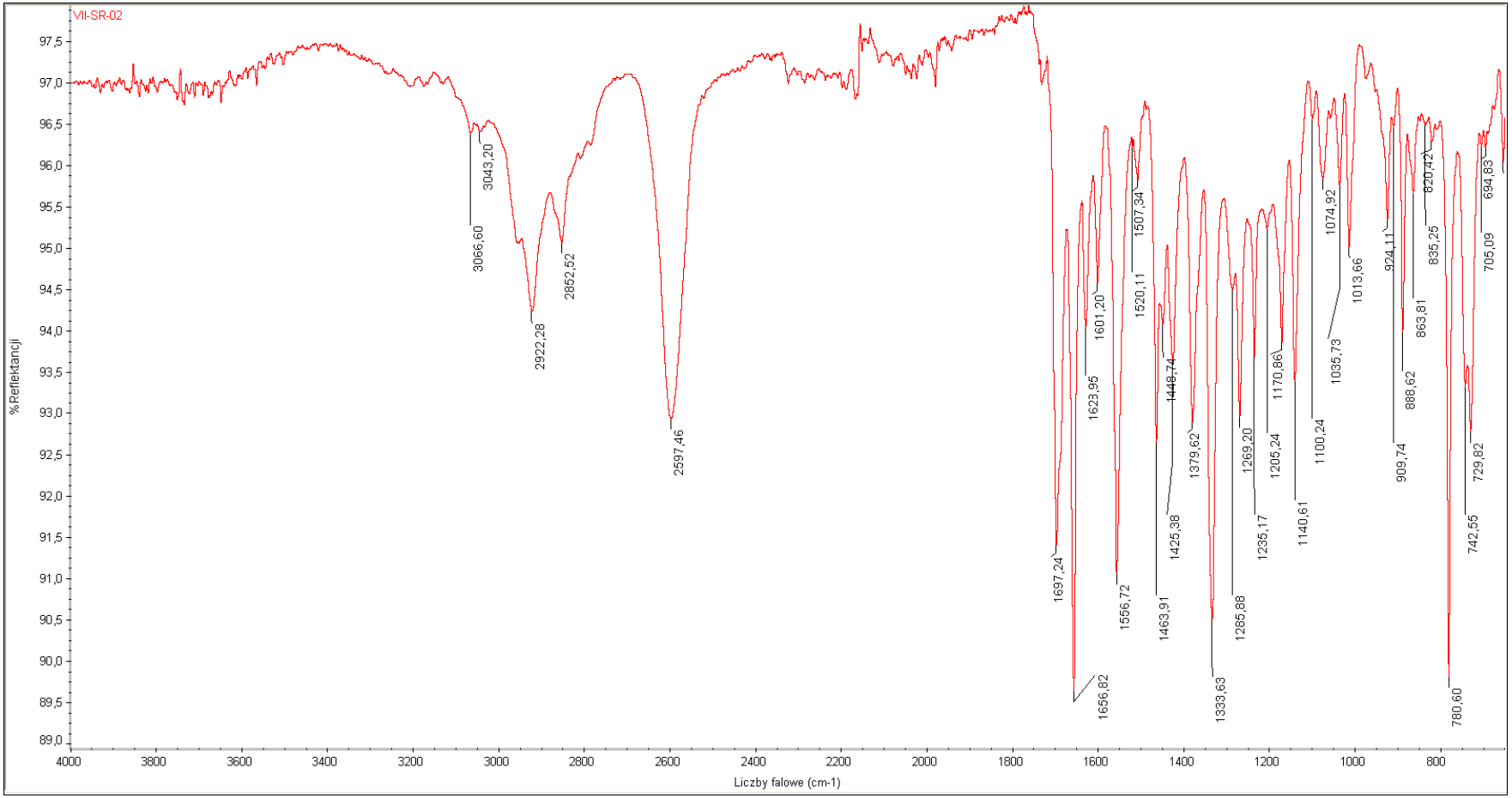

Figure S149. IR spectrum of **41**.

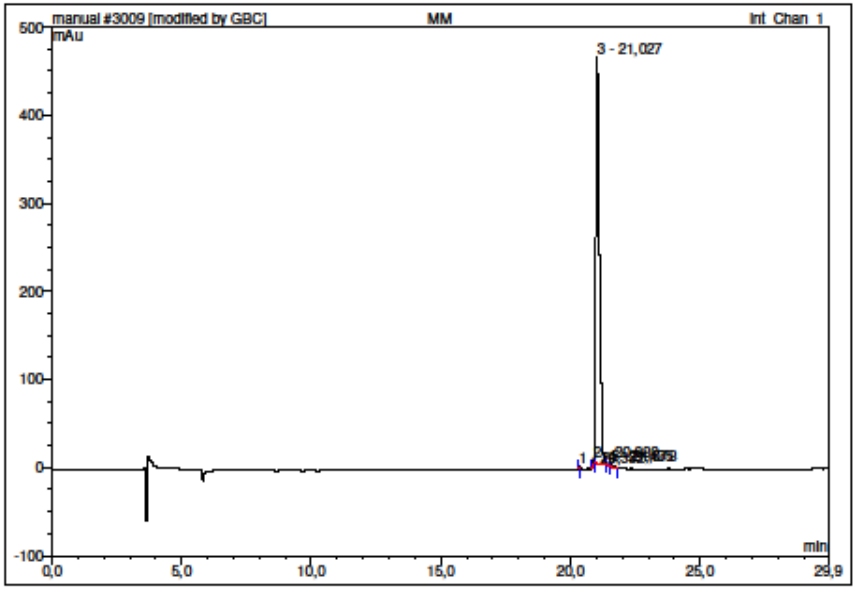

No.	Ret.Time min	Peak Name	Height mAu	Area mAu*min	Rel.Area %	Amount	Type
1	20,33	n.a.	3,809	0,284	0,39	n.a.	BMB*
2	20,88	n.a.	6,404	0,384	0,52	n.a.	BMb*
3	21,03	n.a.	460,312	72,780	98,54	n.a.	bMB*
4	21,44	n.a.	1,057	0,068	0,09	n.a.	BMB*
5	21,58	n.a.	2,437	0,339	0,46	n.a.	BMB*
Total:			474,019	73,856	100,00	0,000	

Figure S150. HPLC analysis of **41**.

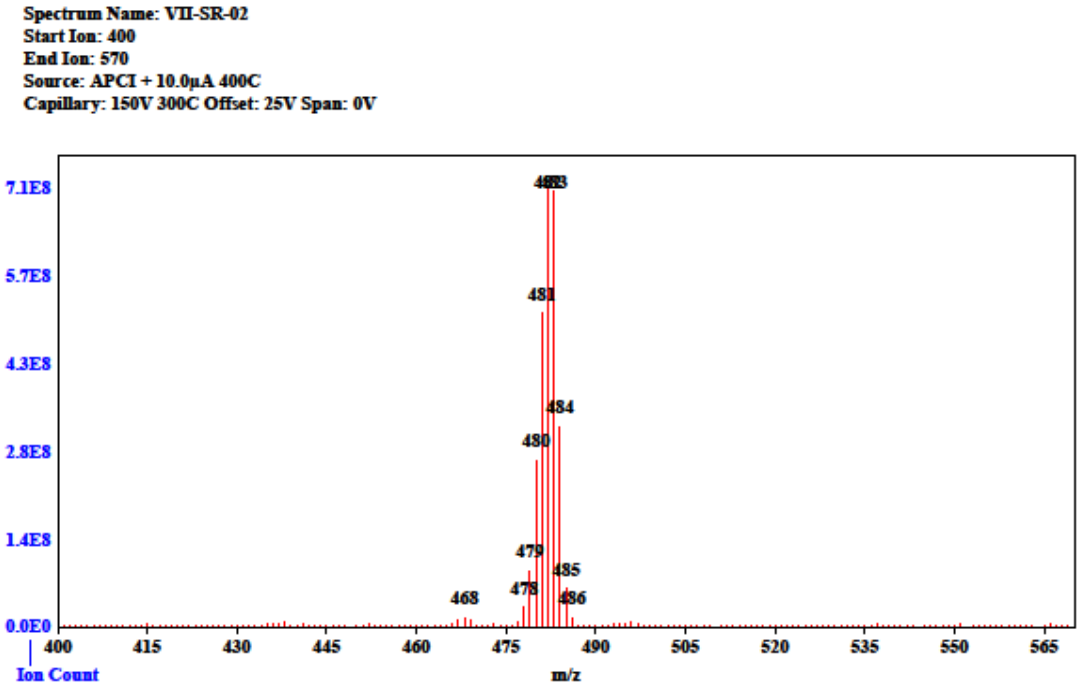

Figure S151. MS spectrum of **41**.

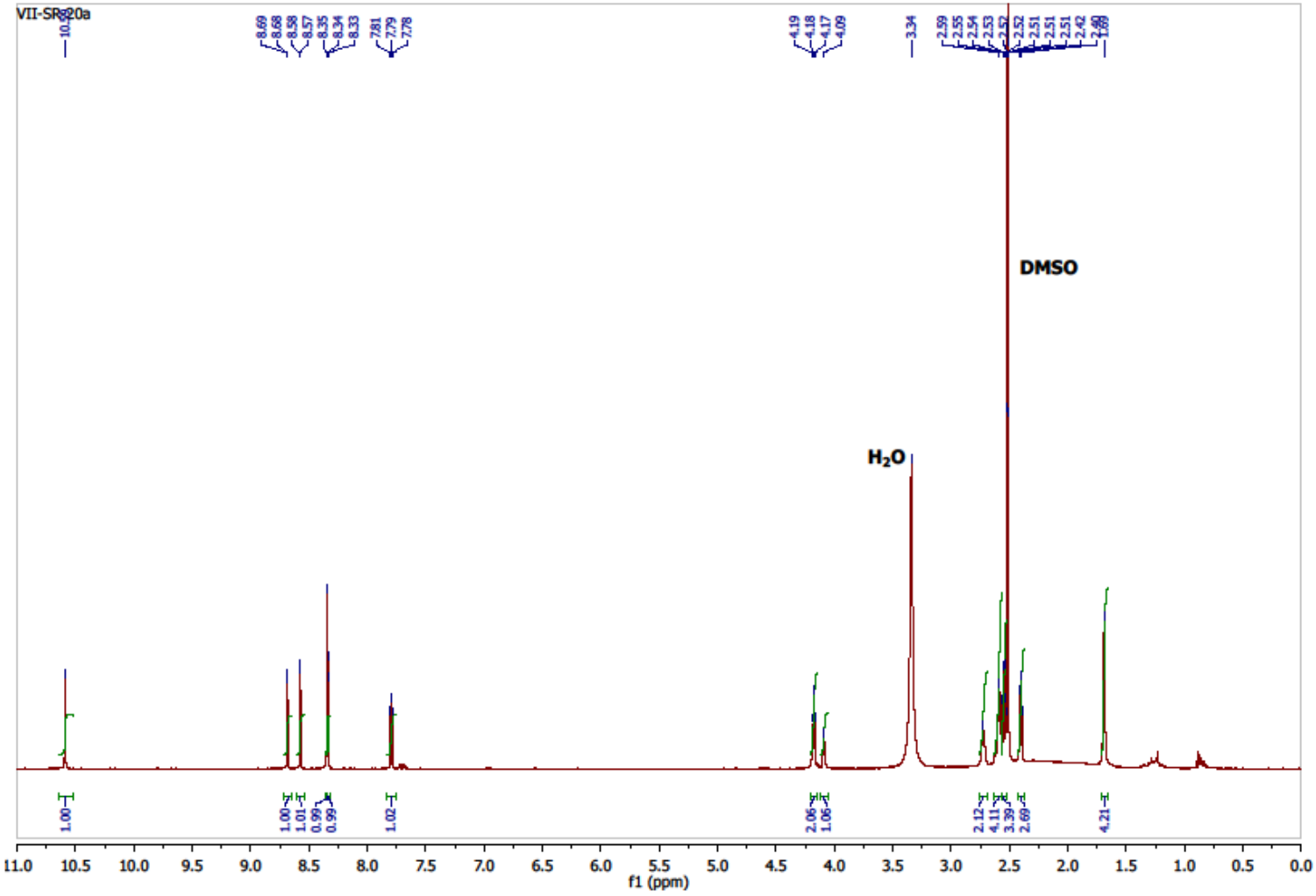

Figure S152. ^{1}H NMR spectrum of **42**.

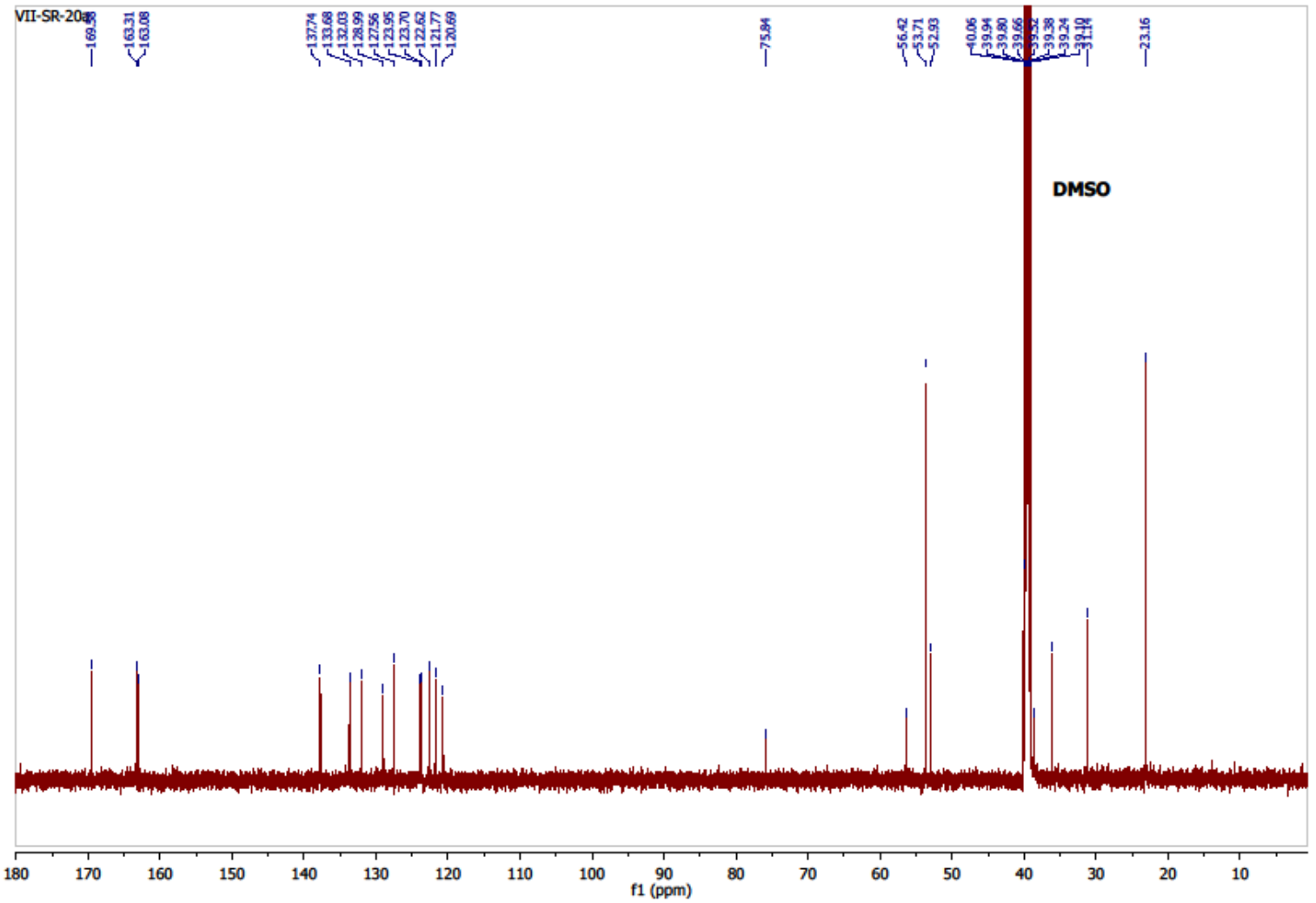

Figure S153. ^{13}C NMR spectrum of **42**.

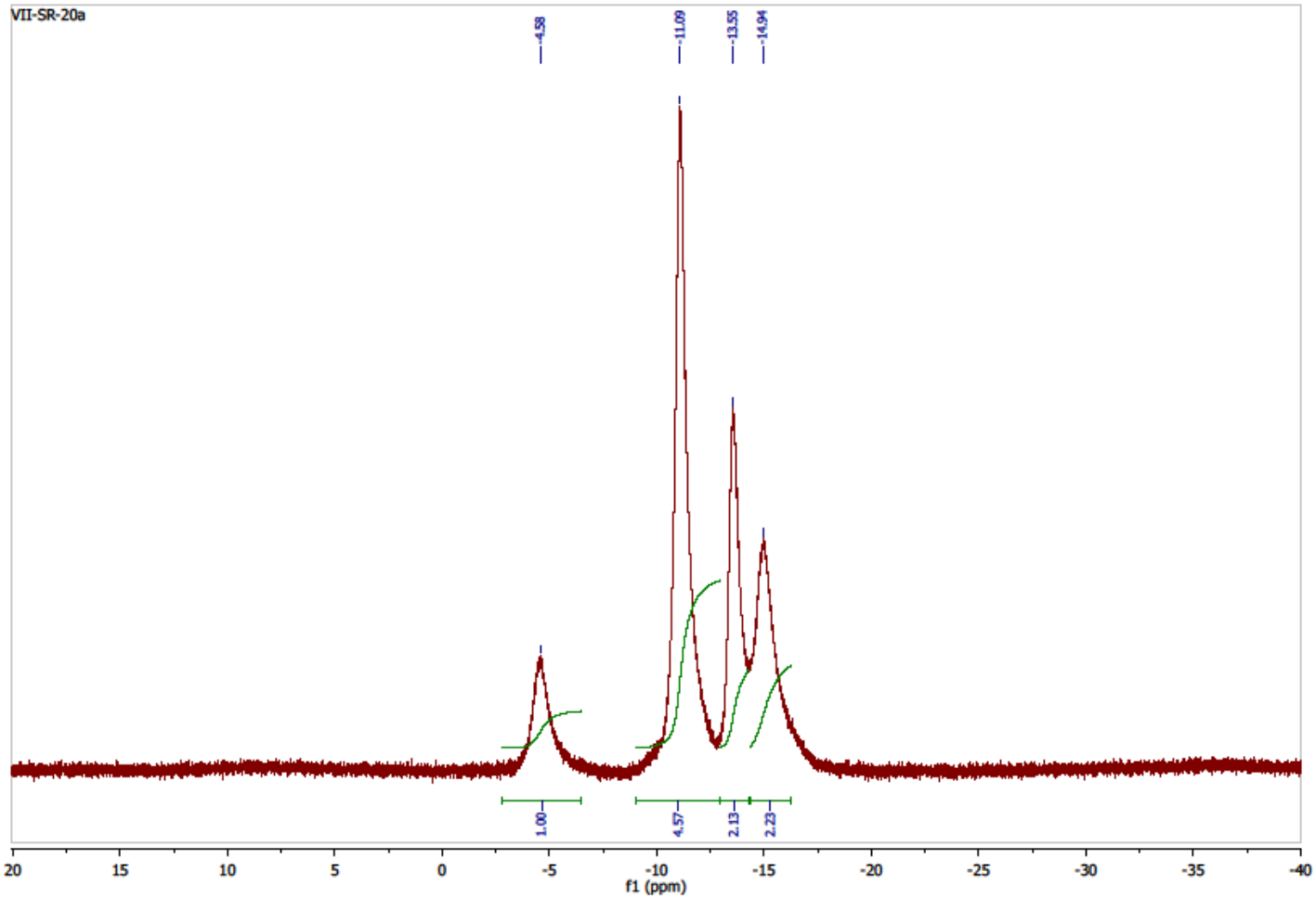

Figure S154. IR spectrum of **42**.

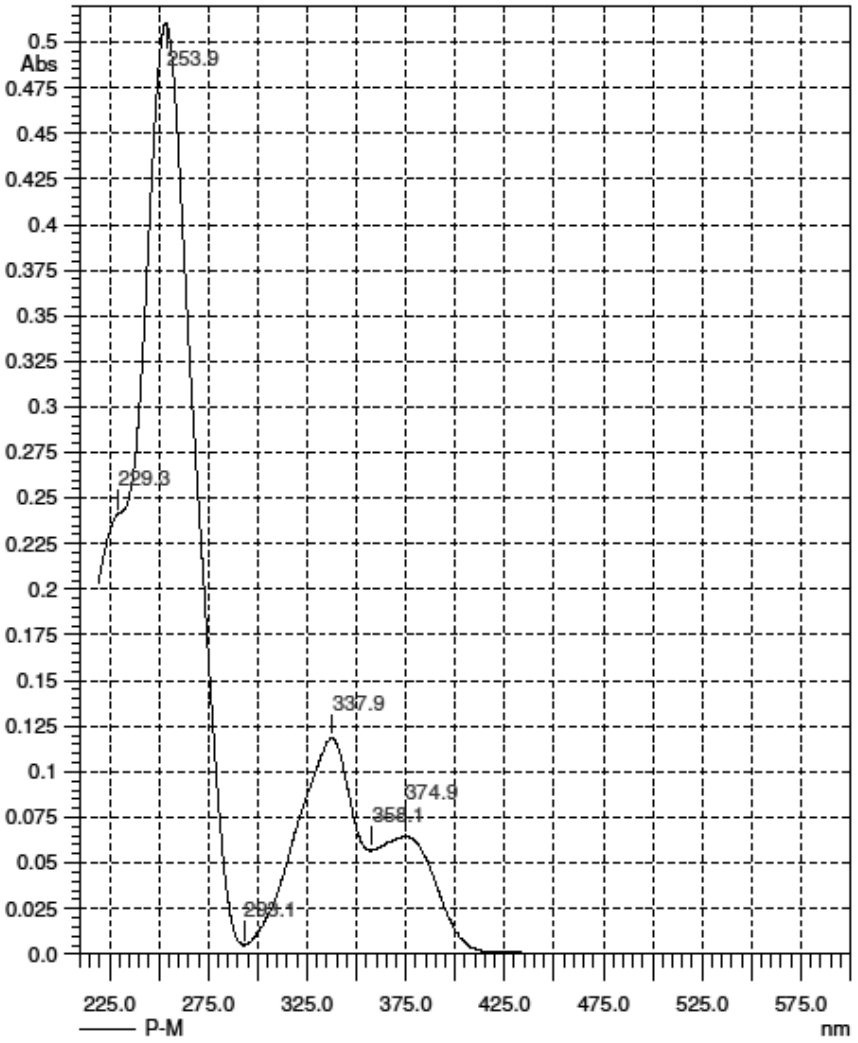

Figure S155. UV spectrum of **42**.

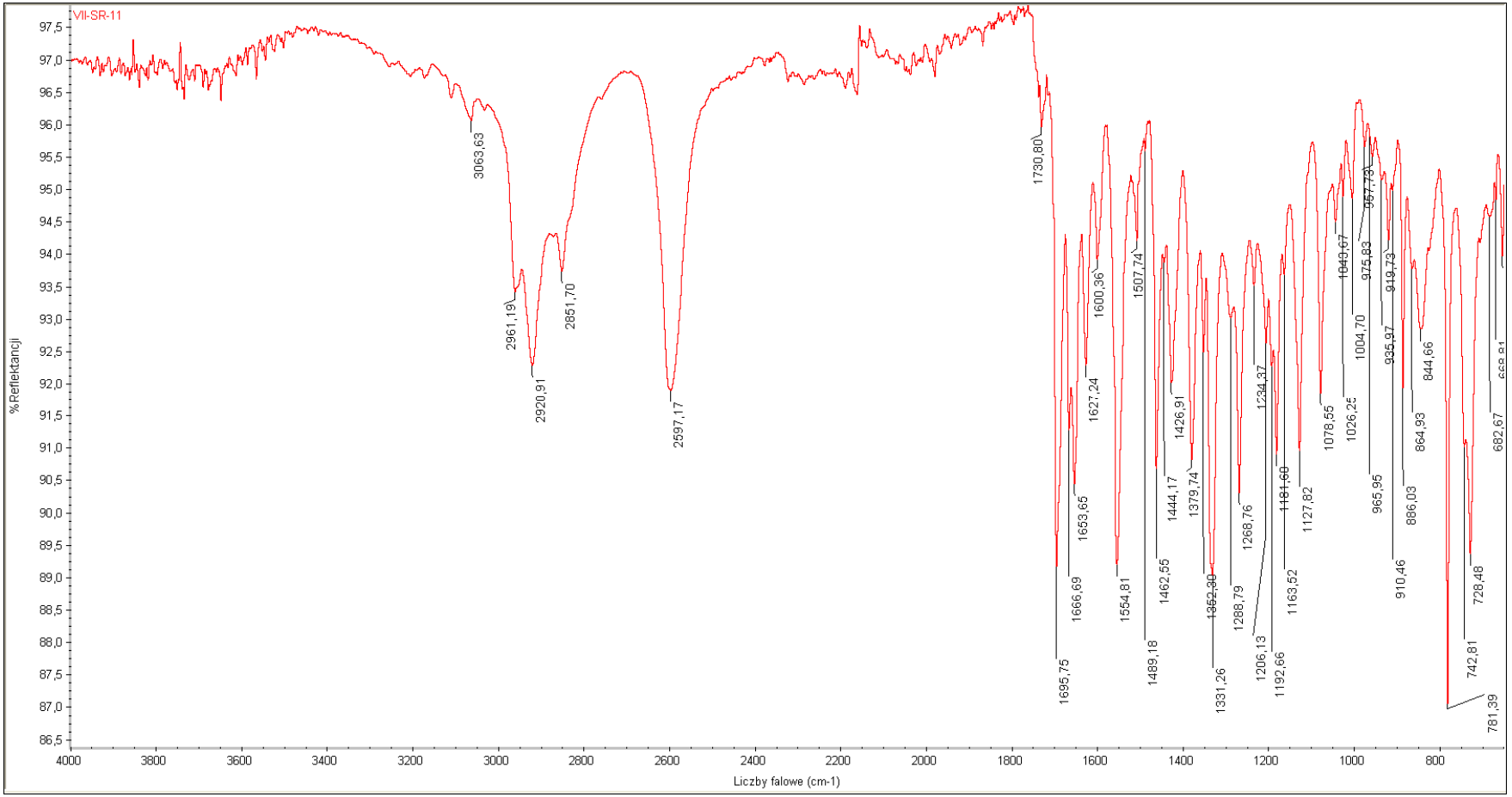

Figure S156. IR spectrum of **42**.

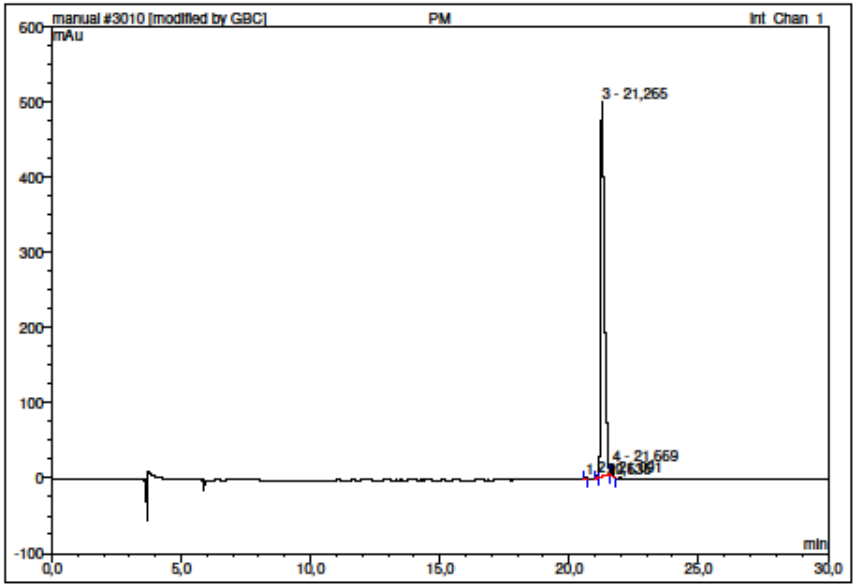

No.	Ret.Time min	Peak Name	Height mAu	Area mAu*min	Rel.Area %	Amount	Type
1	20,63	n.a.	2,620	0,196	0,23	n.a.	BMB*
2	21,09	n.a.	2,455	0,155	0,18	n.a.	BMB*
3	21,27	n.a.	499,429	85,637	98,17	n.a.	BMB
4	21,67	n.a.	14,407	1,245	1,43	n.a.	BMB*
Total:			518,910	87,233	100,00	0,000	

Figure S157. HPLC analysis of **42**.

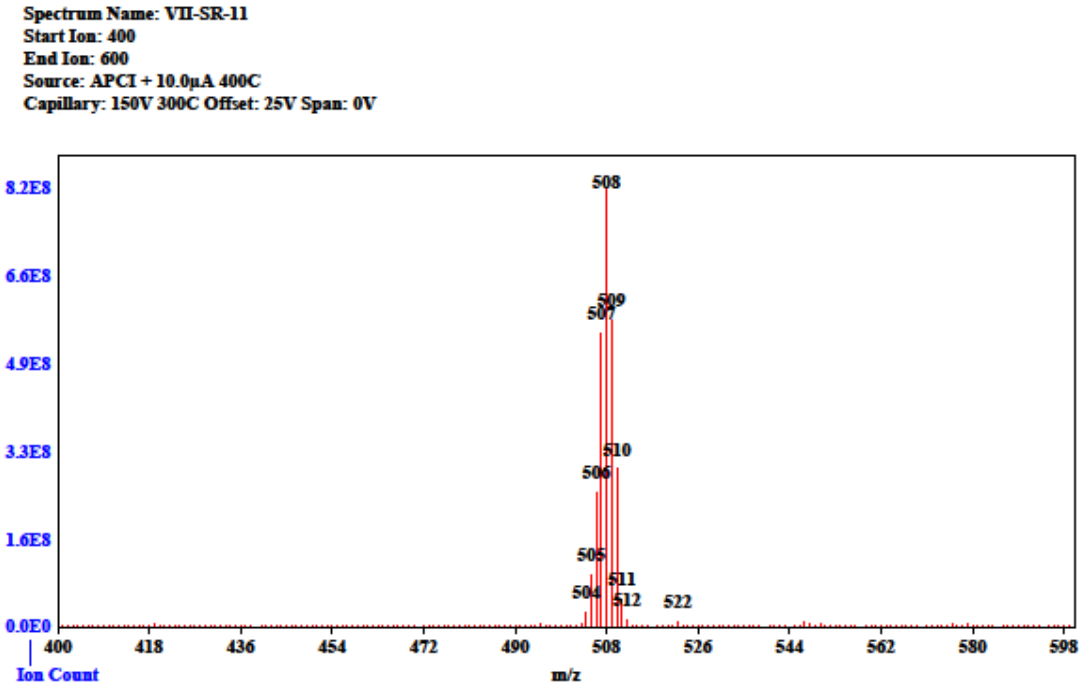

Figure S158. MS spectrum of **42**.

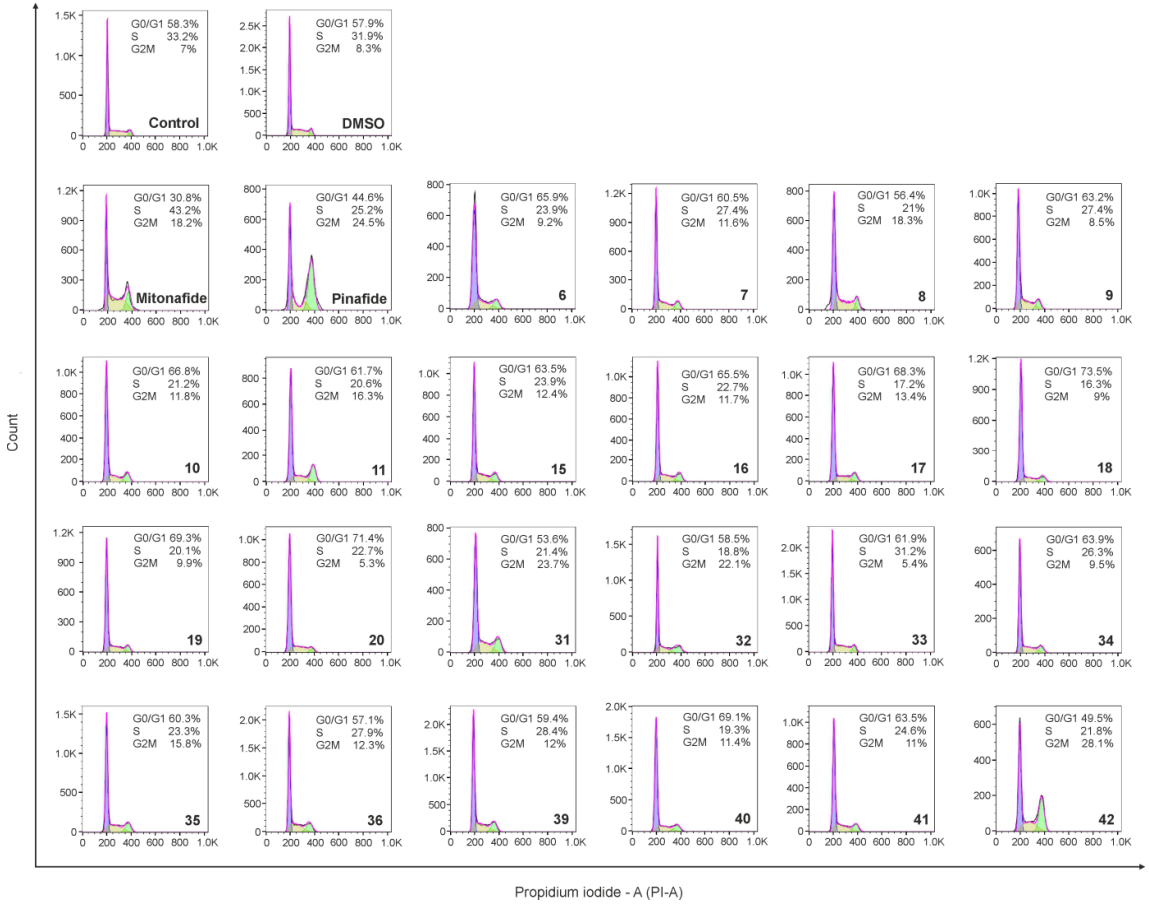

Figure S159. Influence of compound **6** (115 μM), **7** (104 μM), **8** (4 μM), **9** (3 μM), **10** (8 μM), **11** (5 μM), **15** (68 μM), **16** (61 μM), **17** (10 μM), **18** (15 μM), **19** (14 μM), **20** (12 μM), **31**, (53 μM), **32** (42 μM), **33** (5 μM), **34** (8 μM), **35** (9 μM), **36** (6 μM), **39** (11 μM), **40** (13 μM), **41** (10 μM), **42** (6 μM) on cell cycle distribution in HepG2 cells. Flow cytometry analysis of cells treated for 24 h with tested compounds. One representative experiment of three is shown.

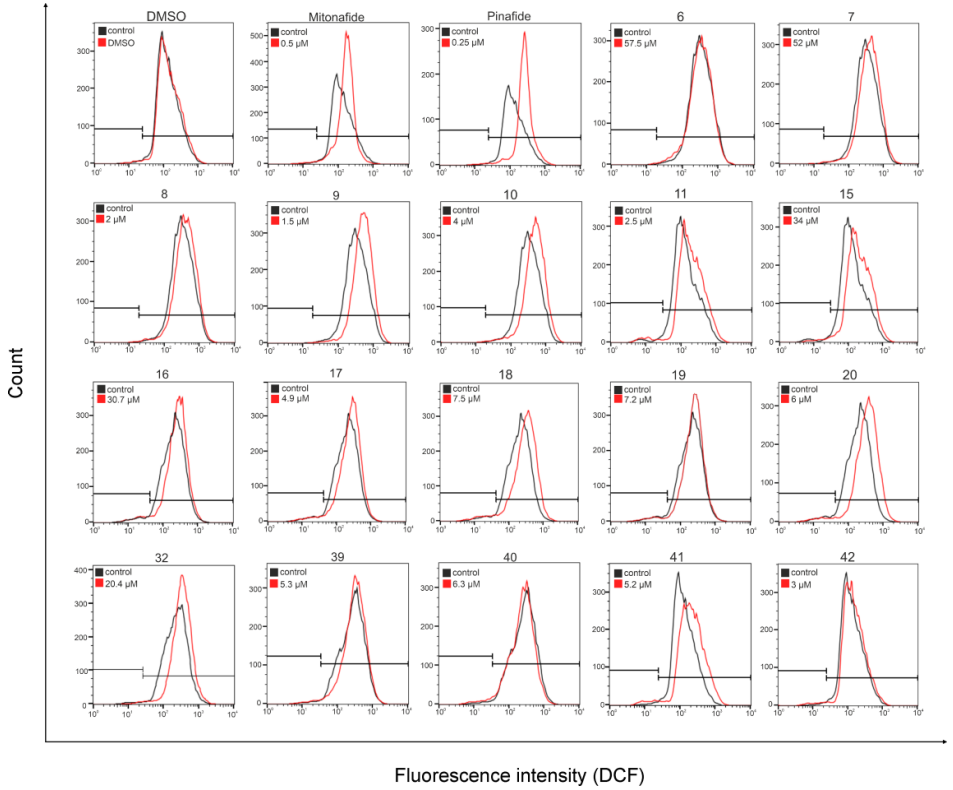

Figure S160. ROS production in HepG2 cells after 24 h incubation with compound **6** (57.5 μM), **7** (52 μM), **8** (2 μM), **9** (1.5 μM), **10** (4 μM), **11** (2.5 μM), **15** (34 μM), **16** (30.7 μM), **17** (4.9 μM), **18** (7.5 μM), **19** (7.2 μM), **20** (6 μM), **32** (20.4 μM), **39** (5.3 μM), **40** (6.3 μM), **41** (5.2 μM), **42** (3 μM). Intracellular production of ROS was measured using dual H_2DCFDA/PI staining. The intensity of DCF fluorescence corresponds to intracellular ROS level in HepG2 cells. The flow cytometric analysis indicated DCF fluorescence shift, which is correlated with higher ROS production after 24 h incubation with the tested compounds compared to control.

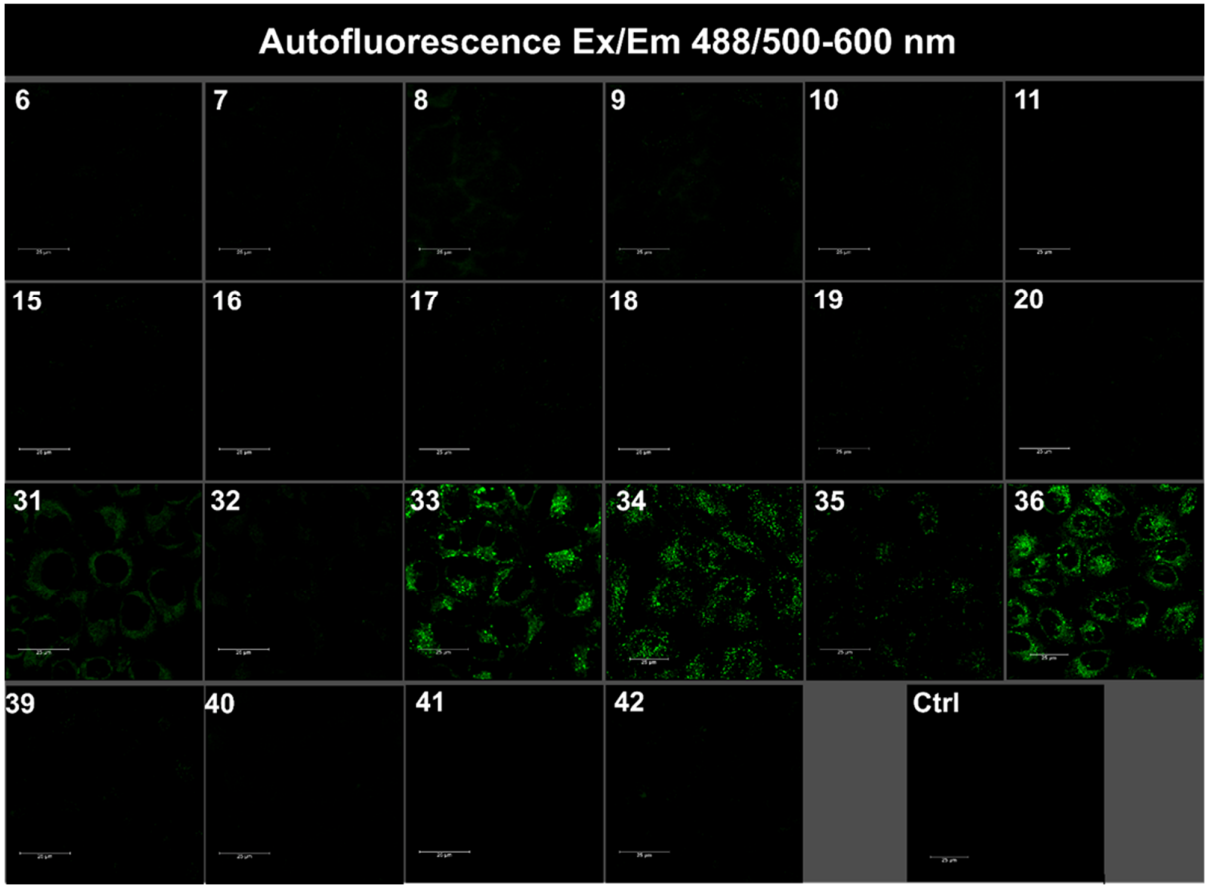

Figure S161. Autofluorescence analysis of the tested compounds in HepG2 cells**.** Confocal microscopy analysis was performed 8 h after treatment with the compounds in the final concentration corresponding to IC_{50}. The number of each compound is placed in the left corner of the picture. The intensity of the autofluorescence was analyzed at Ex/Em 488/500-600 nm.

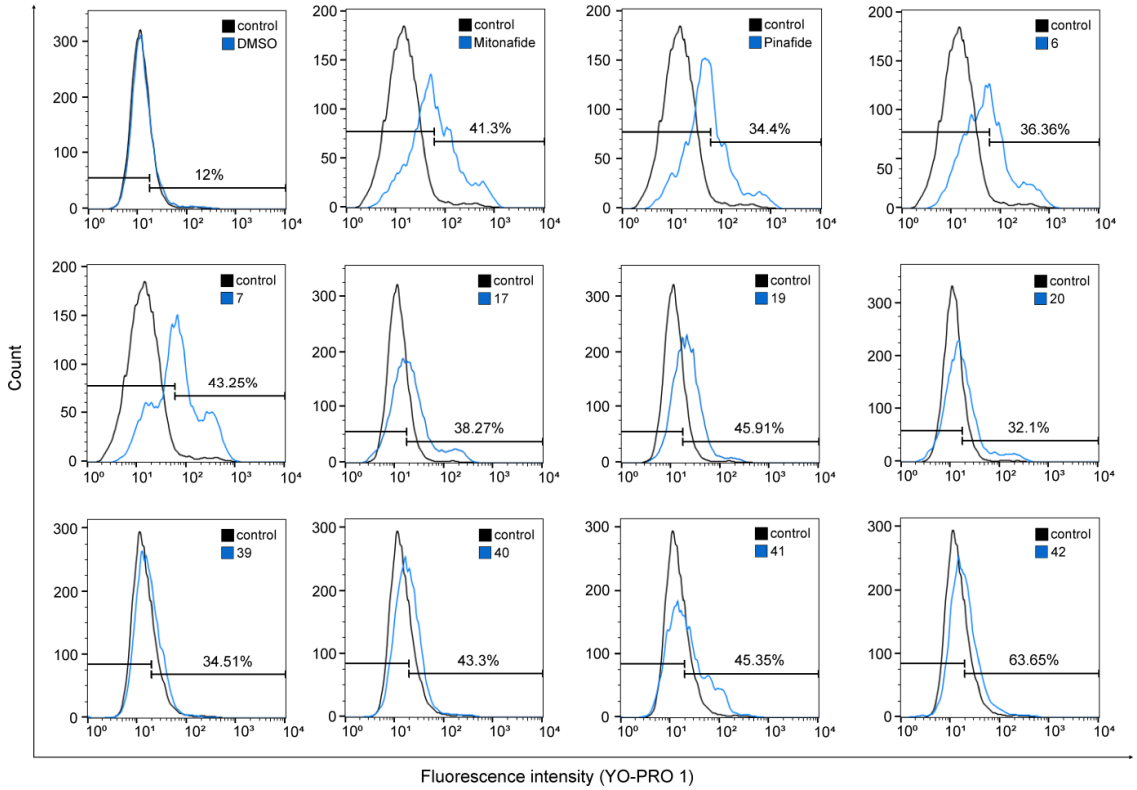

Figure S162. Flow cytometry analysis of apoptosis/necrosis in HepG2 cells after cell toxicity induction with compound **6** (115 μM), **7** (104 μM), **8** (4 μM), **9** (3 μM), **10** (8 μM), **11** (5 μM), **15** (68 μM), **16** (61 μM), **17** (10 μM), **18** (15 μM), **19** (14 μM), **20** (12 μM), **31** (53 μM), **32** (42 μM), **33** (5 μM), **34** (8 μM), **35** (9 μM), **36** (6 μM), **39** (11 μM), **40** (13 μM), **41** (10 μM), **42** (6 μM). The chosen concentration of each compound corresponded to whole IC_{50} values. The number of apoptotic cells for each compound is indicated on histogram. Level of apoptosis was evaluated with dual staining with YO-PRO-1/PI.

Table 1S. Percentage distribution of early and late apoptotic and necrotic cells assessed by flow cytometry.

compound	live cells [%]	early apoptosis [%]	late apoptosis [%]	necrosis [%]
6	47.75 ± 4.78	1.56 ±0.26	28.80 ± 3.72	21.85 ± 1.12
7	25.90 ±0.34	4.55 ± 0.67	38.70 ± 1.72	30.85 ± 2.14
17	60.75 ± 4.49	30.70 ± 4.76	7.57 ± 0.98	0.98 ± 0.33
19	53.40 ± 3.59	39.25 ± 6.30	6.66 ± 2.55	0.72 ± 0.35
20	66.70 ± 2.86	18.75 ± 2.5	13.35 ± 2.69	1.23 ± 0.41
39	65.40 ± 0.88	31.65 ± 1.52	2.86 ± 1.05	0.08 ± 0.02
40	57.40 ± 1.9	32.35 ± 2.49	9.95 ± 2.17	0.35 ± 0.21
41	54.35 ± 3.82	26.75 ± 2.17	18.60 ± 3.01	0.34 ± 0.07
42	36.10 ± 3.8	24.65 ± 1.78	39.00 ± 5.33	0.24 ± 0.04
Mitonafide	37.25 ± 1.09	1.90 ± 0.19	39.40 ± 1.94	21.40 ± 3.13
Pinafide	47.10 ± 1.01	1.40 ± 0.57	33.00 ± 1.19	18.50 ± 1.72

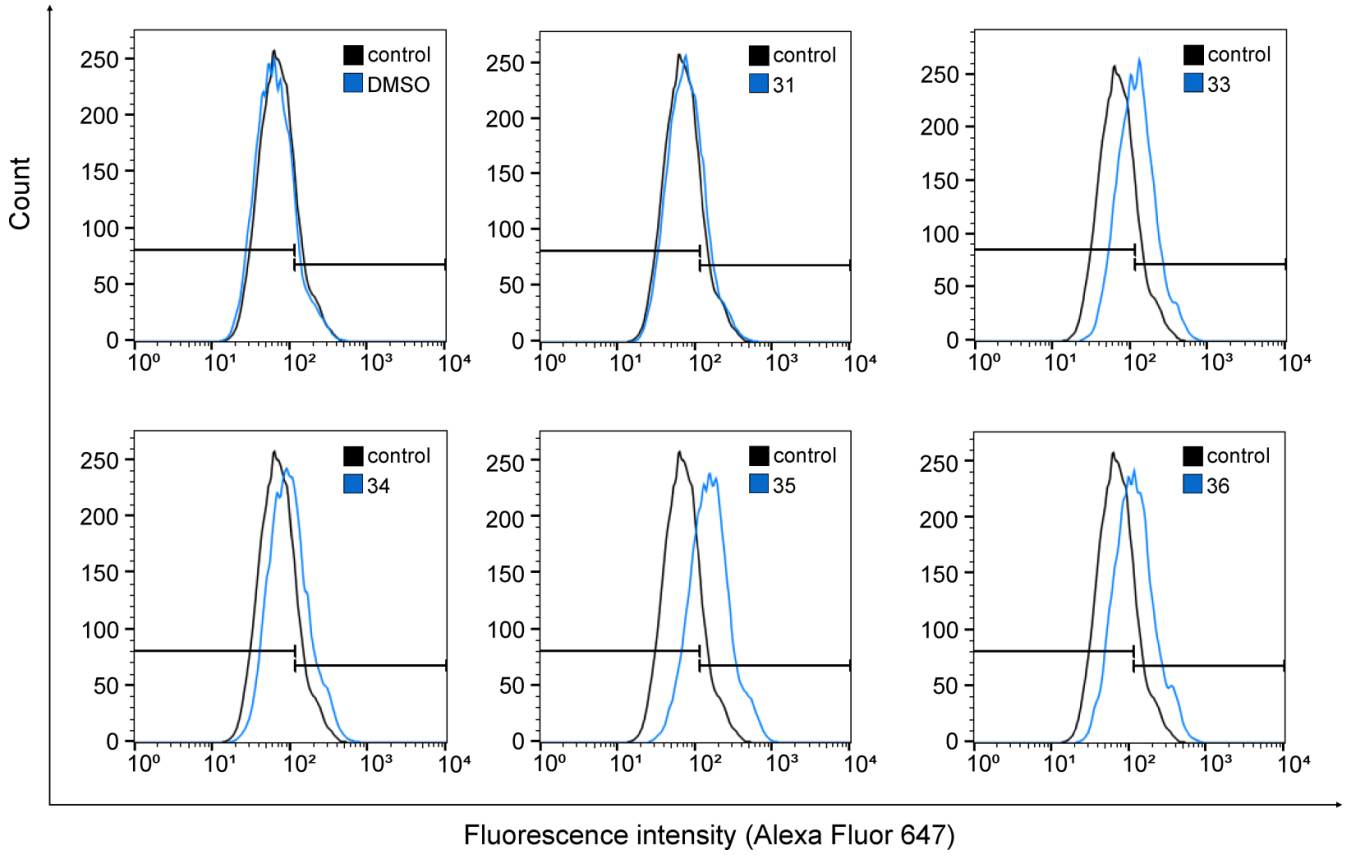

Figure S163. Flow cytometry analysis of apoptosis/necrosis in HepG2 cells after cell toxicity induction with compound **31** (53 μM), **33** (5 μM), **34** (8 μM), **35** (9 μM), **36** (6 μM). The chosen concentration of each compound corresponded to whole IC_{50} values. The number of apoptotic cells for each compound is indicated on histogram. Level of apoptosis was evaluated with Annexin V Alexa Fluor 647 conjugate.

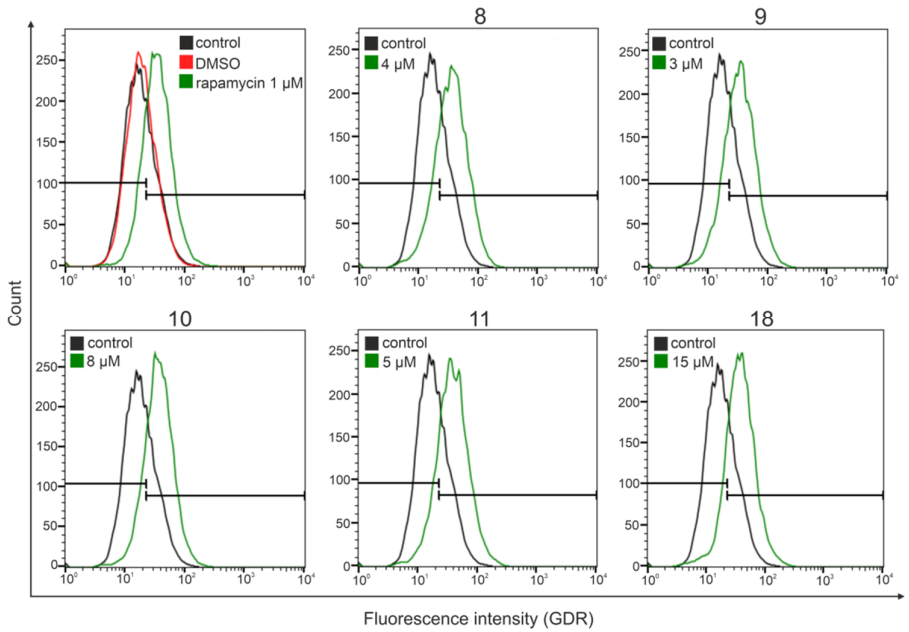

Figure S164. Flow cytometry analysis of autophagy in HepG2 cells after cell toxicity induction with compound **8** (4 µM), **9** (3 µM), **10** (8 µM), **11** (5 µM), **18** (15 µM). The chosen concentration of each compound corresponded to whole IC_{50} values. Level of autophagy was evaluated with Green Detection Reagent. Rapamycin was used as positive control. One representative experiment of three is shown.

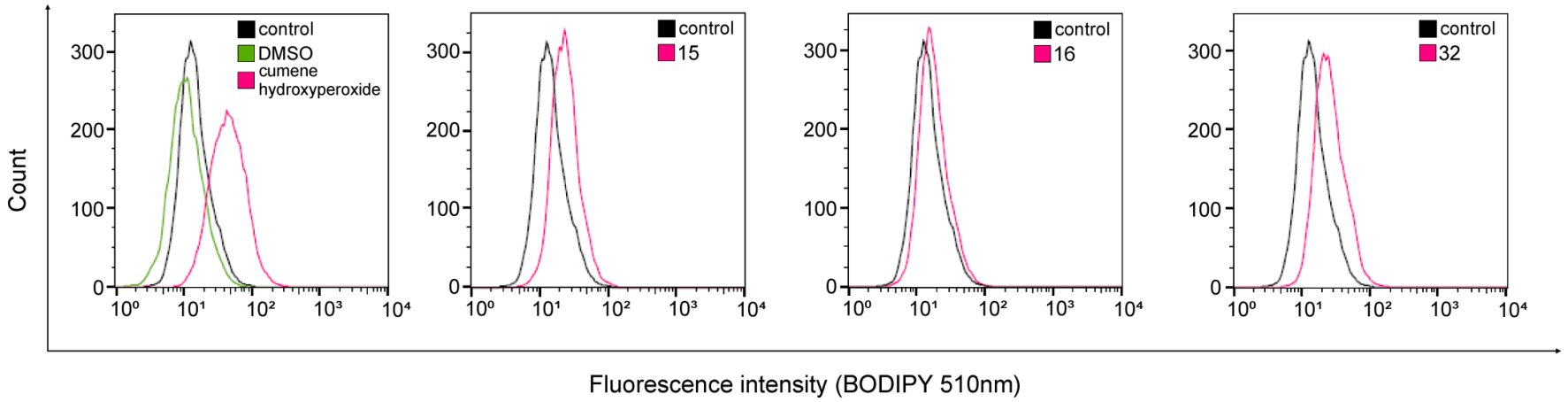

Figure S165. Flow cytometry analysis of lipid peroxidation in HepG2 cells after cell toxicity induction with compound **15** (68 μM), **16** (61 μM), **32** (42 μM). The chosen concentration of each compound corresponded to whole IC_{50} values. Level of lipid peroxidation was evaluated with 581/591 C11 reagent. To induce strong positive signal the cells were incubated with cumene peroxide. One representative experiment of three is shown.

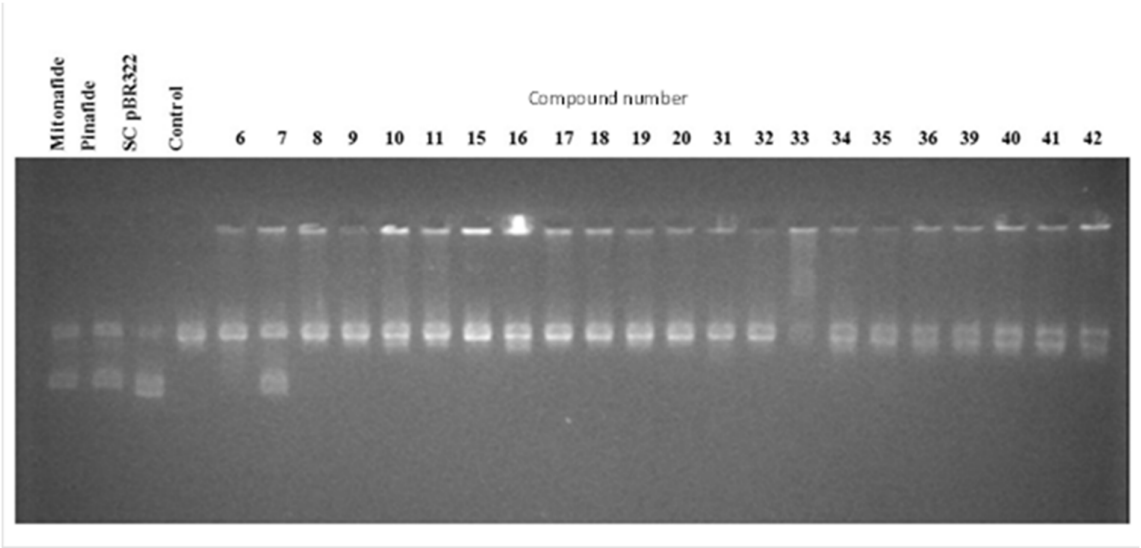

Figure S166. Human Topoisomerase IIα relaxation assay in the presence of modified with carborane cluster naphthalic anhydrides (**6**, **7**, **15**, **16**, **31**, **32**), naphthalimides (**8**-**11**, **17**-**20**, **33**-**36**, **39**-**42**), and the control drugs mitonafide and pinafide at a concentration of 100 μM.
SC – supercoiled DNA.

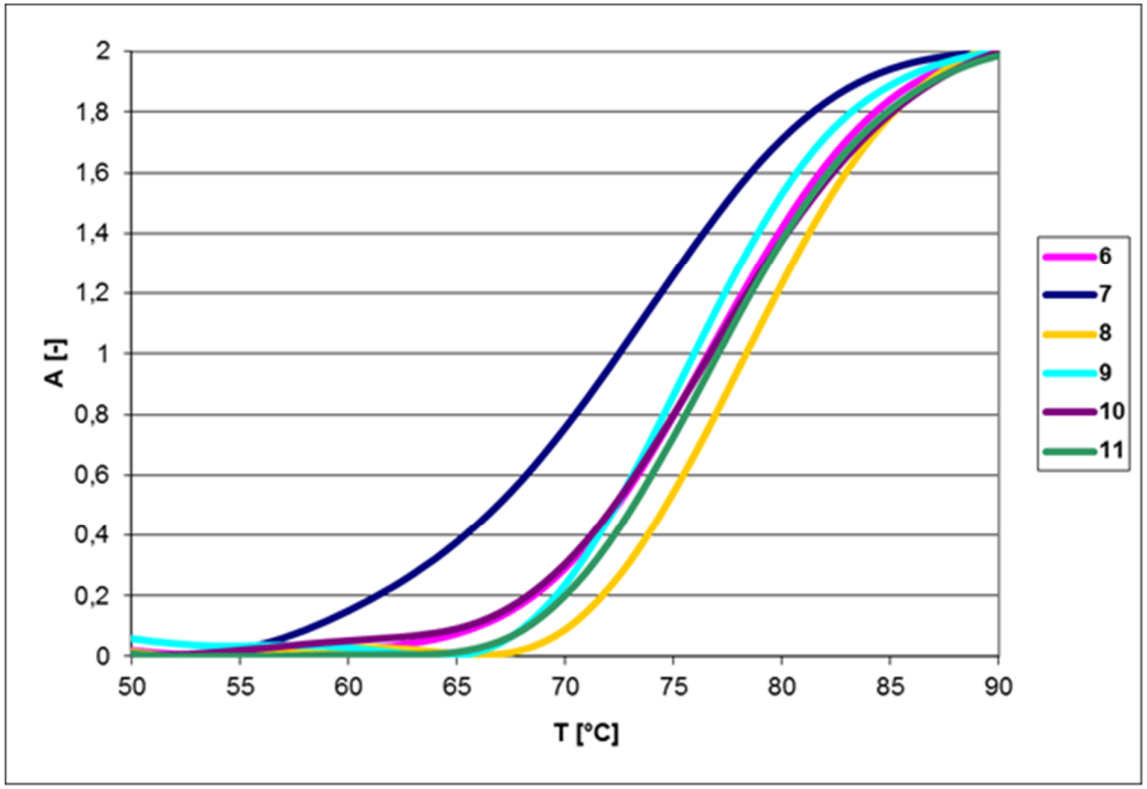

Figure S167. Melting curves of ct-DNA upon addition of **6**-**11** (c (ct-DNA) = 2×10^{-5} mol dm^{-3}) at molar ratio r = 0.3 (r = [compound]/[ct-DNA]), sodium cacodylate buffer (pH 7.0, 20 mM).

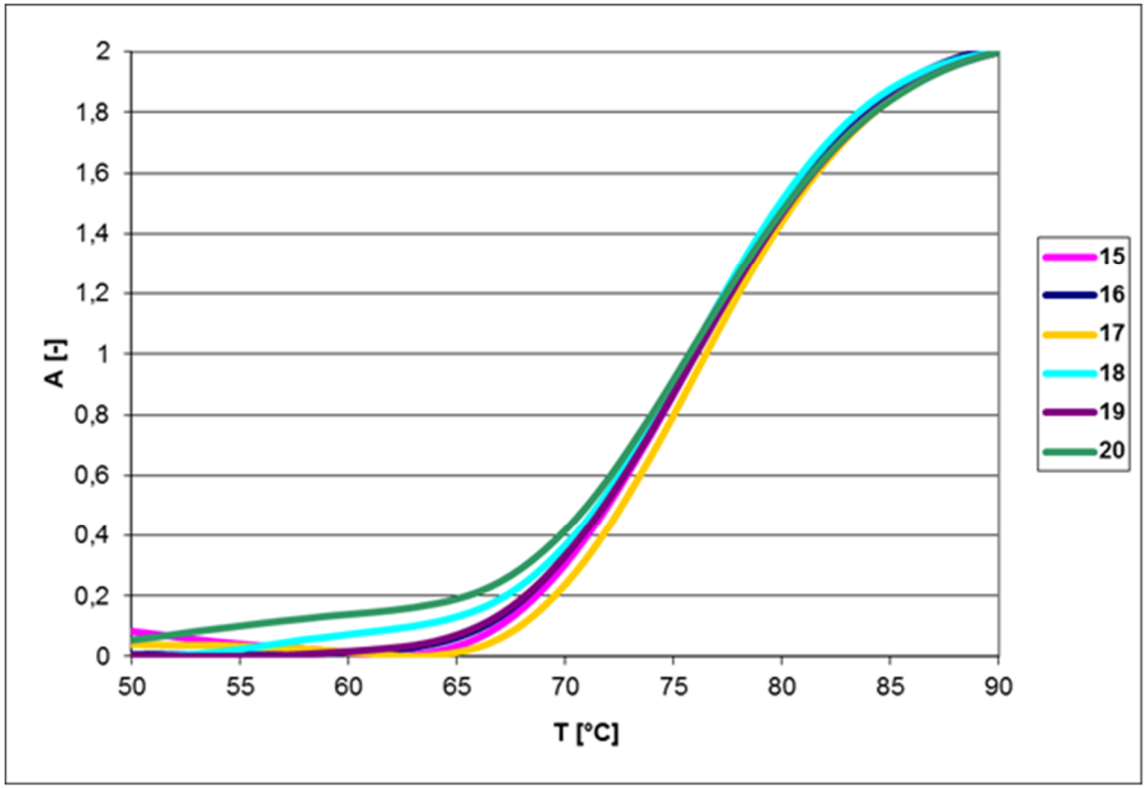

Figure S168. Melting curves of ct-DNA upon addition of **15**-**20** (c (ct-DNA) = 2×10^{-5} mol dm^{-3}) at molar ratio r = 0.3 (r = [compound]/[ct-DNA]), sodium cacodylate buffer (pH 7.0, 20 mM).

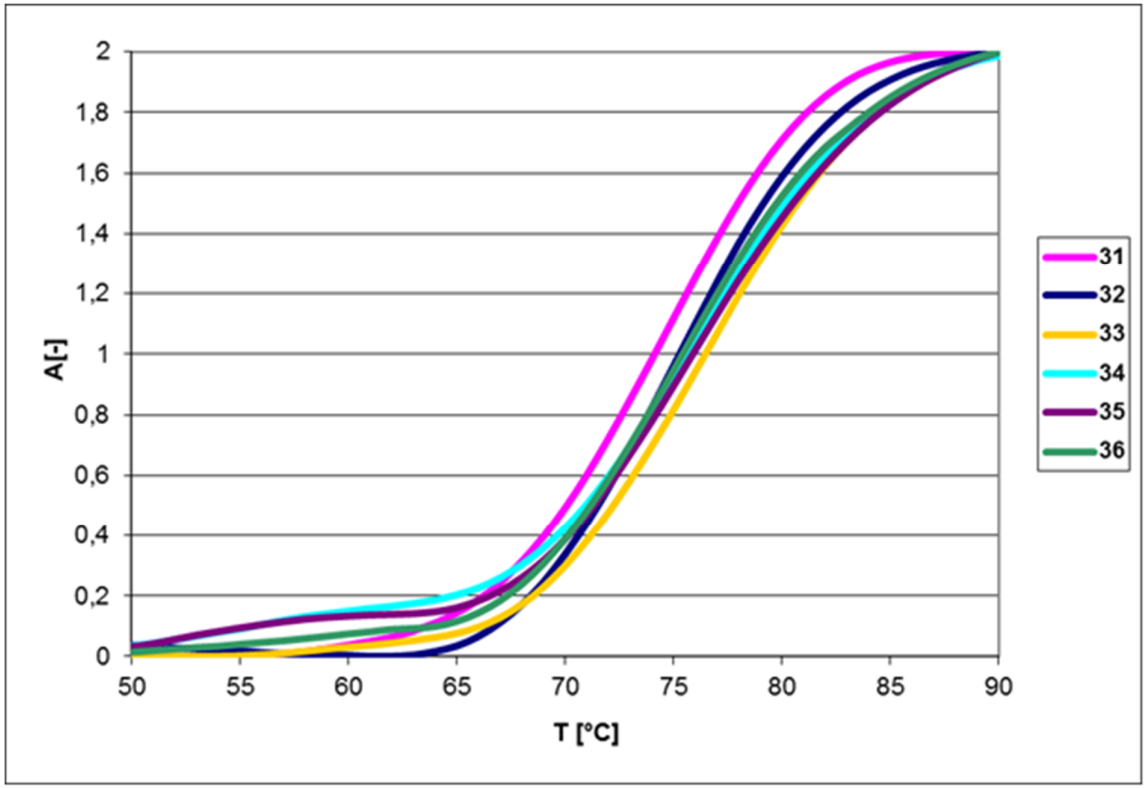

Figure S169. Melting curves of ct-DNA upon addition of **31-36** (c (ct-DNA) = 2×10^{-5} mol dm^{-3}) at molar ratio r = 0.3 (r = [compound]/[ct-DNA]), sodium cacodylate buffer (pH 7.0, 20 mM).

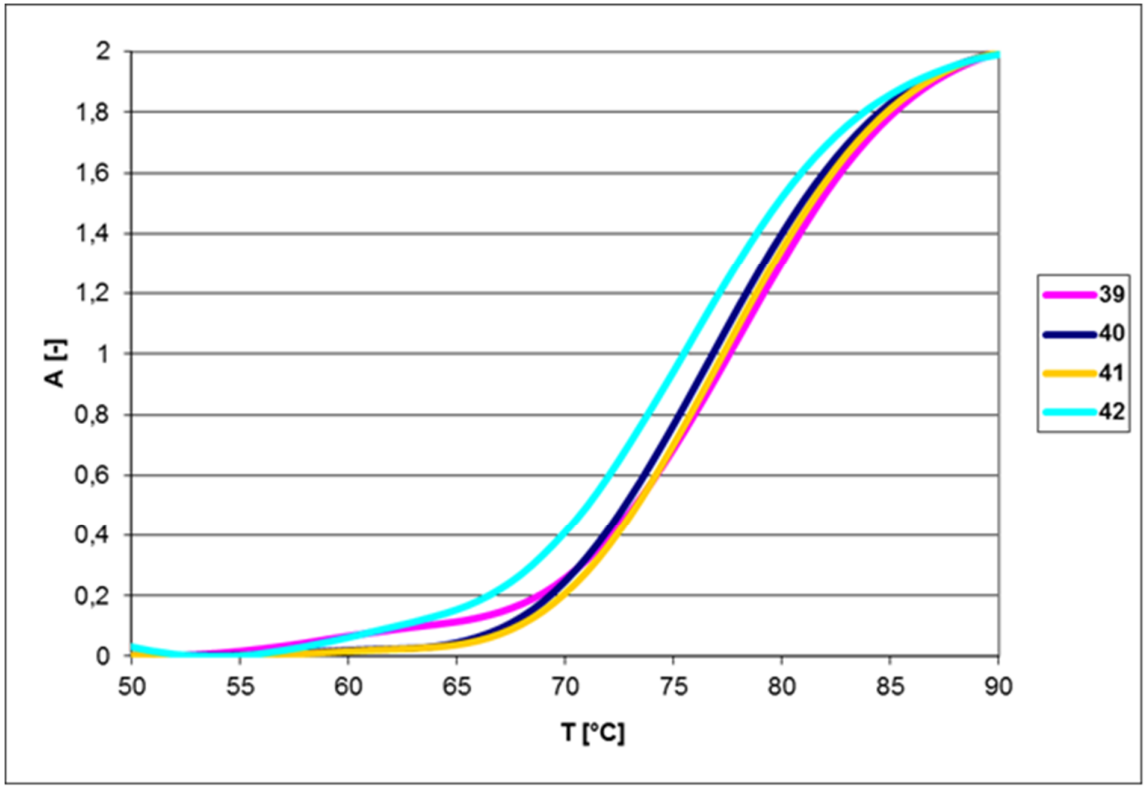

Figure S170. Melting curves of ct-DNA upon addition of **39**-**42** (c (ct-DNA) = 2×10^{-5} mol dm^{-3}) at molar ratio r = 0.3 (r = [compound]/[ct-DNA]), sodium cacodylate buffer (pH 7.0, 20 mM).

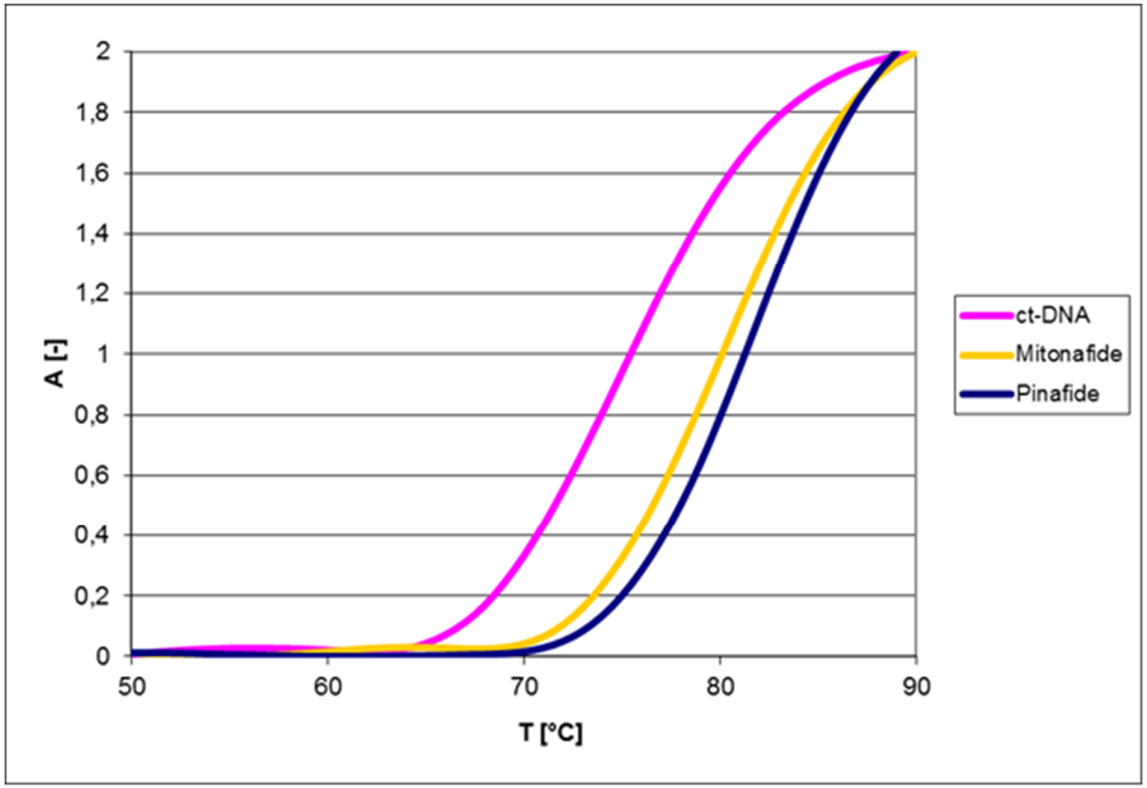

Figure S171. Melting curves of ct-DNA upon addition of mitonafide and pinafide (c (ct-DNA) = 2×10^{-5} mol dm^{-3}) at molar ratio r = 0.3 (r = [compound]/[ct-DNA]), sodium cacodylate buffer (pH 7.0, 20 mM).

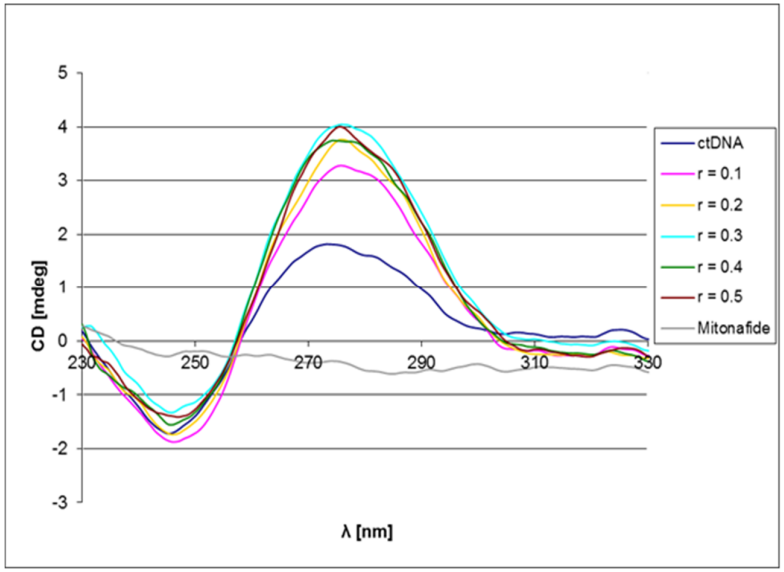

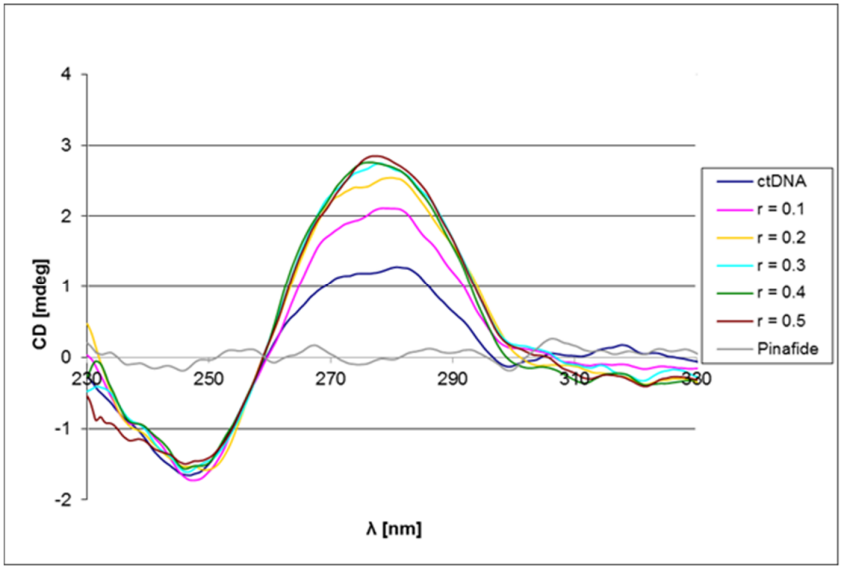

Figure S172. Changes in the CD spectrum of ct-DNA upon addition of mitonafide (left) and pinafide (right) (c (ct-DNA) = 4×10^{-5} mol dm^{-3}) at different molar ratios r = [compound]/[ct-DNA], sodium cacodylate buffer (pH 7.0, 20 mM).

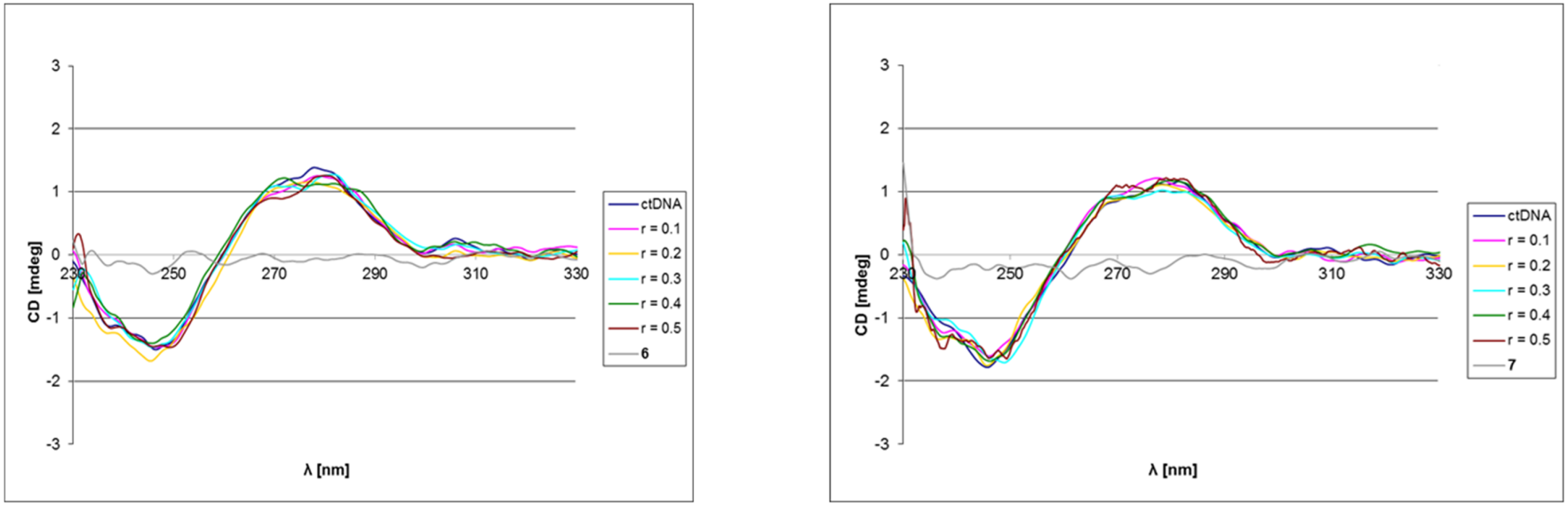

Figure S173. Changes in the CD spectrum of ct-DNA upon addition of **6** (c (ct-DNA) = 4×10^{-5} mol dm^{-3}) (left) and **7** (c (ct-DNA) = 4×10^{-5} mol dm^{-3}) (right) at different molar ratios r = [compound]/[ct-DNA], sodium cacodylate buffer (pH 7.0, 20 mM).

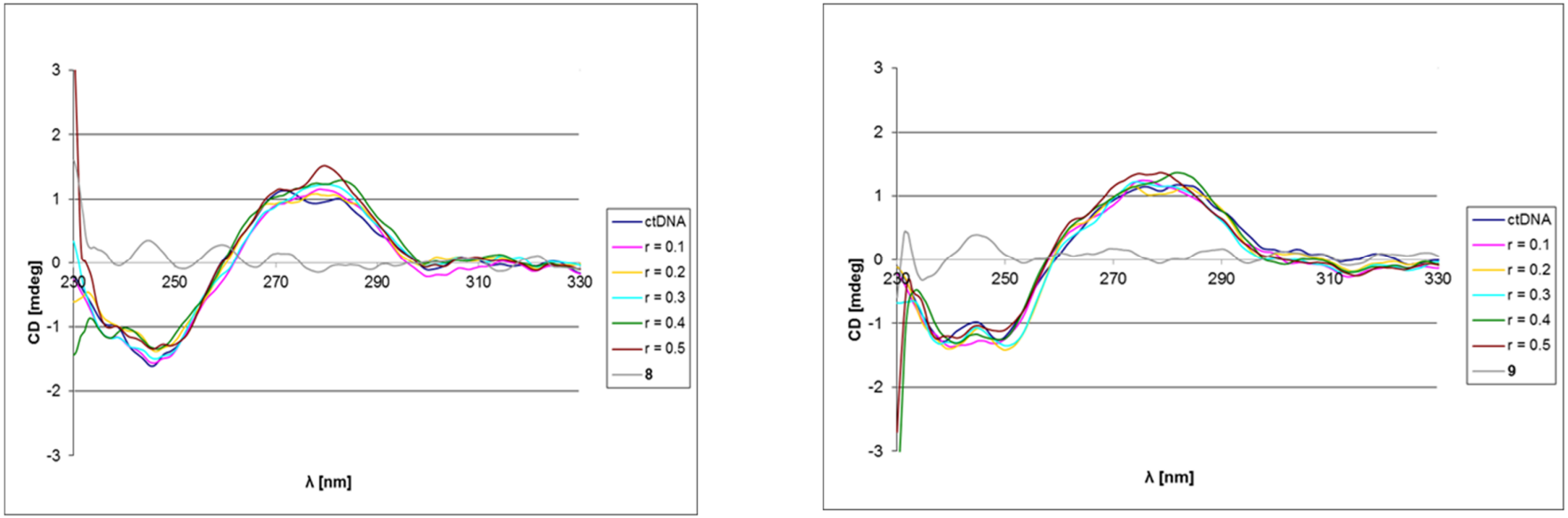

Figure S174. Changes in the CD spectrum of ct-DNA upon addition of **8** (c (ct-DNA) = 4×10^{-5} mol dm^{-3}) (left) and **9** (c (ct-DNA) = 4×10^{-5} mol dm^{-3}) (right) at different molar ratios r = [compound]/[ct-DNA], sodium cacodylate buffer (pH 7.0, 20 mM).

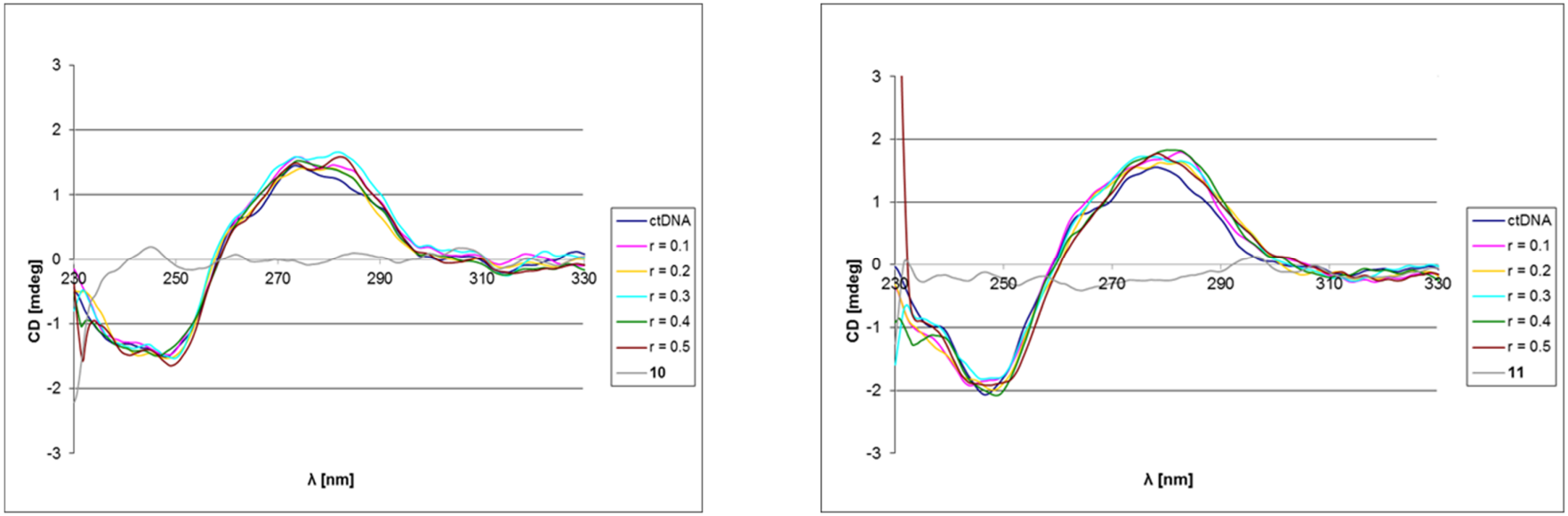

Figure S175. Changes in the CD spectrum of ct-DNA upon addition of **10** (c (ct-DNA) = 4×10^{-5} mol dm^{-3}) (left) and **11** (c (ct-DNA) = 4×10^{-5} mol dm^{-3}) (right) at different molar ratios r = [compound]/[ct-DNA], sodium cacodylate buffer (pH 7.0, 20 mM).

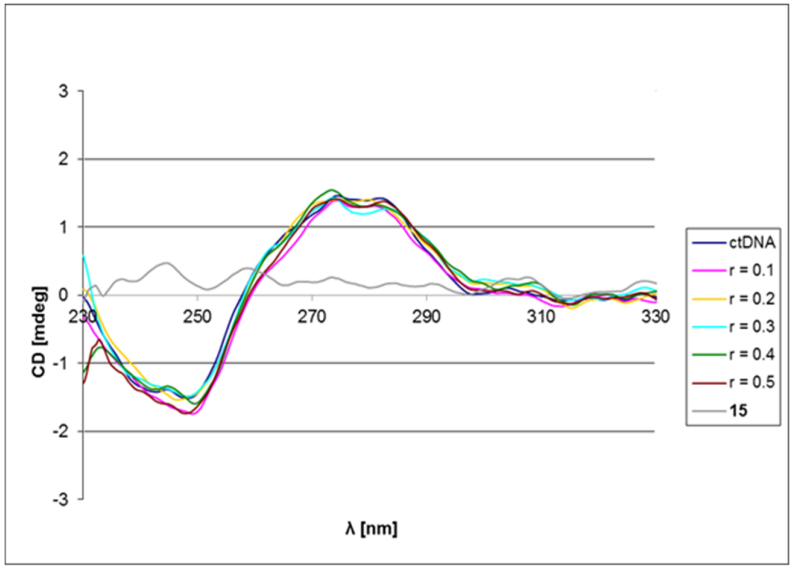

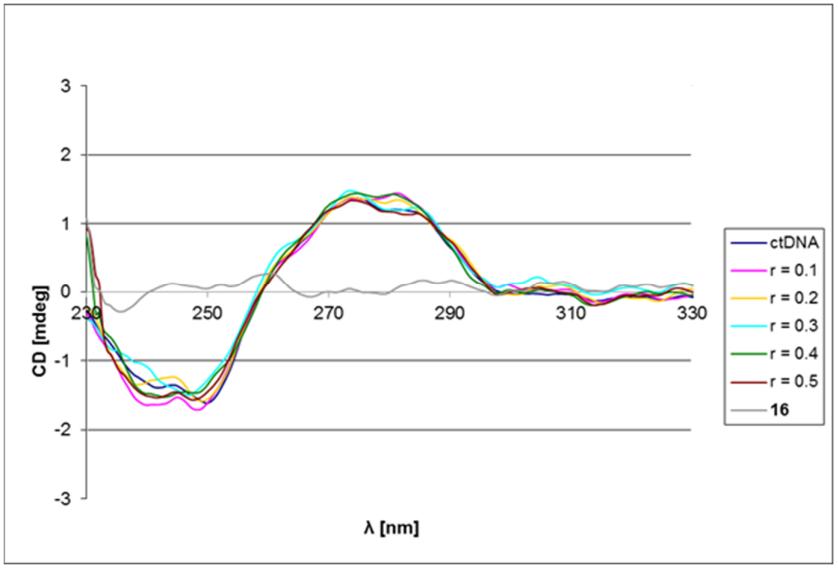

Figure S176. Changes in the CD spectrum of ct-DNA upon addition of **15** (c (ct-DNA) = 4×10^{-5} mol dm^{-3}) (left) and **16** (c (ct-DNA) = 4×10^{-5} mol dm^{-3}) (right) at different molar ratios r = [compound]/[ct-DNA], sodium cacodylate buffer (pH 7.0, 20 mM).

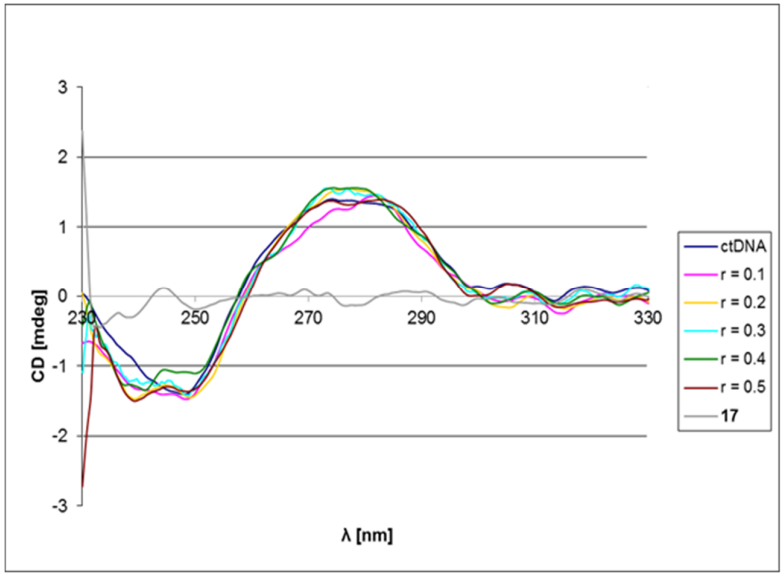

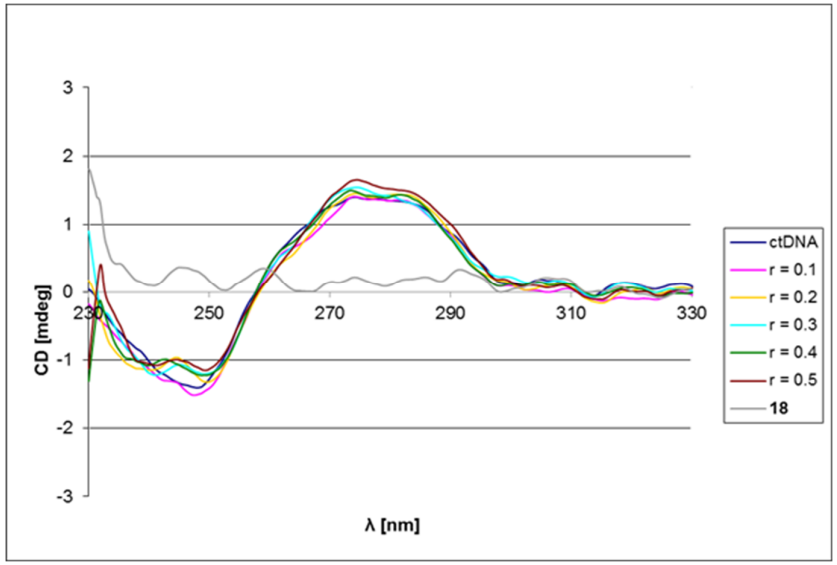

Figure S177. Changes in the CD spectrum of ct-DNA upon addition of **17** (c (ct-DNA) = 4×10^{-5} mol dm^{-3}) (left) and **18** (c (ct-DNA) = 4×10^{-5} mol dm^{-3}) (right) at different molar ratios r = [compound]/[ct-DNA], sodium cacodylate buffer (pH 7.0, 20 mM).

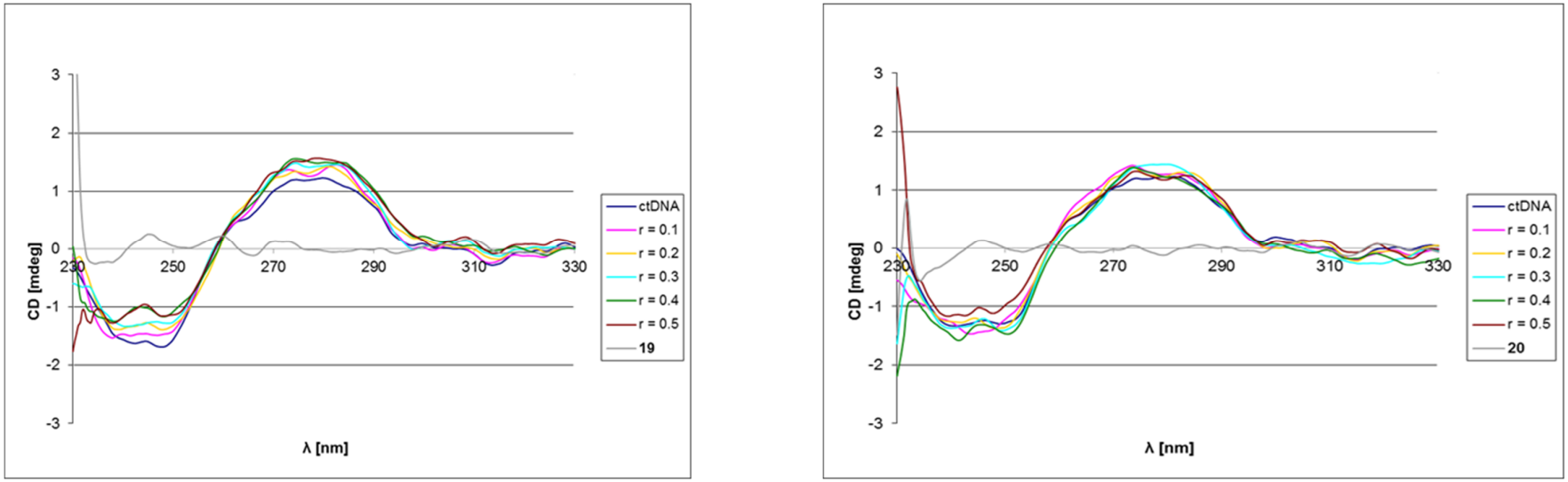

Figure S178. Changes in the CD spectrum of ct-DNA upon addition of **19** (c (ct-DNA) = 4×10^{-5} mol dm^{-3}) (left) and **20** (c (ct-DNA) = 4×10^{-5} mol dm^{-3}) (right) at different molar ratios r = [compound]/[ct-DNA], sodium cacodylate buffer (pH 7.0, 20 mM).

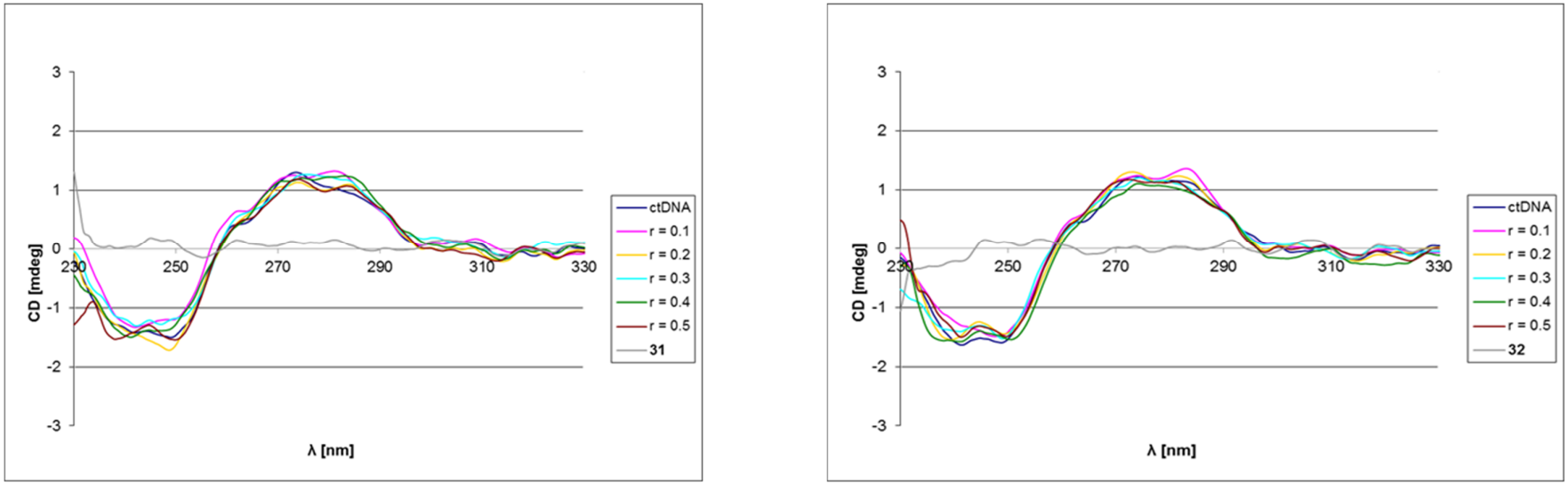

Figure S179. Changes in the CD spectrum of ct-DNA upon addition of **31** (c (ct-DNA) = 4×10^{-5} mol dm^{-3}) (left) and **32** (c (ct-DNA) = 4×10^{-5} mol dm^{-3}) (right) at different molar ratios r = [compound]/[ct-DNA], sodium cacodylate buffer (pH 7.0, 20 mM).

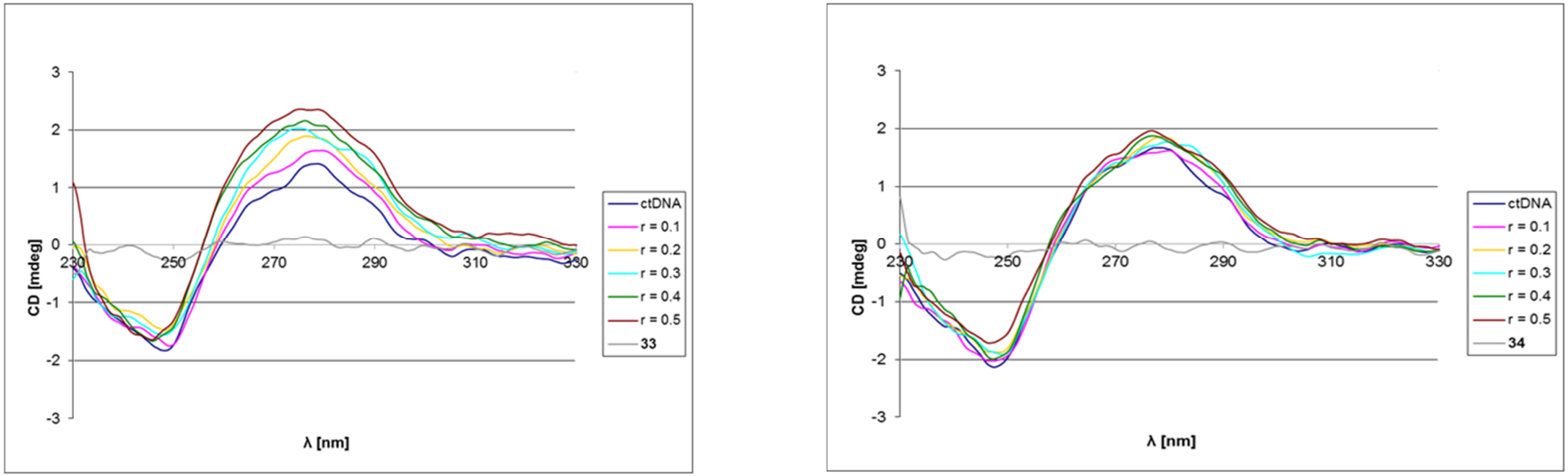

Figure S180. Changes in the CD spectrum of ct-DNA upon addition of **33** (c (ct-DNA) = 4×10^{-5} mol dm^{-3}) (left) and **34** (c (ct-DNA) = 4×10^{-5} mol dm^{-3}) (right) at different molar ratios r = [compound]/[ct-DNA], sodium cacodylate buffer (pH 7.0, 20 mM).

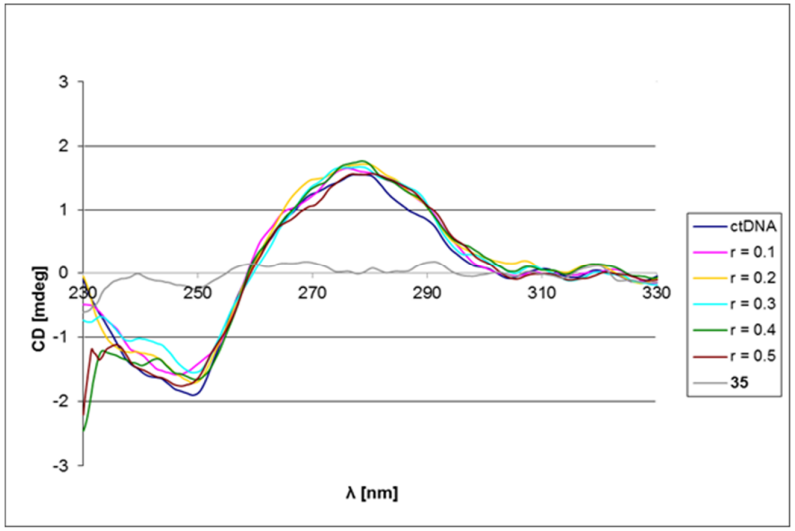

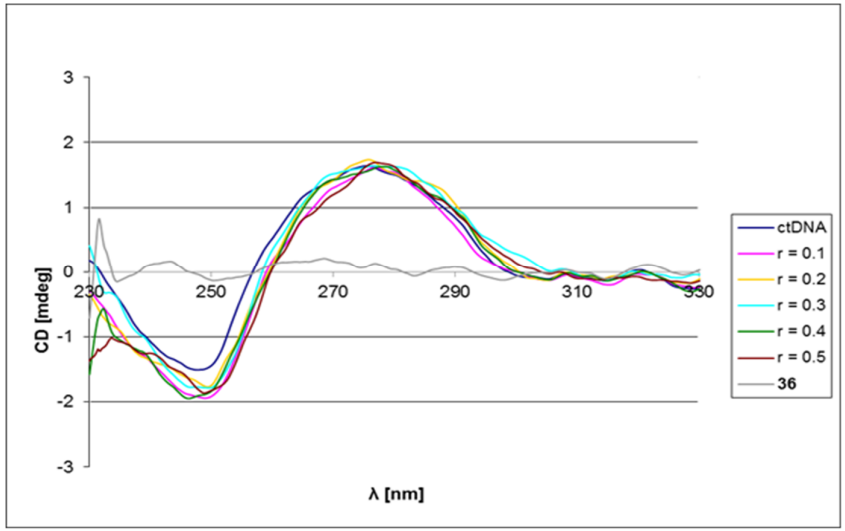

Figure S181. Changes in the CD spectrum of ct-DNA upon addition of **35** (c (ct-DNA) = 4×10^{-5} mol dm^{-3}) (left) and **36** (c (ct-DNA) = 4×10^{-5} mol dm^{-3}) (right) at different molar ratios r = [compound]/[ct-DNA], sodium cacodylate buffer (pH 7.0, 20 mM).

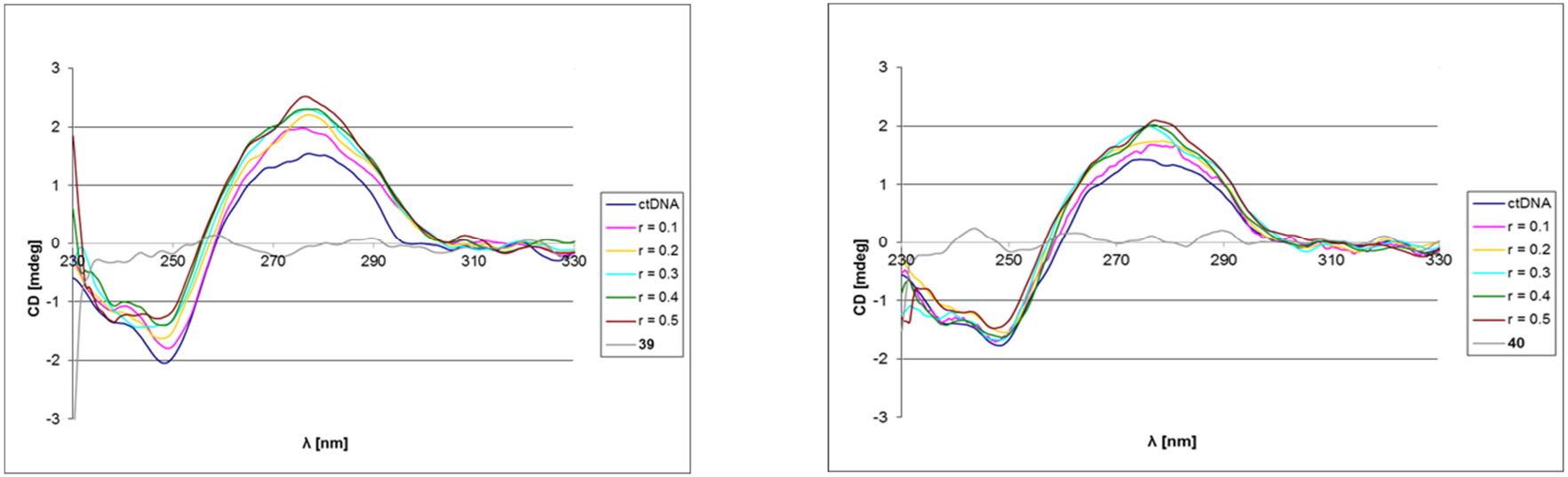

Figure S182. Changes in the CD spectrum of ct-DNA upon addition of **39** (c (ct-DNA) = 4×10^{-5} mol dm^{-3}) (left) and **40** (c (ct-DNA) = 4×10^{-5} mol dm^{-3}) (right) at different molar ratios r = [compound]/[ct-DNA], sodium cacodylate buffer (pH 7.0, 20 mM).

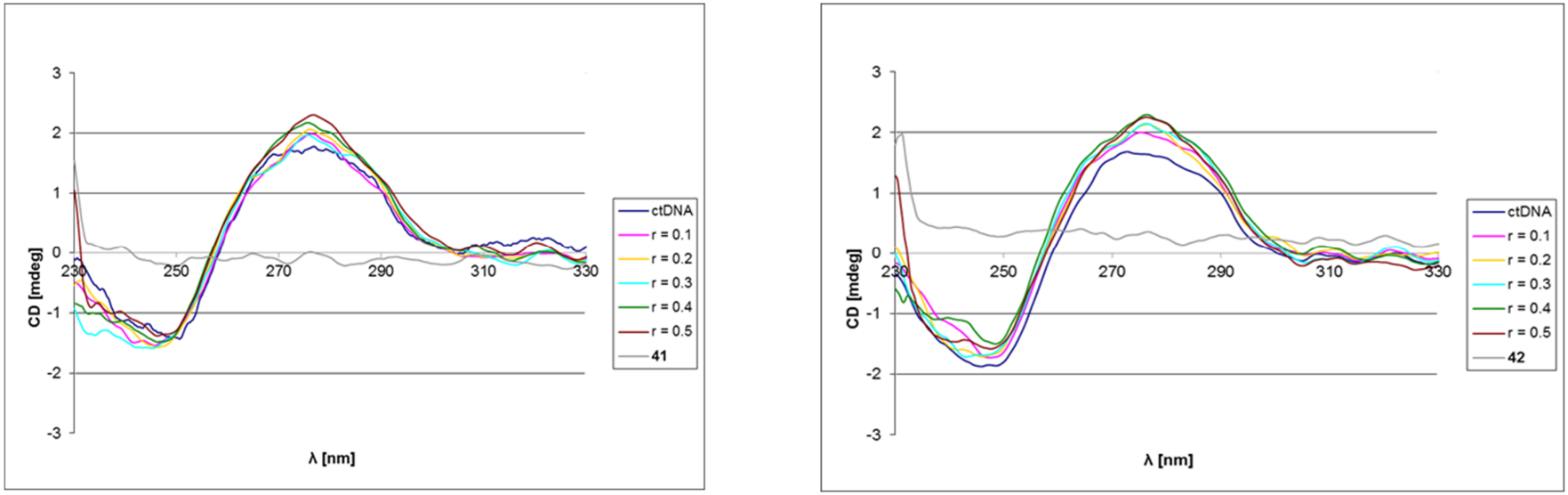

Figure S183. Changes in the CD spectrum of ct-DNA upon addition of **41** (c (ct-DNA) = 4×10^{-5} mol dm^{-3}) (left) and **42** (c (ct-DNA) = 4×10^{-5} mol dm^{-3}) (right) at different molar ratios r = [compound]/[ct-DNA], sodium cacodylate buffer (pH 7.0, 20 mM).

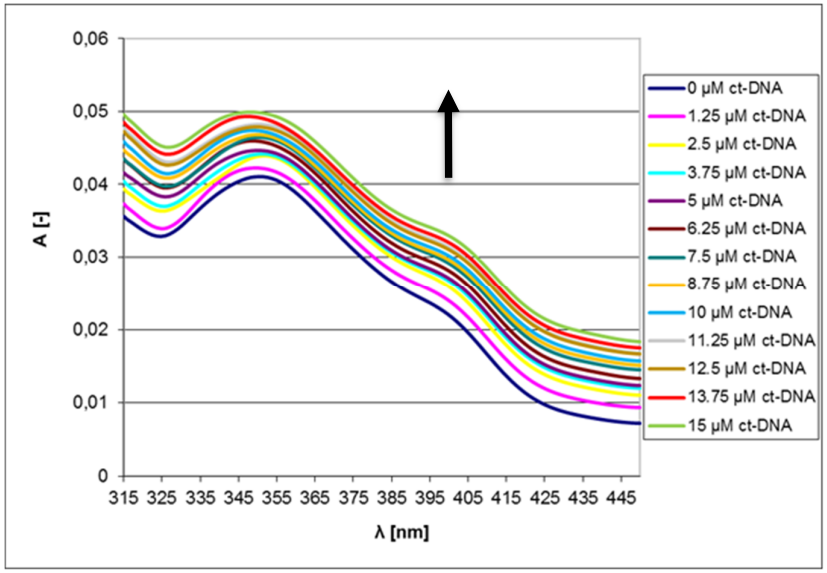

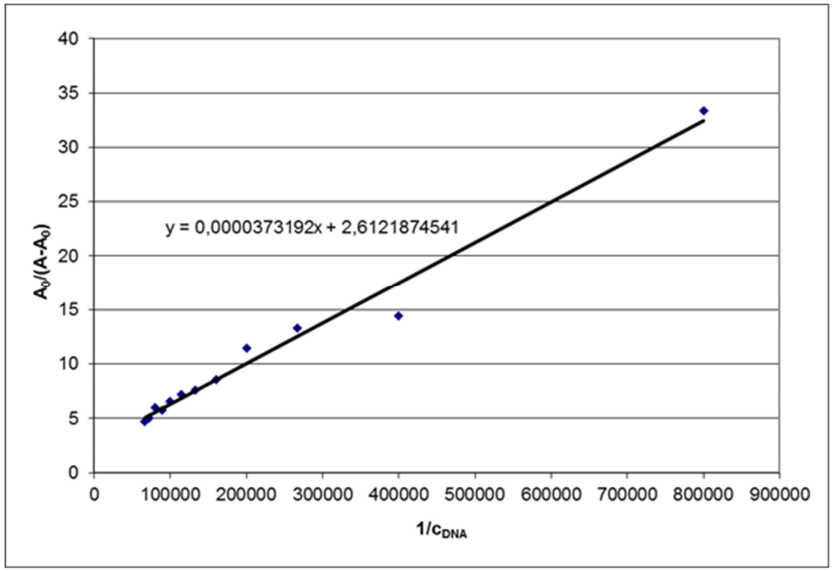

Figure S184. UV-vis absorption spectra of compound **6** (20 µM) in the presence of increasing amount of cf-DNA (0-15 µM) (left). The plot of $A_0/A-A_0$ versus 1/[DNA] yielded the binding constant (right).

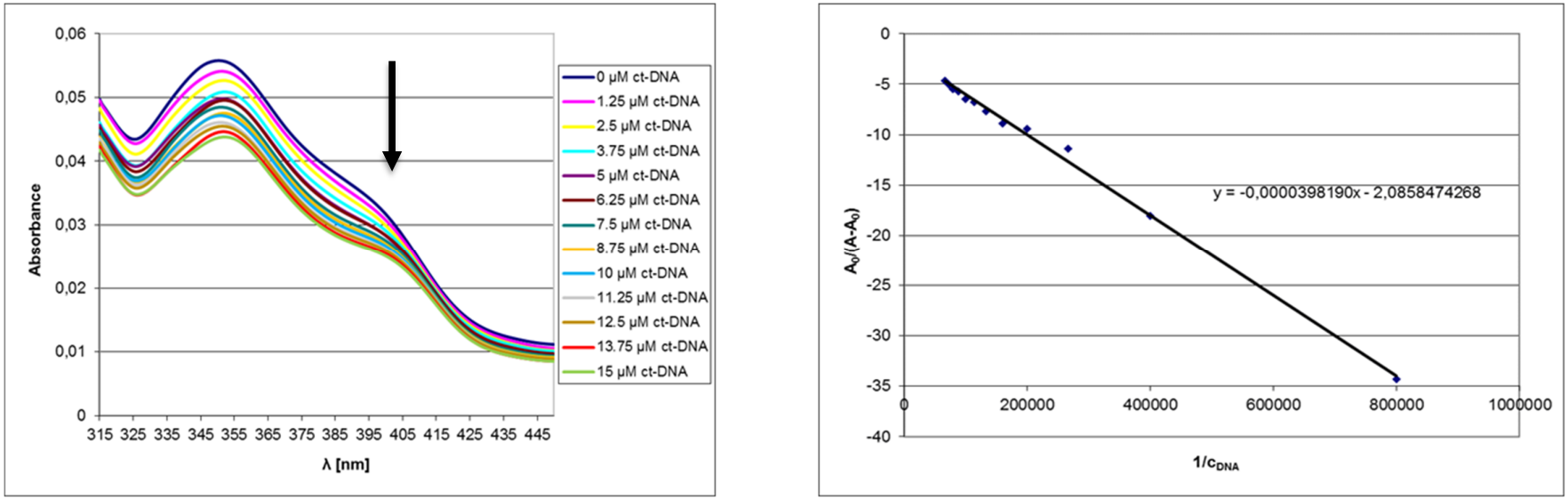

Figure S185. UV-vis absorption spectra of compound **7** (20 µM) in the presence of increasing amount of cf-DNA (0-15 µM) (left). The plot of $A_0/A-A_0$ versus 1/[DNA] yielded the binding constant (right).

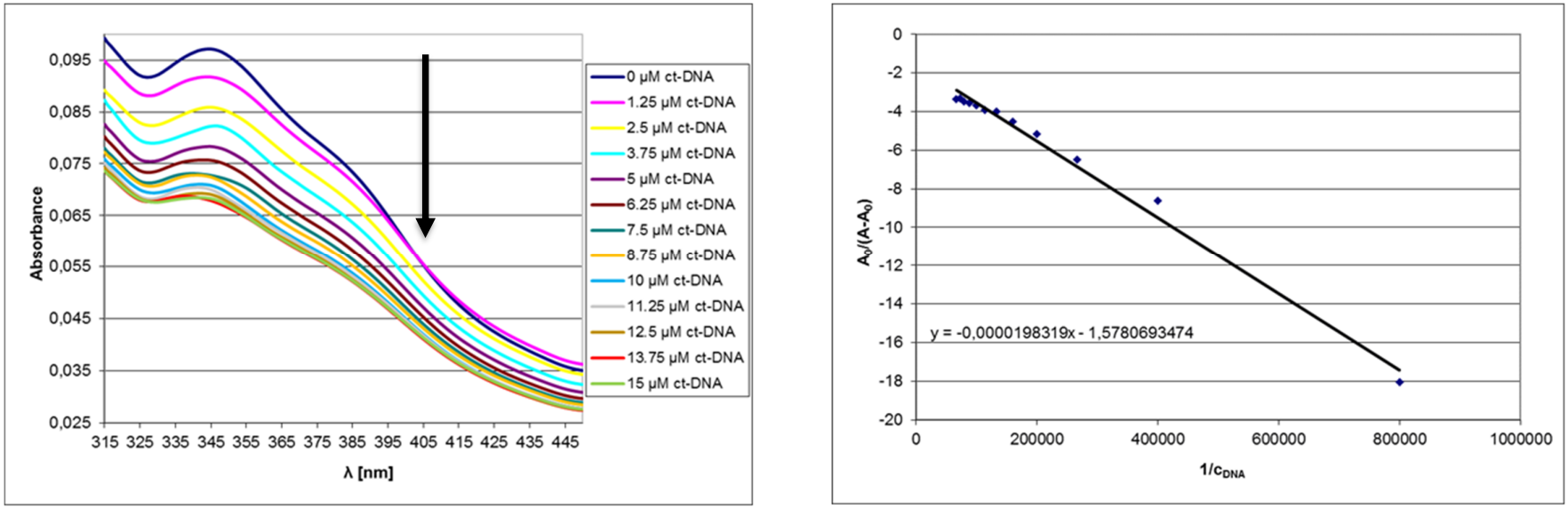

Figure S186. UV-vis absorption spectra of compound **8** (20 μM) in the presence of increasing amount of ct-DNA (0-15 μM) (left). The plot of $A_0/A\text{-}A_0$ versus 1/[DNA] yielded the binding constant (right).

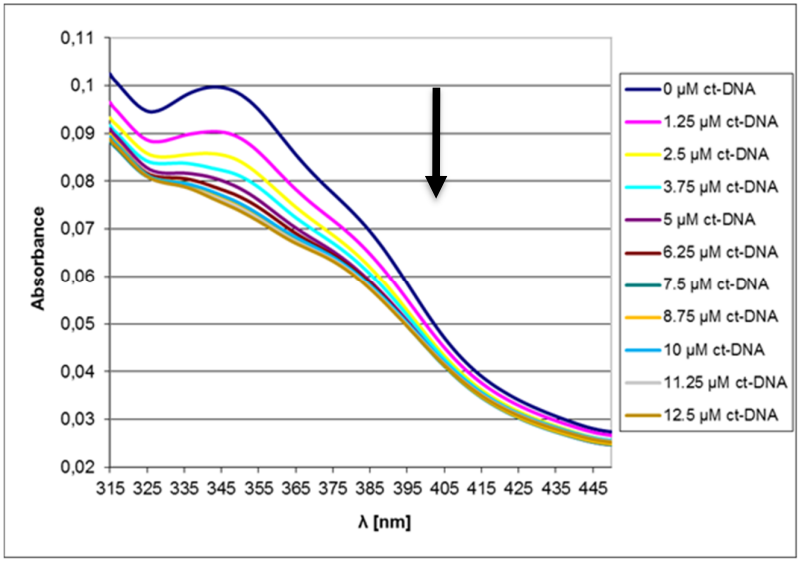

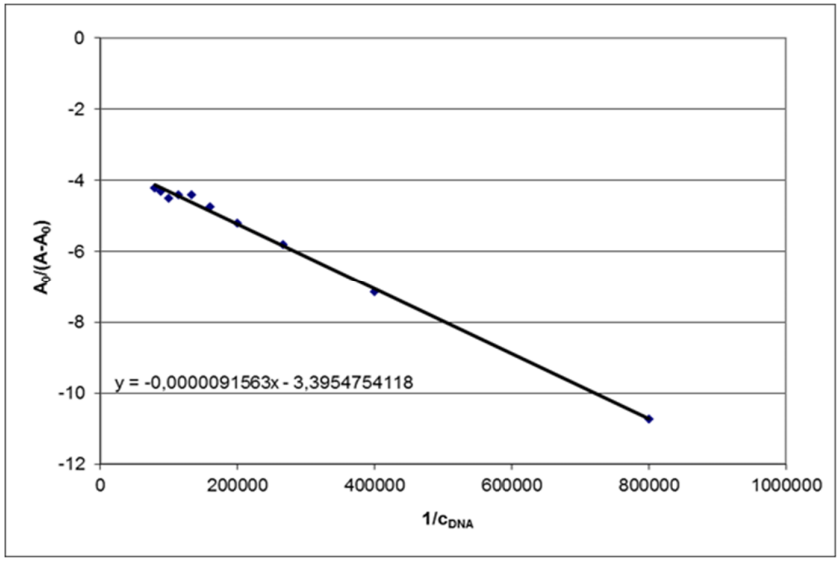

Figure S187. UV-vis absorption spectra of compound **9** (20 μM) in the presence of increasing amount of ct-DNA (0-15 μM) (left). The plot of $A_0/A\text{-}A_0$ versus 1/[DNA] yielded the binding constant (right).

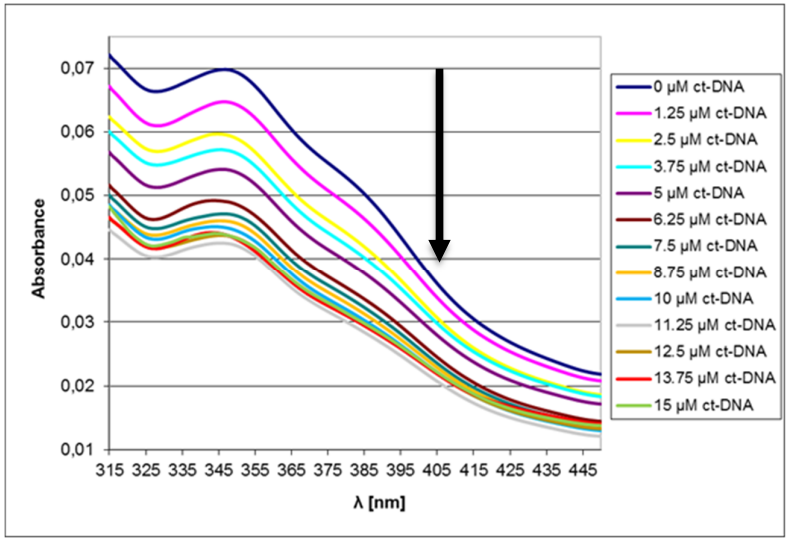

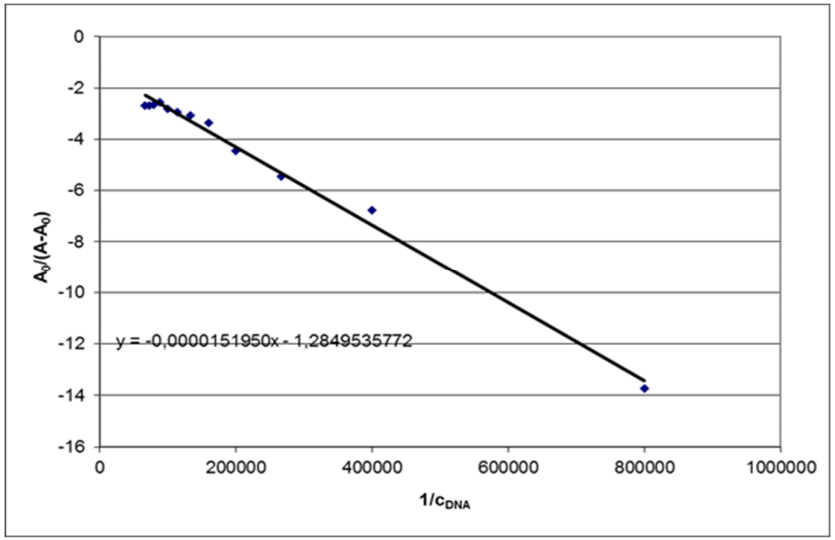

Figure S188. UV-vis absorption spectra of compound **10** (20 µM) in the presence of increasing amount of ct-DNA (0-15 µM) (left). The plot of $A_0/A-A_0$ versus 1/[DNA] yielded the binding constant (right).

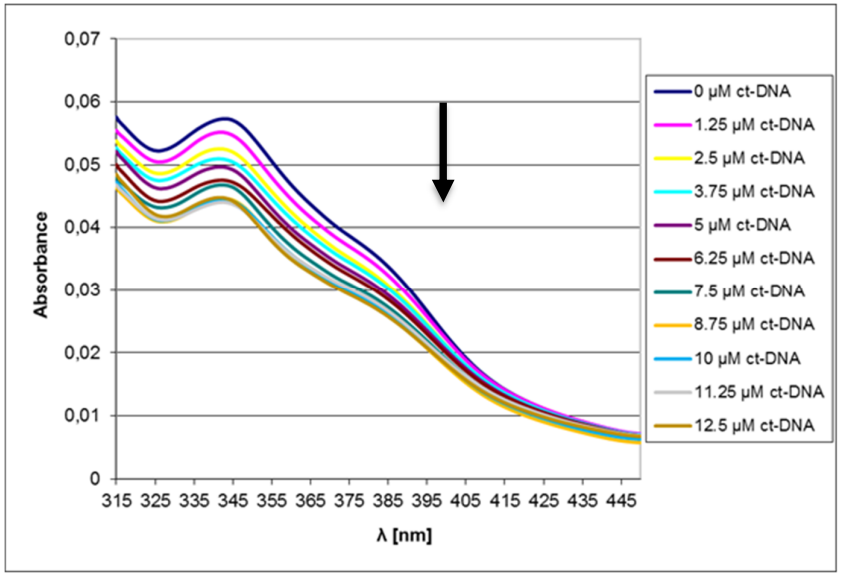

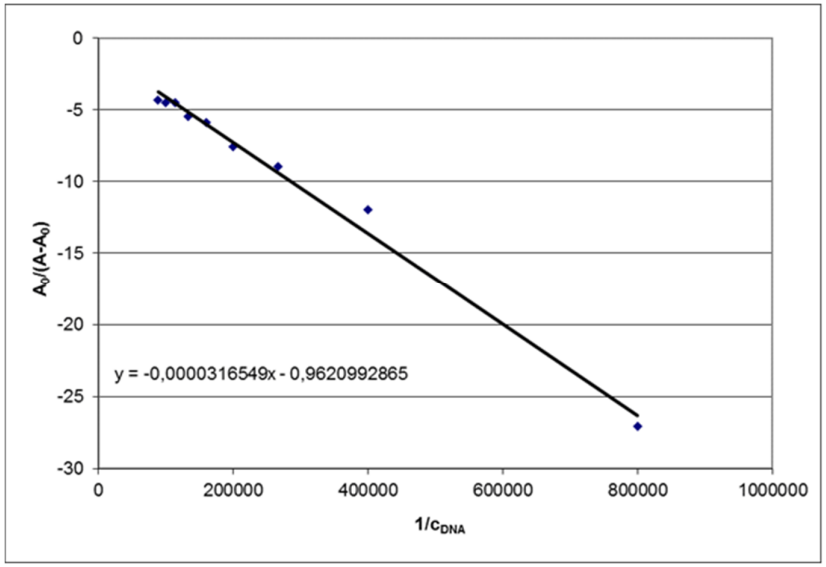

Figure S189. UV-vis absorption spectra of compound **11** (20 μM) in the presence of increasing amount of ct-DNA (0-15 μM) (left). The plot of $A_0/A\text{-}A_0$ versus 1/[DNA] yielded the binding constant (right).

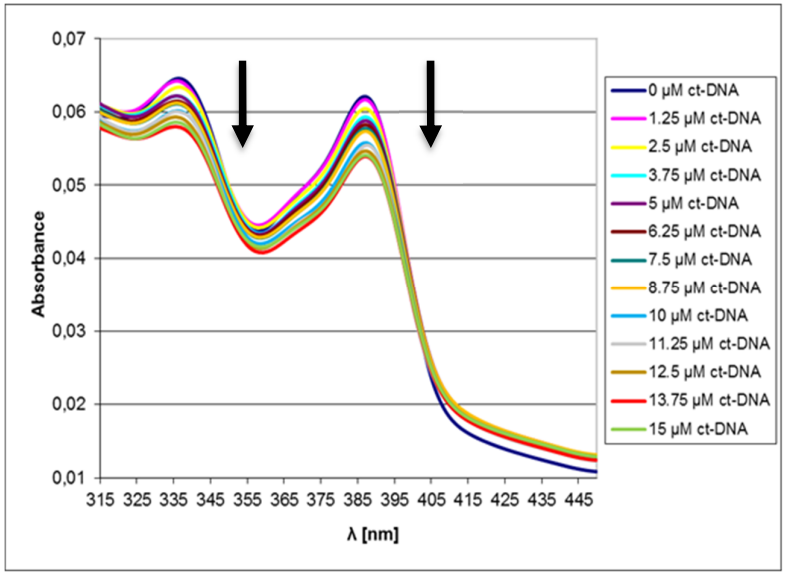

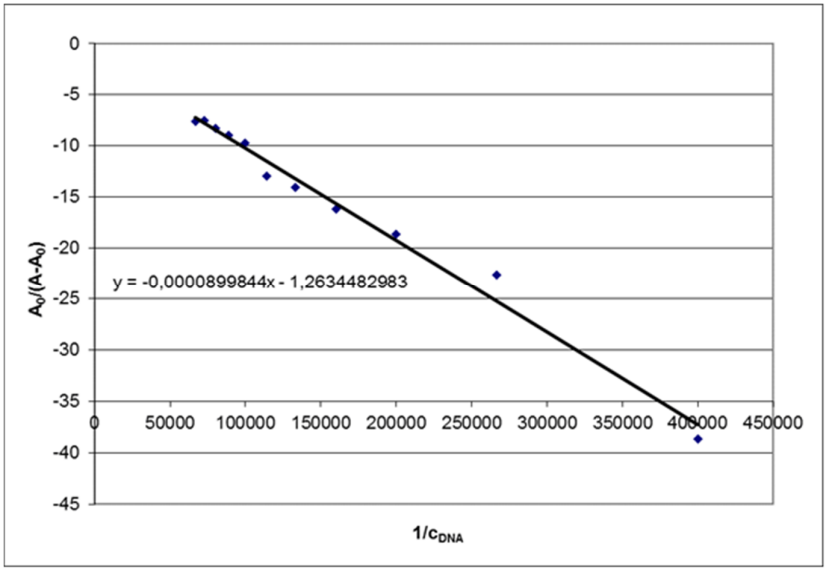

Figure S190. UV-vis absorption spectra of compound **15** (20 μM) in the presence of increasing amount of ct-DNA (0-15 μM) (left). The plot of $A_0/A\text{-}A_0$ versus 1/[DNA] yielded the binding constant (right).

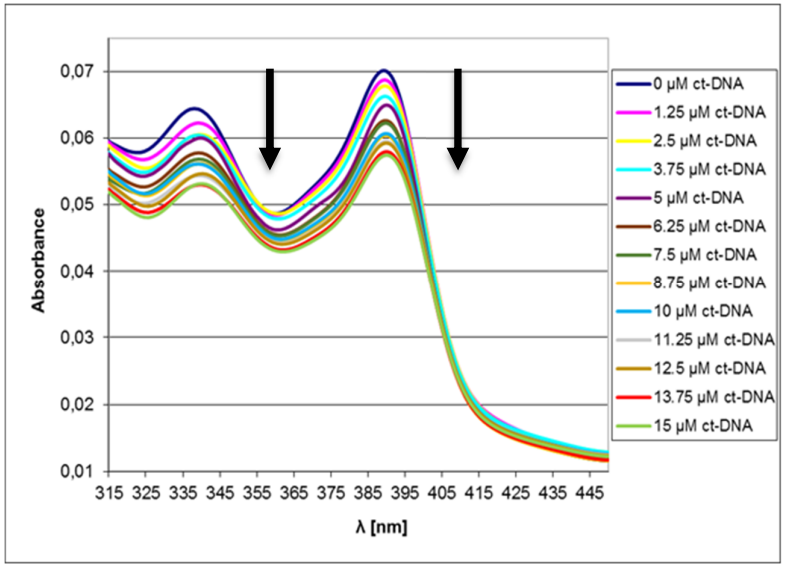

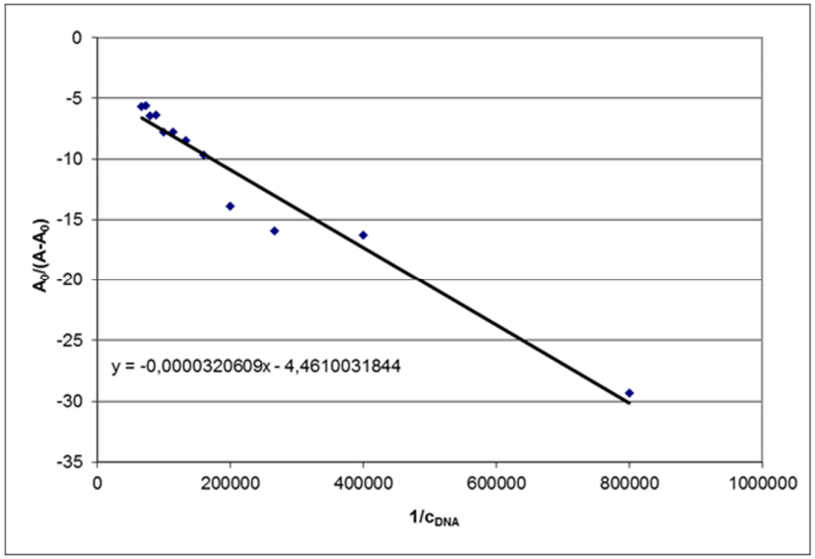

Figure S191. UV-vis absorption spectra of compound **16** (20 µM) in the presence of increasing amount of ct-DNA (0-15 µM) (left). The plot of $A_0/A-A_0$ versus 1/[DNA] yielded the binding constant (right).

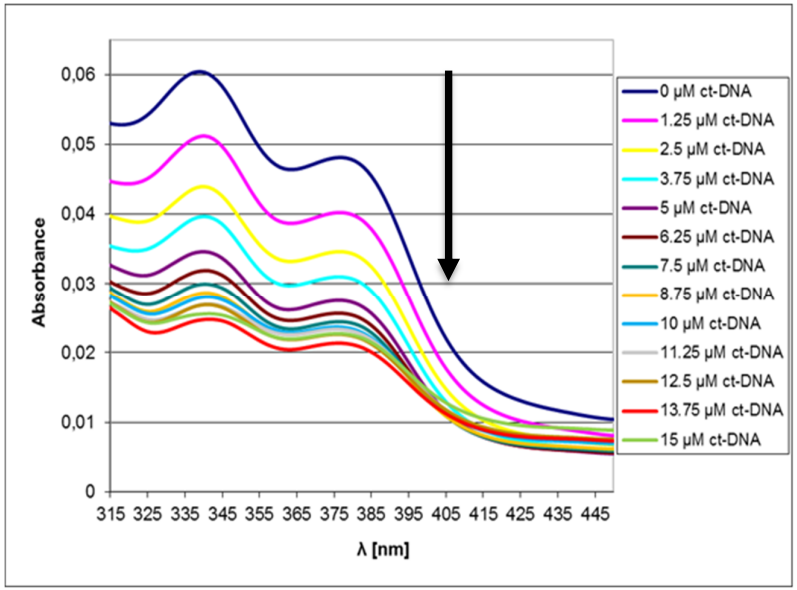

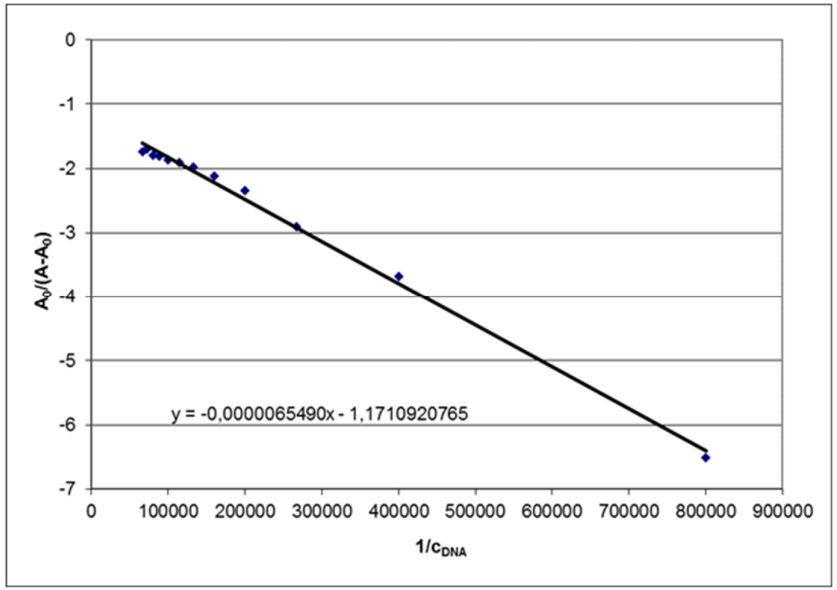

Figure S192. UV-vis absorption spectra of compound **17** (20 µM) in the presence of increasing amount of ct-DNA (0-15 µM) (left). The plot of $A_0/A\text{-}A_0$ versus 1/[DNA] yielded the binding constant (right).

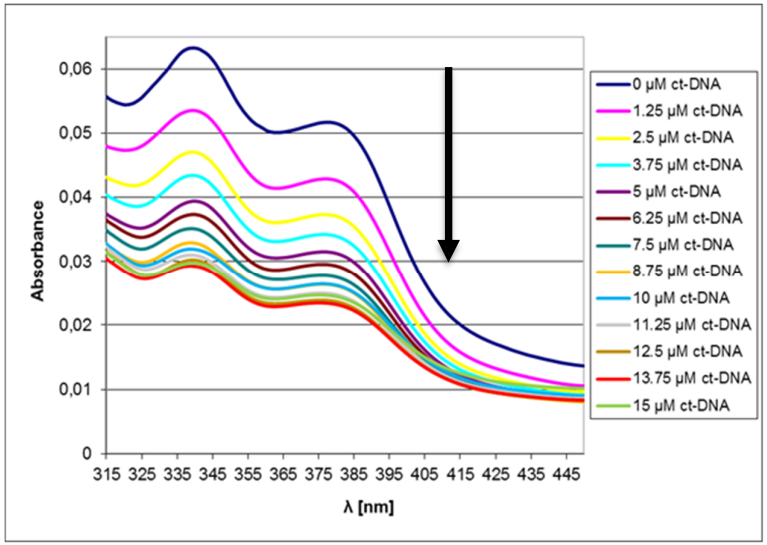

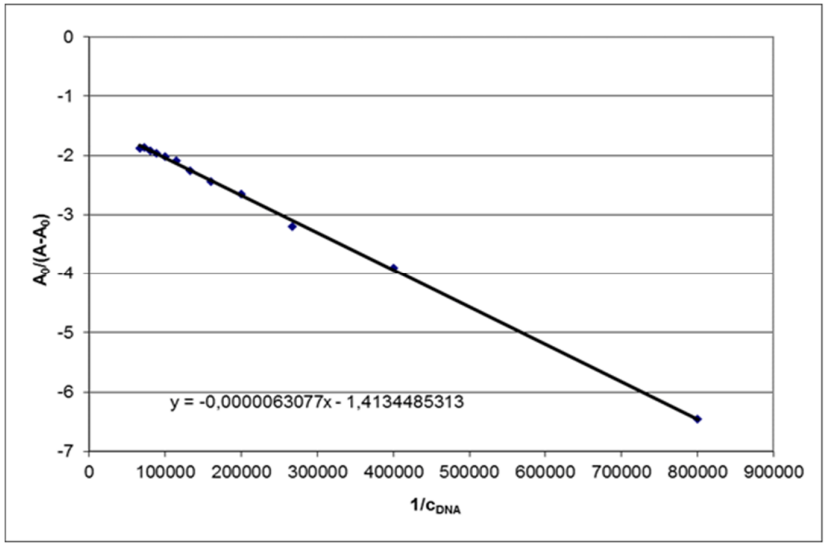

Figure S193. UV-vis absorption spectra of compound **18** (20 µM) in the presence of increasing amount of ct-DNA (0-15 µM) (left). The plot of $A_0/A-A_0$ versus 1/[DNA] yielded the binding constant (right).

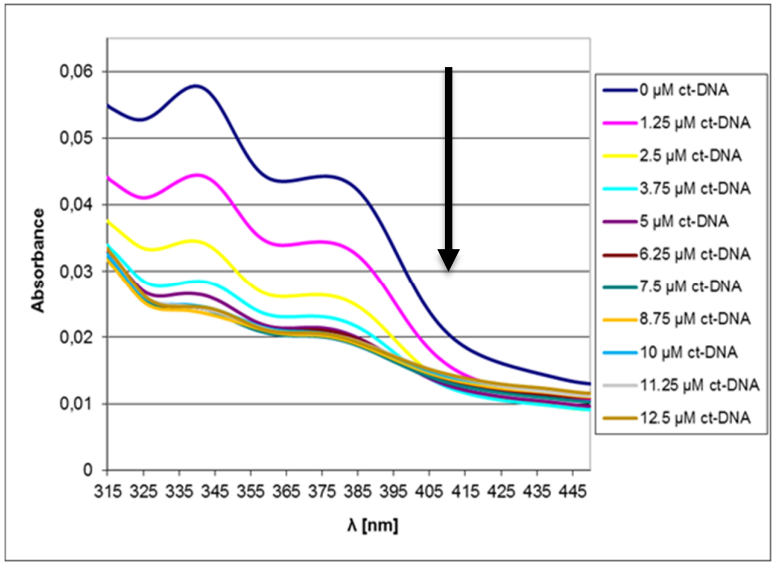

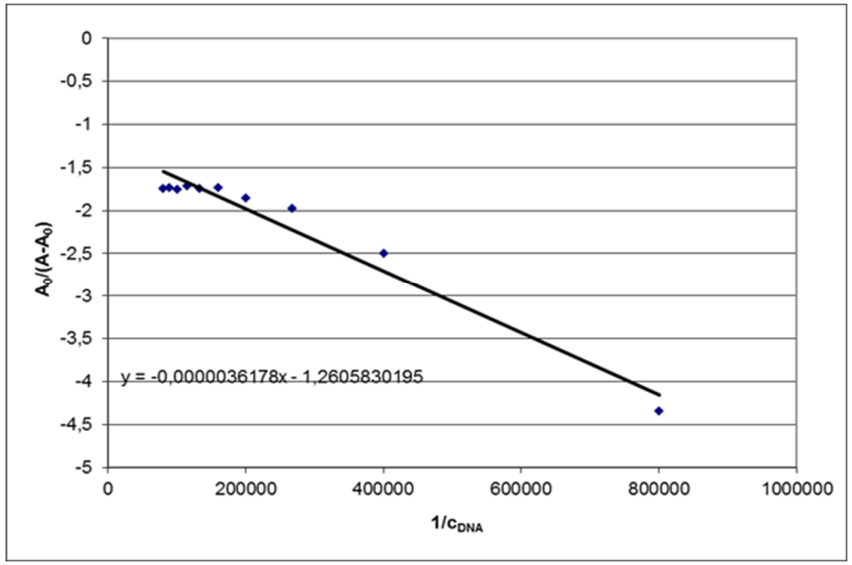

Figure S194. UV-vis absorption spectra of compound **19** (20 µM) in the presence of increasing amount of ct-DNA (0-15 µM) (left). The plot of $A_0/A\text{-}A_0$ versus 1/[DNA] yielded the binding constant (right).

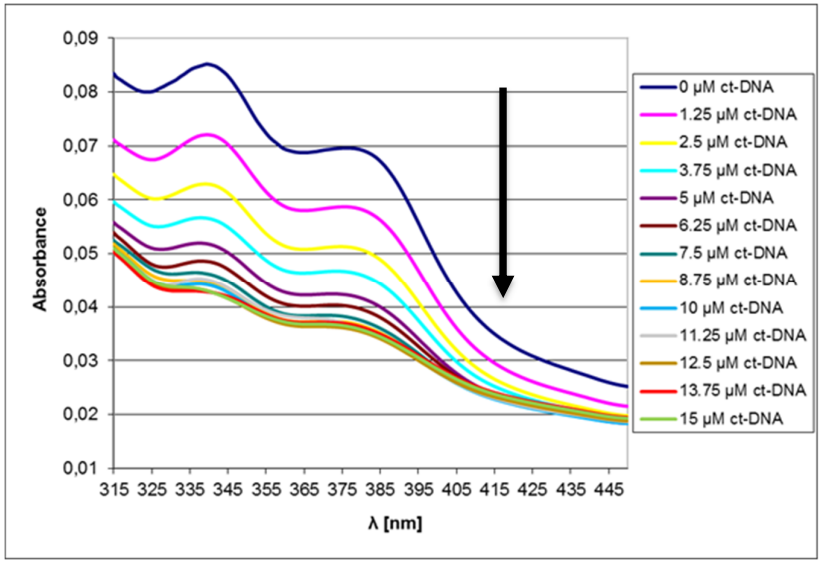

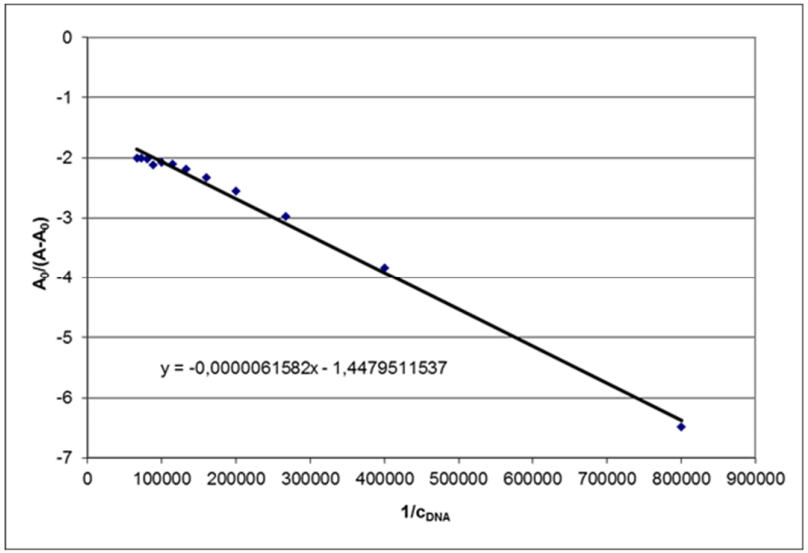

Figure S195. UV-vis absorption spectra of compound **20** (20 µM) in the presence of increasing amount of ct-DNA (0-15 µM) (left). The plot of $A_0/A-A_0$ versus 1/[DNA] yielded the binding constant (right).

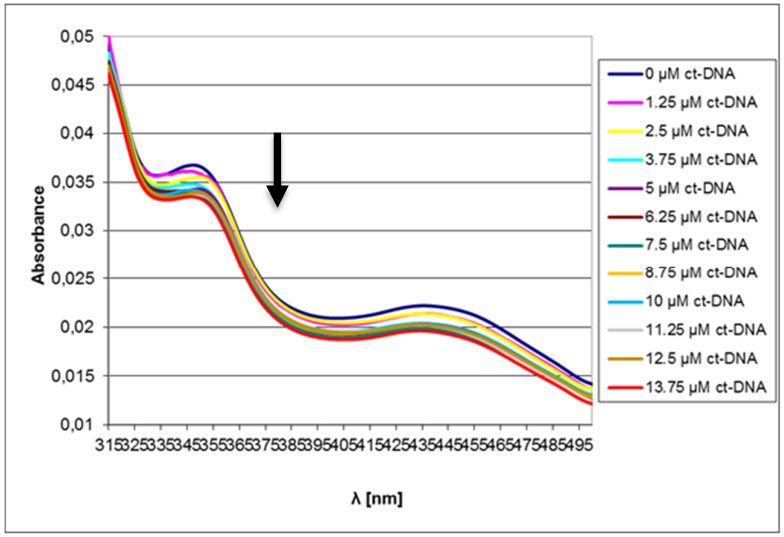

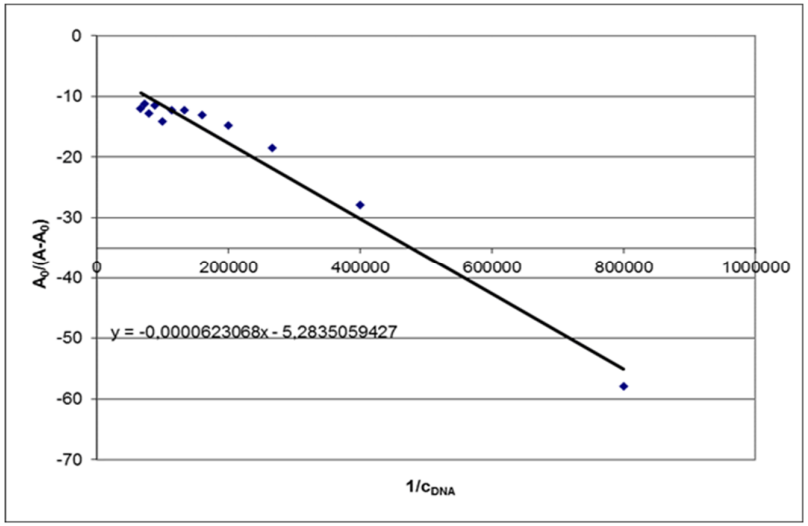

Figure S196. UV-vis absorption spectra of compound **33** (20 µM) in the presence of increasing amount of ct-DNA (0-15 µM) (left). The plot of $A_0/A\text{-}A_0$ versus 1/[DNA] yielded the binding constant (right).

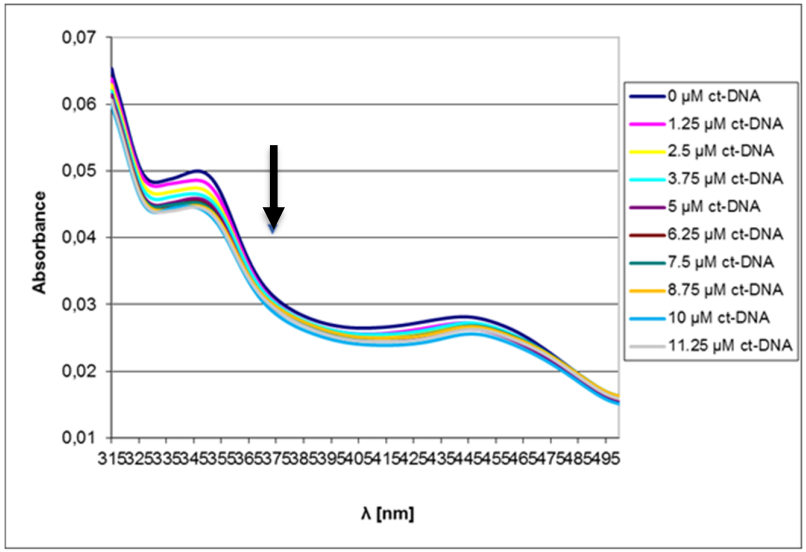

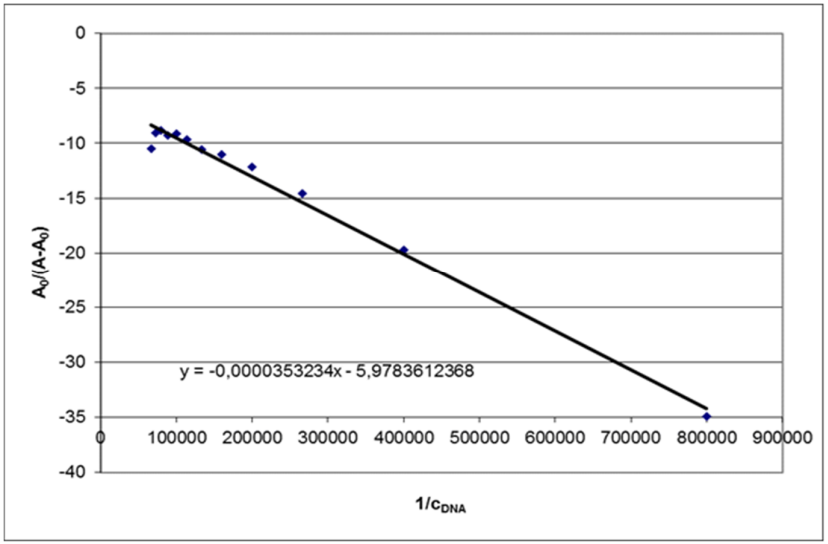

Figure S197. UV-vis absorption spectra of compound **34** (20 µM) in the presence of increasing amount of ct-DNA (0-15 µM) (left). The plot of $A_0/A\text{-}A_0$ versus 1/[DNA] yielded the binding constant (right).

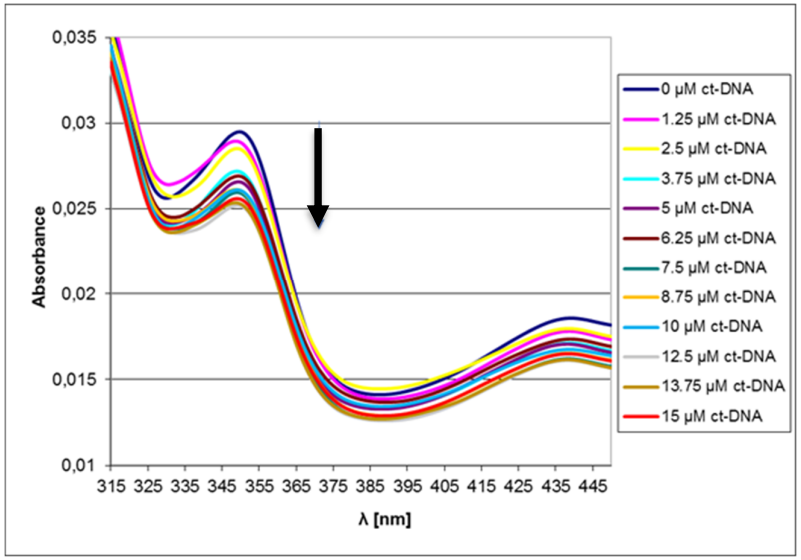

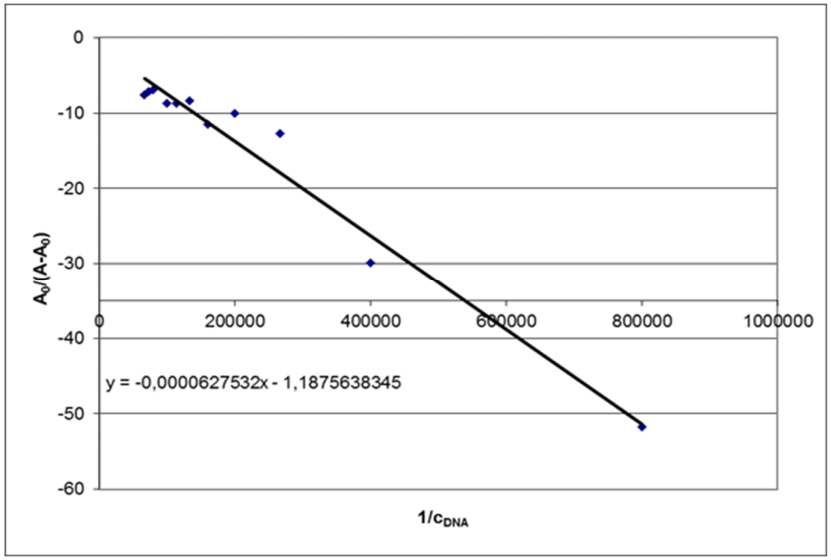

Figure S198. UV-vis absorption spectra of compound **35** (20 µM) in the presence of increasing amount of ct-DNA (0-15 µM) (left). The plot of $A_0/A\text{-}A_0$ versus 1/[DNA] yielded the binding constant (right).

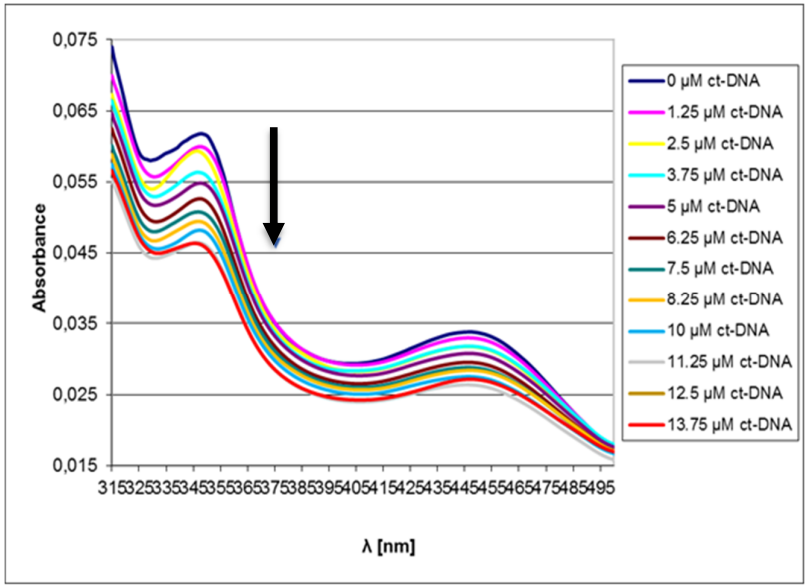

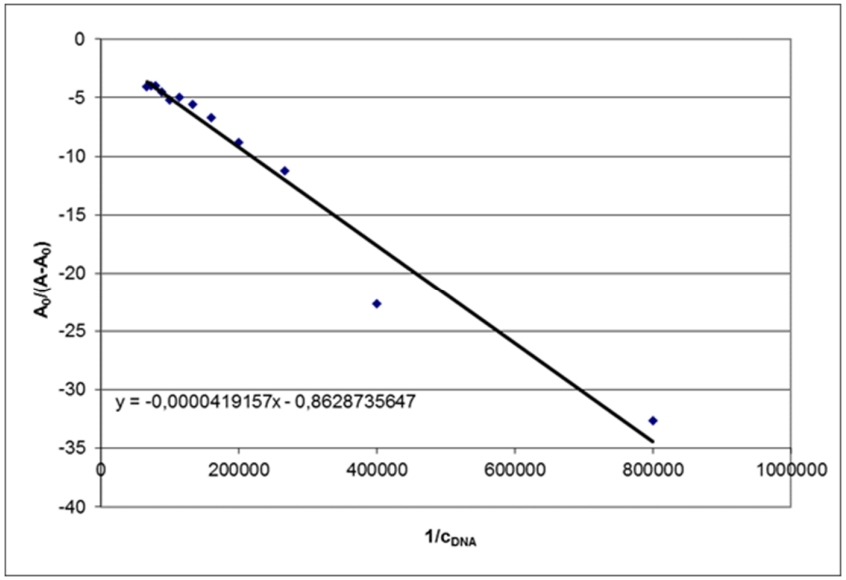

Figure S199. UV-vis absorption spectra of compound **36** (20 μM) in the presence of increasing amount of ct-DNA (0-15 μM) (left). The plot of $A_0/A-A_0$ versus 1/[DNA] yielded the binding constant (right).

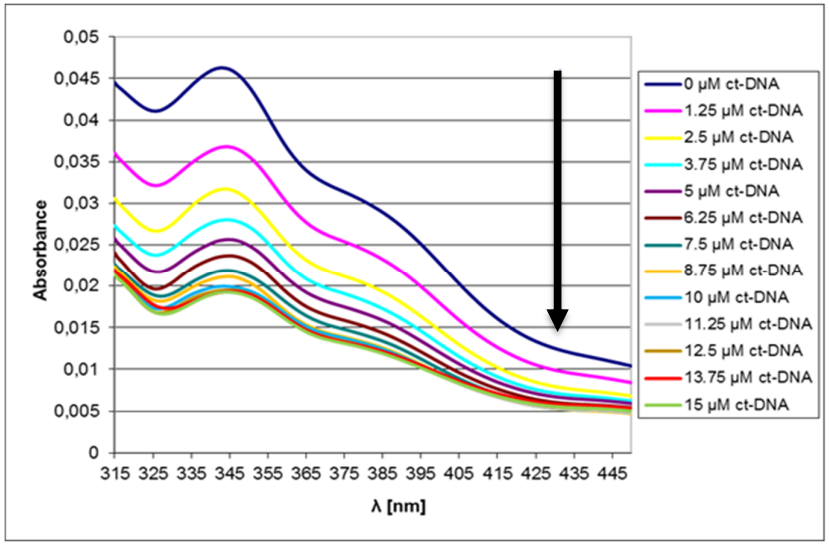

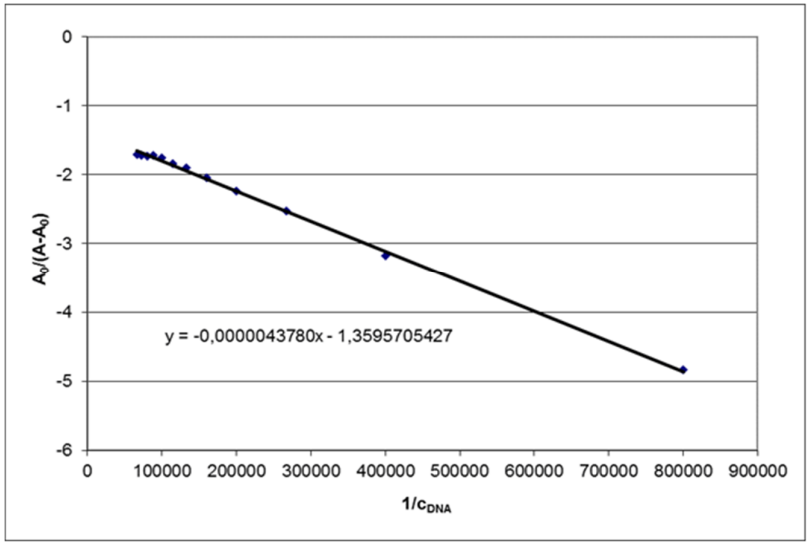

Figure S200. UV-vis absorption spectra of compound **39** (20 µM) in the presence of increasing amount of ct-DNA (0-15 µM) (left). The plot of $A_0/A\text{-}A_0$ versus 1/[DNA] yielded the binding constant (right).

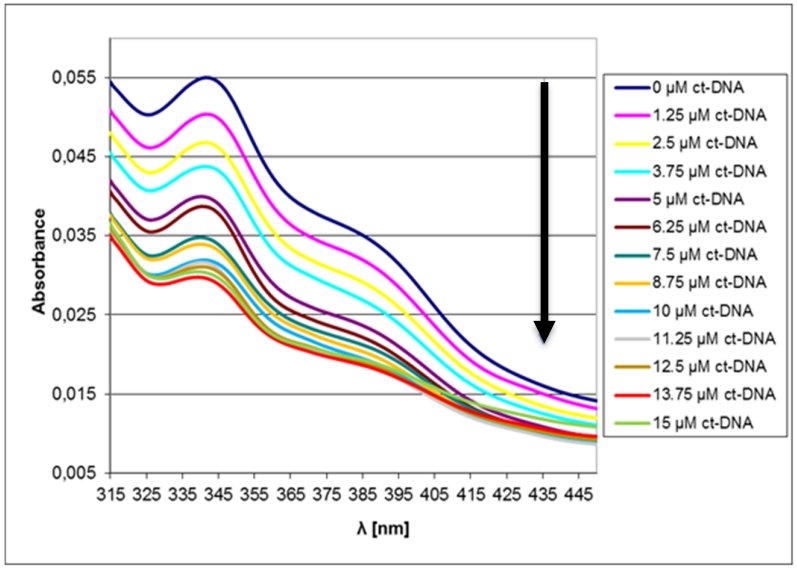

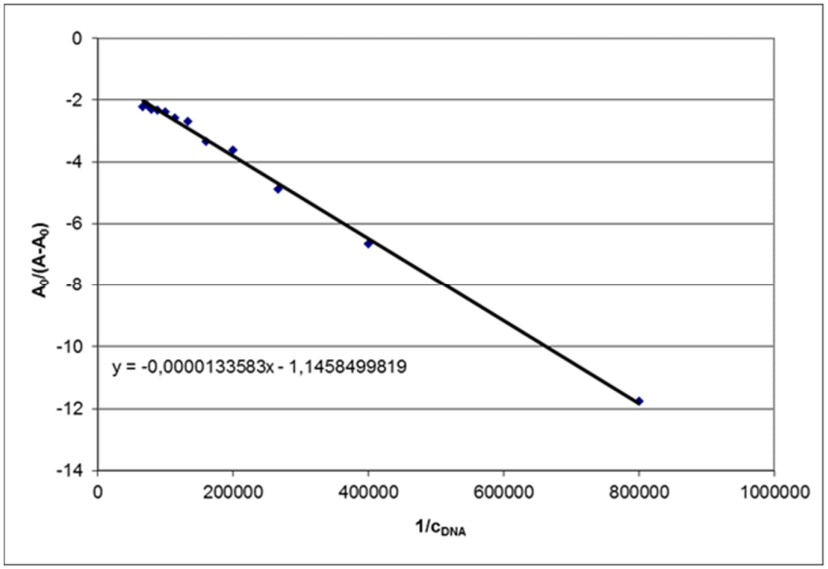

Figure S201. UV-vis absorption spectra of compound **40** (20 μM) in the presence of increasing amount of ct-DNA (0-15 μM) (left). The plot of $A_0/A\text{-}A_0$ versus 1/[DNA] yielded the binding constant (right).

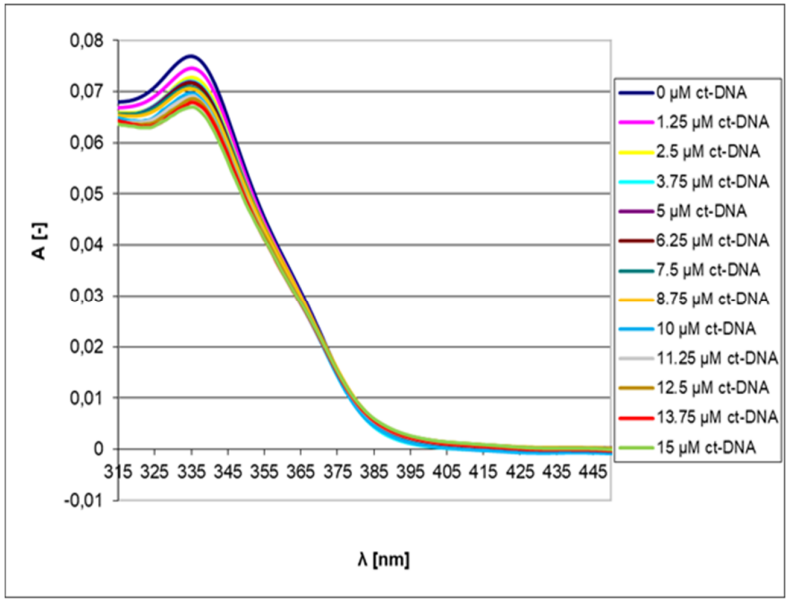

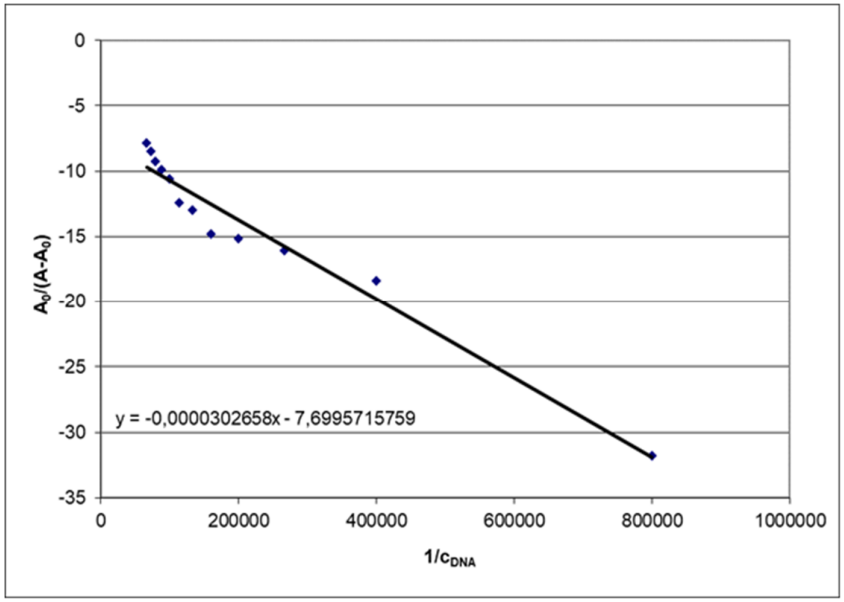

Figure S202. UV-vis absorption spectra of mitonafide (20 µM) in the presence of increasing amount of ct-DNA (0-15 µM) (left). The plot of $A_0/A-A_0$ versus 1/[DNA] yielded the binding constant (right).

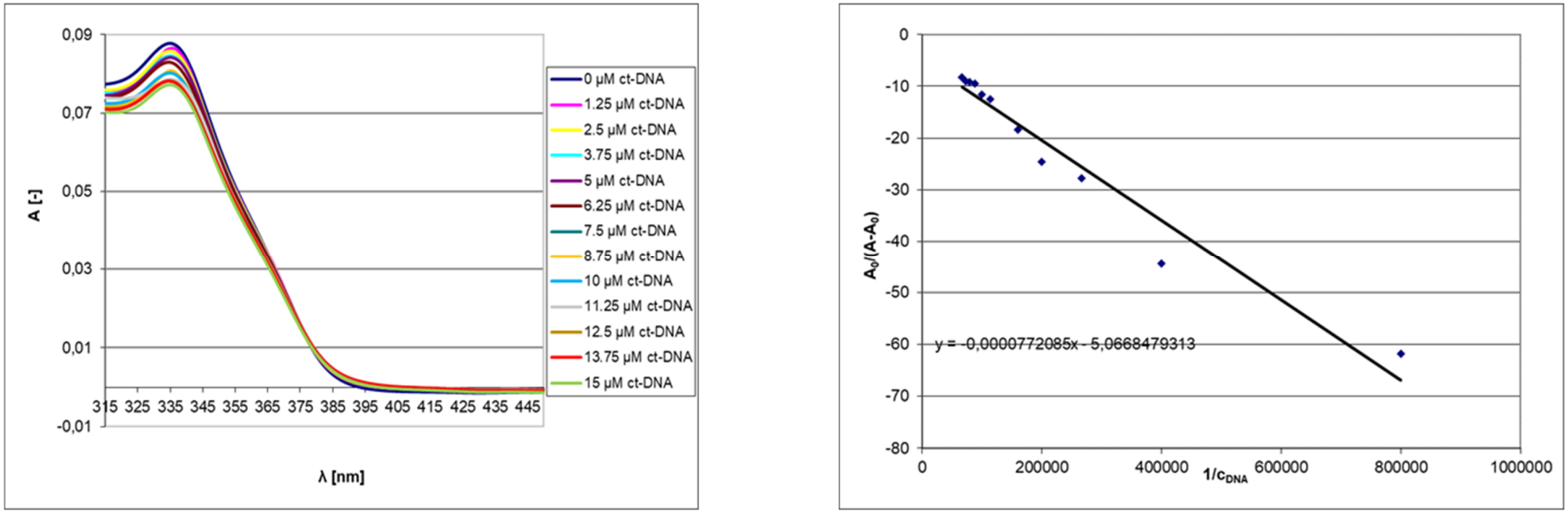

Figure S203. UV-vis absorption spectra of pinafide (20 μM) in the presence of increasing amount of ct-DNA (0-15 μM) (left). The plot of $A_0/A-A_0$ versus 1/[DNA] yielded the binding constant (right).

Table 2S. Crystallographic data.

Compound	**39**	**41**
Wavelength [Å]	0.7749	1.54178
Temperature [K]	100	130
Space group	P-1	P-1
Z	2	2
a [Å]	6.923(2)	7.0385(8)
b [Å]	13.239(8)	9.5223(8)
c [Å]	15.571(3)	21.4413(17)
α [°]	105.721(0)	79.497(7)
β [°]	102.188(3)	81.569(8)
γ [°]	95.815(0)	87.093(8)
R_{int}	0.0550	0.0892
Resolution [Å]	0.79	0.79
% completeness	74.3	94.8
Independent reflections	4262	5628
R/R(for $F_o>4\sigma$)	0.0840/0.1106	0.1012/0.1755
CSD code	2059432	2059431